2007

Autophagy Delivers Viral Antigens for MHC Class II Presentation and is Regulated by Viral Infection

Dorothee Schmid

AUTOPHAGY DELIVERS VIRAL ANTIGENS FOR MHC CLASS II PRESENTATION AND IS REGULATED BY VIRAL INFECTION

A Thesis Presented to the Faculty of

The Rockefeller University

in Partial Fulfillment of the Requirements for

the degree of Doctor of Philosophy

by

Dorothee Schmid

June 2007

Abstract

Autophagy Delivers Viral Antigens for MHC Class II Presentation

and is Regulated by Viral Infection

Dorothee Schmid, Ph.D.

The Rockefeller University 2007

MHC class II molecules generally present peptides derived from exogenous antigens after endocytosis. However, biochemical studies have revealed that MHC class II ligands are frequently derived from intracellular proteins after endogenous processing. Endogenous MHC class II antigen presentation has been described for viral and model antigens and might represent an important mechanism to initiate $CD4^+$ T cell responses to intracellular pathogens.

We studied this unusual MHC class II presentation pathway using the Epstein-Barr virus nuclear antigen 1 (EBNA1) as a model antigen with relevance for human disease. We found that EBNA1 was degraded by lysosomal proteases and detected EBNA1 in double membrane structures by immuno-electron microscopy. Furthermore, inhibition of autophagy led to reduced stimulation of EBNA1-specific $CD4^+$ T cells, suggesting that EBNA1 was delivered for MHC class II presentation by autophagy. This defines a new endogenous MHC class II processing pathway and EBNA1 is the first pathogen-derived antigen found to follow this pathway.

To address the general relevance and the efficacy of this novel MHC class II pathway, we quantified autophagy in MHC class II-positive human cells and demonstrated constitutive autophagosome formation in epithelial, B and dendritic cells. The autophagosome marker Atg8/LC3 strongly overlapped with markers of MHC class II loading compartments (MIICs) by confocal and immuno-electron microscopy, suggesting that autophagosomes frequently fuse with MIICs. Furthermore, this pathway was of functional relevance, because targeting of influenza matrix protein 1 to autophagosomes via LC3 fusion led to strongly enhanced $CD4^+$ T cell stimulation. This suggests that autophagy constitutively and efficiently delivers cytosolic antigens for MHC class II presentation and can be harnessed for improved helper T cell stimulation.

In addition to its role in antigen presentation, autophagy might be an innate immune mechanism to restrict virus replication. We found that autophagosomes strongly accumulated in influenza A virus-infected lung epithelial cells, most likely because they do not fuse with lysosomes anymore. Infected cells contained unusually large autophagosomes filled with amorphous protein or nucleic acid, possibly of viral origin. Inhibition of autophagy led to an increase in influenza virus replication, suggesting that autophagy might be a mechanism to restrict or delay virus replication.

Acknowlegdments

I first and foremost thank my mentor, Dr. Christian Münz, for his guidance throughout my thesis. When I first joined his lab, Christian taught me basic experimental techniques, but even more importantly he trained my as a scientist and encouraged me to think critically and independently. I thank him for his constant advice and support and for always sharing his good mood and enthusiasm with me.

I thank Dr. Ralph Steinman for giving me the chance to join his lab as a visiting student several years ago and for serving as the chair of my thesis committee. I thank him for his interest in my work in countless lab meetings and for giving me helpful advice on many different issues throughout my time at Rockefeller University.

I thank my faculty advisory committee, Dr. Charles Rice and Dr. Thomas Tuschl for their time and helpful suggestions.

I also thank Dr. Ira Mellman for coming all the way from New Haven to serve on my thesis committee.

Dr. Casper Paludan was my collaborator on the EBNA1 project. I thank him for this productive collaboration and for his positive energy and friendship.

Dr. Marc Pypaert was an excellent collaborator and teacher in electron microscopy. I thank him for his generosity during my stay in New Haven and his patience in teaching me the basics of immuno-EM.

I thank my collaborators on the influenza project: Gina Conenello and Tamar Hermesh for help with experiments and Dr. Adolfo Garcia-Sastre and Dr. Peter Pelese for helpful suggestions and their willingness to share important reagents.

I thank Drs. Markus Landthaler, Stefan Stevanović, Ari Helenius, Peter Cresswell, Noburo Mizushima, Mei-Ru Chen, Rajiv Khanna, Martina Vockerodt, Dieter Kube, Jeremy Luban, Thomas Moran and Irene Joab for providing important reagents.

I thank all past and present members of the Munz lab for being excellent colleagues and for keeping up a good lab spirit. Many of them have become good friends and I thank them for many happy lunches, celebrations and hours shared at the bench. My special thanks goes to Till Strowig and Fabienne Brilot for their emotional support, running company and friendship.

I thank the past and present research assistants of the Munz lab, Beza Seyoum, Carolyn Dehner, Gwenola Bougras, Frida Array and Susanne Roberts, for running the daily lab business and all their help with ordering. I also thank Frida for her help in the mouse house and her assistance in the laboratory.

I am grateful to all past and present members of the Steinman lab for their willingness to share reagents and the good atmosphere on the floor. I thank Dr. Sayuri Yamazaki for translating a review article into Japanese and for her kindness and encouragement. I also thank Dr. Adriana Flores-Langarica, Dr. Arnaud Didierlaurent, Juliana Idoyaga and Anthony Bonito for sharing protocols and teaching me basic experimental techniques with mice.

I thank Jacky Chiappetta and Marguerite Nulty for always being so helpful and supportive and for organizing many fun parties.

I appreciate the friendly and professional assistance of the staff at the Bioimaging Resource Center, the Flow Cytometry Resource Center and LARC.

I am indebted to the Rockefeller University and the Dean's office for supporting me as a student in the David Rockefeller Graduate Program.

I am grateful for the financial support that I received from the Schering Founation, the Rockefeller University's Women & Science program, the Cancer Research Institute and the David Rockefeller Graduate Program.

Finally, I thank my family, especially my parents, Wolfgang and Christa Schmid, and my sister Ulrike for their support and constant encouragement. Last but not least I thank Holger Dormann for being there for me every step of the way.

Table of Contents

List of Figures

List of Tables

Chapter 1: Introduction

1.1 General introduction

The vertebrate body is constantly challenged by a variety of pathogens, such as viruses, bacteria, fungi and parasites. In order to respond to this constant threat, vertebrates have evolved an elaborate immune system that - in many cases - confers protective immunity to disease-causing microorganisms. The immune system is commonly divided into two major branches: innate and adaptive immunity. Innate immunity serves as a first line of defence against an invading pathogen and involves the recognition of particular molecular patterns that are common to many pathogens but are absent in the host. However, innate immunity only rarely leads to immunological memory [1], which is primarily a feature of the adaptive immune system [2]. Adaptive immune responses are highly specific for a particular pathogen and can provide long-lasting protection against reinfection. Adaptive immunity is conveyed by two types of lymphocytes: B lymphocytes or B cells, which mature in the bone marrow, and T lymphocytes or T cells, which mature in the thymus [2]. B cells are responsible for the production of antibodies, which are mainly involved in the elimination of extracellular pathogens, such as most bacteria or parasites. In contrast, T cells play an important role in the elimination of intracellular microorganisms, such as viruses: With their T cell receptor (TCR), T cells scan the cell surface for fragments, which are generated within all body tissues and displayed on Major Histocompatibility Complex (MHC) molecules. Detection of a pathogen-derived fragment leads either to direct destruction of the infected cell or to activation of other components of the immune system.

1.2 Antigen presentation on MHC molecules

1.2.1 Major histocompatibility complex (MHC) molecules and antigen recognition by T cells

There are two types of MHC molecules, called MHC class I and MHC class II, which share most of their structural features: Both are transmembrane proteins whose two outer extracellular domains form a long cleft in which a single peptide fragment can be bound (Fig. 1) [2]. However, slight differences in their structures allow them to bind peptides of different length, and differences in their intracellular trafficking allow loading with protein fragments produced in different proteolytic systems: The MHC class I peptide binding cleft can only accommodate peptides that are between 8 and 10 amino acids long (Fig. 1). Peptides that meet these requirements are produced by the proteasome and bind to MHC class I in the endoplasmic reticulum (ER). In contrast, the peptide binding cleft of MHC class II molecules has a more open conformation and therefore can accommodate much longer peptides (Fig. 1). MHC class II ligands mainly are mainly produced by lysosomal degradation and bind to MHC class II in late endosomes. Antigen access to these two proteolytic compartments determines how efficiently T cells detect invaders and, therefore, an understanding of these antigen processing pathways is crucial to our understanding of successful versus insufficient immune responses as well as vaccine efficacy.

MHC class I and II molecules not only present peptides generated in different proteolytic systems. They also activate different classes of T cells that fulfil different functions [2]: MHC class I-peptide complexes activate $CD8^+$ T cells, which are the main killer cells of the adaptive immune system and therefore are called cytotoxic T

Figure 1: Structural features of MHC molecules (adapted from [2]).

A, B: Schematic representation of a MHC class I and MHC class II molecule, respectively. MHC Class I molecules consist of a membrane-spanning α-chain, which folds into three domains (α_1, α_2 and α_3), and a non-covalently associated β_2-microglobulin. In contrast, MHC class II molecules are composed of two transmembrane proteins (α-and β-chain) that have two domains each (α_1, α_2 and β_1 and β_2).

C, D: Crystal structure of a human MHC class I and MHC class II molecule, respectively. Both structures are very similar, with two immunoglobulin-like domains and two domains that together form a peptide-binding cleft.

E, F: Peptide binding cleft with peptide, looking down on the molecule from above. In both molecules, a β-pleated sheet forms the floor and two α-helices form the sides of the cleft. The major differences lie at the ends of the peptide-binding cleft, which are more open in MHC class II molecules. As a consequence, peptides bound to MHC class II molecules can protrude from the cleft and typically are 13-18 amino acids long, whereas MHC class I ligands are completely buried in the peptide binding groove and are not longer than 10 amino acids.

MHC class I | MHC class II

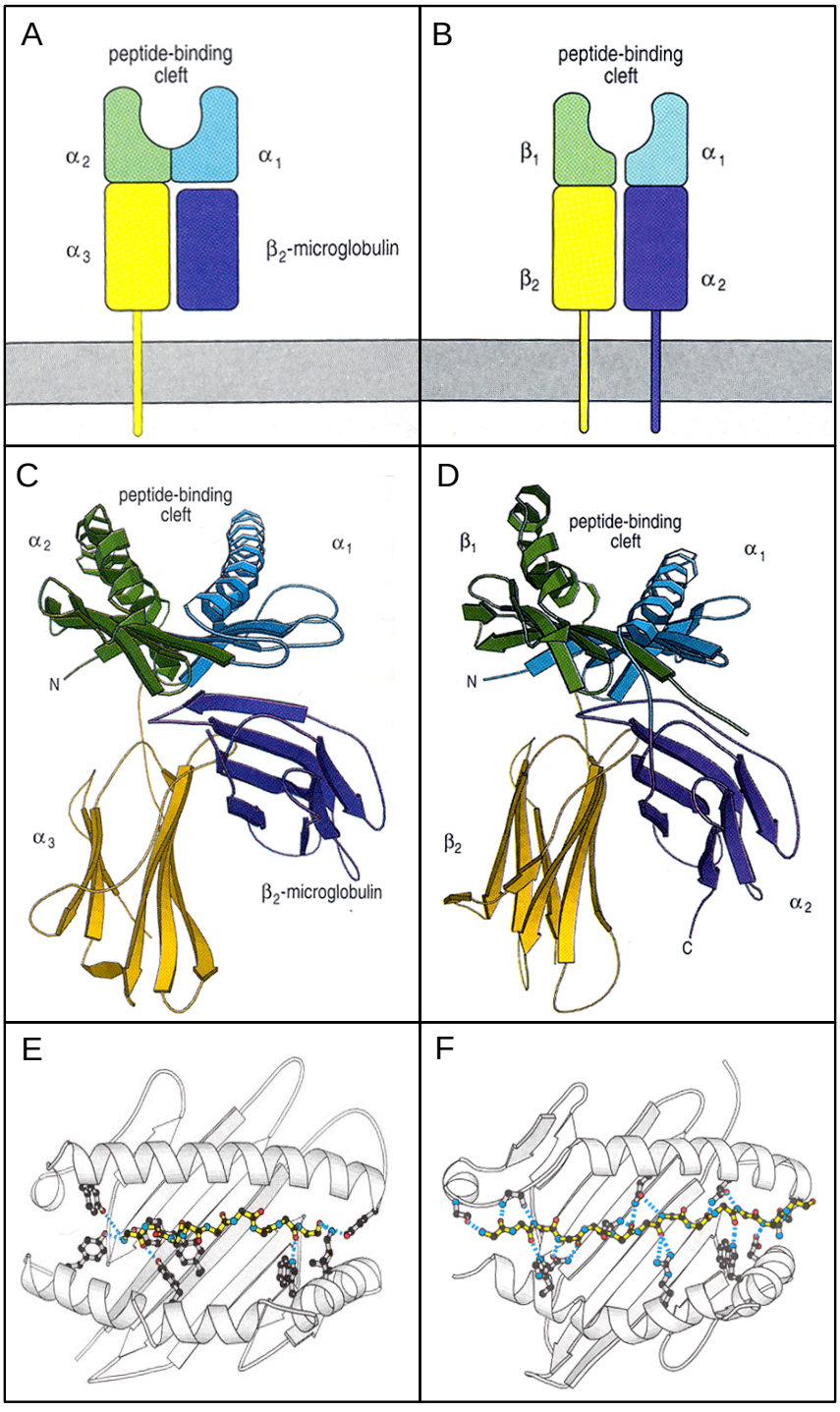

lymphocytes (CTL). In contrast, MHC class II-peptide complexes stimulate $CD4^+$ T cells, whose main function it is to secrete cytokines and to activate other cell types of the adaptive immune system. The functions of $CD8^+$ and $CD4^+$ T cells are discussed in more detail in chapter 1.4.

1.2.2 Classical antigen presentation pathways

MHC class I and II molecules are loaded with their peptide cargo in different cytoplasmic locations [3] (Fig. 2). Antigens for MHC class I presentation are degraded by proteasomes, large multicatalytic proteases found in cytosol and nucleus [4]. Access to proteasomal degradation is primarily regulated via ubiquitinylation of its substrates, and this degradation pathway regulates mostly short-lived proteins [5]. One group of short-lived proteasomal substrates are so called defective ribosomal products (DRiPs), which are degraded by the ubiquitin-proteasome system immediately after misfolding or premature termination of their translation [6]. It was suggested that 30% all of newly synthesized proteins are in some way defective and therefore are immediately ubiquitin-tagged and degraded by the proteasome [7]. This could be especially important in the context of virus infection, as viral antigens would be displayed as soon as viral proteins are translated, allowing the immune system to rapidly detect and destroy the infected cells. Proteasomal products of 8-10 amino acids in length are translocated via the transporter associated with antigen processing (TAP) into the endoplasmic reticulum (ER) (Fig. 2), where they meet newly synthesized MHC class I molecules, which are cotranslationally inserted into the ER membrane. Within the MHC class I loading complex in the ER, which contains chaperones, aminopeptidases and thiol

Figure 2: The classical pathways of antigen presentation on MHC class I and II.

In the classical view of antigen presentation, intracellular antigens are presented on MHC class I molecules (red) and extracellular antigens are presented on MHC class II molecules (blue). Intracellular proteins (yellow) are degraded by the proteasome into short peptides, which subsequently are transported via the transporter associated with antigen processing (TAP) into the endoplasmatic reticulum (ER), where they are loaded into the peptide-binding groove of newly synthesized MHC class I molecules. The MHC class I-peptide complexes then follow the secretory pathway to the cell surface, where they are recognized by cytotoxic $CD8^+$ T cells. Extracellular antigens (pink) are taken up via phagocytosis, macropinocytosis or endocytosis and are delivered to a late endosomal/lysosomal compartment, where they are denatured by low pH and degraded by lysosomal proteases. Newly synthesized MHC class II molecules are targeted from the ER to the same compartment after they associate with a transmembrane glycoprotein called invariant chain (black), which contains a targeting signal for late endosomes. Once MHC class II-inv.chain complexes reach this compartment, invariant chain is degraded by lysosomal proteases and other peptides are loaded into the peptide-binding groove of MHC class II molecules with the help of the peptide-loading chaperone HLA-DM/H2-M (green). Degradation of invariant chain also removes the endosome targeting signal from MHC class II, allowing MHC class II-peptide complexes to traffic to the cell surface for recognition by $CD4^+$ T cells.

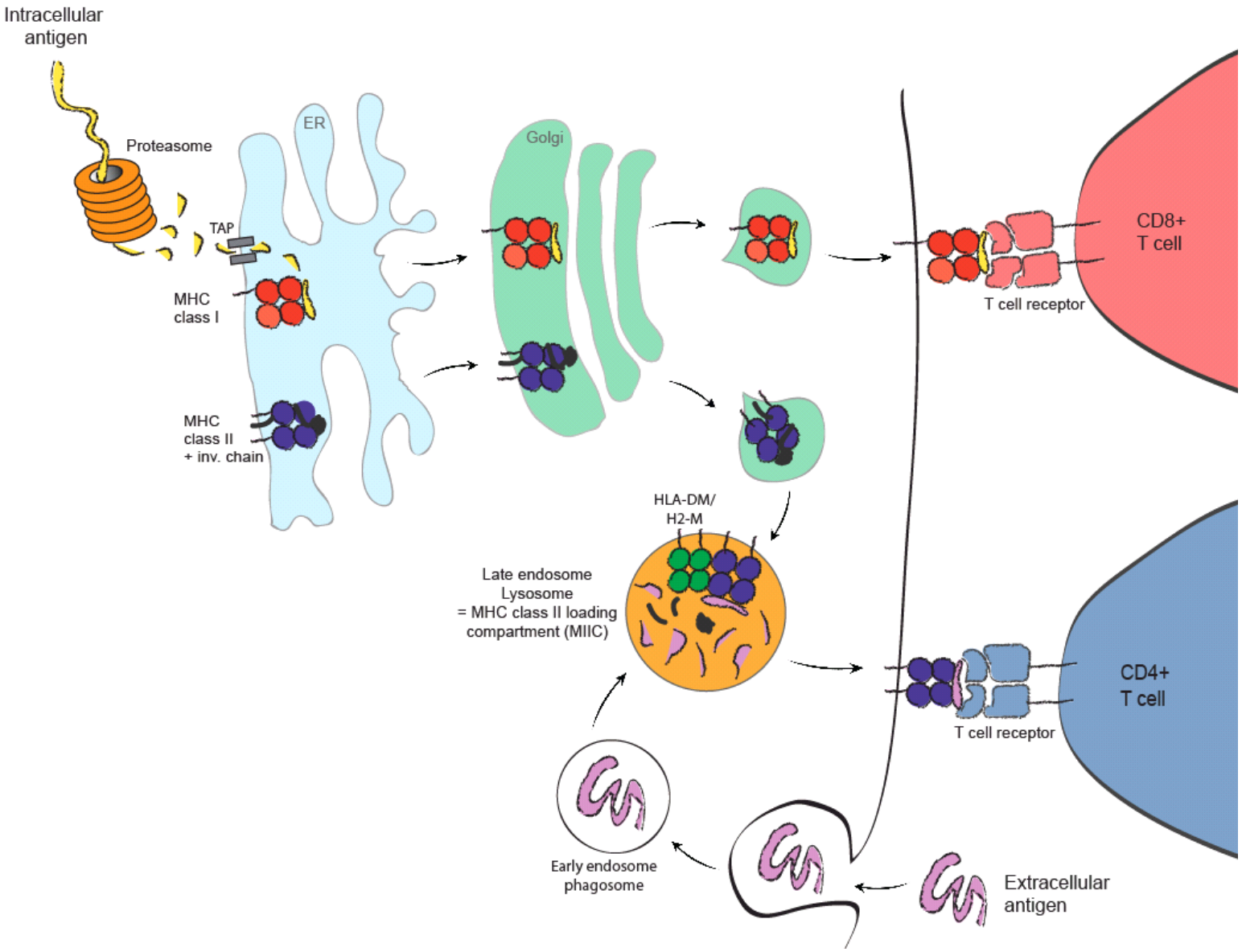
Intracellular antigen
Proteasome
TAP
ER
MHC class I
MHC class II + inv. chain
Golgi
HLA-DM/ H2-M
Late endosome Lysosome = MHC class II loading compartment (MIIC)
Early endosome phagosome
Extracellular antigen
T cell receptor
CD8+ T cell
T cell receptor
CD4+ T cell

oxidoreductases, octamer or nonamer peptides are loaded onto MHC class I molecules [8]. Stably associated MHC class I-peptide complexes are then exported via the Golgi apparatus to the plasma membrane, where they stimulate $CD8^+$ T cells (Fig. 2). As MHC class I ligands are mainly generated in a TAP- and proteasome-dependent fashion, they are thought to mainly originate from cytosolic and nuclear proteins.

MHC class II ligands on the other hand are thought to primarily originate from extracellular antigens after endocytosis and degradation in lysosomes [3]. Newly synthesized MHC class II molecules associate in the ER with a chaperone called invariant chain (Ii) (Fig. 2), which contains a targeting signal that directs MHC class II molecules into late endosomal/lysosomal compartments [9]. In these acidic compartments, which are also called MHC class II loading compartments (MIICs), Ii is degraded by lysosomal proteases and the remaining peptide (CLIP for class II-associated invariant chain peptide) is replaced by lysosomal products under the influence of the chaperone HLA-DM/H2-M [10]. Assembled MHC class II-peptide complexes then migrate to the cell surface for surveillance by $CD4^+$ T cells. As a result of this pathway, MHC class II ligands are mainly generated from extracellular antigens after endocytosis and degradation in lysosomes and therefore are thought to be primarily of extracellular origin.

1.2.3 MHC class II loading compartments and generation of MHC class II ligands

The nature of the MHC class II loading compartment (MIIC) has long been a matter of debate. It is now thought that MIICs are conventional late endosomes or lysosomes that in addition to late endosomal/lysosomal markers contain the MHC class II loading

machinery, such as MHC class II and HLA-DM molecules (Fig. 2). In addition, they should match the following functional criteria: They should be acidic and accessible by endocytosis, and should allow transport of MHC class II-peptide complexes to the plasma membrane [11]. Late endosomes fit these requirements best and are likely to be the major compartments for peptides loading [11, 12].

The importance of lysosomal proteolysis in MHC class II antigen presentation has long been recognized: Drugs that impair lysosomal acidification, such as NH_4Cl or chloroquine, impair proteolysis and thus block antigen presentation on MHC class II molecules [13]. Lysosomal proteases have at least two clear roles in MHC class II function: Generation of antigenic peptides and processing of the invariant chain I_i [14]. Several endo- and exopeptidases are thought to be involved in these processes (Table 1).

Table 1: Lysosomal proteases involved in MHC class II antigen processing.

Class of proteases	Enzyme	Specificity	Role
Cysteine proteases	Cathepsin L (mouse) Cathepsin V (human)	Endo-, after Φ	I_i degrad. in thymic epithelial cells
	Cathepsin S	Endo-, after Φ	I_i degrad. and antigen processing
	Cathepsin B	Carboxy- and Endo-	Antigen processing
	Cathepsin H	Aminopeptidase	Antigen processing
	Cathepsin F	Endo-	I_i degrad. and antigen processing
	Cathepsin Z	Carboxy-	Antigen processing
	AEP	Endo-, after N	Antigen processing
Aspartyl proteases	Cathepsin D	Endo-, after Φ	Antigen processing
	Cathepsin E	Endo-, after Φ	Antigen processing

References: [14-16]

Cysteine proteases, such as cathepsin L, S, B, H, F and Z, aspartyl proteases (cathepsin D and E) and the asparaginyl endopeptidase (AEP) have all been implicated in

antigen processing [16]. Most of these proteases have acidic pH optima and rather broad substrate specificity. The potent endoprotease activities of cathepsin D, E, F, L, S and AEP may be important in revealing antigens, the carboxy-and aminopeptidase activities of cathepsin B, H and Z may fine tune this processing and are likely to account for the heterogenous size of naturally processed MHC class II epitopes (12-24 amino acids) [17]. In addition to proteases, reductases, such as the IFNγ–inducible lysosomal thiol reductase GILT may be involved in the reduction and possibly unfolding of protein antigens [18, 19]. Furthermore, MHC class II molecules may themselves directly participate in antigen processing: The open ends of the class II peptide binding groove are well suited to capture unfolded antigen domains [20] and this might be an essential mechanism to avoid overdigestion and destruction of T cell epitopes.

1.2.4 Professional and non-professional antigen-presenting cells (APCs)

From studying MHC class I and II presentation in different cell types, it has become clear that different cell types can present antigens with vastly different efficiencies [3]. This had led immunologists to term the most efficient antigen-presenting cells (APCs) "professional APCs". These professionals are B cells, macrophages and dendritic cells (DCs). They are characterized by constitutive MHC class II expression and they often have specialized functions of their antigen presentation pathways. For example, B cells express exceptionally high levels of MHC class II [3] and readily internalize antigen via their surface Ig receptor. This allows them to present large quantities of MHC II-peptide that stimulates antigen-specific $CD4^+$ T cells, which in turn provide help for the antigen-presenting B cells (see chapter 1.4.1). Macrophages upregulate MHC class I and II

molecules upon activation by proinflammatory cytokines and bacterial products and readily ingest any form of antigen, either non-specifically or via receptor-mediated endo- or phagocytosis.

The dendritic cell (DC) is the cell type that is most specialized in antigen presentation and is unique among all APCs because it has the capacity for naive T cell activation ("priming"). DCs are enriched in T cell areas of secondary lymphoid organs, where naïve T cells are first activated [21, 22]. They also have unique migratory properties and upon antigen encounter undergo an elaborate maturation process [23]: Immature DCs are highly phagocytic/endocytic and accumulate large amounts of antigens and MHC class II molecules in lysosomal compartments. They continuously circulate through peripheral and lymphoid tissues, where they sample antigens and store them in MHC class II loading compartments. After encountering microbial products or other stimuli (e.g. inflammatory cytokines, CD40 ligand of T cells or innate lymphocytes, such as NK cells), immature DCs transform into mature DCs. They migrate from peripheral sites to secondary lymphoid organs at increased frequency and almost completely downregulate phagocytosis and macropinocytosis and instead process and present the previously ingested antigen, by transporting MHC class II–peptide complexes from lysosomes to the cell surface [23]. In addition, they increase MHC class I and costimulatory molecules on their cell surface, produce proinflammatory cytokines and extend their characteristic dendrites. This allows them to efficiently interact with and activate naïve, antigen-specific T cells. In the absence of a microbial stimulus, dendritic cells can also present self antigen to self-reactive T cells, which in turn get deleted or silenced, i.e. tolerized [24]. The nature of these tolerogenic DCs is still not clear. They

have been suggested to be immature DCs [24], however, immature DCs are inefficient in antigen presentation and migration to T cell areas. Therefore, it seems more likely that tolerogenic DCs have a partially mature phenotype [3]. It is clear that depending on the absence or presence of a microbial stimulus, DCs can be either tolerogenic and immunogenic. However, the exact nature and properties of tolerogenic vs. immunogenic DCs remain to be elucidated.

In addition to these professional APCs, other "non-professional" cell types can present antigens on MHC class I and II molecules. However, in contrast to DCs, they cannot stimulate naive T cells and can only be recognized by previously activated effector T cells. All nucleated cell types express MHC class I molecules and therefore can be recognized by activated $CD8^+$ T cells. Endothelial, epithelial and tumor cells and inflamed tissues can in addition also express MHC class II molecules [25-27] and can, therefore, be recognized by activated $CD4^+$ T cells. These may mediate tissue damage in autoimmune conditions or may contribute to the immune surveillance of tumors.

1.2.5 Non-classical pathways of antigen presentation

Until recently, MHC class I and II molecules were thought to be specialized in presenting peptides derived from distinct sources. MHC class I ligands were thought to be derived from cytosolic and nuclear proteins, whereas MHC class II ligands were believed to be solely generated from extracellular sources. Although these classical pathways of antigen presentation remain correct, it has become apparent that other pathways contribute to antigen presentation, and that antigens from inside and outside the cell can be presented on both MHC class I and II [3].

The classical paradigm of antigen processing was first challenged, when it was discovered that professional APCs, especially dendritic cells (DCs), are able to present extracellular antigen not only on MHC class II, but also on MHC class I [28, 29]. This new exogenous pathway, termed "cross-presentation" pathway, is thought to be important in both immunity and tolerance. It allows dendritic cells to prime $CD8^+$ T cell responses to antigens synthesized by cells other than DCs and to trigger both $CD8^+$ and $CD4^+$ T cell responses at the same time, generating more effective and sustained T cell responses.

The argument that the immune system should be able to survey all cell types and that antigens from all cellular compartments should be presented on both classes of MHC molecules, implies that a similar change in the antigen presentation paradigm might be necessary for MHC class II. Pathogens that replicate in the cytoplasm of professional APCs should be detectable for the immune system via both MHC class I and II presentation. Indeed, it has been shown that MHC class II molecules can present intracellular antigens, including cytosolic and nuclear proteins. This non-classical MHC class II pathway was coined "endogenous MHC class II pathway" and will be further discussed in the next paragraphs.

1.2.6 Endogenous MHC class II processing

The first evidence for the existence of an endogenous MHC class II pathway came from the analysis of natural MHC class II ligands. The analysis of eluted peptides from immunoaffinity purified MHC class II molecules of mouse and human macrophages and B cells, including Epstein-Barr virus (EBV) transformed human B cell lines, revealed that the majority of MHC class II ligands were derived from intracellular proteins [30, 31].

While most ligands were found to originate from transmembrane and secretory proteins, around 20% were found to have nuclear and cytosolic sources (Table 2) [17, 31]. These studies suggested that intracellular proteins gain access to MHC class II presentation by one or more non-classical endogenous antigen processing pathways. The sources of these peptides included cytoskeletal proteins (e.g. actin, tubulin, F-actin capping protein), constitutive metabolic enzymes (e.g. glyceraldehyde-3-phophate dehydrogenase [GAPDH], aspartate aminotransferase [AAT]), heat shock proteins [Hsp70]) and proteins involved in vesicular trafficking (Rab5A) (Table 2). In addition, a few of the identified peptides were derived from nuclear proteins, such as histones [32].

Further evidence for the existence of an endogenous MHC class II pathway came from the fact that $CD4^+$ T cell could recognize cytosolic and nuclear proteins after endogenous processing (Table 3). This pathway for $CD4^+$ T cell recognition was first described by Long and colleagues, who studied presentation of cytosolic measles virus and influenza virus antigens to $CD4^+$ T cells [33-36]. These authors performed cell-mixing experiments to test whether the recognized antigens exit the cell and reenter via endocytosis, i.e. follow the classical MHC class II pathway. They observed, however, that antigen-specific $CD4^+$ T cells did not recognize mixtures of antigen-negative, HLA class II-matched B cells with antigen-expressing, HLA class II-mismatched B cells, but only antigen-expressing, HLA class II- matched B cells, thereby demonstrating that the antigen was not released and then endocytosed for MHC class II presentation [33, 34].

Table 2: Cytosolic/nuclear proteins that give rise to natural MHC class II ligands.

Protein source	Localization	Cell type*
Actin	Cytosol	B, M
Actin-like protein	Cytosol	M
F-actin capping protein	Cytosol	B, M
Tubulin α- and β-chain	Cytosol	B, M
Microtubule-associated protein PB1	Cytosol	B
α-Catenin	Cytosol	B
Clp36	Cytosol	B
GAPDH	Cytosol	B, M, E
Aspartate aminotransferase	Cytosol	B, M
Alcohol dehydrogenase	Cytosol	M
Glucose-6-phosphate isomerase	Cytosol	M
Casein Kinase 1-α	Cytosol	B
Rab5A	Cytosol	B
Cofactor D	Cytosol	B
pp65 macrophage protein	Cytosol	M
ATP citrate lyase	Cytosol	B
Actin interacting protein 1	Cytosol	B
Triosephosphate isomerase 1	Cytosol	B
Peptidylprolyl isomerase A	Cytosol	B
Atg8 (MAP1LC3b)	Cytosol	B
Annexin A2	Cytosol	B
Rab7	Cytosol	B
Acetyl-CoA acyltransferase 1	Cytosol	B
Dipeptidyl peptidase II	Cytosol	B
Phosphoglycerate kinase	Cytosol	B
Pyruvate Kinase	Cytosol	B, E
MIF (Macrophage migration inhibitory factor)	Cytosol	B
GBP-2 (IFN-induced guanylate-binding protein)	Cytosol	B
NADH-cytochrome b_5 reductase	Cytosol	B
c-Myc	Cytosol	B
k-Ras	Cytosol	B
Myosin	Cytosol	E
Fatty acid synthase	Cytosol	E
α-Enolase	Cytosol	B
Elongation Factor 1	Cytosol	B
Hsc70	Cytosol/Nucleus	B
Hsp90-beta	Cytosol/Nucleus	B
Ribosomal proteins S10, S13	Cytosol/Nucleus	B
Ubiquitin	Cytosol/Nucleus	B
EBV Major Capsid Protein	Cytosol/Nucleus	B
Histone H3	Nucleus	B
Histone H2B	Nucleus	B
Rad23b	Nucleus	B
RAN	Nucleus	B

*Cell type: B = B cells, M = macrophages, E = epithelial cells
References: [17, 31, 32, 37-39]

Table 3: Intracellular antigens processed endogenously onto MHC class II.

Type of antigen	Protein	Localization	Cell type	Reference
Viral	Measles Virus Matrix Protein	Cytosol	HLA-DR transf. fibroblasts	[33]
	Measles Virus Nucleocapsid Protein	Cytosol	HLA-DR transf. fibroblasts	[33]
	Influenza A Virus Matrix Protein 1	Cytosol, nucleus	B cells	[35, 36, 40]
	Influenza A Virus Hemagglutinin	Cytosol, ER	HLA-DR-transf. HeLa, B cells	[34, 41]
	Hepatitis C Virus Core protein	Cytosol	B cells	[42]
	Epstein-Barr Virus nuclear antigen 1 (EBNA1)	Nucleus	B cells	[43]
Self	Glutamate decarboxylase (GAD65)	Cytosol	B cells	[44]
	Complement C5	Cytosol	B cells, macroph.	[45]
	Actin, AAT, Rab5	Cytosol	B cells, DCs	[31]
	Igλ light chain	ER	B cells	[46]
Model	Hen egg lysozyme (HEL)	Cytosol, ER, mitoch., nucleus	B cells, MHC class II-transf. sarcoma cells	[47, 48]
	Ovalbumin, Conalbumin	Cytosol	B cells, macroph.	[49]
	Neomycin phosphotransferase II	Cytosol, nucleus	B cells, IFNγ-treated epith. cells	[50]
	β-Galactosidase	Nucleus	Thymic epithelial cells	[51]
	I-E$\alpha_{52\text{-}68}$-GFP	Cytosol	Macroph.	[52]
Tumor	MUC-1	Cytosol	DCs	[53]
	Mutated Cdc27	Cytosol	HLA-DR-transf. 293 cells, melanoma cells	[54]

These experiments showed for the first time that endogenous processing of cytosolic antigens could lead to MHC class II presentation. Subsequently, presentation of endogenous proteins on MHC class II has been described for a number of other viral antigens [41-43, 55, 56] as well as self antigens [31, 44, 45, 57], model antigens [47-52], and tumor antigens [54] [53] (Table 3).

On the basis of these findings, four endogenous MHC class II processing pathways can be postulated [58-60] (Fig. 3). Firstly, secreted/transmembrane proteins (for example influenza hemagglutinin (HA) [41] can associate with newly synthesized MHC class II molecules in the ER, and then follow MHC class II-I_i complexes to endosomal compartments, where processing and peptide-loading occurs. Secondly, cytosolic peptides can be imported into the ER or into endosomes via TAP for binding to MHC class II molecules [34]. In certain APCs, such as dendritic cells, this pathway is even accessed by exogenous antigens like Influenza hemaglutinin and neuraminidase, which leave the endosome for proteasome- and TAP-dependent processing onto MHC class II [61]. A third pathway involves processing of cytosolic or nuclear proteins (for example glutamate decarboxylase 65 (GAD65) by the proteasome and is TAP-independent [44, 52]. For this pathway, peptides seem to be imported directly into endosomal/lysosomal compartments via LAMP-2a, the transporter of chaperone mediated autophagy [62]. In addition, cytosolic/nuclear proteins can be directly imported into endosomes/lysosomes via a fourth, proteasome- and TAP-independent pathway. For example neomycin phosphotransferase II [50] or influenza matrix protein MP1 [36, 40] can be directly imported into endosomes/lysosomes and are degraded by lysosomal proteases. For neomycin phosphotransferase II, autophagy was implicated in the delivery

Figure 3: Proposed processing pathways for presentation of intracellular antigens on MHC class II.

Four different pathways have been postulated: (1) Secreted/transmembrane proteins (e.g. influenza A haemagglutinin) can associate with newly synthesized MHC class II molecules after their cotranslational synthesis into the ER via the Sec61 transporter. Complexes of antigen with MHC class II-I_i then traffic to endosomal compartments, where processing and peptide-loading onto MHC class II occurs. (2) Similar to the classical MHC class I processing pathway, cytosolic peptides (e.g. a 12-mer haemagglutinin peptide) can be imported via TAP into the ER and then associate with MHC class II molecules. It is thought that peptides either bind into the peptide binding groove of MHC class II molecules that failed to associate with invariant chain (I_i) or they co-migrate with MHC class II-I_i complexes and get loaded onto MHC class II in the endosomal MIIC with the help of HLA-DM. (3) Other cytosolic proteins (for example GAD65) are degraded by the proteasome and then follow a TAP-independent pathway onto MHC class II. It is thought that peptides are directly imported into endosomal/lysosomal compartments via a peptide transporter, possibly Lamp-2a. (4) Cytosolic and nuclear proteins (for example neomycin phosphotransferase II) can be processed by lysosomal proteases after direct import into endosomal/lysosomal compartments.

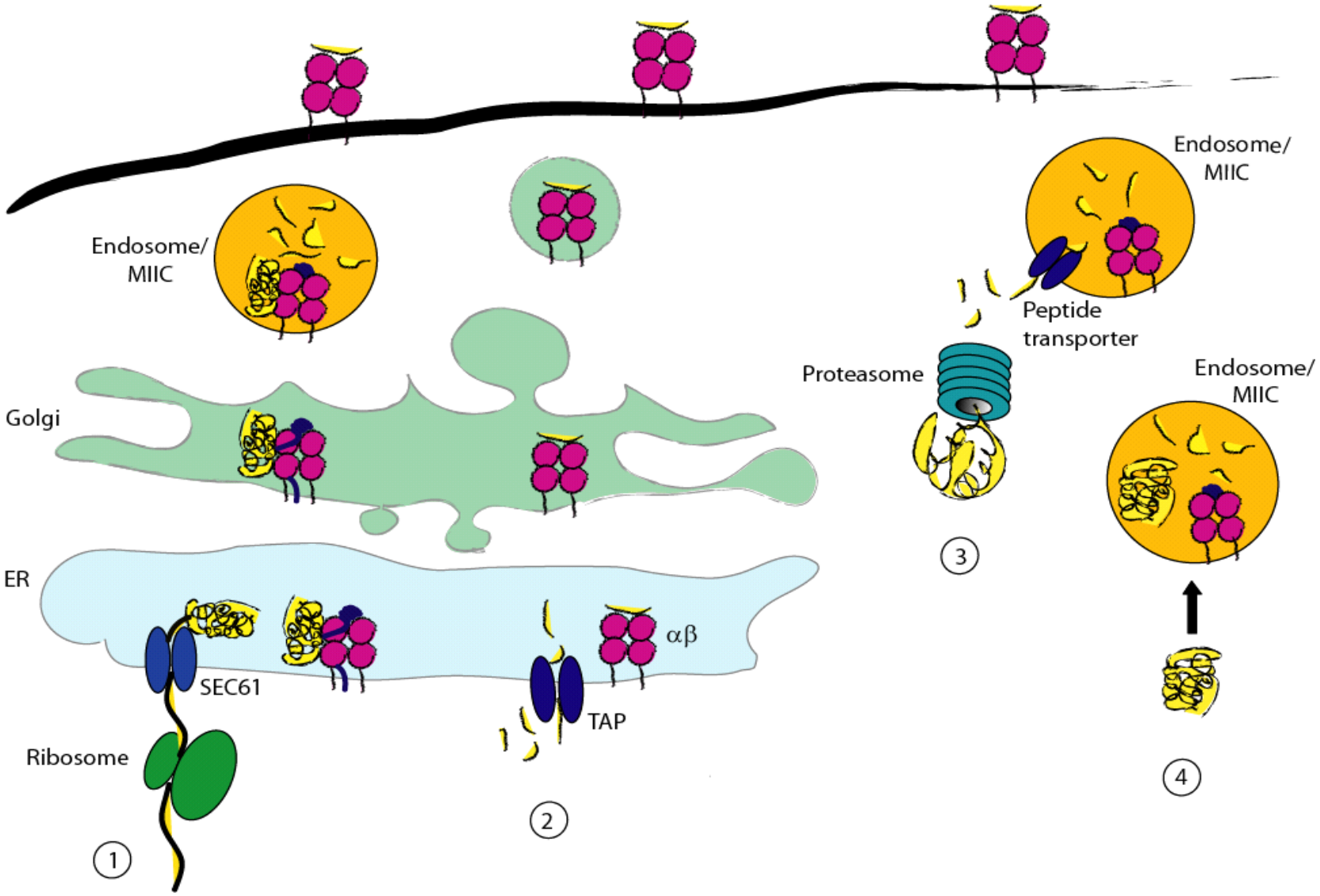
Endosome/
MIIC
Golgi
ER
SEC61
Ribosome
1
αβ
TAP
2
Endosome/
MIIC
Peptide
transporter
Proteasome
3
Endosome/
MIIC
4

of the antigen into lysosomes, while this has not been demonstrated for influenza MP1.

The first pathway (association with MHC class II molecules in the ER) probably contributes the majority (80%) of endogenous MHC class II ligands, which are derived from secreted/transmembrane proteins [17, 31, 32]. The latter three pathways (processing of cytosolic or nuclear proteins by proteasome-dependent or -independent mechanisms) probably contribute the remaining 20% of endogenous MHC class II ligands, which are of cytosolic and nuclear origin. Thus, proteins residing in a compartment that is topologically distinct from the secretory/endocytic route and thus isolated from the classical MHC class II pathway, can gain access to MHC class II molecules and broaden the repertoire of MHC class II ligands.

1.3 Autophagy, a lysosomal degradation pathway

1.3.1 Different pathways of intracellular protein degradation

Intracellular proteins are degraded in two distinct compartments: Short-lived proteins are degraded by the ubiquitin-proteasome pathway [63], while long-lived proteins and organelles are degraded within lysosomes by a process called autophagy [64]. Autophagy, a lysosomal degradation pathway for cytoplasmic material, was originally recognized as a response to starvation [65] and has been recently confirmed to play an essential role during starvation periods in neonates [66]. In addition, autophagy is now accepted as a basal house-keeping mechanism that degrades long-lived proteins and organelles in the steady state [64, 67-70].

Three types of autophagy have been described: chaperone-mediated autophagy, microautophagy and macroautophagy (Fig. 4A). In chaperone-mediated autophagy, cytoplasmic proteins or peptides containing a short signal sequence (KFERQ or related motifs) are imported into lysosomes via the LAMP-2a transporter [71, 72] with the help of cytosolic [73] and lysosomal [74] Hsc70 members. During microautophagy, small amounts of cytoplasm are taken up into the lysosomal lumen via invagination of lysosomal membrane, but this pathway has not been well characterized in mammalian cells so far [75]. Finally, during macroautophagy, cytoplasmic material is engulfed by a characteristic double-membrane vacuole, called autophagosome, which then fuses with lysosomes for degradation of the sequestered material [76]. Macroautophagy is thought to play the most important role for lysosomal degradation of cytosolic constituents, and thus the term autophagy is generally used to describe macroautophagy.

1.3.2 The hallmarks and molecular mechanisms of macroautophagy

During macroautophagy (hereafter simply referred to as autophagy), a double membrane-coated vesicle is formed via elongation of a cup-shaped structure, called isolation membrane (Fig. 4B), whose origin is still debated to date [77, 78]. Cytoplasmic material and organelles are enveloped into this newly forming double membrane vesicle, called autophagosome, which rapidly fuses with lysosomes. The sequestered content is broken down by lysosomal hydrolases, which allows for the recycling of degraded constitutents [79]. Autophagy is seen in all nucleated cell types and is well-conserved from yeast to mammals [64]. The molecular machinery required for autophagosome formation has been identified through genetic screens in yeast. To date, about thirty autophagy-related

Figure 4: Autophagy delivers cytoplasmic constituents to lysosomes.

A: Three autophagy pathways have been described in eukaryotic cells. Chaperone-mediated autophagy delivers signal sequence-dependent cytosolic proteins directly into the lysosomal lumen (1). In this process, cytosolic and lysosomal Hsc70 proteins mediate the import of signal sequence-containing substrates through the Lamp-2a transporter. During microautophagy, small cytosol-containing vesicles bud into the lysosomal lumen, where they are subsequently degraded (2). Finally, macroautophagy involves the formation of a cup-shaped membrane that engulfs cell organelles and long-lived proteins (3). The resulting autophagosome fuses with lysosomes for degradation of its content and of the intravesicular membranes.

B: During the process of macroautophagy, a double-membrane structure, called isolation membrane, surrounds portions of the cytoplasm and organelles. Fusion of the tips of the isolation membrane forms a double-membrane vesicle, called autophagosome, of about 0.5-1 μm diameter. The autophagosome then fuses with late endosomes/lysosomes and the sequestered content and the inner membrane are degraded by lysosomal hydrolases. The fusion of autophagosomes with lysosomes occurs rapidly and hence the half life of autophagosomes is short ($t_{1/2}$ about 8 min).

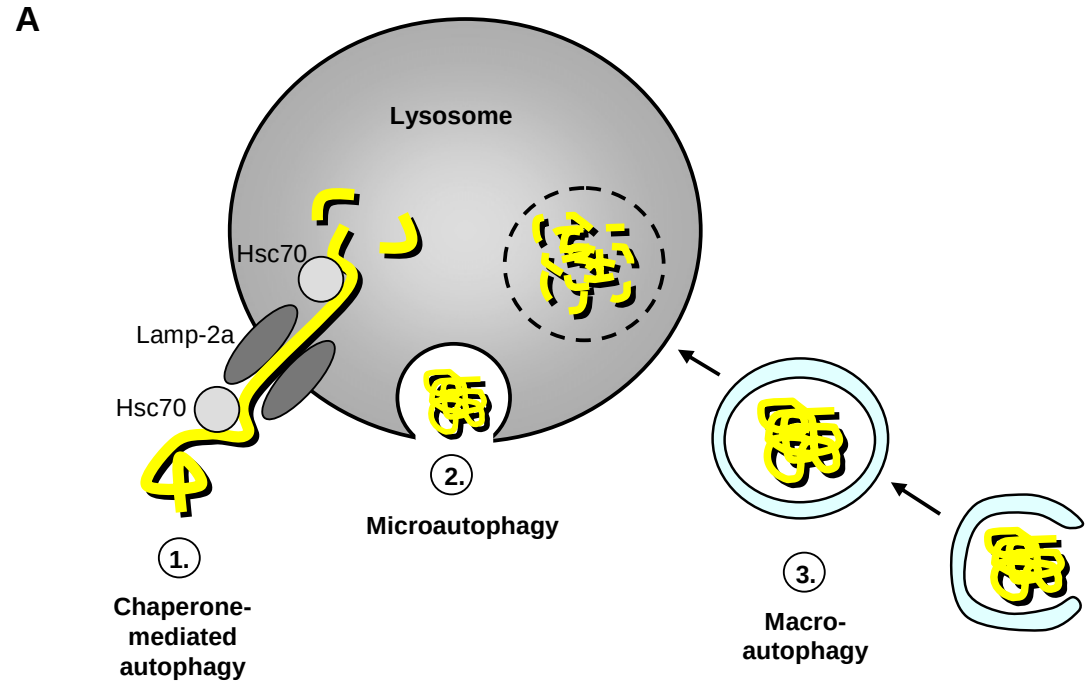
A
Lysosome
Hsc70
Lamp-2a
Hsc70
1.
Chaperone-mediated autophagy
2.
Microautophagy
3.
Macro-autophagy

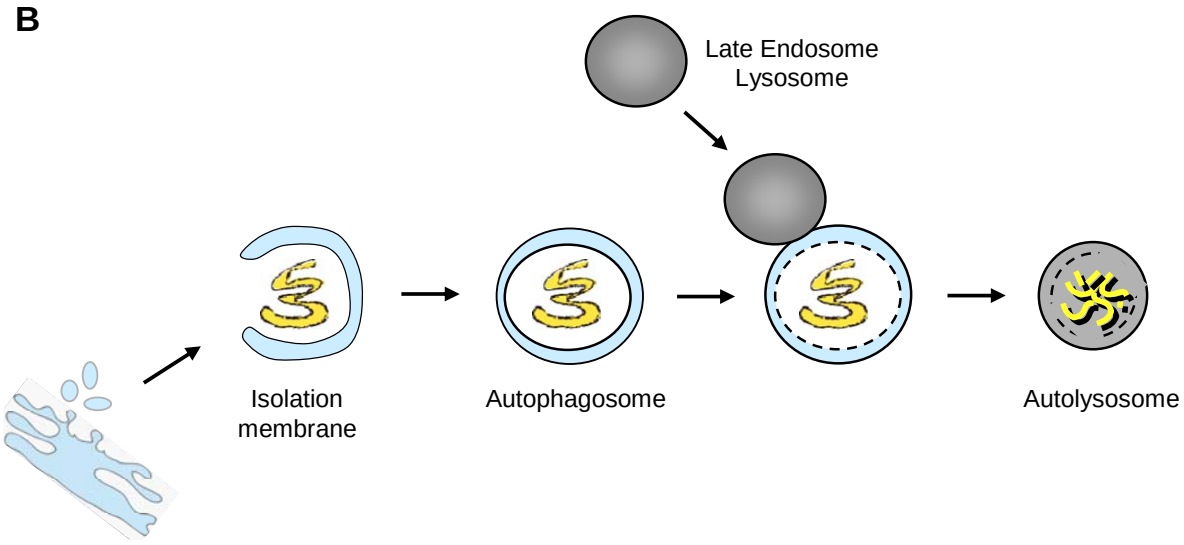
B
Late Endosome
Lysosome
Isolation membrane
Autophagosome
Autolysosome

genes (called Atg) have proven to be involved in macroautophagy in yeast, and mammalian homologues of most of these genes have been identified [80].

Of central importance for the formation of autophagosomes are two ubiquitin-like protein conjugation systems (Fig. 5): First, the ubiquitin-like Atg12 protein is covalently linked to the Atg5 protein by the E1- and E2-like enzymes Atg7 and Atg10, and the resulting complex localizes to the isolation membrane [81]. The Atg5-Atg12 complex is essential for membrane elongation and autophagosome formation [82]. Since it preferentially localizes to the convex membrane of the forming autophagosome, it might determine the curvature of the forming membrane. The mature autophagosome does not carry Atg5 and Atg12. Therefore, it is thought that these proteins leave the isolation membrane just prior to or upon closure of the isolation membrane. The second ubiquitin-like system involves coupling of the ubiquitin-like protein Atg8, also called microtubule-associated protein 1 (MAP1) light chain 3 (LC3), to phosphatidylethanolamine in the autophagosome membrane by the E1- and E2-like enzymes Atg7 and Atg3 [83, 84] (Fig. 5). LC3 is a soluble cytoplasmic protein that first must be cleaved by the Atg4 protease. The C-terminal glycine residue that is generated in this cleavage event is then covalently conjugated to the phospholipid's amino group. In this fashion, LC3 becomes attached to both the inner and the outer autophagosome membrane and is essential for its completion [85, 86]. After autophagosome completion, LC3 remains coupled to the autophagosome and is degraded by lysosomal proteases after fusion with lysosomes [84, 87] (Fig. 5). Due to its covalent attachment to autophagosomal membranes, LC3 and GFP-tagged LC3 are reliable and specific markers to monitor autophagosomes *in vitro* and *in vivo* [68, 88].

Figure 5: Two ubiquitin-like systems participate in autophagosomes formation.

The first ubiquitin-like system involves the ubiquitin-like protein Atg12, whose C-terminal Gly_{140} residue is covalently coupled to a lysine residue (Lys_{130}) in the Atg5 protein. This reaction is catalyzed by the E1- and E2-like enzymes Atg7 and Atg10. The resulting Atg5-Atg12 complex localizes to the isolation membrane and is essential for membrane elongation and autophagosome formation. After closure of the isolation membrane, the Atg5-Atg12 complex leaves the membrane again, so that the mature autophagosome does not carry any Atg5 or Atg12.

The second ubiquitin-like protein Atg8, also called microtubule-associated protein 1 (MAP1) light chain 3 (LC3), is a soluble cytoplasmic protein that first must be cleaved by the Atg4 protease. The C-terminal glycine residue that is generated in this cleavage event (Gly_{120}) is then covalently conjugated to the amino group of a phospholipid in the forming isolation membrane, a reaction catalyzed by the E1- and E2-like enzymes Atg7 and Atg3. In this fashion, LC3 becomes attached to both the inner and the outer autophagosome membrane and thus decorates the autophagosome.

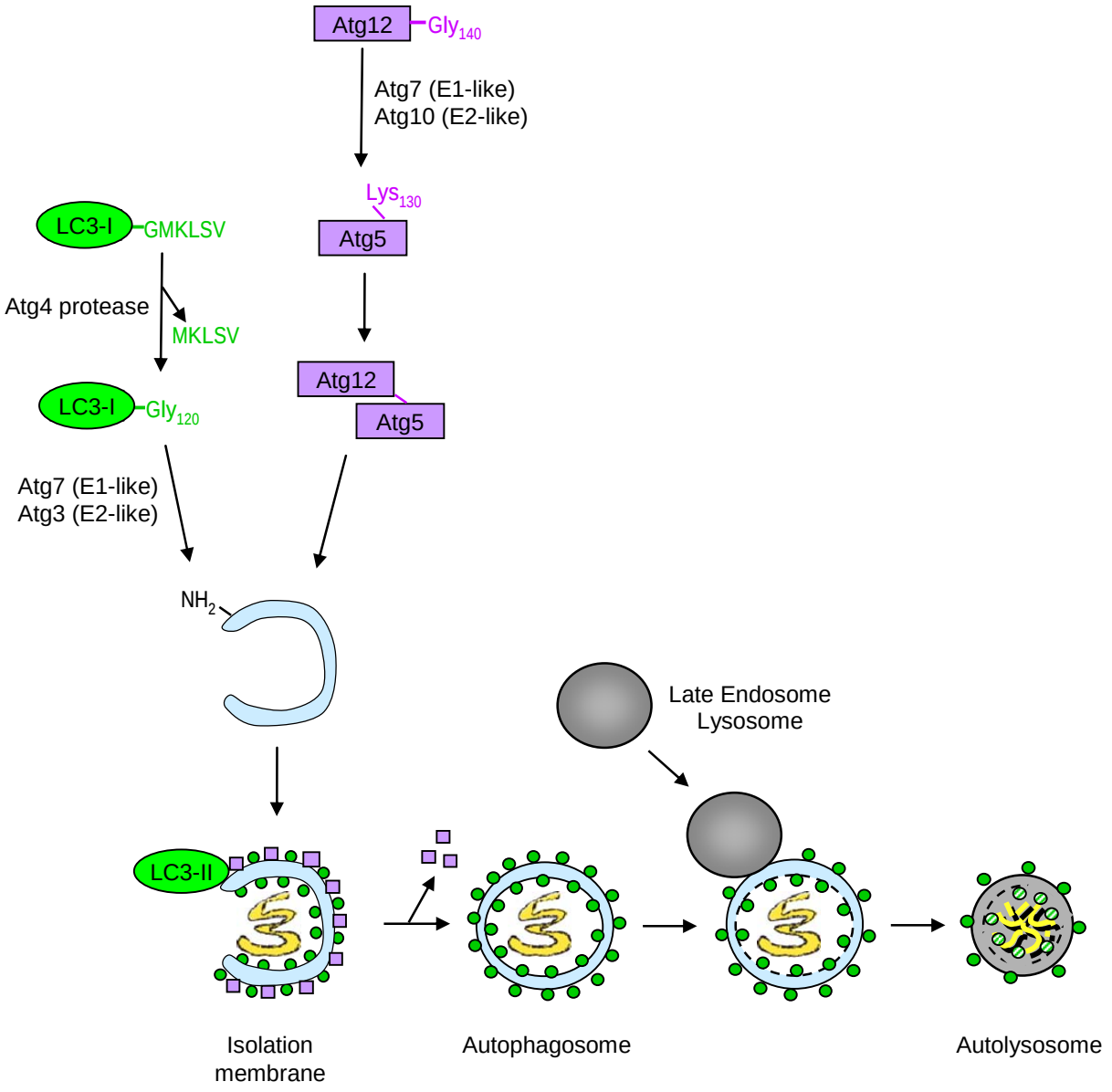
Atg12
Gly140
Atg7 (E1-like)
Atg10 (E2-like)
Lys130
Atg5
LC3-I
GMKLSV
Atg4 protease
MKLSV
LC3-I
Gly120
Atg12
Atg5
Atg7 (E1-like)
Atg3 (E2-like)
NH2
Late Endosome
Lysosome
LC3-II
Isolation membrane
Autophagosome
Autolysosome

In addition to these two ubiquitin-like protein conjugation systems, a number of signaling proteins have been identified to be involved in the regulation of autophagy: Class I PI3 kinase and TOR kinase suppress autophagy, while class III PI3 kinase and its binding partner beclin-1 activate autophagy [89-91]. The class III PI3K-beclin-1 complex seems to be an important signaling checkpoint in starvation-induced autophagy, since beclin$^{-/-}$ cells are unable to upregulate autophagy in response to starvation [92, 93]. Other regulators of the autophagic pathway are the eIF2α kinases GCN2, PERK and PKR [94]. In response to starvation, ER stress and viral infection, respectively, these kinases not only phosphorylate eIF2α to induce translational arrest, but they also upregulate autophagy, most likely via beclin-1 [95].

1.3.3 Autophagy as an innate immune response against bacteria and viruses

Recently it was appreciated that macroautophagy not only contributes to the turnover of cytoplasmic constituents, but also targets intracellular pathogens for degradation during innate immunity [96]. Bacteria and viruses have developed strategies to escape destruction via autophagy, indicating that this is an important mechanism of innate immunity [97].

After phagocytosis, successful bacterial pathogens either leave phagosomes for the cytosol, as is the case for *Listeria monocytogenes,* or stop maturation of phagosomes to acidic vesicles, as for *Mycobacterium tuberculosis*. Both cytosolic and phagosome-resident bacteria can then be targeted by macroautophagy [98]: *Listeria monocytogenes* escapes the phagosome with the help of the protein Listeriolysin O and subsequently replicates in the cytosol. However, when its protein synthesis is inhibited by

chloramphenicol, it is trapped by autophagosomes and is delivered for lysosomal destruction [99]. Similarly, when *Streptococcus pyogenes* manages to leave endosomes of nonphagocytic cells, it becomes enveloped in autophagosomes and the bacterial load decreases after lysosomal degradation [100]. Finally, *Shigella flexneri* lyses phagosome with its gene product IpaB and then prevents degradation via macroautophagy with another gene product IcsB [101]. Furthermore, autophagic degradation of pathogen-containing phagosomes has been reported for *Mycobacterium tuberculosis* (*Mtb*). *Mtb* is degraded in lysosomes after IFN-γ stimulation in macrophages. Recently it was suggested that the IFN-γ-induced guanosine triphosphatase LRG-47 participates in autophagosome formation and these autophagosomes target *Mtb*-containing phagosomes for lysosomal destruction [102, 103]. On the other hand, *Legionella pneumophila, Coxiella burnetii* and *Brucella abortus* all replicate inside autophagosomes, by slowing their maturation and fusion with lysosomes [104-107]. These examples demonstrate that cytosolic and phagosomal bacteria can be degraded via macroautophagy, but many microorganisms have developed strategies to avoid or subvert this innate immune mechanism.

Although several viruses enhance autophagy upon infection, its contribution to anti-viral innate immunity has been less clearly defined. Several single-stranded RNA and double-stranded DNA viruses seem to be sensitive to and subvert autophagy to their benefit [97, 108]. Two main steps in the autophagic process can be targeted by viruses: The generation and the degradation of autophagosomes. The ssRNA viruses poliovirus and mouse hepatitis virus (MHV) block degradation of autophagosomes and use them as scaffolds to assemble their RNA replication complexes [109-111]. Therefore, autophagosomes accumulate after infection with these viruses and stimulation of

autophagy increases viral yield, while inhibition of autophagosome formation decreases virus replication. In contrast, viruses that cannot make use of autophagosomes for their replication have developed strategies to block autophagosome formation and thus escape autophagic degradation. This has been demonstrated for the α- and γ-herpesviruses herpes simplex virus 1 (HSV-1) and Kaposi Sarcoma-associated herpesvirus (KSHV). HSV-1 encodes for an early antigen ICP34.5 that interacts with beclin-1 to inhibit PKR-induced autophagy [95]. KSHV encodes a viral Bcl-2 homologue that interacts with a different domain of beclin-1 and also inhibits autophagy [93]. If these viral escape mechanisms are eliminated or if beclin-1 is overexpressed, autophagy is induced and virus replication and virulence are impaired [93, 95, 112], suggesting that autophagy induction during viral infections might restrict virus replication within infected cells. The fact that viruses have developed effective strategies to prevent autophagy induction, indicates strong evolutionary pressure to escape this innate immune mechanism.

1.3.4 Methods for studying autophagy

The most important methods for studying autophagy include (a) morphological methods, (b) biochemical detection of autophagosomes and (c) inhibition of autophagy via silencing of specific Atg gene. For a long time, morphologic detection of autophagosomes by electron microcopy (EM) has been the only reliable method for monitoring autophagy [88]. Autophagy was first discovered using EM [113] and this method has remained an important tool for studying autophagy. In EM, autophagosomes appear as double membrane vesicles containing cytoplasmic material, while at later stages, they have a single membrane and contain cytoplasmic material at various stages

of degradation [114]. After fusion with endosomes, they may also contain endocytosed or phagocytosed material and it is sometimes difficult to distinguish the different types of autophagic and endocytic vesicles solely by morphology [115]. Immuno-electron microscopy using antibodies against autophagosome marker proteins is probably a more reliable method [84, 88]. Newer morphological methods for monitoring autophagy rely on immunofluorescence microscopy and the specific autophagosome marker protein Atg8/LC3. GFP-tagged LC3 has been used to visualize autophagosomes in cultured cells [68, 84, 102] and GFP-LC3 transgenic mice have been used to quantify constitutive and starvation-induced autophagy in murine tissues [68]. GFP-LC3 localization to autophagosomes can also be observed in real time by live cell imaging [116, 117].

Besides these morphological methods, a biochemical assay is now frequently used to detect and quantify autophagy. Autophagosome-coupled LC3 (LC3-II) and free cytosolic LC3 (LC3-I) migrate with different speed on an SDS-PAGE gel (apparent mobility: 16 and 18 kD, respectively). Consequently, anti-LC3 immunoblots usually gives two bands and the amount of LC3-II or the LC3-I/LC3-II ratio correlates with the number of autophagosomes [84, 88].

Other useful tools for studying autophagy are based on the Atg gene products Atg5, Atg7 and Atg12. The Atg12-Atg5 conjugate is essential for autophagosome formation and Atg7 is required for both Atg12 coupling to Atg5 and Atg8 coupling to phsophatidylethanolamine [82]. Gene targeting of either gene completely inhibits autophagy. Therefore, $Atg5^{-/-}$ or $Atg7^{-/-}$ cells or siRNAs to silence Atg5, Atg7 or Atg12 are important tools for studying autophagy. Inhibition of autophagy with pharmacologic drugs, for example 3-methyladenine (3-MA) [118], which inhibits the class III PI3K-

beclin-1 complex, is also frequently used. However, at higher inhibitor concentrations, the effects of 3-MA are not always specific for autophagy, as 3-MA also inhibits other cellular processes [88]. Therefore, an effect by 3-MA does not always implicate autophagy and results should always be confirmed by more specific Atg gene silencing.

1.4 $CD4^+$ T cell responses in viral and tumor immunity

1.4.1 Effector mechanisms of activated T cells

Antigen-specific T cells play an essential role in eradicating cells that express foreign or abnormal proteins. When T cells detect MHC-bound fragments derived from such proteins, they will be activated to perform specific effector functions – either target cell killing or activation of other components of the immune system [2].

T cells can kill target cells via two different mechanisms: The more rapid mechanism involves the release of the pore-forming protein perforin and proteases called granzymes, which enter through the pores and trigger programmed cell death [119, 120]. The alternative and more slower killing mechanism is via expression of cell surface-associated effector proteins of the TNF family, such as Fas ligand, TRAIL, TNF-α and –β [120]. These molecules can bind to TNF receptor family members on target cells and trigger apoptosis via these death receptors. Target cell killing is the main function of the $CD8^+$ T cells (CTLs). However, as discussed in the next paragraph, $CD4^+$ T cells can also contribute to the killing of infected or transformed cells.

Besides killing, the main effector function of T cells is the activation of other cell types of the immune system, and this function is mainly fulfilled by $CD4^+$ T cells. $CD4^+$

T cells are of two functional types: Th1 cells and Th2 cells [121]. Th1 cells secrete IFN-γ and other cytokines and can activate or kill MHC class II-positive target cells via the cell surface proteins CD40 ligand or Fas ligand, respectively. In addition, a subset of $CD4^+$ Th1 cells is capable of perforin mediated lysis. In contrast, Th2 cells secrete the B cell growth factors IL-4 and IL-5 and activate B cells via CD40 ligand-CD40 interaction to undergo Ig class switching and to become antibody-producing plasma cells.

1.4.2 The contributions of $CD4^+$ T cells to adaptive immunity

The capacity of $CD8^+$ T cells to expand rapidly and to lyse target cells directly has focused previous research efforts mainly on this arm of the adaptive immunity. More recently, however, the equally important contribution of $CD4^+$ T cells to cell-mediated immune responses against viruses and cancer has been appreciated [122-124]. Both direct and indirect $CD4^+$ T cell functions seem to be important in the immune control of malignancies and persistent infections [125, 126]: Direct functions of $CD4^+$ T cells include induction of apoptosis by TNF family members, such as FasL and TRAIL [127], and less frequently perforin/granzyme-mediated cytotoxicity [128-130]. Another direct function of $CD4^+$ T cells is the secretion of cytokines, mainly IFN-γ, which has proven to mediate resistance against viral infections [131, 132] and tumors [133]. Apart from these direct antiviral and cytolytic functions, the $CD4^+$ T cell compartment has been shown to be crucial for the development [134, 135] and maintenance [124, 136-140] of effective $CD8^+$ T cell responses. Therefore, for efficient vaccination against viruses and tumors, $CD4^+$ T cells should be stimulated alongside with $CD8^+$ T cells to allow for the induction of long-lasting $CD8^+$ T cell memory.

1.4.3 Examples of $CD4^+$ T cell responses to viral infections and tumors

$CD4^+$ T cells play a role in controlling both persistent viral infections, such as Epstein-Barr virus (EBV), cytomegalovirus (CMV), and human papillomavirus (HPV) [141] and acute viral infections, such as influenza A virus [142]. Interestingly, many of the predominant $CD4^+$ T cell antigens are localized in the cytoplasm or nucleus of infected cells. For example, the EBV nuclear antigen 1 (EBNA1) is the predominant antigen recognized by EBV-specific $CD4^+$ T cells during latent EBV infection, and nearly all healthy EBV carriers display strong $CD4^+$ T cell responses to this antigen [43, 143]. Two main $CD4^+$ T cell antigens of the high risk HPV type 16 are the viral oncoproteins E6 and E7, which are localized to the cytoplasm and nucleus, respectively [144, 145]. An example of an antigen that is recognized by $CD4^+$ T cells in an acute viral infection is the influenza A virus matrix protein M1, which mediates the transport of viral ribonucleoprotein out of the nucleus [146]. In addition to these viral antigens, different types of melanoma antigens (differentiation antigens, cancer-testis antigens and mutated self antigens) are recognized by melanoma-specific $CD4^+$ T cells [147, 148].

Even though the importance of $CD4^+$ T cells for effective antiviral and antitumor responses is now widely accepted, it is unclear how endogenously expressed viral and tumor antigens are presented onto MHC class II, and hence targeting strategies for this important MHC class II pathway remain elusive. One aim of this thesis project was to characterize the pathway for MHC class II presentation of endogenously expressed viral and tumor antigens and to targting antigens efficiently for MHC class II presentation, to elicit more comprehensive, $CD8^+$ and $CD4^+$ T cell-based immunity against viruses and tumors.

1.5 Epstein-Barr Virus

1.5.1 Epstein-Barr Virus (EBV), a ubiquitous human tumor virus

Epstein-Barr virus (EBV) is a human gamma herpesvirus that preferentially infects B lymphocytes and occasionally other cell types, such as epithelial cells [149]. The virus was originally visualized in Burkitt's lymphoma, a human B cell lymphoma, by Epstein, Achong and Barr in 1964 [150, 151]. When they examined Burkitt's lymphoma-derived cell lines by electron microscopy, these investigators discovered herpesvirus-like particles in a proportion of the cells, and thus discovered the first candidate for a human tumor virus.

EBV is one of the most highly growth transforming viruses known in any species [152]. When B cells are infected by EBV *in vitro*, the cells become immortalized and form permanently growing lymphoblastoid cell lines (LCLs) [153]. *In vivo*, the virus can give rise to a number of different B cell tumors, including Burkitt's lymphoma, nasopharyngeal carcinoma, Hodgkin's disease, post-transplant lymphoproliferative disease (PLD), and AIDS-associated non-Hodgkin's lymphoma as well as epithelial cell cancers, including nasopharyngeal carcinoma and gastric carcinoma [154]. Seroepidemiological studies have shown that more than 95% of the human adult population carry EBV as a lifelong asymptomatic infection [149]. However, despite its strong growth transforming capacity, the virus causes no disease in the vast majority of infected individuals, because a potent EBV-specific cytotoxic T cell response controls the infection and prevents the outgrowth of EBV-positive B cells [155]. Nevertheless, the virus cannot be completely eliminated from the hematopoetic system, but persists in the infected host in a quiescent state for life. Resting memory B cells that express no viral

gene products at the protein level are thought to be the site of EBV-persistence in the body [156]. The ubiquity and persistence of the virus are typical features of all herpes viruses [149].

1.5.2 Primary and persistent EBV infection

After saliva exchange with an infected individual, infectious virus can enter the nasopharyngeal lymphoid system via the tonsils [156]. Once in the lymphoid system, the virus infects naïve B cells and establishes a so-called latent infection. In the latency state, no lytic genes products are expressed and no viral particles are produced. Instead, of the nearly 100 genes encoded in the EBV genome, only a small set of so-called "latency genes" is expressed: six nuclear antigens (EBNA1, EBNA2, EBNA3A, EBNA3B, EBNA3C, and EBNA-LP), three transmembrane proteins (LMP1, LMP2A, and LMP2B) as well as non-translated RNAs, including EBER1 and 2 [BamH1 transcript, microRNAs and maybe more] [149] (Table 4). The combined actions of the latency proteins and the EBERs cause the previously resting B lymphocytes to enter the cell cycle, proliferate continuously and resist apoptosis.

Latently EBV-infected B cells can express four different genetic programs, which are characterized by the expression of specific viral latency genes [149] (Table 5). The so-called latency III program is characterized by the expression of all 11 latency gene products. This program, also referred to as "growth program" [156], activates resting B cells to become proliferating lymphoblasts, and can be observed in newly infected naïve B cells and in *in vitro*-generated lymphoblastoid cell lines (LCLs). In the latency II

Table 4: EBV latency genes and known functions (adapted from [149]).

Latency gene	Function	References
EBNA1	Binds to viral replication origin (oriP) and initiates viral episome replication before mitosis. Also anchors the viral episome to mitotic chromosomes to ensure segregation of the episome.	[157, 158]
EBNA2	Initiates transcription of other viral latency genes (EBNA1, LMP1, LMP2) and of cellular genes (CD23, CD21, c-myc).	[159, 160]
EBNA3A,B,C	EBNA3A and C abrogate cell cycle check points and drive B cells into continuous proliferation. EBNA3B is not essential for transformation	[161, 162]
EBNA-LP	Cooperates with EBNA2 and enhances its effects	[163]
LMP1	Mimics CD40 signalling and thereby rescues B cell from apoptosis (upregulates bcl-2). Also upregulates cellular adhesion molecules (ICAM1, LFA1, LFA3) and activation markers (CD21, CD23, CD40)	[156]
LMP2A,B	LMP2A mimics survival signal from the B cell receptor	[156]
EBER 1, 2	Increases oncogenesis in Burkitt's lymphoma cells (upregulates bcl-2). Antagonized interferon action.	[164, 165]
BamH1 transcripts and microRNAs	Functions not clearly characterized.	[149]

Abbreviations:
EBNA: EBV nuclear antigen, LMP: latent membrane protein, EBER: EBV-encoded RNA

Table 5: Different gene expression programs during latent EBV infection (adapted from [149]).

Gene expression program	Genes expressed	Examples
Latency III program	EBNA1, 2, 3A, 3B, 3C, LP LMP1, 2A, 2B, EBERs and other non-translated RNAs	Newly infected naïve B cells, posttransplant lymphoproliferative disease, LCLs
Latency II program	EBNA1, LMP1, 2A EBERs and other non-translated RNAs	Hodkin's lymphoma, nasopharyngeal carcinoma, nasal T cell lymphoma
Latency I program	EBNA1 EBERs and other non-translated RNAs	Burkitt's lymphoma
Latency 0 program	(EBNA1), (LMP2A) EBERs and other non-translated RNAs	Resting memory cells from peripheral blood of healthy EBV carriers

program, viral gene expression is restricted to EBNA1, LMP1, LMP2A and the non translated RNAs. This expression pattern is found in several EBV-associated malignancies, such as Hodgkin's lymphoma and nasopharyngeal carcinoma. The latency I expression pattern, which can be found in Burkitt's lymphoma cells, is characterized by the presence of a single viral protein, the nuclear antigen EBNA1. Because of its critical functions for the replication and maintenance of the viral DNA during cell division [157, 158], EBNA1 has to be maintained in all proliferating EBV-infected cells. The fourth pattern of latency, called latency 0, is found in resting memory B cells in the blood of healthy EBV carriers. Besides the non-translated RNAs, only EBNA1 and LMP2 are detected in a subset of these cells by RT-PCR [166, 167], suggesting that most memory cells express no EBV proteins. By downregulating the expression of all viral genes, EBV-infected memory cells avoid recognition by the immune system, and therefore provide a site for long-term EBV persistence in the body [156].

In a small fraction of EBV-infected memory B cells, reactivation from latent to lytic infection can occur upon cognate antigen encounter [149]. Accordingly, lytic EBV replication can be found in plasma cells of healthy virus carriers [168]. Thus, even long-term virus carriers continue to secrete low levels of infectious virus into the saliva and help to spread the virus among the human population.

1.5.3 T cell responses in persistent EBV infection

Despite the growth-transforming capacity of EBV, more than 95% of the adult population carry the virus for life without any symptoms. In healthy individuals, the outgrowth of EBV-infected B cells is prevented by a strong adaptive immune response [155]. The

importance of this immune control becomes apparent in immunocompromised hosts, such as immunosuppressed transplant patients or AIDS patients, who frequently develop B cell lymphomas [149].

Both $CD8^+$ and $CD4^+$ memory T cells provide long-term surveillance of EBV-infected B cells [149]. Most $CD8^+$ T cell responses target the EBNA3 proteins [169]. Less frequently, $CD8^+$ T cell responses against epitopes from LMP1 [170] and LMP2 [171] have been reported. Thus, EBV-infected B lymphocytes expressing the latency III expression pattern (Table 5) can be efficiently controlled by EBV-specific $CD8^+$ T cells. $CD4^+$ T cell responses are dominated by EBNA1-specific T cells, which have been identified in all healthy EBV carriers [43, 143]. When isolated from the peripheral blood of healthy donors, these T cells consistently recognize and kill HLA-matched EBV-transformed B cells, including Burkitt's lymphoma cell lines [43, 56]. Thus, EBNA1-specific $CD4^+$ T cells could explain, how latency I and II malignancies, such as Burkitt's and Hodgkin's lymphoma, are avoided in healthy EBV carriers. In these malignancies, EBNA1 is the main T cell target, since EBNA3 proteins are not expressed (Table 5). Thus, EBNA1-specific $CD4^+$ T cells could be the principal effectors in the surveillance of latency I and II expressing cells. EBNA1-specific $CD4^+$ T cells could also be important for the maintenance of an effective $CD8^+$ T cell memory (see chapter 1.4.2).

1.5.4 EBNA1 and its processing in B cells

EBNA1 was originally identified as an EBV nuclear antigen that is present in all EBV-infected B cells [172]. It is localized in the nucleus, where it is responsible for replication and maintenance of the EBV genome in the infected cell [173]. Like all nuclear proteins,

EBNA1 is synthesized at cytosolic ribosomes and is subsequently imported into the nucleus by virtue of its nuclear localization sequence (NLS). A unique feature of the EBNA1 protein is the long, irregular glycine-alanine (GA) repeat domain that stretches from amino acid 90 to 327. The repeat was shown to prevent EBNA1 mRNA translation [174] as well as EBNA1 protein degradation by the ubiquitin-proteasome system [175] in *cis* and thus strongly decreases MHC class I presentation of EBNA1. Presumably, only truncated EBNA1 DRiPs (defective ribosomal products) immediately after their synthesis can be processed by the proteasome and give rise to some $CD8^+$ T cell epitopes [176, 177]. Thus, the virus has evolved a unique mechanism to specifically suppress $CD8^+$ T cell recognition of an essential viral protein [178].

In contrast to the weak MHC class I presentation, EBNA1 is consistently presented on MHC class II molecules of infected B cells, and hence can be targeted by EBNA1-specific $CD4^+$ T cells [43, 143]. Münz et al. demonstrated that MHC class II presentation of EBNA1 is not due to the uptake of dying EBNA1-expressing B cells (classical exogenous pathway), but to the direct processing of the protein in the infected cell (non-classical endogenous pathway) [43]. Even though endogenous MHC class II presentation has been described for other cytosolic and nuclear antigens (see chapter 1.2.6), its molecular basis is not very well understood so far.

1.6 Influenza A virus

1.6.1 Influenza A virus (IAV) and its life cycle

Influenza is a contagious, acute respiratory disease caused by infection of respiratory tract epithelial cells by influenza A virus (IAV). In the industrialized world, it is the leading viral cause of mortality and it remains a major public health concern due to its potential to cause devastating pandemics [179].

IAV is an enveloped single-stranded RNA virus that belongs to the family of *Orthomyxoviridae* [180]. Its genome is composed of eight single-stranded RNA segments of negative polarity, encoding 11 proteins (Fig. 6A). These RNA segments are always tightly associated with viral proteins, forming ribonucleoprotein (RNP) complexes [181]. The main protein components of RNPs are nucleoprotein (NP) and the trimeric polymerase complex (PB1, PB2, PA). The RNP core is surrounded by the viral matrix protein (MP1 or M_1), which associates with RNPs and the lipid envelope (Fig. 6A). Three integral membrane proteins are inserted into the lipid bilayer: Haemagglutinin (HA), neuraminidase (NA) and small amounts of the M_2 ion channel.

The influenza life cycle is depicted in Fig. 6B. During entry into cells, HA binds to sialic acid residues on cell surface glycoproteins or glycolipids and mediates endocytosis of viral particles. Acidification of endosomes results in a conformational change in HA, leading to fusion of the viral envelope with the endosomal membrane [182] and release of viral RNPs into the host cell cytoplasm. M_2 ion channel activity is essential for this uncoating process, as it permits the flow of ions into the virion core, leading to the disruption of RNP-MP1 interactions [183]. Once RNPs are in the

Figure 6: Influenza A virus structure and life cycle.

A: Schematic diagram of the structure of the influenza A virus particle (adapted from). IAV is an enveloped virus whose genome consists of eight different segments of single-stranded RNA. The genomic segments encode for a total of 11 proteins. The major structural proteins are the matrix protein M1 (green), which underlies the lipid envelope (grey), and the transmembrane glycoproteins haemagglutinin (HA) and neuraminidase (NA), which are inserted into the lipid bilayer.

B: Schematic diagram of the life cycle of influenza A virus (adapted from [180]).

A

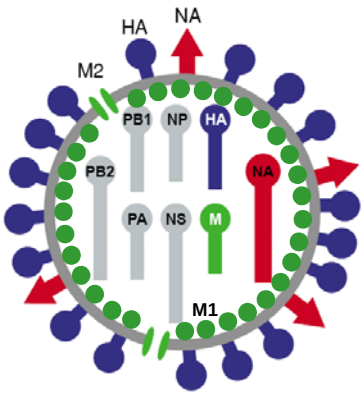

Influenza A

B

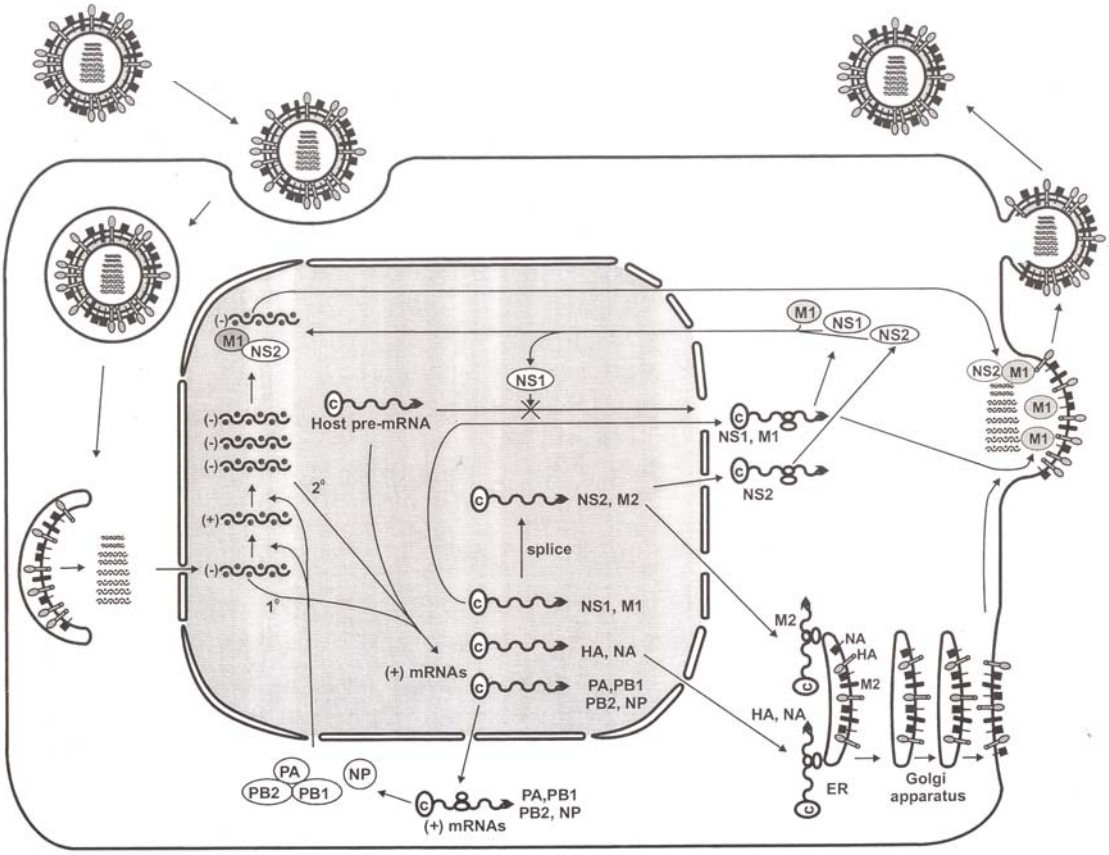

cytoplasm, they get imported into the nucleus for transcription and replication [184]. MP1 also enters the nucleus, where is associates with newly generated RNPs and mediates their export from the nucleus [185]. Newly synthesized positive-stranded mRNAs are also exported into the cytoplasm for translation. The integral membrane proteins HA, NA and M_2 are cotranslationally synthesized into the ER and then are transported to the plasma membrane for virion assembly and budding [180].

1.6.2 Adaptive immune responses to influenza A virus

Both humoral and cellular immune responses are important for protective immunity to IAV. Neutralizing antibodies are mainly directed against the viral envelope proteins HA and NA and therefore they are usually only effective against homologous virus strains, but not heterologous virus strains with serologically distinct glycoproteins [186]. In contrast to antibodies, T cells can recognize internal virus proteins (e.g. NP, MP1, NS2, PA, PB1 and PB1-F2), which are more conserved among heterologous virus strains. Both $CD8^+$ and $CD4^+$ T cell responses are stimulated by IAV [142, 186]. Priming and expansion of influenza-specific $CD8^+$ T cells occur in draining mediastinal lymph nodes 3-4 days after infection [187]. 5-7 days after infection, they appear in the airway epithelium and secrete antiviral cytokines and lyse influenza-infected target cells [188]. Secondary influenza-specific CTL responses arise about 2 days faster than the primary response and have a greatly increased level of activity. Influenza-specific $CD4^+$ T cell responses are much less well characterized than their $CD8^+$ counterparts. Studies in $CD4^+$ T cell-deficient mice have shown that influenza-specific $CD4^+$ T cells seem to play an important role for $CD8^+$ memory T cell expansion and function [189], although this

defect was mainly seen in the draining lymph node and spleen and not in the lung [190]. In addition, it has been suggested that $CD4^+$ T cells have direct effector functions against IAV and may contribute to immunopathology [142].

1.6.3 Innate immune mechanisms to restrict influenza A virus

In addition to the above described adaptive immune responses, innate defense mechanisms, such as the production of type I IFNs, can restrict virus replication [191]. In virus-infected cells, toll-like receptor (TLR) family members (TLR 7, 8 and 3) and cytoplasmic RNA helicases (RIG-I and mda-5) can sense viral dsRNA or ssRNA and induce the expression of IFN-α and –β [192]. These in turn then stimulate the expression of more than 100 IFN-stimulated genes (ISGs), whose concerted action leads to the generation of an antiviral state [191]. Among the best characterized ISGs is protein kinase R (PKR), whose activity results in an inhibition of protein translational and in autophagy induction (see chapter 1.3.2).

It is not surprising that many viruses, including IAV, have evolved ways to down-modulate the IFN response. In the case of IAV, the viral non-structural protein 1 (NS1) binds viral dsRNA and thus prevents its recognition by cellular sensors [179, 193]. In addition, IAV activates a cellular inhibitor of PKR, p58IPK, and thus inactivates one of the most important ISGs [194]. In the face of these effective anti-IFN mechanisms, it is conceivable that host cells have evolved other innate immune mechanisms to restrict IAV replication at early stages, before the adaptive immune response can take over.

Chapter 2: Material and methods

2.1 Reagents

2.1.1 Inhibitors, synthetic peptides and cytokines

Ammonium chloride, chloroquine, 3-methyladenine, E64, Leupeptin and Pepstatin A were purchased from Sigma and lactacystin was from Calbiochem. Peptides $EBNA1_{481-501}$, $EBNA1_{514-527}$ and $EBNA3A_{325-333}$ were synthesized by the Fmoc solid phase method on a peptide synthesizer (model 432A, Applied Biosystems). Peptide purity and identity were confirmed by reverse phase HPLC (System Gold, Beckman) and mass spectrometry (LD-TOF G2025A, Hewlett-Packard). Lyophilized peptides were dissolved in 1% DMSO to a concentration of 1 mM. The MP1 peptide mix was purchased from the Proteomics Resource Center of the Rockefeller University. Lyophilized MP1 peptides were dissolved in 10% DMSO to a concentration of 1 mM. Recombinant human IL-4 was from Peprotech and recombinant human GMCSF was "Leukine" from Berlex. IL-1β, IL-6 and TNF-α were from R&D Systems. Recombinant human IFN-γ was from ProSpec-Tany TechnoGene LTD and was used at 200 U/ml to induce MHC class II expression. Recombinant human IFN-α-2b was from Schering Corporation.

2.1.2 Antibodies

Anti-LC3 antiserum was generated by immunizing two rabbits with the N-terminal peptide $LC3_{1-15}$ (MPSEKTFKQRRTFEQR) conjugated to KLH carrier protein (Cocalico Biologicals). Animals were boosted 5 times (2, 3, 7, 11 and 15 weeks after initial inoculation) and then sacrificed to obtain terminal bleeds. Antiserum collected from one

rabbit showed good LC3 reactivity by ELISA and Western blot and was used for Western blots at a dilution of 1:2000. All other antibodies are listed in Table 6.

Table 6: List of antibodies.

1° antibodies	Dilution	Source
Rat anti-EBNA1ΔGA (clone 1H4), monoclonal	1:200 (WB)	[195]
Mouse anti-EBNA1$_{408-641}$ (clone 5F12), monoclonal	1:10 (IF) 1:50 (EM)	[196]
Mouse anti-HLA-A,B,C (clone w6/32), monoclonal	1:10	ATCC
Mouse anti-HLA-DR,DP,DQ (clone IVA12), monocl.	1:10	ATCC
Mouse anti-HLA-DM (clone MaP-DM1), monoclonal	1:400 (IF)	BD Pharmingen
Mouse anti-transferrin receptor (clone DF1513), monocl.	1:800 (IF)	Sigma
Mouse anti-actin (clone AC-40), monoclonal	1:2500 (WB)	Sigma
Mouse anti-LAMP1 (clone H4A3), monoclonal	1:400 (IF)	Southern Biotech
Mouse anti-LAMP2 (clone H4B4), monoclonal	1:200 (IF)	Southern Biotech
Rabbit anti-EBNA3A, polyclonal	1:1000 (WB)	Oncogene
Rabbit anti-GFP, polyclonal	1:50 (EM)	Molecular Probes
Rabbit anti-HLA-DR (C6861), polyclonal	1:50 (EM)	Peter Cresswell
Rabbit anti-influenza A-MP1 (7648), polyclonal	1:1000 (IF) 1:2000 (WB)	[184]
Goat anti-EEA1, polyclonal	1:300 (IF)	Santa Cruz Biotech

2° (HRP or biotin-conjugated) antibodies	Dilution	Source
Goat anti-mouse-IgG-HRP	1:10,000 (WB)	BioRad
Goat anti-rabbit IgG-HRP	1:50,000 (WB)	Jackson ImmunoRes
Goat anti-rat IgG-HRP	1:1000 (WB)	Amersham
Goat anti-mouse IgG-biotin	1:300 (EM)	Hercules

2° (Fluorochrome-conjugated) antibodies	Dilution	Source
Mouse anti-HLA-DR-FITC (clone TÜ36), monoclonal	1:20 (FACS)	BD PharMingen
Mouse anti-human CD4-PE, monoclonal	1:20 (FACS)	BD PharMingen
Mouse anti-human CD8-PE, monoclonal	1:120 (FACS)	BD PharMingen
Donkey anti-mouse IgG-Rhodamine Red-X, F(ab)$_2$	1:300 (IF)	Jackson ImmunoRes
Donkey anti-rabbit IgG-Rhodamine Red-X, F(ab)$_2$	1:300 (IF)	Jackson ImmunoRes
Donkey anti-goat IgG-Rhodamine Red-X, F(ab)$_2$	1:300 (IF)	Jackson ImmunoRes

2.2 Cell lines and primary cells

2.2.1 Cell lines

A variety of epithelial and B cell lines were used in this study. All epithelial cell lines were routinely cultured in DMEM with 10% fetal calf serum (FCS, Sigma), 2 mM glutamine, 110 μg/ml sodium pyruvate and 2 μg/ml gentamycin, except MLE-12, which was cultured in a 50:50 mix of DMEM:Ham's F12, supplemented with 2% FCS, 5 μg/ml insulin, 10 μg/ml transferrin, 30 mM sodium selenite, 10 nM hydrocortisone, 10 nM beta-estradiol, 2 mM glutamine and 2 μg/ml gentamycin. Epithelial cell monolayers were detached by one wash in PBS/0.5 mM EDTA followed by incubation in 0.05% trypsin/0.53 mM EDTA (Gibco). B cell lines and hybridomas were maintained as suspension cultures in RPMI-1640 medium with 10% FCS, 2 mM glutamine and 2 μg/ml gentamycin. All cell lines are listed in Table 7.

2.2.2 PBMC isolation and preparation of monocytes and dendritic cells (DCs)

Human peripheral blood mononuclear cells (PBMCs) were isolated from leukocyte concentrates (buffy coats) from the New York Blood Center or blood donations from healthy lab donors, which provided informed consent for this Rockefeller University Internal Review board approved study. PBMCs were isolated by density gradient centrifugation on Ficoll-Paque Plus (GE Healthcare). $CD14^+$ monocytes/macrophages were isolated by positive magnetic cell separation (MACS) using anti-CD14 MicroBeads (Miltenyi Biotec). To generate monocyte-derived DCs, $3x10^6$ $CD14^+$ cells were plated into each well of a 6-well plate in 3ml of RPMI-1640 + 1% single-donor plasma +

Table 7: List of cell lines.

Name of cell line	Type of cell line	Source
HaCat	Human keratinocyte	Rajiv Khanna, Brisbane, Australia
MDAMC	Human breast carcinoma	Irene Joab, Paris, France
HeLa	Human cervical carcinoma	ATCC
293	Human kidney epithelium	ATCC
A549	Human lung carcinoma	Thomas Moran, New York, U.S.
MLE-12	Mouse lung epithelium	Arnaud Didierlaurent, London, UK
MDCK	Canine kidney epithelium	Peter Palese, New York, U.S.
SL-LCL	EBV-transformed B lymphoblastoid cell line (B-LCL)	Generated by culturing PBMCs of a healthy donor with supernatant of the marmoset cell line B95.8
MS-LCL	EBV-transformed B-LCL	Generated as described above
CM-LCL	EBV-transformed B-LCL	Generated as described above
BM-LCL	EBV-transformed B-LCL	Rajiv Khanna, Brisbane, Australia
LG2	EBV-transformed B-LCL	ATCC [197]
LCL721.221	MHC class I-negative EBV-transformed B-LCL	ATCC
Ag876	EBV-positive Burkitt's lymphoma	Rajiv Khanna, Brisbane, Australia
RPMI6666	EBV-positive Hodgkin's lymphoma	ATCC
L591	EBV-positive Hodgkin's lymphoma	Martina Vockerodt and Dieter Kube, Göttingen, Germany
L428	EBV-negative Hodgkin's lymphoma	Martina Vockerodt and Dieter Kube, Göttingen, Germany [198]
L428E1PC5	EBNA1-transfected L428	Martina Vockerodt and Dieter Kube, Göttingen, Germany [198]
IVA12	Mouse hybridoma (anti-HLA-DR,DP,DQ)	ATCC
W6/32	Mouse hybridoma (anti-HLA-A,B,C)	ATCC
5F12	Mouse hybridoma (anti-EBNA1)	Jen-Yang Chen, Teipei, Taiwan [196]

glutamine + gentamycin + recombinant human IL-4 (rhIL-4, 500 U/ml, Peprotech) and rhGMCSF (1000 U/ml, "Leukine" from Berlex). rhIL-4 and rhGMCSF were added again on day 2 and 4 and floating immature DCs were collected on day 5. For maturation, immature DCs were transferred to new plates on day 5 and half of the medium was replaced with fresh medium containing proinflammatory cytokines [IL-1β (10 ng/ml), IL-6 (1000 U/ml), TNF-α (10 ng/ml) from R&D Systems, and PGE_2 (1 μg/ml, Sigma)] or 200 ng/ml lipopolysaccharide (LPS, Sigma). For lentiviral transduction of DCs, $CD14^+$ monocytes were infected with lentivirus at an MOI of 10 on day 1 after isolation, in the presence of 8 μg/ml polybrene (Sigma), rhIL-4 and rhGM-CSF and immature/mature DCs were generated as described above.

2.2.3 EBNA1- and EBNA3A-specific T cell clones

The EBNA1-specific $CD4^+$ T cell clones A4.E116 and RJD.79 were generated as described in [56] and [199]. Briefly, EBNA1-specific $CD4^+$ T cell lines were obtained after stimulation of MACS-purified $CD4^+$ T cells with irradiated autologous vvEBNA1ΔGA-infected or $EBNA1_{514-527}$ peptide-pulsed autologous DCs for one week and one week restimulation with irradiated autologous rEBNA1-loaded DCs. The EBNA3A-specific $CD8^+$ T cell clone MS.B11 was derived from an EBNA3A-specific T cell line, which was obtained from an HLA-$B8^+$ donor by two weeks of stimulation with the autologous LCL, followed by magnetic separation with $EBNA3A_{325-333}$/HLA-B8 tetramer-PE and αPE-MACS beads (Miltenyi Biotec). T cells were cloned by limiting dilution at 10, 1, or 0.3 T cells/well and expanded in RPMI-1640 + 8% PHS + 150 U/ml rhIL-2 (Chiron) + 1 μg/ml PHA-L (Sigma) + glutamine + gentamycin. 10^5 irradiated

PBMCs/well and 10^4 irradiated LCLs/well were added as feeder cells. After 14 days, expanded cells were tested in split-well IFNγ–ELISPOT assays for peptide specificity and MHC-restriction and specific clones were expanded under the same conditions [200]. The EBNA1-specific $CD4^+$ T cell clone P3-B7 was a gift from Drs. Kui Shin Voo and Rong-Fu Wang, Houston, TX [176]. A4.E116 recognizes the peptide $EBNA1_{514-527}$ restricted by HLA-DR1. RJD.79 specifically recognizes peptide $EBNA1_{481-501}$ in the context of HLA-DQ2/3. P3-B7 specifically recognizes peptide $EBNA1_{519-532}$ in the context of HLA-DP3. MS.B11 recognizes peptide $EBNA3A_{325-333}$ bound to HLA-B8 and the QIMR-WIL EBV strain transformed HLA-$B8^+$ LCL BM-LCL. Peptides were pulsed on target cells at 1-10 μM and 37°C for 1h in RPMI, followed by two washes.

2.2.4 Influenza A virus matrix protein (MP1)-specific T cell clones

The MP1-specific $CD4^+$ T cell clones 9.26, 10.9, 11.46 and the MP1-specific $CD8^+$ T cell clone 9.2 were generated as described in [199]. Briefly, CD14-negative PBMCs were stimulated with autologous mature DCs electroporated with in vitro transcribed influenza MP1-RNA, a gift from Irina Tcherepanova, Durham, NC (PBMC:DC ratio = 30:1, medium: RPMI-1640 with 5% human serum + glutamine + gentamycin). DCs were electroporated with 10 μg RNA in Opti-MEM at 300 V and 150 μF with a BioRad Gene Pulser plus Capacitance Extender (BioRad). On day 8 of PBMC/DC coculture, the stimulation was repeated and 10 U/ml IL-2 were added to enhance T cell survival. On day 21, the surviving cells were cloned by limiting dilution as described above for the EBNA1-specific T cell clones. On day 40, expanded cells were tested in split-well IFNγ ELISPOT assays for recognition of an MP1 peptide mix (64 15-mer peptides overlapping

by 10 amino acids) and the HLA-A2 immunodominant epitope $MP1_{58-66}$ (GILGFVFTL). Clones 9.26 and 10.9 are specific for the epitope $MP1_{62-72}$ and clone 11.46 is specific for $MP1_{103-113}$. The $CD8^+$ T cell clone 9.2 specifically recognizes $MP1_{58-66}$ bound to HLA-A2.

2.3 Experimental procedures

2.3.1 Lysate preparation, SDS-PAGE and immunoblotting

Cells were lysed in ice cold lysis buffer (50 mM Tris-HCl pH 8.0, 140 mM NaCl, 1.5 mM $MgCl_2$, 0.5% NP-40 with Complete protease inhibitor cocktail from Roche) for 5 min on ice (about 10^6 cells/200 µl). Whole cells and cell debris were pelleted by low speed centrifugation (400 g, 3 min) and cleared supernatants were transferred to a new tube. Protein concentration was determined by BCA protein assay (Pierce). Samples were boiled for 5 min in the presence of 4x SDS-PAGE-loading buffer (250 mM Tris-HCl pH 6.8, 40% glycerol, 8% SDS, 0.57 M β-mercaptoethanol, 0.12% bromophenol blue). Equal amounts of protein were run on 11 or 12% SDS-PAGE gels and transferred onto a PVDF membrane (Hybond-P, Amersham Biosciences). Primary antibodies were visualized with HRP-conjugated goat anti-rabbit or anti-mouse IgG and the ECL plus detection system (Amersham Biosciences).

2.3.2 Immunofluorescence (IF) staining of EBNA1

The EBV-transformed B lymphocyte cell line SL-LCL was washed in RPMI, left to sediment on poly-lysine treated printed-well slides (Carlson Scientific) for 30 minutes in

RPMI at 37°C and fixed in 4% paraformaldehyde/PBS/0.1% saponin (Sigma Aldrich) for 20 minutes at 4°C. The cells were then washed three times with blocking buffer from the TSA amplification kit (NEN Life Sciences). For EBNA1 detection, the cells were blocked for 30 minutes at room temperature with blocking buffer and incubated with the 1H4 or 5F12 monoclonal antibodies in RPMI containing 0.1% saponin and 5% normal goat serum for two hours at 4°C. After three blocking buffer washes, the cells were incubated with HRP-conjugated goat anti-rat or goat anti-mouse antibody in RPMI containing 0.1% saponin, for two hours at 4°C. The Cyanin-3 TSA amplification kit (NEN Life Sciences) was used according to the manufacturer's instructions. After labeling, all cells were washed three times and incubated for one minute with DAPI (Sigma). After three washes the cells were mounted using Aqua Polymount (Polysciences). The slides were analyzed using a fluorescence wide-field microscope (Olympus). Pictures were taken with an Olympus digital camera and pictures were processed with Metamorph software (Universal Imaging Corporation).

2.3.3 Subcellular fractionation

Subcellular fractionation was performed as previously described [201]. 1-3x 10^7 L428E1PC5 or 10^8 LG2 cells were washed three times in cold PBS before resuspension in 10 ml of ice cold homogenization buffer (10 mM Tris-HCl pH 7.4, 250 mM sucrose, 1 mM DTT, 1 mM EDTA, 30 μg/ml DNase, 0.1 mM PMSF, 1 μg/ml Leupeptin, 1 μg/ml Pepstatin A) and homogenization in a 15 ml Dounce homogenizer. Whole cells, cell debris, and nuclei were pelleted by two low speed spins (3,000 g, 10 min). Microsomes and mitochondria were pelleted by a subsequent high speed spin (100,000 g, 1h). Pellets

were resuspended in 1 ml homogenization buffer and were loaded on top of a two-step sucrose gradient (2M, 0.5 M). After centrifugation at 100,000 g for 1 h, microsomes were collected from the interphase. Aliquots were taken from all fractions and were analyzed by SDS-PAGE/immunoblotting antibodies specific for EBNA1, EBNA3A and LAMP1.

2.3.4 Electron miscroscopy of EBNA1-transfected cells

L428 Hodgkin's lymphoma cells, transfected with full-length EBNA1, were used for these studies. The cells were first synchronized with medium containing 100 nM colchicine for 48 hours. After washing, lysosomal acidification was blocked in 50 μM chloroquine-containing medium or medium alone, for another 48 hours. Then the cells were prepared for electron microscopy: Cells were plated on Alcian Blue coated petri dishes, fixed in PLP fixative (periodate-lysine-paraformaldehyde fixative [202], and permeabilized in 0.01% Saponin/0.1% BSA/PBS (Buffer A). For the EBNA1 and isotype control staining, the 5F12 anti-EBNA1 antibody or the isotype control antibody was diluted 1/50, goat anti-mouse-biotin 1/300, and neutravidin-HRP (Molecular Probes), in buffer A. After another fixation step in 0.5% glutaraldehyde, stable DAB was applied for 10 minutes, and the cells were postfixed and stained in reduced Osmium tetroxide [1% OsO4, 1%(K4Fe(CN)6]. Then the cells were dehydrated in a graded series of ethanol washes (70%, 95%, 100%), and removed from the petri dishes by adding propylene oxide and gently pipeting. After rinsing the cells several times in propylene oxide to remove dissolved plastic from the culture dishes, the cells were resuspended in Embed (Electron Microscopy Sciences), microfuged into a pellet in the resin and allowed to polymerize in a 60° oven for 48 hours. Thin sections were cut in an Ultracut E and viewed and

photographed at 80kV in a JEOL100CXII electron microscope. The morphology studies were carried out as follows: Cells were fixed in 2.5% glutaraldehyde fixative and microfuged into a pellet. After postfixing in 1% OsO4 on ice and block staining in 0.5% uranyl acetate, cells were dehydrated and processed into Embed as stated above. Sections were post-stained with uranyl acetate and lead before viewing.

2.3.5 IFN-γ ELISPOT assay

Enzyme-linked immunospot (ELISPOT) assays for IFN-γ-secreting cells were performed as described previously [203]. Briefly, MAHA S45 plates (Millipore) were coated with anti-IFN-γ-antibody 1-D1K (Mabtech) overnight at 4°C. Plates were blocked with RPMI + 5% pooled human serum. Afterwards, 10^5 T cell clones and $5x10^4$ stimulator B cells were added per well and incubated overnight. Then plates were incubated with biotinylated anti-IFN-γ-antibody 7-B6-1 (Mabtech). Afterwards, preassembled avidin-peroxidase complexes (Vectastain ABC kit, Vector Laboratories) were added. Spots were developed by addition of stable DAB (Research Genetics). Plates were washed three times with water and air-dried. SFCs (spot forming cells) were counted using a stereomicroscope (mean counts of duplicates).

2.3.6 Flow cytometry assays

MHC class I and II surface levels on T cell targets were measured by staining cells with IVA12 or w6/32 hybridoma supernatants and AlexaFluor488-conjugated rabbit anti-mouse IgG (Invitrogen-Molecular Probes). T cell clones were analyzed for CD4/CD8 expression by staining with anti-CD4-PE and anti-CD8-PE (BD Pharmingen). Cell

viability was analyzed by staining cells with Annexin-V-PE for 10 min in Annexin-V-staining buffer (BD Pharmingen) and the addition of 7-AAD (BD Pharmingen) directly before flow cytometry. Cells were analyzed on a FACScalibur instrument (Becton-Dickinson).

2.3.7 siRNA-mediated gene silencing

All siRNAs were a gift of Markus Landthaler and Thomas Tuschl, New York, except *lamin A/C*-specific siRNAs, which were purchased from Dharmacon. siRNA duplexes (20 or 100 μM) were prepared by heating sense and antisense oligos for 1 min at 90ºC in siRNA-annealing buffer (Dharmacon), followed by 1 h incubation at 37ºC. siRNA duplexes were stored in aliquots at -80ºC. For delivery of siRNAs into B-LCLs, cells were washed in serum-free Opti-MEM medium and $5x10^6$ cells in 300 μl Opti-MEM in a 2 mm gene pulser cuvette were electroporated with 10 μM siRNA at 300 V and 150 μF using a Biorad gene pulser II. Cells were used for T cell stimulation 4-5 days after the knockdown, to allow for turnover of preexisting MHC class II-peptide complexes. For delivery of siRNAs into epithelial cell lines, siRNAs were transfected with lipofectamine 2000 (Invitrogen), using 30 pmol siRNA + 1.5 μl lipofectamine/well in a 24-well format. Effect of knockdown was analyzed after 2-3 days. siRNA sequences are listed in Table 8.

Table 8: List of 21-nt siRNA oligos

Name	Sequence
Atg12.1 sense	5'-GUGGGCAGUAGAGCGAACAUdT-3'
Atg12.1 antisense	5'-UCAUGUAGUAGCAAGUUGAUdT-3'
Atg12.2 sense	5'-UCAACUUGCUACUACAUGAUdT-3'
Atg12.2 antisense	5'-UCAUGUAGUAGCAAGUUGAUdT-3'
GFP sense	5'-CUUGAAGAAGUCGUGCUGCUdT-3'
GFP antisense	5'-GCAGCACGACUUCUUCAAGUdT-3'
Lamin A/C sense	5'-CUGGACUUCCAGAAGAACAdTdT-3'
Lamin A/C antisense	5'-UGUUCUUCUGGAAGUCCAGdTdT-3'
Firefly luciferase sense	5'-CGUACGCGGAAUACUUCGAdTdT-3'
Firefly luciferase antisense	5'-UCGAAGUAUUCCGCGUACGdTdT-3'

2.3.8 RT-PCR

2-4 days after siRNA delivery into B-LCLs, total RNA was isolated using the RNeasy mini kit (Qiagen) and reverse transcription and PCR was carried out by using the OneStep RT-PCR kit (Qiagen). Different cycle numbers were used to amplify the PCR product and the lowest cycle number for which a band was detectable on an agarose gel was used to quantify the mRNA level.

2.3.9 Generation of expression plasmids and lentiviral constructs

The cDNA of human MAP1LC3B sequence (NM_022818) was PCR-amplified from a human B-LCL by RT-PCR with gene specific primers and cloned into the multiple cloning site of the mammalian expression vector pEGFP-C2 (Clontech). The cDNA of Influenza A/WSN/33 matrix protein 1 (MP1) was PCR-amplified from the

pCAGGS/MCS-MP1 vector (a gift from Peter Palese, New York) with or without a stop codon at the 3' end. The PCR products then were inserted into the pEGFP-LC3 vector in place of the EGFP sequence to obtain MP1-LC3 fusion constructs. For lentiviral constructs, the EGFP-LC3, MP1-LC3 or MP1Stop-LC3 sequences were subcloned into the lentiviral vector pHR-SIN-CSGWΔNotI (a gift from Jeremy Luban, Bellinzona, Switzerland). For production of lentiviral particles, lentiviral vectors were co-transfected with the helper plasmids pCMVΔR8.91 and pMDG into 293T cells by calcium phosphate transfection. Culture supernatants containing recombinant viral particles were harvested on day 1, 2 and 3 after transfection, filtered through a 0.45 μm filter and frozen at –80ºC. For lentiviral transduction of cells, cells were infected with an MOI of 10-40.

2.3.10 Immunocytochemistry and confocal microscopy

Epithelial cells were grown on microscopy cover glasses in 24 well plates overnight, whereas B cells or dendritic cells were plated onto polylysine-coated cover glasses immediately before the staining procedure. Cells were fixed in 3% paraformaldehyde in PBS for 15 min and permeabilized in 0.1% Triton X-100 in PBS for 5 min. Cells were blocked for 30 min in blocking buffer (from Perkin Elmer's TSA kit) + 0.1% saponin. Primary and secondary antibodies were applied in blocking buffer + 0.1% saponin + 5% normal donkey serum for 30-60 min, followed by three 5 min-washes in PBS + 0.1% saponin. Finally, cells were stained with DAPI nucleic acid stain (0.5 μg/ml, Invitrogen-Molecular Probes) for 1 min and cover glasses were mounted onto microscope slides using Aqua Polymount (Polysciences) or Prolong Gold antifade reagent (Invitrogen-Molecular Probes). All steps were carried out at room temperature. Cells were analyzed

either on an Olympus wide-field microscope with a 60x or 100x/1.4 N.A. oil immersion lens and pictures were processed with the Metamorph Software (Universal Imaging Corporation) or on an inverted LSM 510 laser scanning confocal microscope (Zeiss Axiovert 200) with a 63 or 100x/1.4 N.A. oil immersion lens using a pinhole diameter of 1 Airy unit. Pictures were taken with the LSM 510 confocal software (Zeiss). Colocalization of markers was quantified using the profile tool of the LSM 510 software. The number of double-positive vesicles compared to the total number of red vesicles was determined in 10-15 double-positive cells/condition.

2.3.11 Immuno-electron microscopy analysis of MHC class II loading compartments

MDAMC cells stably transfected with GFP-LC3 were fixed for 1h at RT with 4% paraformaldehyde (PFA, Electron Microscopy Sciences) in 0.25 M Hepes, pH 7.4, followed by overnight fixation at 4°C in 8% PFA/Hepes. Cells were embedded in 5% gelatin in PBS, small pieces of gelatin pellets were infiltrated overnight at 4°C with 2.3 M sucrose in PBS, mounted onto cryospecimen pins and frozen in liquid nitrogen. Ultrathin sections (80 nm) were cut using a Leica ultracut ultramicrotome with an FCS cryoattachment at -108°C and collected on formvar- and carbon-coated nickel grids using a 1:1 mixture of 2% methyl cellulose (25 centipoises; Sigma) and 2.3 M sucrose in PBS. Cells were quenched with 0.1 M NH_4Cl in PBS, blocked in 1% fish skin gelatin (FSG, Sigma) in PBS and subsequently labeled with rabbit anti-HLA-DR antiserum and 10 or 15 nm protein A–gold (purchased from the Department of Cell Biology, University of Utrecht, Netherlands). After fixation in 1% glutaraldehyde and quenching with 0.1 M

NH_4Cl, the same labeling procedure was repeated for the rabbit anti-GFP antibody. After final fixation in 1% glutaraldehyde, grids were washed 8x in HPLC-grade water. Sections were infiltrated for 10 min on ice with a mixture of 1.8% methylcellulose and 0.5% uranyl acetate (Electron Microscopy Sciences), washed 3x in 0.5% uranyl acetate/1.8% methylcellulose and air-dried. Samples were analyzed in a Tecnai 12 Biotwin (FEI) microscope and pictures were taken using Kodak 4489 film.

2.3.12 Target cell-T cell coculture and IFN-γ ELISA

Target cells were cocultured overnight with EBNA1-, EBNA3A- or MP1-specific T cell clones in 5% PHS medium (RPMI-1640 with 5% PHS + glutamine + gentamycin) in 96-well round bottom plates (10^5 T cells/well + variable target cell numbers). HaCat target cells were treated with 200 U/ml IFN-γ 24h before the coculture to upregulate MHC class II expression and were washed 3x in DMEM before addition of T cells to remove IFN-γ. After coculture, IFN-γ in culture supernatants was measured using the human IFN-γ ELISA kit from Mabtech according to the manufacturer's instructions. Recombinant human IFN-γ (Mabtech) at concentrations of 30-2,000 pg/ml was used as a standard. If IFN-γ levels in supernatants exceeded 2000 pg/ml, supernatants were diluted in 5% PHS medium and IFN-γ was remeasured by ELISA.

2.3.13 Statistics

Paired or homocedastic, one-tailed student's T test statistics were applied where indicated.

2.3.14 Influenza A virus infection

For most experiments, influenza A virus strain Aichi X:31 (A/Aichi/68, H3N2, purified virus, purchased from Charles River Laboratories) was used. Where indicated, influenza A/PR8/34 (H1N1) or the isogenic deletion mutant A/PR8/34ΔNS1 (a gift of Adolfo Garcia-Sastre, New York), influenza A/WSN/33 (H1N1) or the isogenic deletion mutant A/WSN/33ΔPB1-F2 (a gift of Peter Palese, New York) were used. Before infection, cells were washed three times in RPMI-1640 to remove FCS and then were incubated with influenza virus in a small volume of RPMI-1640 for 1 h at 37ºC at an MOI of 0.1-0.2, unless indicated otherwise. After one hour, cells were washed once in culture medium (DMEM + 10% FCS + glutamine + gentamicin) and then were kept in culture medium for the indicated amount of time, usually 24 hours. For heat-inactivation, virus was incubated in a 56ºC water bath for 30 min and then was added to cells as described above.

2.3.15 Transmission electron microscopy of influenza-infected cells

A549 cells (uninfected or 24 hours post-infection with influenza A/Aichi/68) were washed 3x in PBS, fixed in 2.5 % glutaraldehyde (Electron Microscopy Sciences) in 0.1M sodium cacodylate buffer (pH 7.4) for 1 hour at room temperature and then washed 3x 5 min in 0.1M sodium cacodylate buffer. Cells were scraped off the culture plates with a cell scraper and postfixed in 1% osmium tetroxide (Electron Microscopy Sciences) in cacodylate buffer for 1 h at room temperature. Cells were stained in 2% aqueous uranyl acetate, dehydrated in a graded series of ethanol, and embedded in epoxy resin (Embed-812, Electron Microscopy Sciences). Ultrathin sections (60 nm) were cut with a Reichert

ultracut E ultramicrotome, stained with 2% uranyl acetate and lead citrate and examined in a Tecnai 12 Biotwin electron microscope. Micrographs were generated using a Morada CCD camera (Olympus Soft Imaging Solutions).

2.3.16 Live cell imaging

Cells were grown on 35 mm culture dishes with No. 1.5 coverglass inserts (MatTek Corporation) and infected with influenza virus as described in section 2.3.14. 24 hours post-infection, medium was replaced by CO_2-independent Medium 199 supplemented with 10% FCS, 2 mM glutamine and 25 mM Hepes (Gibco) prewarmed to 37ºC. For staining of acidic compartments, 50 nM Lysotracker Red (Molecular Probes) was added to the medium. After 30 min, medium was replaced with fresh supplemented Medium 199 and cells were analyzed on an inverted Zeiss Axiovert 200 microscope equipped with an UltraView spinning disk confocal head (Perkin-Elmer) and a 37ºC environmental chamber, using a 63x/1.4 N.A. oil immersion lens. Pictures were taken at various intervals with a Hamamatsu Orca ER cooled CCD camera using Metamorph Software (Universal Imaging Corporation). Vesicles that had a minimum diameter of 0.5 μm were tracked over time using Imaris software (Bitplane). For each condition, > 200 vesicle tracks total were analyzed (uninfected: n=222, infected: n=269) and average vesicle speed was calculated with the Imaris software.

2.3.17 Determination of virus titer by plaque assay

Culture supernatants were centrifuged for 5 min at 300g to pellet any floating cells and supernatant was transferred to a new tube and frozen at -80ºC. For titer determination,

supernatants were thawed on ice and serially diluted (1:10 dilutions, 8 dilutions total) in infection medium (EMEM, 0.2% BSA, glutamine, pen/strep). Dilutions were added to 100% confluent MDCK cells growing in a 6-well plate (100 µl/well) for 1 h at room temperature. Then, inoculum was removed and cells were covered with 2ml/well plaquing medium (MEM, 0.2%BSA, 0.01% DEAE Dextran, 2 µg/ml TPCK trypsin, 0.6% oxoid purified agar, glutamine, pen/strep). Agar was allowed to solidify at room temperature, then plates were placed upside down in 37ºC incubator for 2 days. Cells were fixed in 4% paraformaldehyde for 10 min and agar plugs were washed off with running water. Then, cells were stained with crystal violet for 10 min. Plates were washed in water and after drying plaques were counted to determine titers.

Chapter 3: Results

3.1 Endogenous MHC class II processing pathway of the EBV nuclear antigen 1 (EBNA1)

As described in chapter 1.2.6, intracellular antigens can be endogenously processed for presentation on MHC class II molecules, but the exact processing pathway has remained unclear, especially for cytosolic and nuclear antigens that usually don't gain access to the secretory pathway or endocytic system. The first aim of this thesis project was to dissect the intracellular route by which cytosolic/nuclear antigens gain access to MHC class II loading compartments.

EBNA1 is an ideal antigen to study endogenous MHC class II presentation of a viral protein relevant for disease: First, it is the dominant $CD4^+$ T cell antigen during latent EBV infection and can be detected by $CD4^+$ T cells after endogenous processing in EBV positive lymphoma cells [43]. Second, presentation of EBNA1 epitopes on MHC class I for $CD8^+$ T cell recognition is decreased because the full-length form of EBNA1 prevents its own proteasomal processing and therefore presentation on MHC class I [175, 178]. Instead, EBNA1 is endogenously processed for MHC class II presentation and can be detected by $CD4^+$ T cells in nearly all healthy virus carriers [43]. Third, EBNA1's processing under physiologic conditions of latent EBV infection can easily be studied in B-lymphoblastoid cell lines (LCLs). Hence, we studied endogenous MHC class II processing of EBNA1, in order to gain insight into the cell biology of this non-classical pathway of MHC class II presentation.

3.1.1 EBNA1 is degraded by lysosomal, not cytosolic proteases

EBNA1 was found to be endogenously processed and presented on MHC class II molecules in B cells [43]. However, the protease(s) responsible for degradation of EBNA1 have not been identified so far. To identify the proteolytic pathway in which EBNA1 is degraded, we investigated the effect of various protease inhibitors on whole cell EBNA1 protein levels. To test whether lysosomal proteases are involved in the degradation of EBNA1, EBNA1-expressing B cell lines were treated with inhibitors of lysosomal acidification (NH_4Cl or chloroquine) and their effect on EBNA1 levels was monitored by Western blot. Initially, experiments were carried out with the EBV-negative Hodgkin's lymphoma cell line L428 stably transfected with EBNA1 (L428-E1). EBNA1 expression in this cell is about 10-fold higher than in EBV-transformed B lymphocytes [198] so that EBNA1 can be detected more easily in Western blot. We found that total cellular EBNA1 levels were increased upon blocking lysosomal acidification for 48 hours with NH_4Cl or chloroquine (Fig. 7A). At earlier time points, EBNA1 accumulation was small to undetectable (data not shown). Since none of these inhibitors affect the rate of protein synthesis, the enrichment of EBNA1 must be due to a reduced rate of degradation. This suggests that endosomal/lysosomal proteolysis is responsible for degradation of EBNA1.

In order to specify the proteases responsible for EBNA1 degradation, we treated L428-E1 cells with protease inhibitors specific for particular families of lysosomal proteases. We observed that EBNA1 levels increased upon inhibition of aspartyl proteases with pepstatin A (Fig. 7B). Possible candidates are the aspartyl proteases cathepsin D and E, which are abundantly expressed in lysosomes of B cells and have

Figure 7: Accumulation of EBNA1 after inhibition of lysosomal proteolysis.

A and B: The EBV-negative Hodgkin's lymphoma cell line L428 and the stably EBNA1-transfected cell line L428-E1 were treated with increasing concentrations of the lysosomal acidification inhibitors NH_4Cl and chloroquine (A) or the lysosomal protease inhibitors leupeptin and pepstatin A (B) for 48 hours and levels of EBNA1 and the control protein β-actin in whole cell lysates were visualized by Western blot. One representative experiment of three is shown.

C: The EBV-transformed B lymphocyte cell line (LCL) LG2 and the Burkitt lymphoma (BL) cell line Ous were cultured with different concentrations of the lysosomal protease inhibitor pepstatin A for 48 hours, and EBNA1 and β-actin were visualized by Western blot. The Western blots for LG2 and Ous required longer exposure times due to 10 fold lower EBNA1 expression levels present in these cells compared to EBNA1-transfected L428 cells.

D: As in A, except that the cytosolic protease inhibitors lactacystin or calpeptin were used. One representative experiment of two is shown.

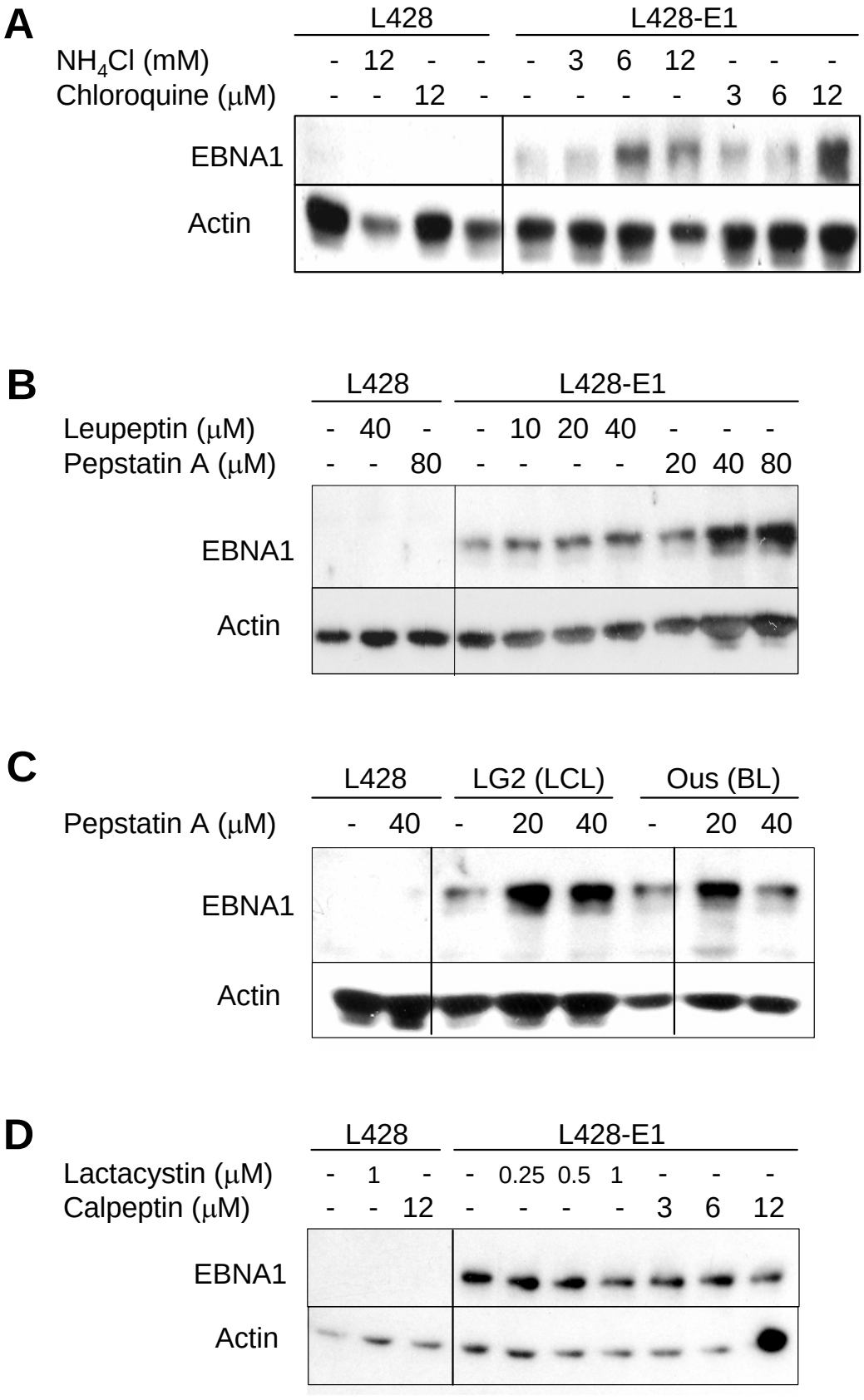
A
L428
L428-E1
NH4Cl (mM) - 12 - - - 3 6 12 - - -
Chloroquine (μM) - - 12 - - - - - 3 6 12
EBNA1
Actin
B
L428
L428-E1
Leupeptin (μM) - 40 - - 10 20 40 - - -
Pepstatin A (μM) - - 80 - - - - 20 40 80
EBNA1
Actin
C
L428
LG2 (LCL)
Ous (BL)
Pepstatin A (μM) - 40 - 20 40 - 20 40
EBNA1
Actin
D
L428
L428-E1
Lactacystin (μM) - 1 - - 0.25 0.5 1 - - -
Calpeptin (μM) - - 12 - - - - 3 6 12
EBNA1
Actin

previously been implicated in antigen processing [204-208]. In contrast, cysteine proteases such as cathepsin L, S and B, seem to play a minor role in EBNA1 degradation, since treatment with the cysteine protease inhibitor leupeptin had no effect on EBNA1 protein levels (Fig. 7B). Even leupeptin concentrations, that were sufficient to inhibit invariant chain degradation and cause downregulation of the MHC class II surface level as determined by flow cytometry (40 μM leupeptin reduced MHC class II levels by 40%; data not shown), had no effect on overall EBNA1 levels. An accumulation of EBNA1 after pepstatin A treatment could also be observed in EBV transformed cells of a lymphoblastoid cell line (LCL LG2) and a Burkitt lymphoma cell line (Ous, Fig. 7C), which express physiological levels of EBNA1. This suggests that EBNA1 is degraded by aspartyl proteases in both EBV-transformed cell lines and EBNA1-transfected B cell lines.

In addition to lysosomal proteases, cytosolic proteases, such as proteasomes and calpains, have been shown to play a role in the endogenous pathway of MHC class II presentation [44, 49]. However, they do not seem to be involved in the degradation of EBNA1. The proteasome inhibitor lactacystin had no effect on the steady state level of EBNA1 (Fig. 7D), which is consistent with the finding that EBNA1 is resistant to proteasomal degradation [175]. Furthermore, treatment with the calpain inhibitor calpeptin did not affect the EBNA1 level either (Fig.7D). While a role for additional proteases cannot be excluded, our data indicate that EBNA1 is mainly degraded by aspartyl proteases in the endosomal/lysosomal pathway.

3.1.2 EBNA1 accumulates in lysosomal compartments after inhibition of lysosomal acidification

Since we had detected an accumulation of EBNA1 in whole cell lysates after lysosomal protease inhibition, we wanted to address in which compartments EBNA1 accumulated under these conditions. Immunofluorescence microscopy showed that EBNA1 accumulated in cytosolic vesicles that partially costained with the lysosomal marker protein LAMP1 (Fig 8A).

Subcellular fractionation confirmed that upon blocking lysosomal acidification, EBNA1 was enriched in microsomes (Fig. 8B and C): In L428-E1 cells without lysosomal protease inhibition, EBNA1 was confined to the whole-cell lysate and the nuclear fraction, whereas after chloroquine treatment, EBNA1 could be found in the postnuclear supernatant and the highspeed pellet derived thereof. Discontinuous sucrose gradient centrifugation to further purify microsomes revealed that EBNA1 had accumulated in microsomes after chloroquine treatment. EBNA1 fractionated with the lysosomal marker LAMP1. We confirmed accumulation of EBNA1 in microsomes in the EBV-transformed B cell line LG2, which in contrast to L428-E1 expresses physiological levels of EBNA1 (Fig. 8C). This cell line also expresses other EBV latency antigens and therefore allowed us to examine how other nuclear EBV antigens behave after lysosomal protease inhibition. EBNA3A, another nuclear EBV antigen and prominent $CD8^+$ T cell antigen [209], was not enriched in the microsomal fraction after chloroquine treatment (Fig. 8C). These results demonstrate that EBNA1 is degraded in cytosolic and partially lysosomal vesicles and confirm our previous finding that EBNA1 is degraded by lysosomal proteases.

Figure 8: EBNA1 accumulates in lysosomal/microsomal compartments after inhibition of lysosomal acidification.

A: The B lymphoblastoid cell line SL-LCL was left untreated (first row) or treated with 20 mM NH_4Cl for 48 h (second and third row) and then stained for EBNA1, LAMP1 and DNA content (DAPI). Arrows indicate cells with EBNA1/LAMP1 colocalization. One of three experiments is shown. *(Experiment performed in collaboration with Casper Paludan, Laboratory of Viral Immunobiology, Rockefeller University).*

B and C: The EBNA1-transfected Hodgkin's lymphoma cell line L428-E1 (B) or the EBV-transformed B-LCL LG2 (C) were treated with 50 μM chloroquine for three days (+CQ). After homogenization (H), intact cells and nuclei (N) were pelleted (2x 3000 g, 10 min) and the postnuclear supernatant (S1) was centrifuged at 100,000 g for 1 h to obtain a microsomal pellet (P) and a postmicrosomal supernatant (S2). The microsomal pellet was resuspended in homogenization buffer and purified over a two-step sucrose gradient (2M/ 0.5M sucrose) and microsomal vesicles were collected from the interphase (M). The amount of EBNA1 within each fraction was determined by Western blot. The same blots were reprobed with antibodies specific for the lysosomal marker LAMP1 (B and C) and the EBV nuclear antigen EBNA3A (C). One of nine experiments is shown.

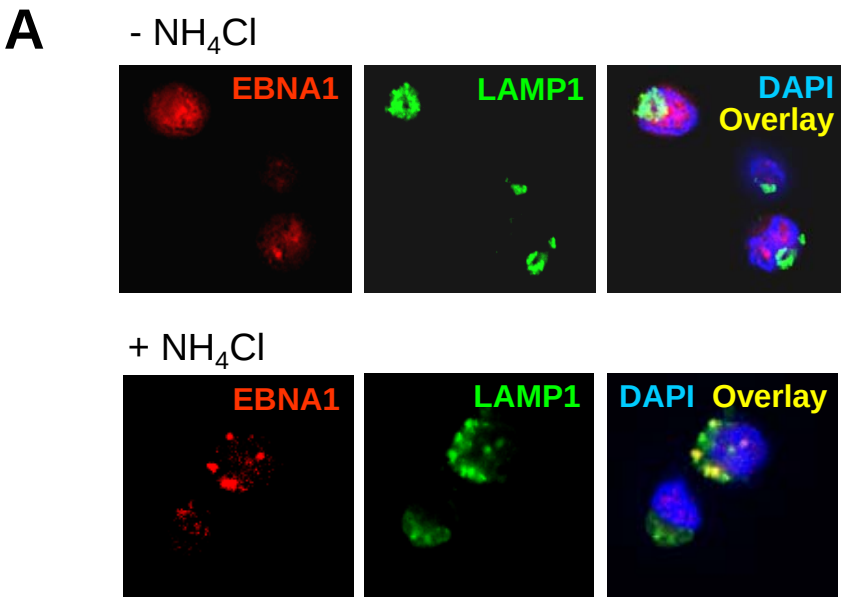
A
- NH4Cl
EBNA1
LAMP1
DAPI
Overlay
+ NH4Cl
EBNA1
LAMP1
DAPI Overlay

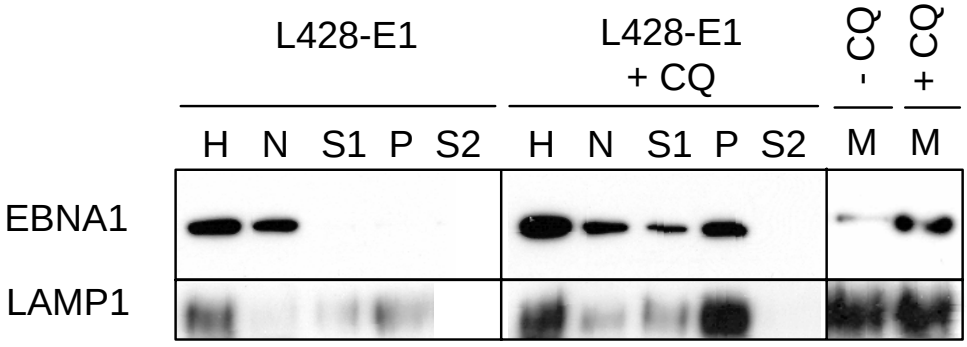
B
L428-E1
L428-E1
+ CQ
CQ
-
CQ
+
H N S1 P S2 H N S1 P S2 M M
EBNA1
LAMP1

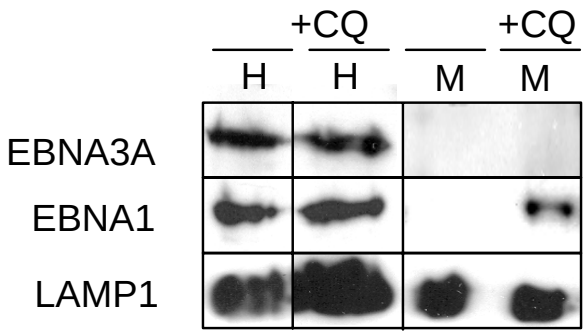
C
+CQ
+CQ
H H M M
EBNA3A
EBNA1
LAMP1

3.1.3 EBNA1 is taken up into double-membrane vesicles

Our immunofluorescence microscopy and cell fractionation experiments suggested that EBNA1 was degraded in lysosomal compartments. The resolution of these methods is however limited and therefore these experiments are only able to provided a first evidence that EBNA1 is degraded in lysosomes. To confirm our findings, we performed immuno-electron microscopy (IEM), which allowed us to assess the ultrastructural features of EBNA1-containing vesicles. In collaboration with Casper Paludan, Laboratory of Viral Immunobiology and Eleana Sphicas, Bioimaging Resource Center, Rockefeller University, EBNA1-transfected L428 Hodgkin's lymphoma cells were stained for EBNA1 and analyzed by electron microscopy. Upon inhibition of lysosomal acidification, EBNA1 could be observed in cytosolic vesicles, surrounded by double membranes (Fig. 9B, black arrows). Some of these structures had the cup-shaped appearance of forming autophagosomes/isolation membranes (Fig. 9B, middle panel). An isotype control antibody produced no staining (data not shown). Without lysosomal protease inhibition, no cytosolic/vesicular EBNA1 staining could be detected (data not shown), presumably because EBNA1 is degraded by lysosomal proteases. The observation that EBNA1 is taken up by cup-shaped structures and accumulates in double-membrane vesicles suggest that autophagy participates in the delivery of EBNA1 to lysosomes.

Figure 9: Electron micrographs of EBNA1-transfected B cell line show that EBNA1 is taken up into autophagosomes. *(Experiment performed in collaboration with Casper Paludan, Laboratory of Viral Immunobiology and Eleana Sphicas, Bioimaging Resource Center, Rockefeller University).*

A: The EBNA1-transfected Hodgkin's lymphoma cell line L428-E1 was left untreated (-CQ) or was treated with 50 μM chloroquine (+CQ) for 48 hours to inhibit EBNA1 degradation. Then cells were fixed and processed for electron microscopy. Pictures show morphology of untreated and chloroquine-treated cells. Black arrows indicate electron-dense autophagosomes/lysosomes, which are stabilized by chloroquine.

B: L428-E1 cells treated with chloroquine for 48 hours were stained with the EBNA1-specific monoclonal antibody 5F12 before processing for electron microscopy. Blue arrows indicate nuclear EBNA1, black arrows show EBNA1 in forming or mature autophagosomes. One of three experiments is shown.

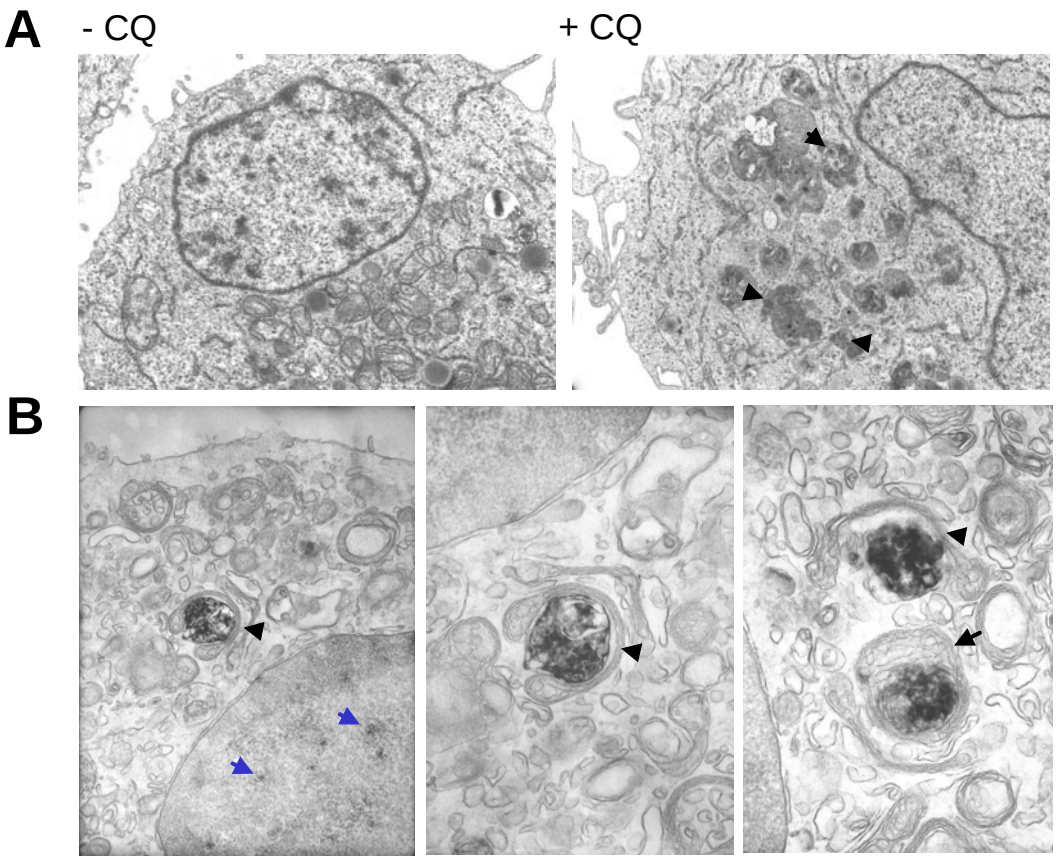
A
- CQ
+ CQ
B

3.1.4 Inhibition of autophagy with a pharmacologic inhibitor leads to decreased MHC class II-restricted $CD4^+$ T cell recognition of EBNA1

In order to test whether autophagy indeed leads to endogenous MHC class II presentation of EBNA1, we determined whether inhibition of this pathway would block antigen presentation to EBNA1-specific $CD4^+$ T cell clones [43, 56, 210]. As a first indication, we used 3-methyladenine (3-MA), which is a frequently used pharmacologic inhibitor of autophagy [118]. 3-MA inhibits the class III PI3K kinase complex, which is essential for autophagosome formation [89]. Therefore, 3-MA inhibits macroautophagy. When we treated EBV-transformed B cells or EBNA1-transfected Hodgkin's lymphoma cells with 3-MA for 2 to 4 days, EBNA1-specific $CD4^+$ T cell recognition of the cells was decreased by 30-70% in IFN-γ ELISPOT assays, while the proteasome inhibitor lactacystin [211] had little effect (Fig. 10A). In contrast, the IFN-γ response of an EBNA3A-specific $CD8^+$ T cell clone was not affected by 3-MA but decreased upon lactacystin treatment by 50% (Fig. 10A). The inhibition time of 2-4 days was chosen since high affinity MHC class II-peptide complexes have a half life around 24 h [212]. MHC class II surface expression was not decreased by 3-MA or lactacystin at the reported concentrations, as assessed by flow cytometry (Fig. 10B). Moreover, recognition of inhibitor-treated target cells was completely restored by pulsing cells with the cognate peptide (Fig. 10C), demonstrating that the MHC class II levels were not affected by inhibitor treatment. Together, these experiments indicate that autophagy might be involved in MHC class II presentation of EBNA1, but not the presentation of the MHC class I-restricted antigen EBNA3A. Furthermore, inhibition of EBNA3A presentation by lactacytin confirmed that the proteasome is involved in processing EBNA3A for MHC

Figure 10: Blocking of autophagy with the pharmacological inhibitor 3-methyladenine leads to decreased MHC class II-restricted $CD4^+$ T cell recognition of EBNA1.

A: IFN-γ ELISPOT assays with EBNA1-specific $CD4^+$ T cell clones A4.E116 and RJD.79 or EBNA3A-specific $CD8^+$ T cell clone MS.B11. T cell clones were stimulated with untreated, 3-methyladenine- or lactacystin-treated cognate target cells. As negative control, non-cognate target cells (same restriction element, but EBV-negative or different EBV strain) were used. As positive control, non-cognate target cells were pulsed with the specific peptide. Target cells treated with 10 mM 3-methyladenine and 1 μM lactacystin were added for 3 days prior to the T cell stimulation, but were not present during the stimulations. One of four experiments is shown.

B: HLA-DR surface levels on the target cell line L428-E1 after treatment with 3-methyladenine or lactacystin for 3 days were evaluated by flow cytometry. Mean fluorescence values are given in the FACS blots. One of two experiments is shown.

C: IFN-γ ELISPOT assay with EBNA1-specific $CD4^+$ T cell clones A4.E116 and EBV^+ (LCL721.221) or EBV^- (HDLM-2) cells as target cells. Target cells were either left untreated or were treated with 10 mM 3-methyladenine or 1 μM lactacystin for 3 days. Then cells were either cocultured with T cell clones directly, or were pulsed with the specific EBNA1 peptide before T cell coculture. Under all conditions, maximal T cell activation was restored, demonstrating that MHC class II levels were not affected by inhibitor treatments. One of two experiments is shown.

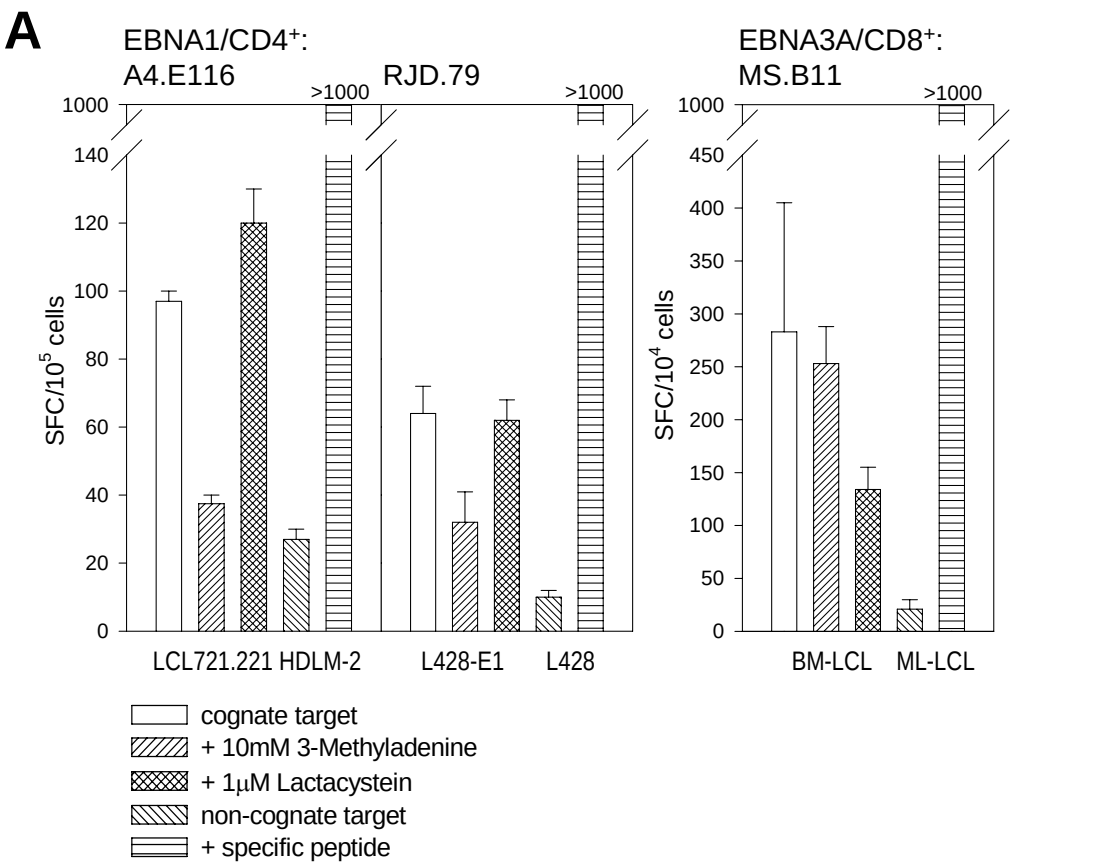
A
EBNA1/CD4+:
A4.E116
RJD.79
EBNA3A/CD8+:
MS.B11
>1000
SFC/10^5 cells
SFC/10^4 cells
LCL721.221
HDLM-2
L428-E1
L428
BM-LCL
ML-LCL
cognate target
+ 10mM 3-Methyladenine
+ 1μM Lactacystein
non-cognate target
+ specific peptide

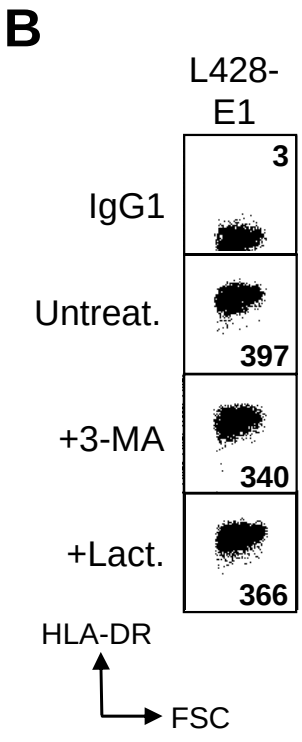
B
L428-E1
IgG1
Untreat.
+3-MA
+Lact.
3
397
340
366
HLA-DR
FSC

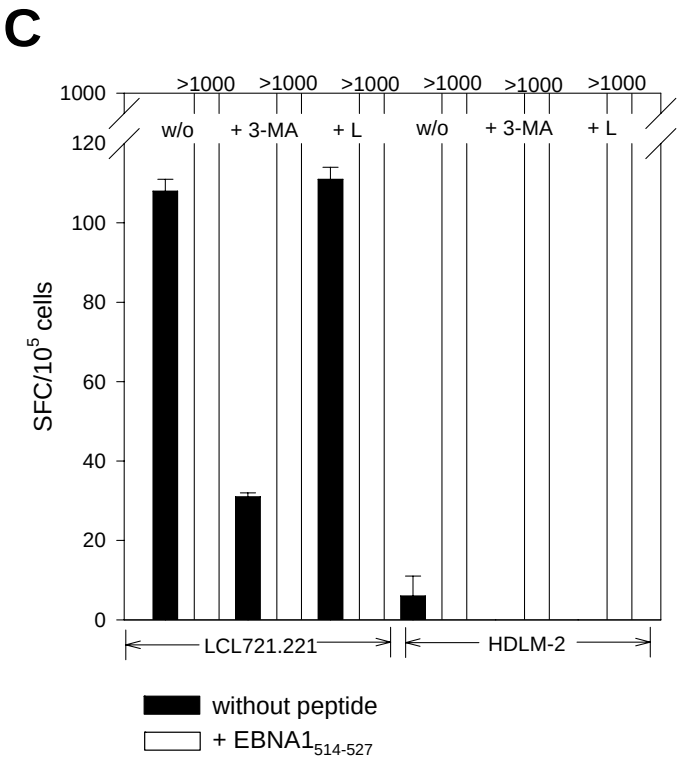
C
>1000
w/o
+ 3-MA
+ L
SFC/10^5 cells
LCL721.221
HDLM-2
without peptide
+ EBNA1514-527

MHC class I presentation, but is not involved in the degradation of EBNA1 for endogenous MHC class II presentation.

3.1.5 Specific inhibition of autophagy by RNA interference leads to decreased MHC class II-restricted CD4$^+$ T cell recognition of EBNA1

3-MA-induced inhibition of class III PI3 kinase also inhibits other intracellular vesicle trafficking processes, such as endocytosis [88], and therefore 3-MA effects have to be interpreted with caution. Therefore, we used RNA interference to silence the essential autophagy gene *atg12* [79, 82, 213] and thereby specifically inhibit autophagy and no other vesicle transport process. siRNAs against two different regions of *atg12* (Atg12.1 and Atg12.2), but not a *GFP*-specific siRNA, efficiently down-regulated the *atg12* mRNA level in EBV-transformed B cells (Fig. 11A). Knock-down of *atg12* with both siRNA duplexes decreased the IFN-γ response of EBNA1-specific CD4$^+$ T cell clones by 40-60% ($p=0.003$), whereas treatment with the GFP siRNA had no effect. In contrast, MHC class I presentation of the nuclear EBV antigen EBNA3A was not affected by *atg12* knockdown, since EBNA3A was still efficiently recognized by the CD8$^+$ T cell clone MS.B11 (Fig. 11B). Treatment with *atg12*-specific siRNAs did not affect the MHC class II surface levels on the B cells (Fig. 11C). Exogenous MHC class II processing of EBNA1 could be excluded, since LCLs were unable to sensitize bystander B cells for EBNA1-specific CD4$^+$ T cell recognition [43]. In addition, EBNA1 was undetectable in supernatants of LCLs and EBNA1-transfected L428 cells with the use of ELISA assays (detection limit was 0.1 μg/ml), whereas 1 to 10 μg/ml were necessary to increase CD4$^+$ T cell recognition of EBV$^+$ and EBV$^-$ B cell lines (data not shown). Thus, blocking of

Figure 11: Specific inhibition of autophagy by RNA interference leads to decreased MHC class II-restricted CD4$^+$ T cell recognition of EBNA1.

A: mRNA levels of *atg12* and *GAPDH* were analyzed on day 4 after knock-down by semi-quantitative RT-PCR from whole cell RNA isolated from T cell targets. The results are representative of five experiments and the example shown here corresponds to the experiment shown in B.

B: IFN-γ-ELISA assays of the EBNA1-specific CD4$^+$ T cell clone P3-B7 and the EBNA3A-specific CD8$^+$ T cell clone MS.B11. Target cells (P3-B7: HLA-DP3$^+$ Ag876 cells; MS.B11: HLA-B8$^+$ BM-LCL cells) were electroporated with 10 μM siRNA (*GFP*- or *atg12*-specific) on day 0 and 2 and on day 4 targets were cocultured with T cell clones overnight. IFNγ in culture supernatants was measured in IFN-γ-ELISA assays. One of three experiments is shown.

C: HLA-DR surface levels on the target cell line Ag876 after knock-down of *atg12*. Mean fluorescence values are given in the FACS blots. One of two experiments is shown.

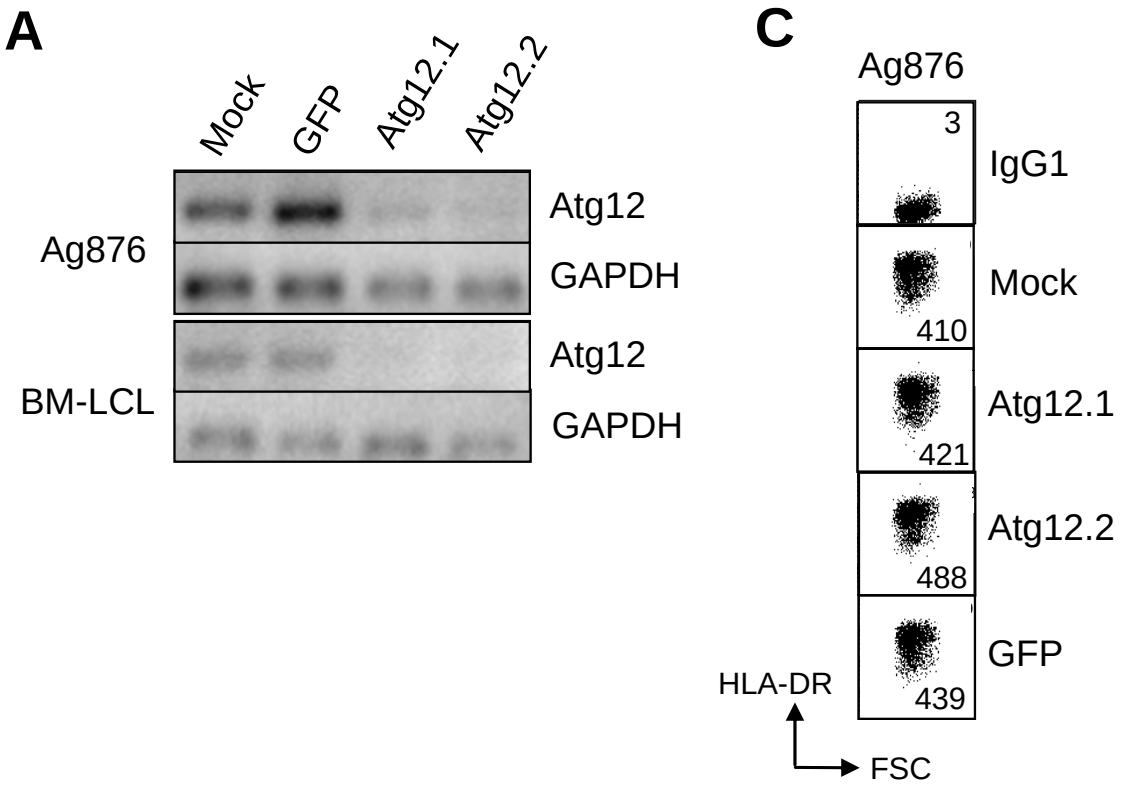
A
Mock
GFP
Atg12.1
Atg12.2
Ag876
Atg12
GAPDH
BM-LCL
Atg12
GAPDH
C
Ag876
3
IgG1
Mock
410
Atg12.1
421
Atg12.2
488
GFP
439
HLA-DR
FSC

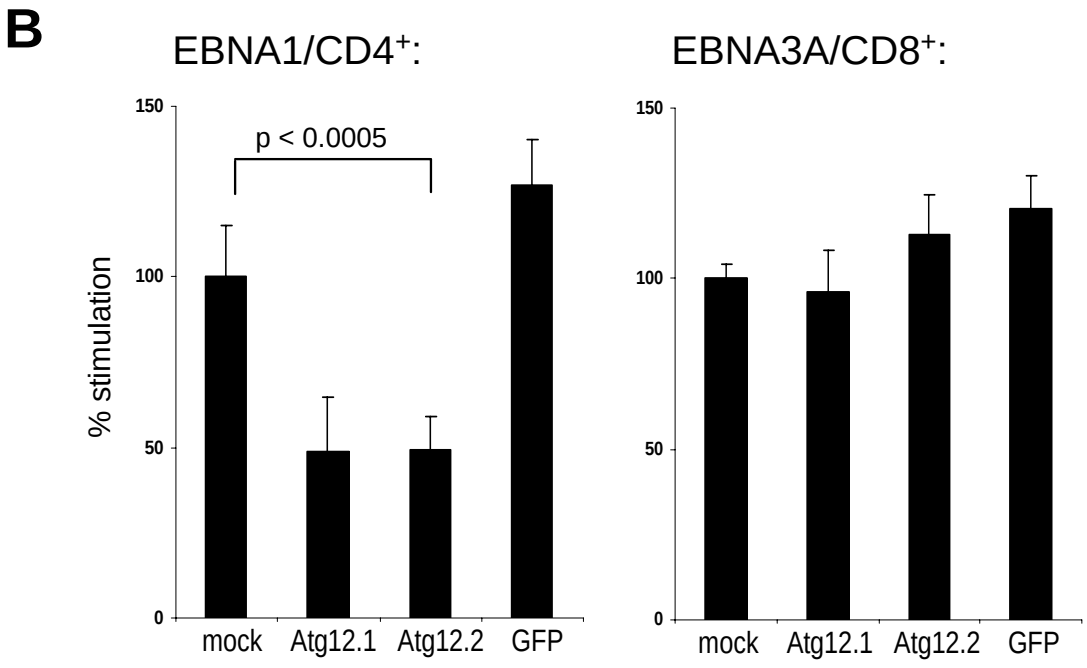
B
EBNA1/CD4+:
EBNA3A/CD8+:
p < 0.0005
% stimulation
150
100
50
0
mock
Atg12.1
Atg12.2
GFP

autophagy by siRNA-mediated silencing of *atg12* inhibits endogenous MHC class II presentation of EBNA1, but not presentation of the MHC class I-restricted EBV antigen EBNA3A.

3.1.6 Conclusion: EBNA1 is processed for MHC class II presentation by autophagy

Using various protease inhibitors, we could show that EBNA1 is degraded by lysosomal proteases, especially aspartyl proteases, whereas cytosolic proteases, such as the proteasome and calpains, are not involved in EBNA1 degradation. Furthermore, when lysosomal proteolysis was inhibited, EBNA1 was detected in the microsomal fraction and could be visualized in partially LAMP1-positive compartments by immunofluorescence microscopy. Furthermore, EBNA1 localized to cup-shaped isolation membranes of double-membrane vesicles by immuno-electron microscopy. Finally, inhibition of autophagy with pharmacologic drugs or *atg12*-specific siRNAs showed that autophagy was involved in delivering EBNA1 for MHC class II presentation and $CD4^+$ T cell stimulation. Together, these data provide strong evidence that EBNA1 is delivered for endogenous MHC class II presentation by autophagy. Thus, autophagy probably contributes to the immune control of Epstein-Barr virus (EBV) and represents a novel pathway by which intracellular protein antigens can be loaded endogenously onto MHC class II molecules.

3.2 General relevance of autophagy for MHC class II presentation and targeting of autophagy to boost $CD4^+$ T cell stimulation

Our studies of the EBNA1 processing pathway have shown that autophagy plays a role in endogenous MHC class II presentation of this viral antigen [214]. Autophagy was also implicated in MHC class II presentation of one model antigen (neomycin phosphotransferase II) [50], one self antigen (Complement C5) [45] and one tumor antigen (MUC-1) [53], but the general relevance of this pathway for MHC class II presentation is not known. We wondered whether macroautophagy is a general and efficient pathway for MHC class II presentation of intracellular antigens in a variety of antigen-presenting cells. In order to address this question, we analyzed the autophagy level in different MHC class II-positive human cell types, to see if they exhibit constitutive autophagy and therefore might be predisposed for immune surveillance by $CD4^+$ T cells. Furthermore, we analyzed the overlap of autophagosomes with MHC class II loading compartments (MIICs) to see how frequently MHC class II loading compartments receive input from the autophagy pathway. Finally, we determined the efficiency with which a cytosolic antigen is presented on MHC class II molecules if it is specifically targeted for autophagic degradation.

3.2.1 GFP-LC3 as a tool to visualize autophagosome formation

To quantify the autophagy level in MHC class II-positive human cells, we made use of the specific autophagosome marker autophagy-related gene 8 (Atg8), also called light chain 3 (LC3). LC3 is an ubiquitin-like protein that is covalently coupled via its C-

terminus to a phospholipid in the newly forming inner and outer autophagosomal membranes and thus is specifically incorporated into autophagosomes [84]. GFP-tagged LC3 has been used to visualize autophagosomes in cultured cells [68, 84, 102] and GFP-LC3 transgenice mice have been established to quantify constitutive and starvation-induced autophagy in murine tissues [68]. It has been shown previously that overexpression of GFP-LC3 does not alter the autophagic activity [68], and we confirmed this in our own experimental system (see section 3.2.3, Fig. 14).

To visualize autophagosomes in MHC class II-positive human cells, we generated a construct encoding for GFP-LC3, by cloning the cDNA of human LC3 into the mammalian expression vector pEGFP-C2 (Fig. 12A). Expression of the construct after transient transfection into 293 cells was tested by immunoblotting and fluorescence microscopy (Fig. 12B and C). Western blots with an anti-GFP antibody showed a single band of the predicted molecular weight (42kD) (Fig. 12B). In fluorescence microscopy, GFP-LC3 was seen to be evenly distributed throughout the cytoplasm and to localize to small, cytosolic vesicles (Fig. 12C, left). Since only few GFP-LC3-positive vesicles were observed in most cells, we treated cells with the lysosomal acidification inhibitor chloroquine in order to inhibit degradation of autophagosomes by lysosomes. Already 2 hours after chloroquine treatment, many more GFP-labeled vesicles were observed in GPF-LC3 transfected 293 cells (Fig. 12C, middle). These vesicles were also larger in size and were more brightly labeled with GFP-LC3 than vesicles observed in untreated cells, indicating that GFP-LC3 had accumulated inside these vesicles. The accumulation of GFP-LC3$^+$ vesicles was even more pronounced 10 hours after chloroquine treatment (Fig. 12C, right). This suggests that large numbers of autophagosomes have formed and fused

Figure 12: GFP-LC3 as a tool to visualize autophagosomes.

A: Schematic diagram of the EGFP-LC3 construct. EGFP is fused in frame to the human LC3 sequence via a short linker region. The five C-terminal residues MKLSV are cleaved off by the Atg4 protease and subsequently the protein is coupled to the autophagosome membrane via Gly_{120}.

B: Expression of GFP-LC3 in 293 cells as tested by anti-GFP Western blot.

C: 293 cells stably transfected with a GFP-LC3 reporter construct were left untreated (no CQ) or were treated with 50 μM chloroquine (CQ) for 2 or 10 hours. Cells were fixed, stained with DAPI and analyzed in an epifluorescence microscope. Inhibition of lysosomal acidification with CQ leads to a gradual accumulation of GFP-LC3-labeled autophagosomes over time. Representative fields from one experiment out of two are shown.

D: MDAMC cells stably expressing GFP-LC3 were either mock transfected or with siRNA duplexes specific for lamin A/C or *atg12*. After 2 days, cells were treated with 50 μM CQ for 6 h (+CQ) or were left untreated (no CQ), stained with DAPI and examined in an epifluorescence microscope. Inhibition of autophagy by *atg12* knockdown abrogates CQ-mediated autophagosome accumulation. One of two experiments is shown.

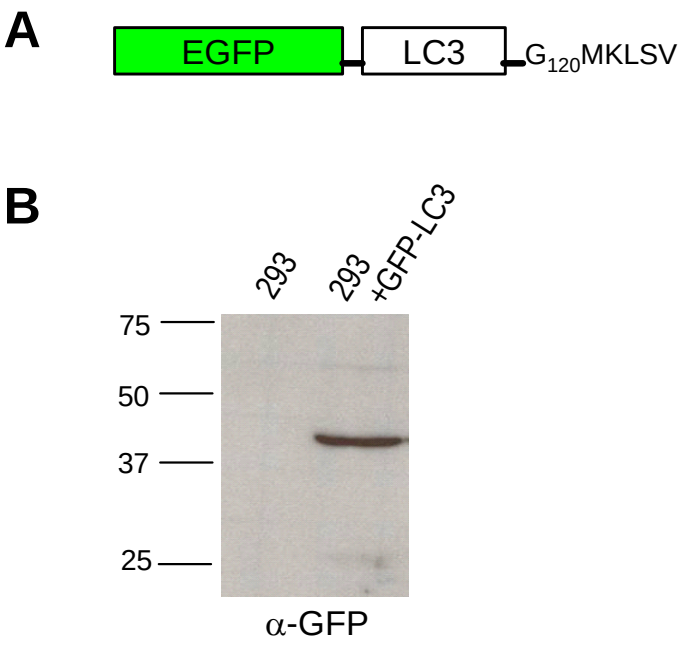
A
EGFP
LC3
G120MKLSV
B
293
293 +GFP-LC3
75
50
37
25
α-GFP
C
Untreated
2h CQ
10h CQ
D
Mock
Lamin siRNA
Atg12 siRNA
GFP-LC3
GFP-LC3
GFP-LC3
No CQ
+ CQ

with lysosomes during the 10 hour observation period. The accumulation of GFP-LC3$^+$ vesicles upon CQ treatment was dependent on autophagosome formation, because siRNA-mediated knockdown of *atg12*, a gene essential for autophagosome formation [79] completely abrogated accumulation of these vesicles (Fig. 12D). This demonstrates that the accumulation of GFP-LC3-positive vesicles upon CQ-treatment is indeed due to autophagosome formation and therefore can be used to assess the autophagy level of a given cell type.

3.2.2 Generation and characterization of a rabbit polyclonal anti-LC3 antiserum

To analyze autophagosome formation more quantitatively and to look at endogenous LC3, we generated a LC3-specific antiserum. Autophagosome-coupled LC3 (LC3-II) and free cytosolic LC3 (LC3-I) can be distinguished by their apparent molecular weights in SDS-PAGE gel electrophoresis (16 and 18 kD, respectively) and thus can be quantified separately in anti-LC3 immunoblots [84]. Therefore, anti-LC3 Western blots can be used to quantify autophagosome-associated LC3-II, which is proportional to the number of autophagosomes [84, 88].

We generated a polyclonal rabbit antiserum against the N-terminal peptide of human LC3 (PSEKTFKQRRTFEQRC, $LC3_{1\text{-}15}$) coupled to KLH carrier protein and tested it in ELISA and Western blot assays. The second and third bleed from rabbit RU1129 recognized the $LC3_{1\text{-}15}$ peptide, but not a control EBNA1 peptide in an ELISA assay, whereas the prebleeds did not show any $LC3_{1\text{-}15}$ reactivity (Fig. 13A). In Western blots, the antiserum recognized the GFP-LC3 fusion protein (42 kD) in lysates of GFP-LC3 transfected-293 cells and showed little cross-reactivity to other proteins (Fig. 13B).

Figure 13: Characterization of polyclonal rabbit anti-LC3 antiserum.

Polyclonal antiserum against the N-terminal LC3 peptide was raised in rabbit RU1129. After the second and third boost, bleeds were collected and analyzed by ELISA and Western blot (A and B). After an additional boost, terminal bleed were collected and used in Western blots to visualized endogenous LC3 in different cell lines (C).

A: ELISA plates were coated with the $LC3_{1-15}$ peptide or a control EBNA1 peptide and serial dilutions of rabbit bleeds (prebleeds, second and third bleeds) were tested for LC3 reactivity.

B: Third bleed from rabbit RU1129 was tested for LC3 reactivity in Western blots on lysates of 293 cells, untreated and chloroquine (CQ)-treated GFP-LC3-transfected 293 cells. As a control, lysates were probed in parallel with GFP-specific antiserum (left). Both antisera specifically recognize two forms of GFP-LC3 (cytosolic and autophagosome-coupled).

C: Final bleed of rabbit RU1129 was tested on lysates of untreated or chloroquine (CQ)-treated HaCat and MDAMC cells. The antiserum strongly recognizes endogenous LC3-II and more weakly LC3-I. A cross-reacting band around 28 kD is indicated by an asterisk. Two different exposures of the same blot are shown.

On

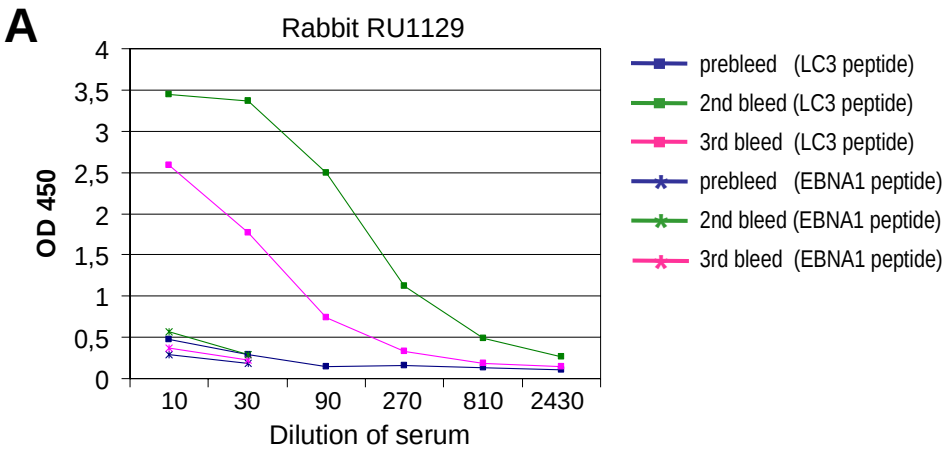
A
Rabbit RU1129
OD 450
4
3,5
3
2,5
2
1,5
1
0,5
0
10
30
90
270
810
2430
Dilution of serum
prebleed (LC3 peptide)
2nd bleed (LC3 peptide)
3rd bleed (LC3 peptide)
prebleed (EBNA1 peptide)
2nd bleed (EBNA1 peptide)
3rd bleed (EBNA1 peptide)

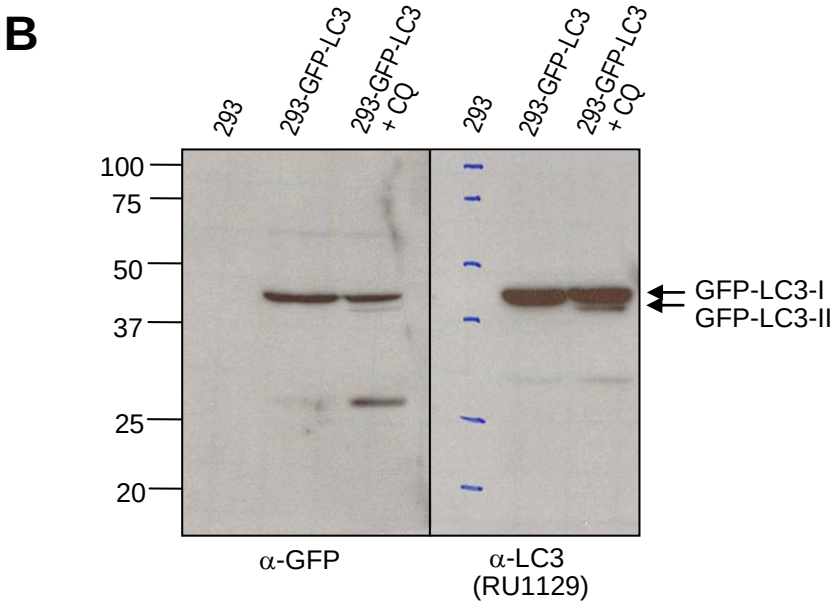
B
293
293-GFP-LC3
293-GFP-LC3 + CQ
293
293-GFP-LC3
293-GFP-LC3 + CQ
100
75
50
37
25
20
GFP-LC3-I
GFP-LC3-II
α-GFP
α-LC3 (RU1129)

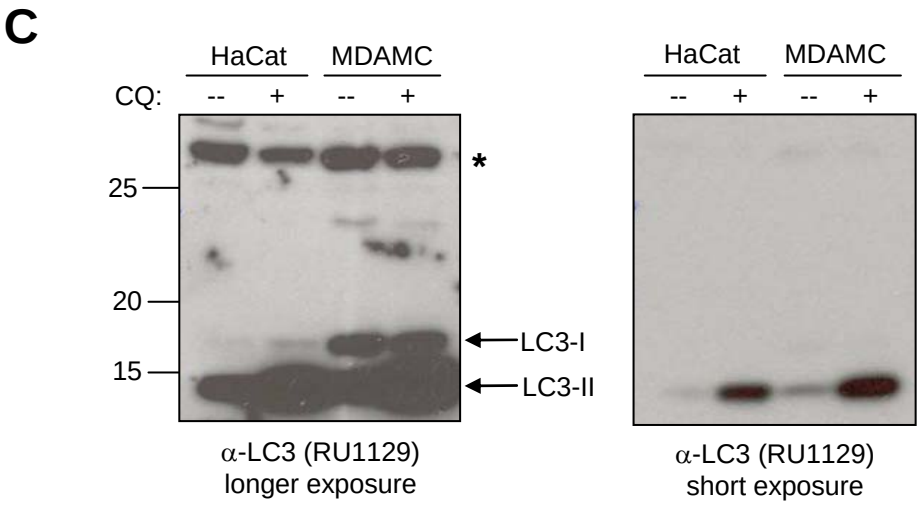
C
HaCat
MDAMC
CQ:
--
+
--
+
*
25
20
15
LC3-I
LC3-II
α-LC3 (RU1129) longer exposure
HaCat
MDAMC
--
+
--
+
α-LC3 (RU1129) short exposure

chloroquine-treated cells, a second band of slightly lower molecular weight (40 kD) appeared, which most likely corresponds to lipidated GFP-LC3-II that migrates with a smaller apparent molecular weight. The antiserum also recognized endogenous 16/18 kD LC3 in lysates of different epithelial cell lines and revealed a strong accumulation of endogenous LC3-II upon chloroquine treatment (Fig. 13C). Since LC3-II is proportional to the number of autophagosomes, a strong LC3-II accumulation reflects a strong autophagosome accumulation and therefore a high rate of autophagosome formation. Therefore, anti-LC3 Western blots can be used to quantify the autophagic activity of a given cell type. Furthermore, the LC3 antiserum can be used to show that expression of GFP-LC3 does not change the autophagic activity [68]: As shown in Figure 14, expression of GFP-LC3 does not alter the LC3-I/LC3-II ratio, indicating that autophagy is not enhanced by overexpression of GFP-LC3.

3.2.3 Autophagosomes are formed constitutively in human epithelial cell lines

To test whether MHC class II-positive human cells exhibit constitutive autophagy, we first analyzed the autophagy level in human epithelial cell lines. Epithelial cells readily up-regulate MHC class II molecules in response to inflammatory cytokines both *in vitro* and *in vivo* [215]. Because they have only limited endocytic potential, we wondered whether these cell lines might rely on endogenous degradation pathways, such as autophagy, to generate peptide ligands for their MHC class II molecules.

To assess the autophagy level in human epithelial cell lines, we transfected cell lines derived from different organs [HaCat (skin), HeLa (cervix), MDAMC (breast), 293 (kidney)] with a GFP-LC3 construct and treated them with chloroquine (CQ) to block

Figure 14: GFP-LC3 expression does not enhance autophagosome formation.

A: Human epithelial cell lines HaCat and MDAMC transfected with GFP-LC3 or untransfected were analyzed by Western blot with the LC3-specific antiserum. In GFP-LC3-transfected cells, strong GFP-LC3 (42/40 kD) expression can be seen. The longer exposure shows that levels of endogenous LC3-I and –II and therefore autophagy levels are not affected by GFP-LC3 overexpression.

B: The experiment shown in A was repeated on 293 cells that were in addition subjected to 50 μM chloroquine (CQ) for 10 h to visualize autophagosome turnover. CQ leads to an accumulation of LC3-II and GFP-LC3-II. In GFP-LC3 transfected cells, the ratio of LC3-I/LC3-II is slightly increased in comparison to untransfected cells, presumably because some GFP-LC3 is incorporated into autophagosomes instead of LC3. However, no increase in LC3-II and therefore no increase in autophagosome formation can be observed after GFP-LC3 overexpression.

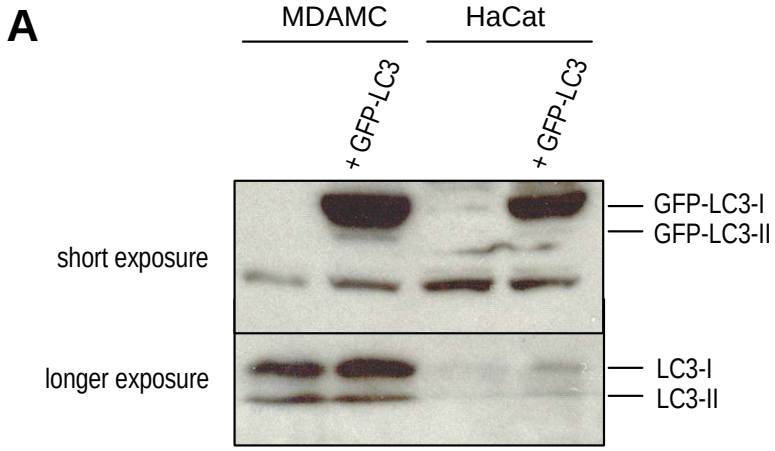
A
MDAMC
HaCat
+ GFP-LC3
+ GFP-LC3
short exposure
longer exposure
GFP-LC3-I
GFP-LC3-II
LC3-I
LC3-II

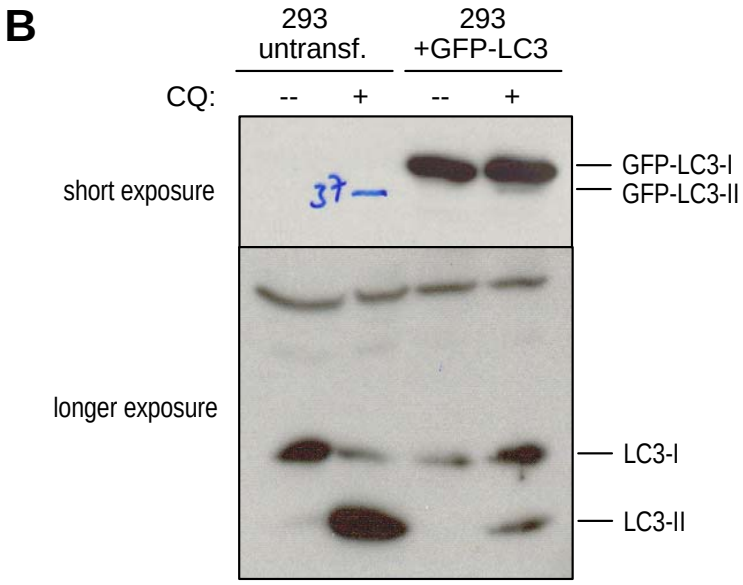
B
293
untransf.
293
+GFP-LC3
CQ:
--
+
--
+
37
short exposure
longer exposure
GFP-LC3-I
GFP-LC3-II
LC3-I
LC3-II

lysosomal proteolysis and thus visualize the accumulation of GFP-LC3 in autolysosomes. In the steady state (no CQ), most cells had only a few GFP-LC3-labeled autophagosomes (typically 0-5) and only a small fraction of cells had >10 GFP-LC3-positive vesicles (Fig. 15A, left). However, after 10 hours of CQ-treatment, GFP-LC3 strongly accumulated in cytosolic vesicles in all cell lines examined (Fig. 15A, right), suggesting that large numbers of GFP-LC3 labeled autophagosomes had formed and fused with lysosomes during the 10-hour observation period.

To measure autophagosome formation more quantitatively and to extend our results with GFP-LC3 to endogenous LC3, we analyzed the same four epithelial cell lines by Western blot with the anti-LC3 antiserum described in section 3.2.2. We cultured the cell lines in the presence or absence of the lysosomal protease inhibitor chloroquine (CQ) for 10 hours and quantified LC3-II accumulation by immunoblotting. In all cell lines, autophagosome-associated LC3-II strongly accumulated upon CQ-treatment (Fig. 15B), demonstrating that LC3-II labeled autophagosomes were constitutively forming over the course of 10 hours. As shown in Fig. 15C for the HaCat cell line, cellular LC3-II levels were already increased 1 hour after CQ-treatment and gradually accumulated after longer treatment times, confirming that autophagosomes are being produced continuously and that their accumulation is not just an effect of long-term inhibitor treatment. Density quantification of immunoblots revealed that LC3-II accumulated 5-fold in HaCat and MDAMC, 15-fold in HeLa and 30-fold in 293 cells after 10 hours of CQ-treatment (Fig. 15D). LC3-II accumulated to similar levels when cells were treated with inhibitors of lysosomal cathepsins for 10 hours (Fig. 15E). In comparison to starvation, lysosomal protease inhibition led to a much stronger LC3-II accumulation (Fig. 15E), demonstrating

Figure 15: Constitutive autophagosome formation in human epithelial cell lines under nutrient-rich conditions.

A: Human epithelial cell lines HaCat (keratinocyte), HeLa (cervical carcinoma), MDAMC (breast carcinoma), and 293 (kidney) were stably transfected with a GFP-LC3 reporter construct. To assess turnover of GFP-LC3 in endosomal and lysosomal compartments, cells were treated with 50 μM chloroquine for 10 h (+CQ) or were left untreated (no CQ). Cells were fixed, stained with DAPI nucleic acid stain and analyzed by confocal microscopy. Scale bars: 20 μm. Representative fields from one experiment out of three are shown.

B: Human epithelial cell lines (HaCat, HeLa, MDAMC, and 293) were treated for 10 h with 50μM CQ (+) or were left untreated (--). Whole cell lysates were analyzed by anti-LC3 immunoblots. Actin blots show general protein amounts. One of three experiments is shown.

C: HaCat cells were treated with 50 μM CQ for 0, 1, 2, 10 or 24 h and gradual accumulation of LC3-II was visualized by anti-LC3 immunoblot. Anti-actin blot controls for sample loading. One of two experiments is shown.

D: LC3-II accumulation in Western blots as quantified with OpenLab software.

E: MDAMC cells were left untreated (--), cultured in Hanks Balanced Salt Solution (starv.), treated with 50 μM chloroquine (+CQ) or with the protease inhibitors E64 (28 μM), Leupeptin (40 μM) and Pepstatin A (15 μM) (+Prot. inhib.) for 10 hours. Whole cell lysates were analyzed by anti-LC3 Western blotting. Actin blot demonstrates equal protein loading. While nutrient starvation induces LC3-II only weakly, inhibition of lysosomal proteases by treatment with CQ or the protease inhibitors E64, Leupeptin and Pepstatin A leads to a strong accumulation of LC3-II. One of two experiments is shown.

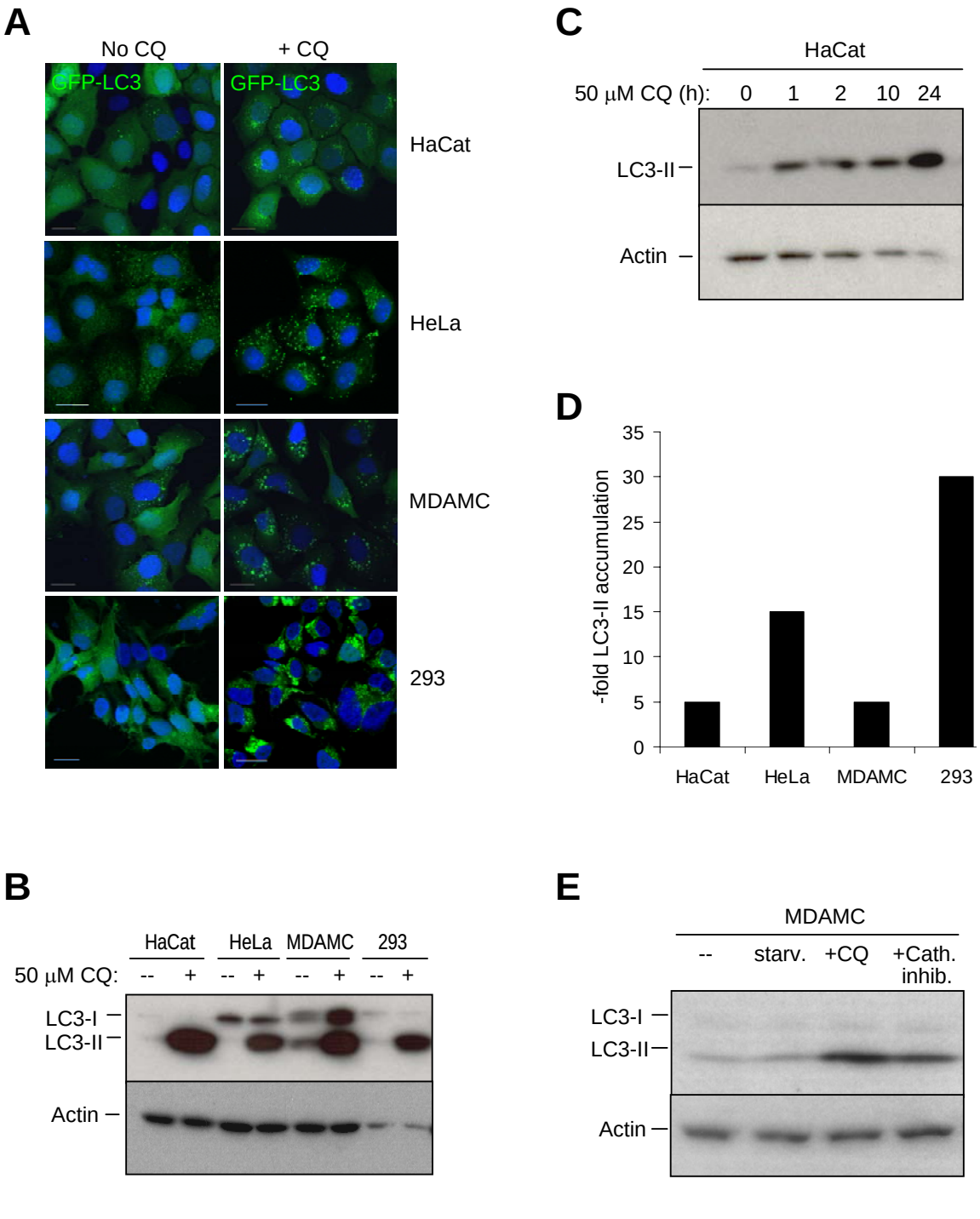
A
No CQ
+ CQ
GFP-LC3
GFP-LC3
HaCat
HeLa
MDAMC
293
C
HaCat
50 μM CQ (h): 0 1 2 10 24
LC3-II
Actin
D
-fold LC3-II accumulation
35
30
25
20
15
10
5
0
HaCat
HeLa
MDAMC
293
B
HaCat
HeLa
MDAMC
293
50 μM CQ: -- + -- + -- + -- +
LC3-I
LC3-II
Actin
E
MDAMC
--
starv.
+CQ
+Cath. inhib.
LC3-I
LC3-II
Actin

that lysosomal protease inhibition does not equal starvation of cells.

Taken together, these experiments confirm that autophagy is a constitutively active process in all human epithelial cell lines analyzed. Although autophagy can be associated with nutritional deprivation [216], the gradual accumulation of LC3 demonstrates that autophagosomes continuously deliver LC3 for lysosomal degradation, i.e., that autophagy is constitutively active in human epithelial cell lines under nutrient-rich conditions.

3.2.4 Autophagy is a constitutively active process in professional antigen-presenting cells

Next, we sought to analyze the autophagic activity of professional antigen-presenting cells (APCs) that are constitutively MHC class II-positive, such as B cells and dendritic cells. Dendritic cells (DCs) are the most efficient professional APCs and exist in two functionally and phenotypically distinct states, immature and mature [23]. Immature DCs continuously circulate through tissues and lymphoid organs to present antigens to T cells for tolerance induction [24]. In contrast, mature DCs have an exceptional capacity to initiate adaptive and innate immune responses. Given the crucial role of DCs in both tolerance and immunity, we were wondering whether autophagy might contribute to MHC class II presentation in these cells.

To quantify autophagy in human B cells and dendritic cells, we visualized the turnover of lentivirally delivered GFP-LC3 in EBV-transformed B lymphoblastoid cell lines (LCLs) and in monocyte-derived immature and mature DCs. In all three cell types, GFP-LC3-labeled autophagosomes strongly accumulated after treatment with CQ for 10

h (Fig. 16A), indicating constitutive autophagosome formation. Although LCLs only contained up to 10 autophagosomes after CQ exposure, as previously observed [214], immature DCs accumulated up to 100 GFP-LC3$^+$ vesicles, similar to epithelial cell lines. Accumulation of GFP$^+$ vesicles did not occur upon CQ-treatment of GFP-transfected immature DCs, showing that GFP$^+$ vesicles are not due to phagocytic uptake of neighboring GFP$^+$ DCs or debris (Fig. 16B). Furthermore, LC3 immunoblots confirmed that endogenous LC3 was continuously degraded by lysosomal proteases in human B cell lines, in freshly isolated CD14$^+$ monocytes as well as in monocyte-derived immature and mature dendritic cells (Fig. 16C). These experiments demonstrated that autophagy is a steady-state process not only in epithelial cells, which present antigens on MHC class II only upon immune activation, but also in professional APCs. Furthermore, constitutive autophagy is not restricted to transformed human cell lines, but is also a feature of primary human cells, as demonstrated for primary monocytes and dendritic cells.

3.2.5 GFP-LC3 colocalizes with markers of MHC class II loading compartments in IFN-γ-treated human epithelial cell lines

To test whether autophagosomes fuse with MHC class II loading compartments (MIICs), we examined by confocal microscopy whether the autophagosome marker GFP-LC3 would colocalize with markers of MIICs. MIICs have been characterized as conventional late endosomal compartments that in addition to late endosomal and lysosomal markers, such as LAMP-1 and –2, contain the components for MHC class II loading, namely MHC class II and the peptide-loading chaperone HLA-DM [3].

Figure 16: Autophagy is a constitutive process in professional antigen-presenting cells (APCs), including dendritic cells.

A: To assess autophagosome formation in professional APCs, an EBV-transformed B lymphocyte cell line (B-LCL) stably expressing GFP-LC3 and GFP-LC3-expressing immature and mature DCs (iDC and mDC) were treated with 50 μM chloroquine for 10 h (+CQ) or were left untreated (no CQ). Cells were fixed, stained with DAPI and analyzed by confocal microscopy. Scale bars: 20 μm. Representative fields from one experiment out of two are shown.

B: GFP-transfected mature DCs were treated with 50 μM CQ for 10 hours and analyzed for GFP^+ vesicles by confocal microscopy. No GFP^+ vesicles appear in GFP-expressing iDCs after 10 hours of CQ treatment.

C: Human B cell lines (MS-LCL, RPMI6666 and L591, left) and $CD14^+$ monocytes (Mono.), immature DCs (iDC) and LPS-matured DCs (mDC) (right) were treated for 10 h with 50 μM CQ (+) or were left untreated (--). Whole cell lysates were analyzed by anti-LC3 immunoblotting. Actin blots demonstrate that CQ-treatment did not affect general protein levels. One of three experiments is shown.

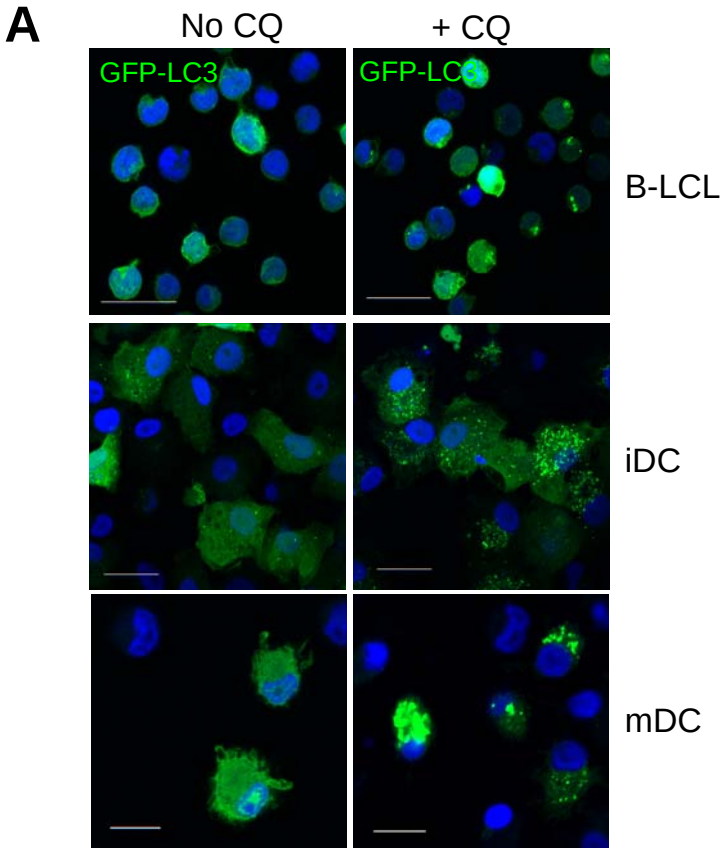
A
No CQ
+ CQ
GFP-LC3
GFP-LC3
B-LCL
iDC
mDC

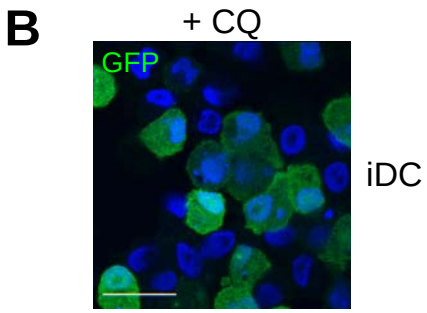
B
+ CQ
GFP
iDC

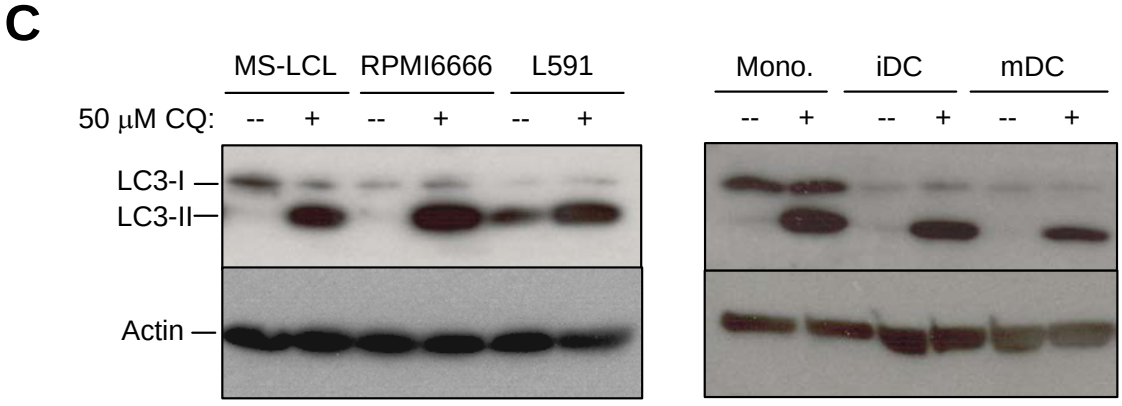
C
MS-LCL
RPMI6666
L591
Mono.
iDC
mDC
50 μM CQ:
-- + -- + -- + -- + -- + -- +
LC3-I
LC3-II
Actin

We initially focused our analysis on epithelial cells, because they might rely heavily on endogenous MHC class II antigen processing due to their limited endocytic potential compared to classical APCs, such as DCs. We confirmed that most of our human epithelial cell lines, with the exception of 293 cells, expressed MHC class II molecules after IFN-γ treatment (Fig 17A). In the human cell lines used in this study, IFN-γ treatment did not lead to a detectable upregulation of autophagy, as determined by immunoblot (Fig. 17B), although we cannot exclude that the IFN-γ treatment slightly influenced the autophagy activity, in addition to inducing MHC class II-positive compartments.

For colocalization analysis, cells were treated with IFN-γ, transiently transfected with the GFP-LC3 reporter construct, and stained with antibodies specific for the MIIC markers MHC class II, HLA-DM and LAMP-2 in MDAMC (Fig. 18A) and HaCat cells (data not shown). MHC class II positive compartments frequently colocalized with GFP-LC3 (Fig. 18A). When we quantified colocalization of MHC class II and HLA-DM with GFP-LC3 using the LSM510 software's profile tool, which overlays the intensity profiles along a cross section through a cell, we found that in double-positive cells, 58% (± 10%) of MHC class II^+ and 52% (± 20%) of HLA-DM^+ compartments contained GFP-LC3. An example of the profile analysis is shown in Fig. 18B.

To assess the proportion of MIICs that showed no colocalization with GFP-LC3 due to degradation of the autophagosome marker protein, we performed the same experiments on CQ-treated MDAMC and HaCat cells. Colocalization of GFP-LC3 with MHC class II, HLA-DM and LAMP-2 was more pronounced under these conditions (Fig. 18C and data for HaCat not shown). Colocalization analysis with the LSM 510 profile

Figure 17: Effect of recombinant IFNs on human epithelial cell lines.

A: Human epithelial cell lines (HaCat, HeLa, MDAMC and 293) were treated for 48 h with 200 U/ml recombinant human IFN-γ and MHC class II surface levels were analyzed by flow cytometry. With the exception of 293 cells, all epithelial cell lines upregulate MHC class II after IFN-γ treatment. One of two experiments is shown.

B: Human epithelial cell lines (293T, HaCat and MDAMC) were treated for 24 h with 1000 U/ml recombinant human IFN-α or IFN-γ or were left untreated (--). Whole cell lysates were prepared and equal amounts of protein were run on a 12% SDS-PAGE gel. LC3-I and –II were visualized by anti-LC3 Western blotting. The high molecular weight bands marked with an asterisk (*) are proteins that cross-react with the LC3 antiserum and demonstrate equal protein loading. LC3-II levels and hence autophagy are not affected by IFN treatment.

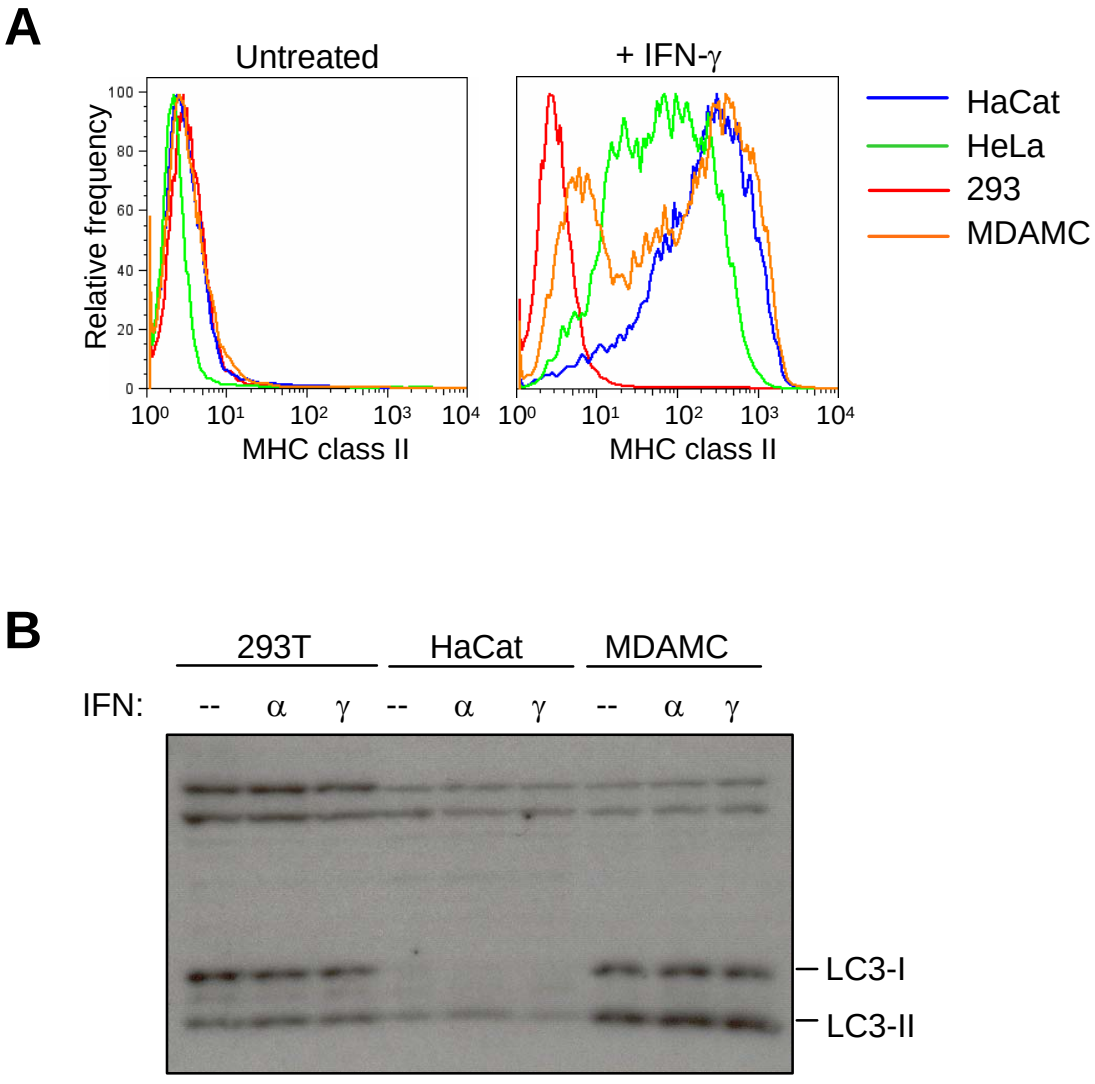
A
Untreated
+ IFN-γ
Relative frequency
100
80
60
40
20
0
10⁰
10¹
10²
10³
10⁴
MHC class II
HaCat
HeLa
293
MDAMC
B
293T
HaCat
MDAMC
IFN:
--
α
γ
LC3-I
LC3-II

Figure 18: GFP-LC3 colocalizes with markers of MHC class II loading compartments (MIICs) in human epithelial cell lines.

A: MDAMC cells were treated with 200 U/ml IFN-γ, transiently transfected with a GFP-LC3 reporter construct and 48 h later stained with antibodies to MHC class II, HLA-DM, LAMP-2 and DAPI for DNA content. Colocalization of GFP-LC3 with MIIC markers was analyzed by confocal microscopy. Scale bars: 10 μm. Representative cells from one experiment out of three are shown.

B: Example of the colocalization analysis performed with the LSM 510 software's profile tool. Graph shows fluorescence intensities of GFP-LC3 (green) and MHC class II (red) along the profile path shown to the left. In the given example, 12 out of 18 MHC II^+ vesicles contain significant amounts of GFP-LC3 (fluorescence intensity >100).

C: Same as A, except that 50 μM chloroquine (CQ) was present during the last 10 h of the culture. Scale bars: 10 μm. Representative cells from one experiment out of three are shown.

A

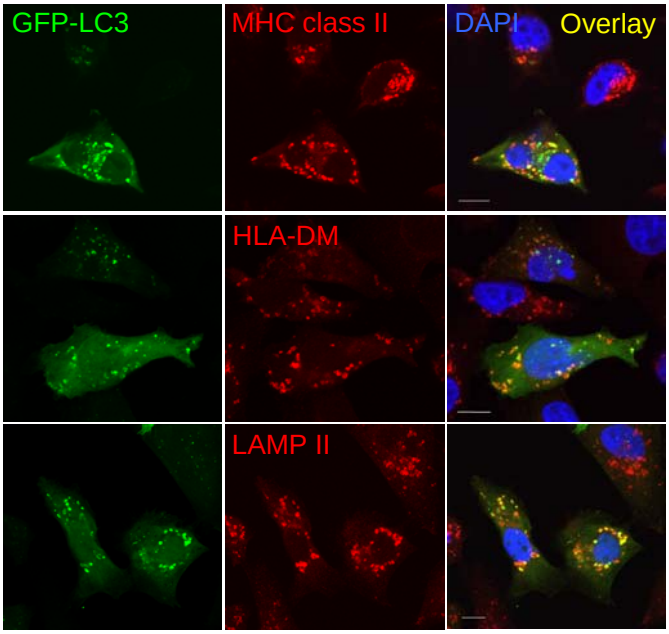
GFP-LC3
MHC class II
DAPI
Overlay
HLA-DM
LAMP II

No CQ

B

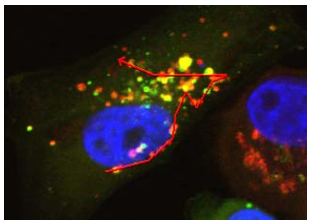

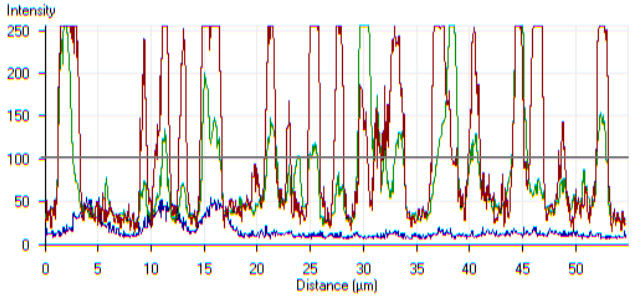
Intensity
250
200
150
100
50
0
0
5
10
15
20
25
30
35
40
45
50
Distance (µm)

C

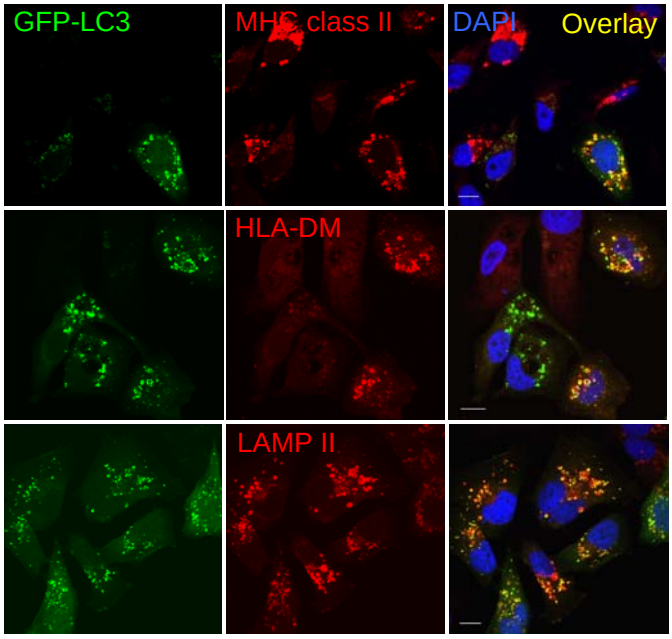
GFP-LC3
MHC class II
DAPI
Overlay
HLA-DM
LAMP II

+ CQ

tool showed that after CQ treatment, colocalization increased to 86% (± 9%) for MHC class II^+ and to 71% (± 12%) for HLA-DM^+ vesicles. This demonstrates that the majority of MHC class II loading compartments obtain input from autophagosomes in human epithelial cell lines. The CQ-induced accumulation of GFP-LC3 inside MIICs furthermore shows that GFP-LC3 is degraded in MHC class II loading compartments, suggesting that other autophagosomal cargo proteins might also be degraded in MIICs for MHC class II loading.

3.2.6 GFP-LC3 and MHC class II colocalize in electron-dense multivesicular compartments

To identify GFP-LC3 and MHC class II double-positive compartments by electron microscopy, we prepared ultrathin cryosections of untreated or CQ-treated, stably GFP-LC3 transfected MDAMC cells, stained them with antibodies specific for HLA-DR and GFP, and applied antibodies labeled with 10 and 15 nm protein A-Gold particles (in collaboration with Dr. Marc Pypaert, Yale University, New Haven). In both untreated and CQ-treated cells, the two antibodies strongly labeled large (1-2 μm), electron-dense, multivesicular compartments (Fig. 19A). Other organelles, such as nuclei and mitochondria, were mostly gold-negative, however some GFP-LC3 staining was observed in the cytosol and MHC class II staining could be seen on the ER, on the Golgi and at the cell membrane (Fig. 19B). The morphology of the double-labeled compartments was very similar in untreated and CQ-treated cells, but they were found much more frequently in CQ-treated cells and some of them displayed the characteristic swollen phenotype of lysosomal compartments under chloroquine treatment (Fig. 19C).

Figure 19: GFP-LC3 and MHC class II colocalize in electron-dense multivesicular compartments.

A: Untreated (I and II) or CQ-treated (III and IV) MDAMC cells stably expressing GFP-LC3 and MHC class II-positive due to IFN-γ induction were fixed in 4% paraformaldehyde and cut into 80 nm-thin cryosections. Sections were labeled with an HLA-DR-specific antiserum and 10 nm protein A-Gold (PAG10) and antibody-PAG complexes were irreversibly fixed with glutaraldehyde. Subsequently, sections were labeled with a GFP-specific antibody and 15 nm protein A-Gold (PAG15) and were analyzed by electron microscopy. As a control, PAG10 and PAG15 were interchanged and were shown to produce the same labeling pattern (I/II vs. III/IV). Scale bar: 1 μm. Inserts from panels I and III are shown at higher magnification in panels II and IV, respectively. Representative fields from one experiment out of three are shown.

B: Same experiment as in A, with MHC class II labeled by 15 nm gold and GFP-LC3 by 10 nm. MHC class II labeling (15 nm gold) can be seen both on GFP-LC3-positive electron-dense multivesicular compartments and on the plasma membrane. Scale bar: 1 μm.

C: MDAMC-GFP-LC3 cells were treated with 50 μM CQ for 10 h and ultrathin crysections were double-labeled for MHC class II (10 nm gold) and GFP (15 nm gold). After CQ treatment, double-labeled multivesicular compartments frequently appear expanded and swollen, with a diameter of >1 μm and some empty space. Three representative fields from one experiment out of three are shown. Scale bar: 1 μm.

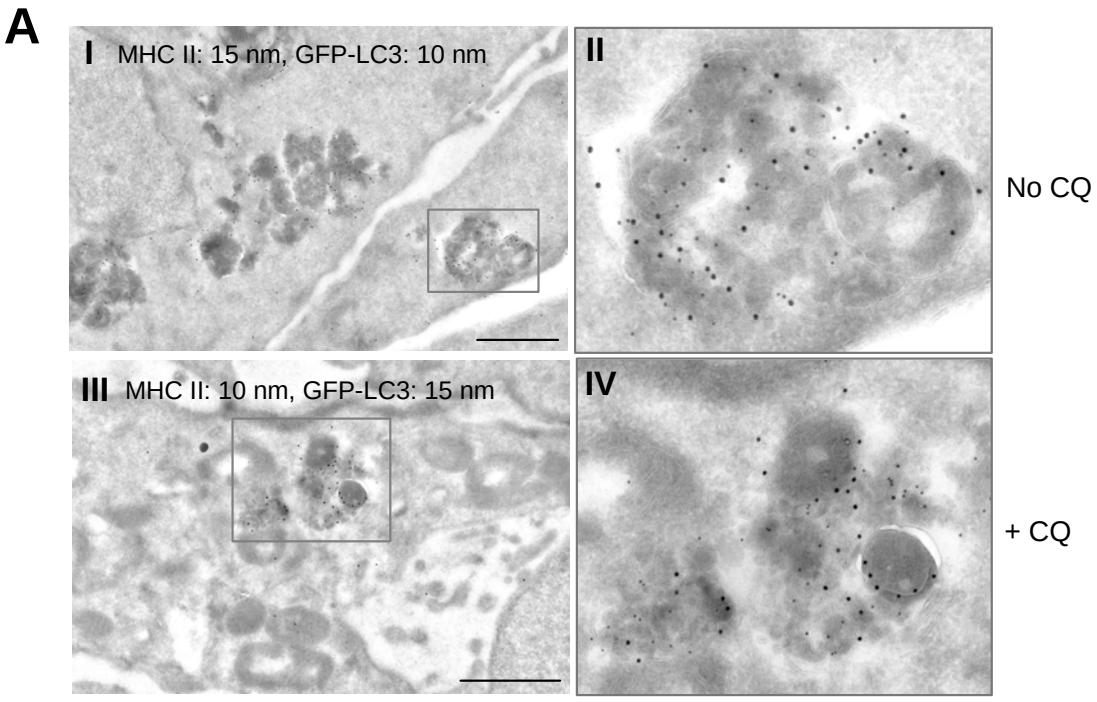
A
I MHC II: 15 nm, GFP-LC3: 10 nm
II
No CQ
III MHC II: 10 nm, GFP-LC3: 15 nm
IV
+ CQ

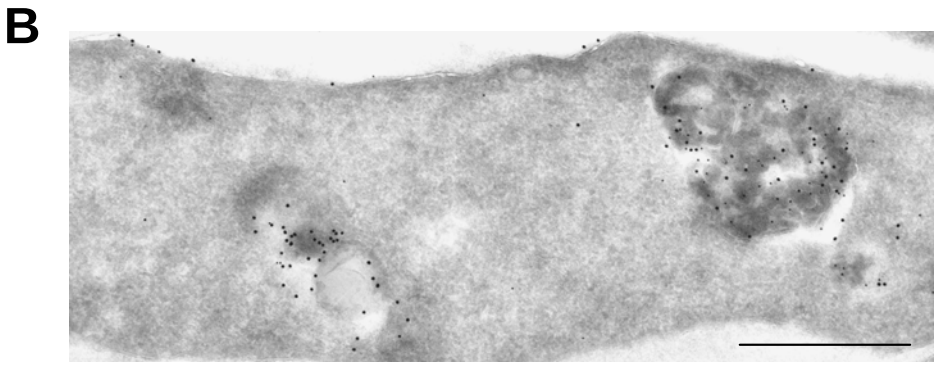
B

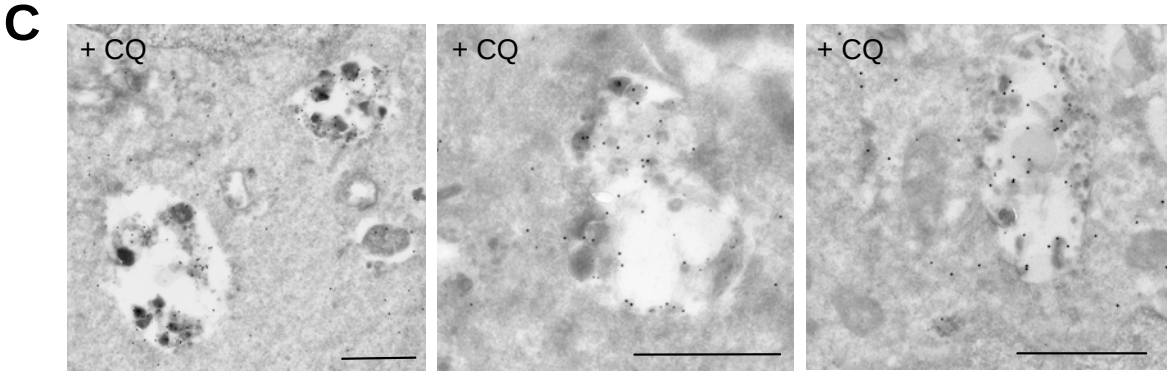
C
+ CQ
+ CQ
+ CQ

At higher magnification, the presence of electron-dense material, numerous small vesicles and sometimes larger lipid membranes became apparent (Fig. 19A). Both GFP-LC3 and MHC class II molecules were often found in close proximity to each other on intraluminal lipid membranes. This suggests that autophagosomes frequently fuse with MHC class II compartments, giving rise to multivesicular compartments that contain both MHC class II molecules and LC3 on internal membranes.

3.2.7 GFP-LC3 is degraded in MHC class II loading compartments of dendritic cells

After having observed an overlap of autophagosomes with MHC class II loading compartments in human epithelial cell lines, we wondered whether we could observe the same colocalization in professional APCs, most notably dendritic cells. To address this question, we transfected $CD14^+$ monocytes with a lentiviral GFP-LC3 reporter construct, generated immature and mature DCs and stained them with an MHC class II-specific antibody. Because DCs are constitutively MHC class II-positive, no IFN-γ treatment was necessary for these experiments. In the absence of the lysosomal acidification inhibitor CQ, GFP-LC3 was mainly present in the cytosol and only very few GFP-$LC3^+$ vesicles could be observed in both immature and mature DCs (Fig. 20, upper rows, also see Fig. 16A). Therefore, no colocalization analysis could be performed for untreated DCs. However, when cells were treated for 10 hours with chloroquine, MHC class II compartments of immature DCs frequently contained the autophagosome marker GFP-LC3 (Fig. 20 bottom rows). Colocalization analysis showed that 41% (±7%) of MHC class II-labeled compartments were positive for GFP-LC3. In the majority of mature

Figure 20: GFP-LC3 colocalizes with MHC class II loading compartments in dendritic cells.

Untreated or chloroquine (+CQ)-treated GFP-LC3-expressing immature and mature dendritic cells (iDCs and mDCs) were stained with an MHC class II-specific antibody and DAPI and were analyzed by confocal microscopy. Scale bar: 10 μm. Without CQ, (upper rows), no or few GFP-LC3$^+$ vesicles were observed and therefore, no colocalization analysis with MHC class II could be performed. After CQ treatment, many GFP-LC3$^+$ vesicles accumulated (bottom rows), which partially overlapped with MHC class II molecules. In the majority of mature DCs, MHC class II was mainly localized at the cell surface (second and fourth row), but a subset of cells had intracellular MHC class II compartments (fourth row, white arrow). Scale bar: 10 μm. Representative cells from one experiment out of three are shown.

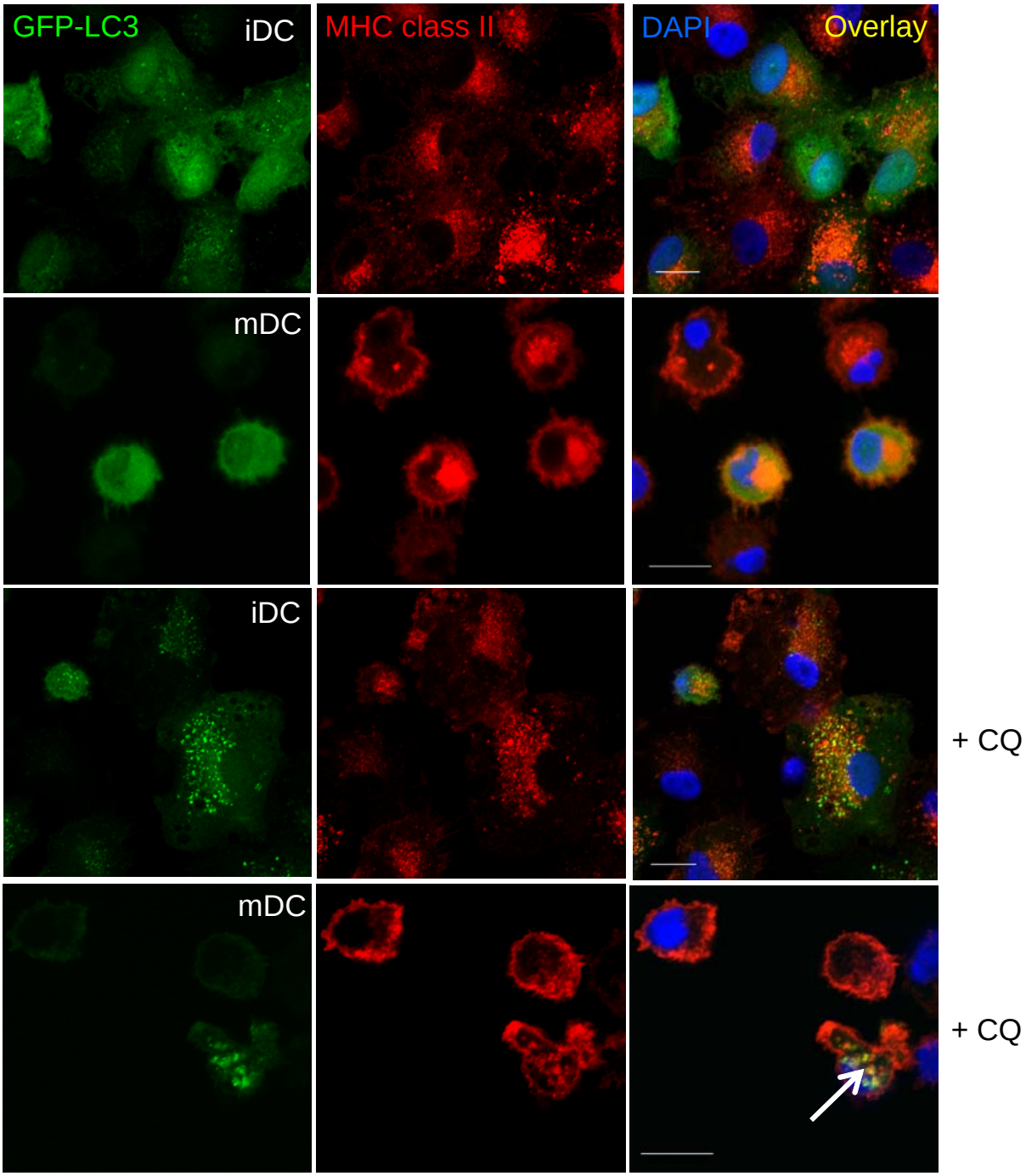
GFP-LC3
iDC
MHC class II
DAPI
Overlay
mDC
iDC
+ CQ
mDC
+ CQ

DCs, MHC class II molecules were mainly localized at the cell surface (Fig. 20, second and fourth row) and therefore the overlap with autophagosomes was minimal. However, in a subset of cells that still had some intravesicular MHC class II staining, GFP-LC3 was frequently localized within these MIICs after CQ treatment (Fig. 20, white arrow in fourth row). The accumulation of GFP-LC3 in MIICs of CQ-treated immature and mature DCs showed that autophagosomes feed into the MHC class II pathway not only in epithelial cell lines but also in professional APCs, namely dendritic cells.

3.2.8 GFP-LC3 minimally colocalizes with markers of early endosomes or MHC class I loading compartments

To determine if autophagosomes selectively fuse with MIICs, we analyzed the overlap of GFP-LC3 with markers of other endocytic compartments, specifically early endosomes (positive for early endosomal antigen, EEA1) and recycling endosomes (positive for transferrin receptor, TR). For the MDAMC cell line, GFP-LC3 did not show a pronounced overlap with either EEA1 or transferrin receptor, even in the presence of chloroquine (Fig. 21A). When we quantified colocalization of EEA1 with GFP-LC3, colocalization was low in untreated MDAMC cells (9%), but slightly increased after chloroquine treatment (to 26%) (Fig. 21B). The difference between GFP-LC3 colocalization with MHC class II or HLA-DM versus EEA1 was statistically significant in the presence and absence of CQ ($p < 0.001$) (Fig. 21B). In HaCat cells, the overlap of GFP-LC3 with EEA1 or transferrin receptor was also minimal (data not shown). Furthermore, also in IFN-γ treated cells, GFP-LC3 rarely entered early or recycling endosomes (data not shown).

Figure 21: GFP-LC3 minimally colocalizes with markers of early endosomes or MHC class I loading compartments.

A: MDAMC cells were transiently transfected with a GFP-LC3 reporter construct and 36 h later treated with 50 μM chloroquine for 10 h. Cells were stained with antibodies to early endosomal antigen (EEA1) or transferrin receptor (TR) and DAPI and analyzed by confocal microscopy. Scale bars: 10 μm. Representative cells from one experiment out of two are shown.

B: Quantitative analysis for colocalization of GFP-LC3 with MHC class II, HLA-DM and EEA1 in untreated or CQ-treated MDAMC cells. Results were obtained using the LSM 510 software's profile tool. Data represent means from 10-15 cells from one representative experiment out of two. Error bars indicate standard deviations. P-values from homocedastic, one-tailed student's T test statistics are shown.

C: As in A, except that cells were stained with an MHC class I-specific antibody.

A

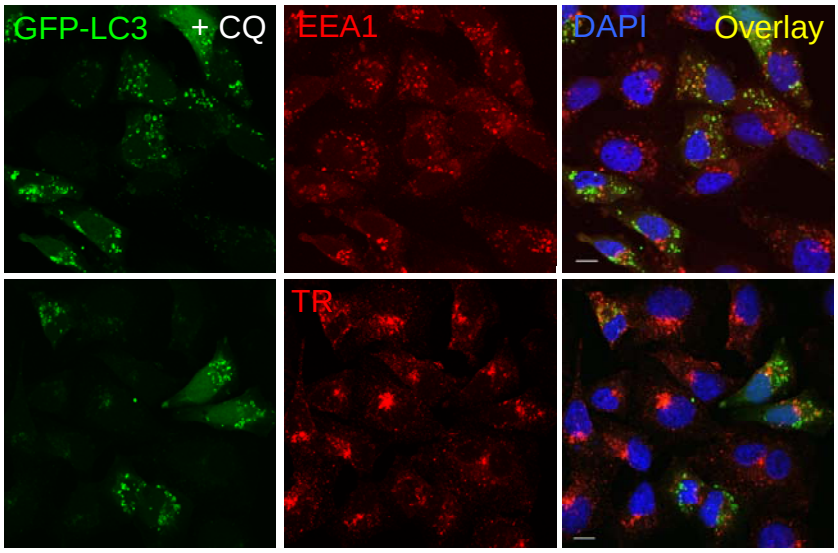
GFP-LC3
+ CQ
EEA1
DAPI
Overlay
TR

B

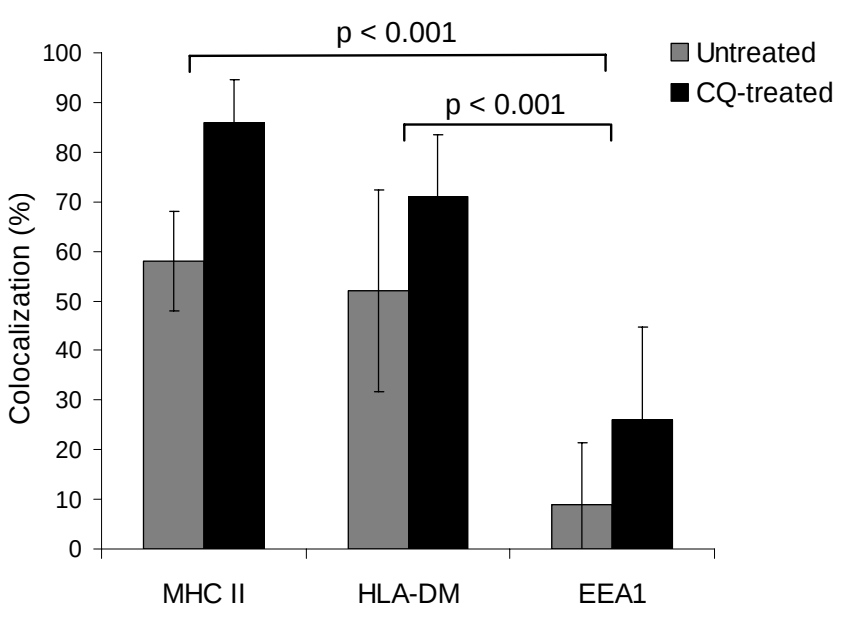
p < 0.001
p < 0.001
Untreated
CQ-treated
Colocalization (%)
100
90
80
70
60
50
40
30
20
10
0
MHC II
HLA-DM
EEA1

C

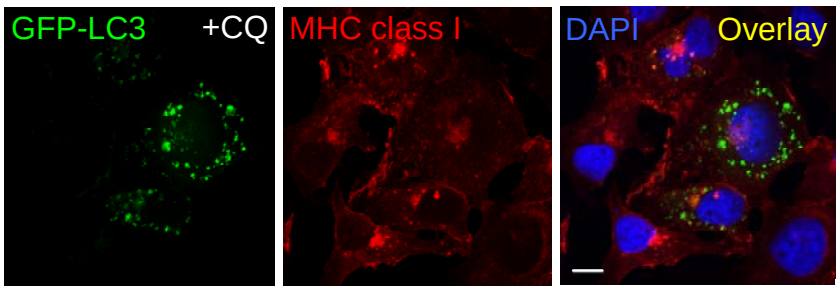
GFP-LC3
+CQ
MHC class I
DAPI
Overlay

Macroautophagy has been implicated in the presentation of intracellular antigens on MHC class II, but does not seem to influence MHC class I presentation [50, 214]. To further address this issue, we analyzed the overlap of GFP-LC3 with MHC class I-molecules. As expected, MHC class I was mainly found in perinuclear ER and Golgi regions and on the plasma membrane and did not colocalize with the more peripherally distributed GFP-LC3-positive vesicles (Fig. 21C). Together, our data suggest that autophagosomes mainly fuse with MIICs in MHC class II-positive cells, but only rarely with early and recycling endosomes or MHC class I compartments.

3.2.9 Cytosolic/nuclear antigens can be targeted for autophagic degradation by fusion to LC3

The observation that autophagosomes continuously fuse with MHC class II loading compartments suggests that this pathway might deliver cytosolic antigens efficiently for MHC class II presentation to $CD4^+$ T cells. To test this hypothesis, we investigated whether the targeting of a cytosolic antigen for autophagy would lead to enhanced $CD4^+$ T cell recognition. For this purpose, we generated a fusion construct of the Influenza matrix protein 1 with the autophagosome marker protein LC3, reasoning that the LC3 portion of such a fusion protein should target the antigen to autophagic membranes and subsequently degradation in MIICs. We stably expressed the MP1-LC3 fusion protein or the MP1 wild-type protein (Fig. 22A) in the human epithelial cell lines HaCat and MDAMC. Immunoblot analysis showed that the antigens were expressed in both cell lines and had the expected molecular weights (MP1: 28 kD; MP1-LC3: 43 kD) (Fig. 22B). Notably, the MP1-LC3 fusion protein was present at slightly lower amounts than

Figure 22: Targeting of influenza A matrix protein 1 (MP1) to autophagosomes by fusion to Atg8/LC3.

A: Schematic diagram of the two constructs encoding for MP1 and MP1-LC3, respectively. The influenza A virus matrix protein 1 (MP1) coding sequence was fused to the N-terminus of the human LC3 sequence, either with or without a stop codon at the 3' end of MP1.

B: HaCat and MDAMC cell lines were stably transfected with lentiviral MP1 and MP1-LC3 constructs and protein expression was analyzed by Western blot with anti-MP1 antiserum. Actin blot shows equal protein loading. Note that MP1-LC3 levels are slightly lower than MP1 levels.

C: MDAMC cells stably expressing GFP-LC3 were infected with lentivirus encoding for MP1 or MP1-LC3. To inhibit degradation of autophagosome substrates in lysosomes, cells were treated with 50 μM chloroquine for 10 h (+CQ). Cells were stained with anti-MP1 antiserum and DAPI and analyzed by confocal microscopy. MP1-LC3 localizes to GFP-LC3$^+$ compartments, whereas MP1 is homogenously distributed in cytosol and nucleus and does not accumulate in autophagosomes even after CQ treatment. Scale bars: 10 μm. Representative fields from one experiment out of two are shown.

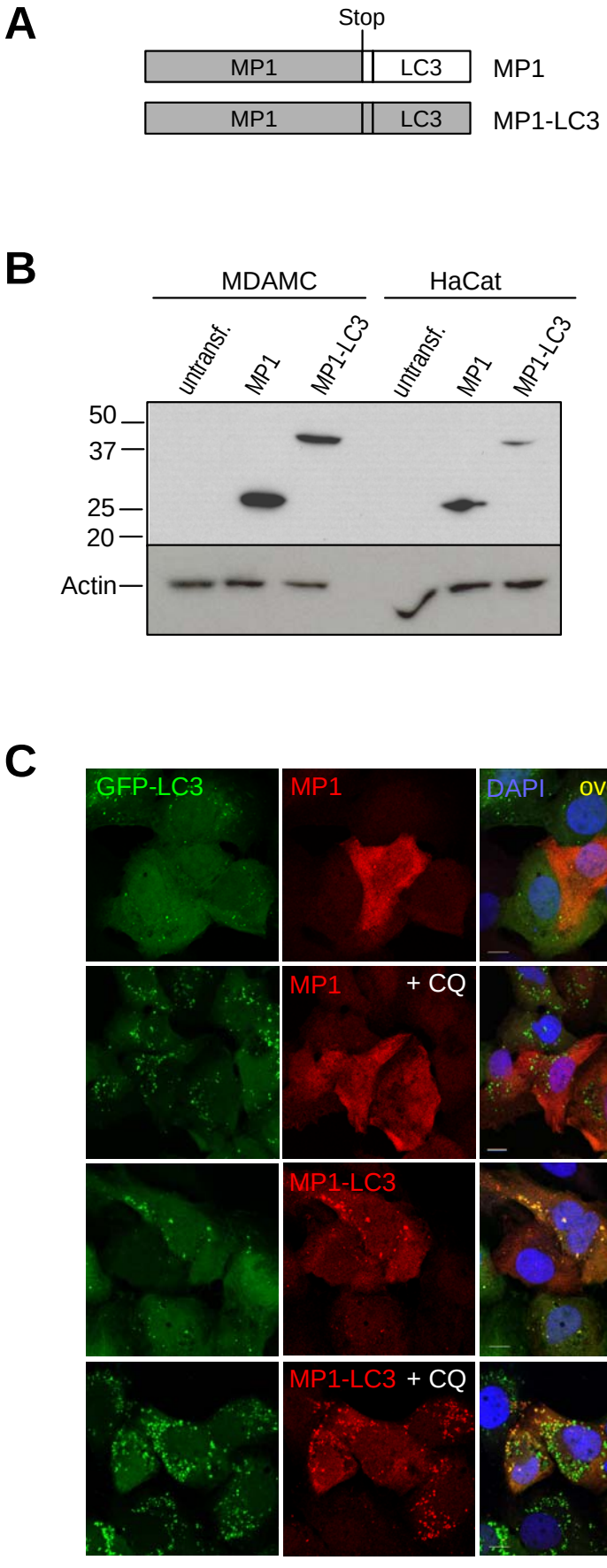
A
Stop
MP1
LC3
MP1
MP1
LC3
MP1-LC3
B
MDAMC
HaCat
untransf.
MP1
MP1-LC3
untransf.
MP1
MP1-LC3
50
37
25
20
Actin
C
GFP-LC3
MP1
DAPI
overlay
MP1
+ CQ
MP1-LC3
MP1-LC3
+ CQ

MP1 in both cell lines. In order to test whether the fusion protein would indeed localize to autophagosomes, we coexpressed GFP-LC3 and the MP1-constructs in MDAMC cells (Fig. 22C) and HaCat cells (data not shown) and analyzed their colocalization by confocal microscopy. As expected, wild-type MP1 was homogenously distributed in the cytosol and nucleus, and this pattern did not change after CQ-treatment (Fig. 22C, top rows). In contrast, the MP1-LC3 fusion protein showed punctate cytosolic staining, which overlapped with GFP-LC3-positive autophagosomes (Fig. 22C, bottom rows). Furthermore, after CQ-treatment for 10 hours, GFP-LC3 and MP1-LC3 accumulated in the same cytosolic vesicles, demonstrating that the LC3 tag indeed targets the influenza matrix protein 1 to autophagosomes for subsequent degradation by lysosomal proteases.

3.2.10 Targeting of antigens for autophagic degradation leads to enhanced $CD4^+$ T cell recognition

To test the hypothesis that targeting of cytosolic and nuclear antigens for autophagic degradation via LC3 fusion leads to enhanced MHC class II presentation, we analyzed the recognition of MP1- versus MP1-LC3-expressing target cells by MP1-specific $CD4^+$ T cell clones (Fig. 23). For this purpose, we generated MP1-specific $CD4^+$ T cell clones from a healthy lab donor that was HLA-DR and –DQ matched to the HaCat cell line, so that IFN-γ–treated HaCat cells could be used as target cells. To analyze the effect of the LC3 fusion on MHC class I presentation, we also generated an HLA-A2-restricted $CD8^+$ T cell clone from the same donor (Fig. 23), which then could be tested for recognition of HLA-A2-positive MDAMC target cells. Furthermore, autologous EBV-transformed B-

Figure 23: Characterization of Influenza MP1-specific $CD4^+$ and $CD8^+$ T cell clones.

A: CD4 and CD8 expression of T cell clones as analyzed by flow cytometry. Clones 9.26, 10.9 and 11.46 were homogenously $CD4^+CD8^-$ and clone 9.2 was homogenously $CD8^+CD4^-$.

B: Recognition of MP1 peptides by T cell clones in IFN-γ ELISPOT assays. An MP1 peptide library (64 15-mer peptides overlapping by 10 amino acids) was divided in 6 subpools covering MP1 amino acid positions 1-51 (pool I), 41-88 (pool II), 78-128 (pool III), 118-163 (pool IV), 152-203 (pool V) and 193-252 (pool VI). Clones 9.2, 9.26 and 10.9 responded specifically to pool II and clone 11.46 to pool III. In addition, the $CD8^+$ T cell clone 9.2, but not the $CD4^+$ T cell clones, recognized the HLA-A2-restricted MP1 epitope 58-66. Error bars indicate standard deviations.

C: MP1-specific $CD4^+$ T cell clones were tested for recognition of individual peptides covering MP1 amino acid sequence 29-128, including all peptides of MP1 pools II and III. Clones 9.26 and 10.9 specifically recognized peptide epitope $MP1_{62-72}$ and clone 11.46 was specific for epitope $MP1_{103-113}$. Error bars indicate standard deviations.

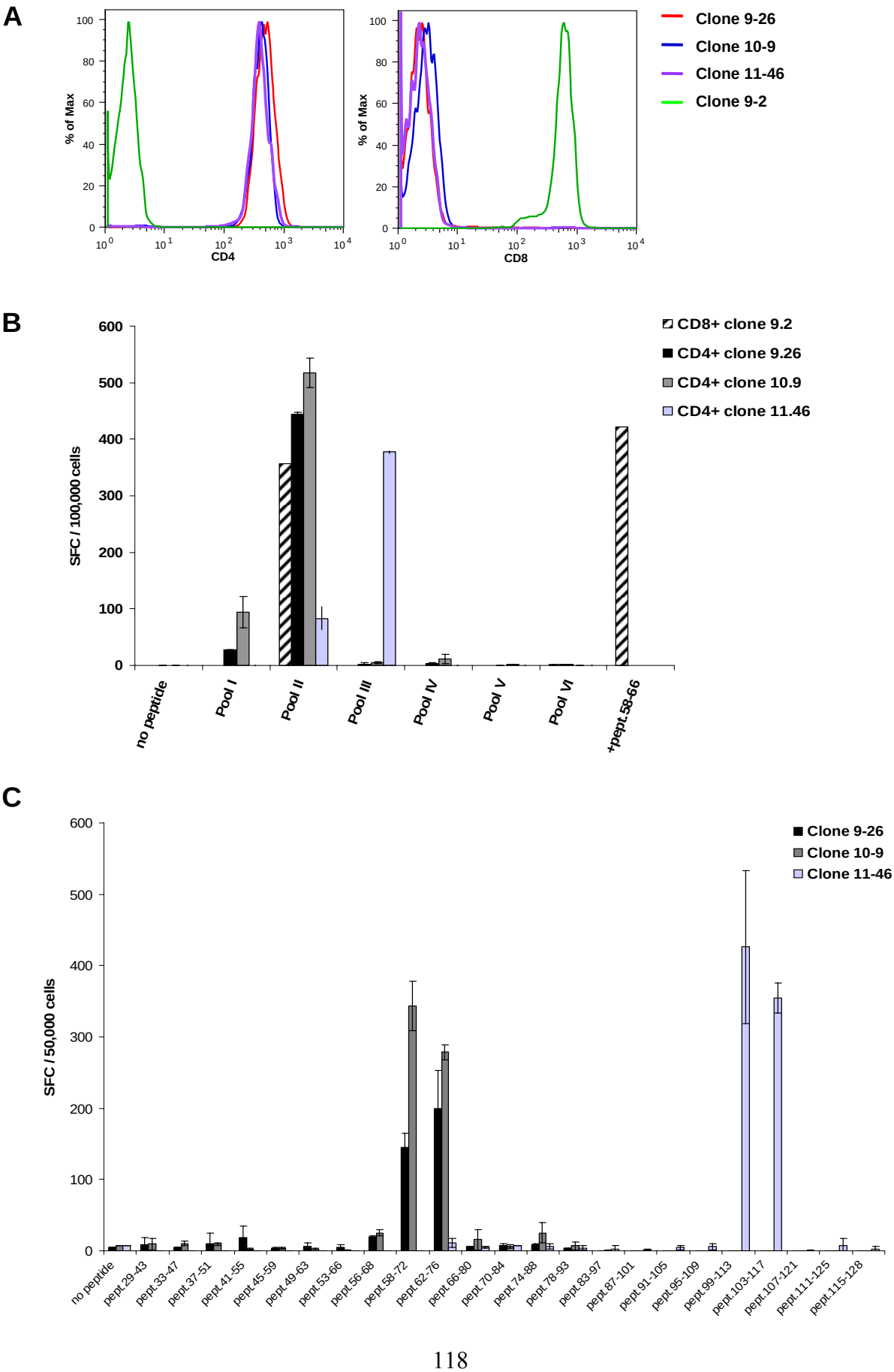
A
% of Max
CD4
CD8
Clone 9-26
Clone 10-9
Clone 11-46
Clone 9-2
B
SFC / 100,000 cells
CD8+ clone 9.2
CD4+ clone 9.26
CD4+ clone 10.9
CD4+ clone 11.46
no peptide
Pool I
Pool II
Pool III
Pool IV
Pool V
Pool VI
*pept.58-66
C
SFC / 50,000 cells
Clone 9-26
Clone 10-9
Clone 11-46
no peptide
pept.29-43
pept.33-47
pept.37-51
pept.41-55
pept.45-59
pept.49-63
pept.53-66
pept.56-68
pept.58-72
pept.62-76
pept.66-80
pept.70-84
pept.74-88
pept.78-93
pept.83-97
pept.87-101
pept.91-105
pept.95-109
pept.99-113
pept.103-117
pept.107-121
pept.111-125
pept.115-128

LCLs and monocyte-derived DCs from the same donor could be used as target cells for both $CD4^+$ and $CD8^+$ T cell clones.

To assess how well the two different forms of MP1 could be presented on MHC class II, we measured IFN-γ secretion of three MP1-specific $CD4^+$ T cell clones in response to MP1 or MP1-LC3-expressing target cells (HaCat epithelial cells, B-LCLs or DCs). The response of the $CD4^+$ T cell clones (clone 9.26, 10.9 and 11.46) was strongly increased by the LC3 fusion (Fig. 24A). This effect was seen for all types of target cells, epithelial, B and DCs. Although at the lowest ratio of T cell clone to cellular targets (effector to target or E:T ratio) MP1-LC3 typically elicited only 2-4 fold higher IFN-γ production, the difference in IFN-γ secretion was especially pronounced at higher E:T ratios, when the target cells and thus MHC class II-peptide complexes became limiting. At these E:T ratios, IFN-γ secretion by the $CD4^+$ T cell clones in response to MP1-LC3 compared to MP1 was increased 12-17 fold for HaCat epithelial targets, 4-8 fold for B-LCL targets, 5-17 fold for immature DCs and 7-20 fold for mature DCs. Untransfected and GFP-LC3 transfected target cells were not recognized above background (Fig. 24A). Although the IFN-γ response to MP1 transfectants of the HaCat cell line never exceeded 30% of the amount secreted upon recognition of the peptide-pulsed HaCat positive control, MP1-LC3 transfectants were able to stimulate up to 95% of the maximal $CD4^+$ T cell recognition achieved with peptide pulsed targets. Mixing experiments demonstrated that MHC class II presentation of MP1 and MP1-LC3 was indeed due to endogenous processing, because the mixing of HLA-matched HaCat cells with mismatched MP1- or MP1-LC3 expressing MDAMC cells did not stimulate any T cell responses (Fig. 24A, upper panel). Furthermore, when MHC class II was not induced on HaCat cells by IFN-γ,

Figure 24: Fusion of MP1 to LC3 enhances $CD4^+$ T cell recognition.

A: MP1-specific $CD4^+$ T cell clones 9.26, 10.9 and 11.46 were stimulated at various effector to target cell (ET) ratios with different MP1 or MP1-LC3 expressing target cells: HaCat cells (IFN-γ-treated to induce MHC class II), CM-LCL or immature/mature DCs. The next day, IFN-γ in culture supernatants was measured by ELISA to assess MHC class II presentation of MP1. As a positive control, target cells were pulsed with cognate peptide (+pept.) and as negative controls, untransfected and GFP-LC3-transfected target cells were used. For HaCat cells, further negative controls included no IFN-γ pretreatment to demonstrate MHC class II-restriction. Furthermore, coculture of untransfected HaCat cells with MHC class II-mismatched MP1- or MP1-LC3-expressing MDAMC cells demonstrated that the presentation occurred after endogenous, not exogenous processing. Error bars indicate standard deviations. P-values for paired, one-tailed student's T test statistics across all E:T ratios are shown. For each target cell type, one representative clone out of three is shown (HaCat: 10.9, CM-LCL: 11.46, DCs: 9.26) and the experiments were performed twice.

B: MHC class II surface levels on target cells as analyzed by flow cytometry. Enhanced $CD4^+$ T cell recognition of MP1-LC3-expressing cells is not due to a higher MHC class II level.

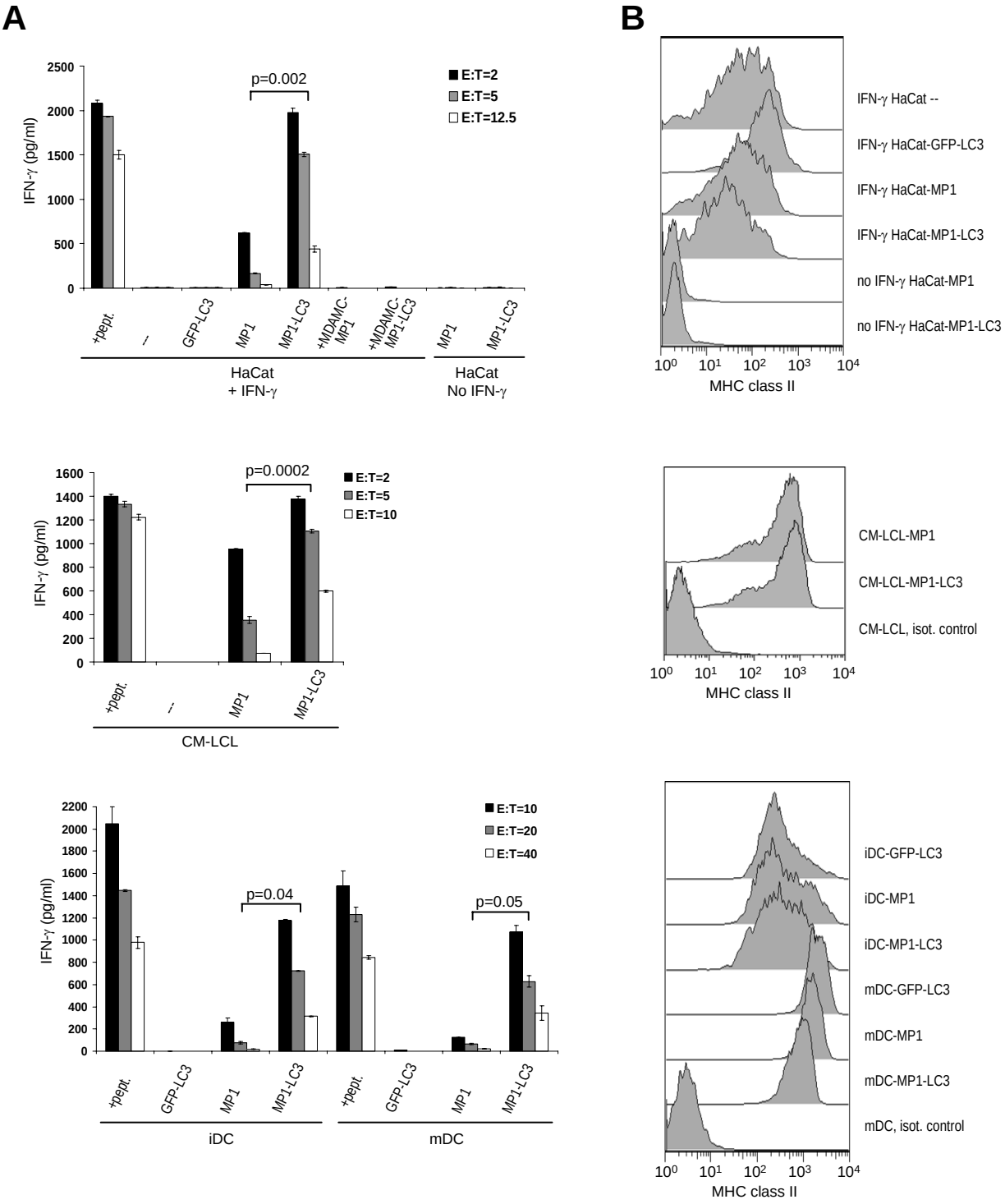
A
B
IFN-γ (pg/ml)
p=0.002
E:T=2
E:T=5
E:T=12.5
+pept.
--
GFP-LC3
MP1
MP1-LC3
+MDAMC-MP1
+MDAMC-MP1-LC3
MP1
MP1-LC3
HaCat + IFN-γ
HaCat No IFN-γ
IFN-γ HaCat --
IFN-γ HaCat-GFP-LC3
IFN-γ HaCat-MP1
IFN-γ HaCat-MP1-LC3
no IFN-γ HaCat-MP1
no IFN-γ HaCat-MP1-LC3
MHC class II
p=0.0002
E:T=2
E:T=5
E:T=10
CM-LCL
CM-LCL-MP1
CM-LCL-MP1-LC3
CM-LCL, isot. control
E:T=10
E:T=20
E:T=40
p=0.04
p=0.05
iDC
mDC
iDC-GFP-LC3
iDC-MP1
iDC-MP1-LC3
mDC-GFP-LC3
mDC-MP1
mDC-MP1-LC3
mDC, isot. control

MP1- and MP1-LC3-expresssing cells were unable to stimulate $CD4^+$ T cell responses (Fig. 24A, upper panel), confirming that the presentation was MHC class II-restricted. In addition, MHC class II surface staining showed that approximately equal MHC class II surface levels were present on all MP1- and MP1-LC3-expressing target cells (Fig. 24B), demonstrating that the enhanced recognition of MP1-LC3 was not due to enhanced MHC class II expression.

3.2.11 LC3 fusion does not influence MHC class I presentation and $CD8^+$ T cell recognition

To assess the effect of the LC3 fusion on MHC class I presentation, we analyzed the IFN-γ response of an MP1-specific $CD8^+$ T cell clone to MP1- and MP1-LC3-expressing target cells (MDAMC epithelial cells, B-LCLs or DCs). For all types of target cells and across all E:T ratios, similar amounts of IFN-γ were secreted by $CD8^+$ T cells in response to MP1- and MP1-LC3 expressing targets (Fig. 25). This suggests that the LC3 fusion does not impair MHC class I presentation and both constructs give rise to similar amounts of defective ribosomal products (DRiPs), which are then efficiently processed for $CD8^+$ T cell recognition [6]. This was observed for both IFN-γ-treated MDAMC target cells and untreated MDAMC cells, although MHC class I presentation seemed to be slightly enhanced by the IFN-γ treatment (Fig. 25, upper panel), which is consistent with an enhanced MHC class I processing machinery [3]. Taken together, our data suggest that targeting of cytosolic and nuclear antigens for autophagic degradation via LC3 fusion can strongly increase $CD4^+$ T cell recognition, without impairing $CD8^+$ T cell recognition.

Figure 25: $CD8^+$ T cell recognition is not affected by LC3 fusion.

The MP1-specific $CD8^+$ T cell clone 9.2 was stimulated at various effector to target cell (ET) ratios with different MP1 or MP1-LC3 expressing target cells: MDAMC cells (IFN-γ-treated or untreated), CM-LCL or immature/mature DCs. The next day, IFN-γ in culture supernatants was measured by ELISA to assess MHC class I presentation of MP1. As a positive control, target cells were pulsed with the HLA-A2-restricted $MP1_{58-66}$ peptide (+pept.) and as negative controls, untransfected and GFP-LC3-transfected target cells were used. MP1- and MP1-LC3-expressing target cells stimulated the $CD8^+$ T cell clone to similar levels. Error bars indicate standard deviations. One of two experiments is shown.

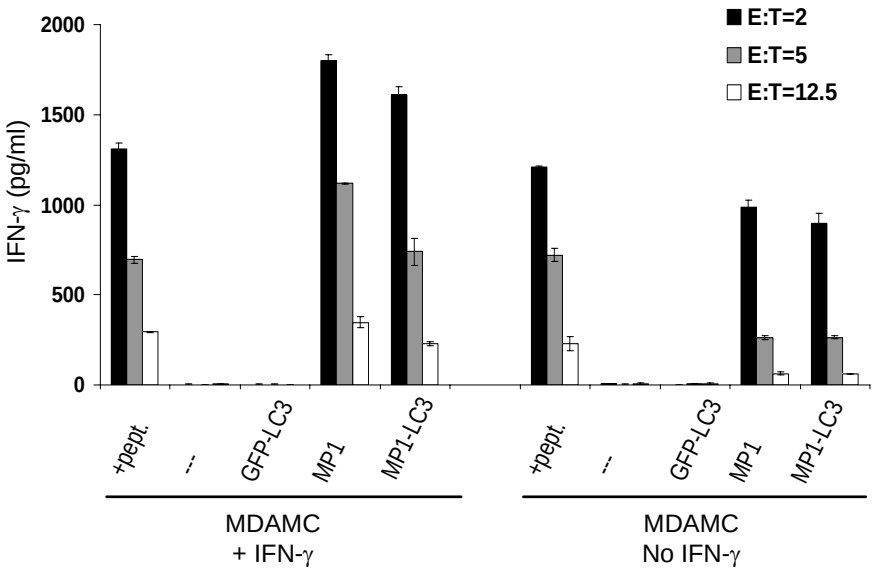
E:T=2
E:T=5
E:T=12.5
IFN-γ (pg/ml)
2000
1500
1000
500
0
+pept.

GFP-LC3
MP1
MP1-LC3
+pept.

GFP-LC3
MP1
MP1-LC3
MDAMC
+ IFN-γ
MDAMC
No IFN-γ

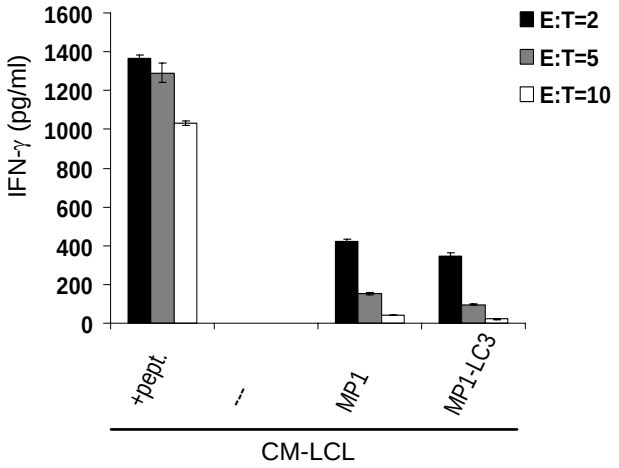
E:T=2
E:T=5
E:T=10
IFN-γ (pg/ml)
1600
1400
1200
1000
800
600
400
200
0
+pept.

MP1
MP1-LC3
CM-LCL

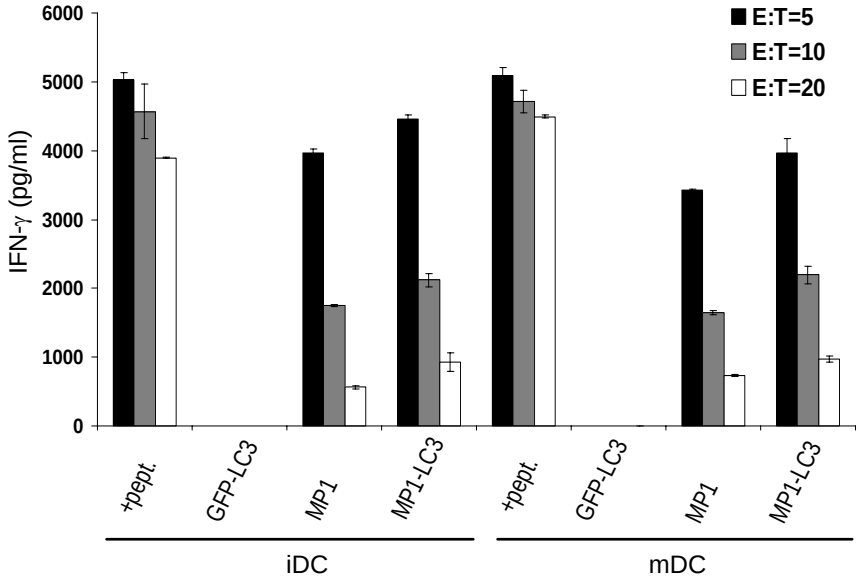
E:T=5
E:T=10
E:T=20
IFN-γ (pg/ml)
6000
5000
4000
3000
2000
1000
0
+pept.
GFP-LC3
MP1
MP1-LC3
+pept.
GFP-LC3
MP1
MP1-LC3
iDC
mDC

3.2.12 Autophagosome targeting depends on the molecular machinery of macroautophagy

In order to determine whether coupling to the autophagosomal membrane was crucial for antigen targeting to enhance MHC class II presentation, we mutated the amino acid Gly_{120} of LC3 to Ala in our fusion construct (MP1-LC3(G_{120}A)). Gly at position 120 is crucial for cleavage of the 125 amino acid LC3 precursor protein by the Atg4 protease (see Fig. 5), and it has been shown that mutation of Gly_{120} to Ala abrogates coupling of LC3 to the autophagosome membrane [84, 102]. When we expressed our MP1-LC3(G_{120}A) construct in MDAMC epithelial cells, the mutant protein failed to localize to GFP-$LC3^+$ autophagosomes (Fig. 26A). In addition, the preferential targeting for MHC class II presentation was completely abrogated by this point mutation: Influenza MP1-specific $CD4^+$ T cell recognition of MP1-LC3(G_{120}A) was similar to MP1 after transfection into HaCat cells (Fig. 26B). All constructs were expressed to similar amounts in HaCat and MDAMC cells (Fig. 26C) and elicited comparable Influenza MP1-specific $CD8^+$ T cell stimulation (Fig. 26B). These data suggest that the ubiquitin-like conjugation of LC3 to the autophagosomal membrane is crucial for LC3-mediated targeting to enhance MHC class II presentation.

To further confirm that autophagy is required for targeting of LC3 fusion antigens to MHC class II loading compartments, we analyzed colocalization of MP1-LC3 with MHC class II molecules, with and without *atg12*-specific RNA interference. In cells transfected with control siRNA, MP1-LC3 colocalized substantially with MHC class II in cytosolic vesicles of IFN-γ-treated MDAMC cells (Fig. 27). In contrast, in cells transfected with *atg12*-specific siRNA, MP1-LC3 was diffusely distributed and did not

Figure 26: Autophagosome targeting depends on covalent coupling of LC3 to the autophagosome membrane via Gly_{120}.

A: MDAMC cells stably expressing GFP-LC3 were infected with lentivirus encoding for MP1, MP1-LC3 or MP1-LC3(G_{120}A). To visualize autophagosome formation, cells were treated with 50 μM chloroquine for 10 h (+CQ) and were stained with anti-MP1 antiserum and DAPI and analyzed by confocal microscopy. Scale bars: 10 μm. Mutation of Gly_{120} to Ala abrogates autophagosome targeting and degradation of MP1-LC3.

B: The MP1-specific $CD4^+$ T cell clone 11.46 or the MP1-specific $CD8^+$ T cell clone 9.2 were stimulated at various effector to target cell (ET) ratios with target cells expressing either MP1, MP1-LC3 or MP1-LC3(G_{120}). The next day, IFN-γ in culture supernatants was measured by ELISA to assess presentation of MP1 on MHC class II or I, respectively. MP1-LC3(G_{120}) stimulates the $CD4^+$ T cell clone as weakly as MP1 does, indicating that Gly_{120} is required for enhanced MHC class II presentation. Error bars indicate standard deviations and P-values for paired, one-tailed student's T test statistics across all E:T ratios are shown. One of two experiments is shown.

C: Expression level of different MP1 constructs in HaCat and MDAMC cell lines, analyzed by Western blot with anti-MP1 antiserum. Actin blot shows equal protein loading. MP1-LC3 and MP1-LC3(G_{120}) are expressed at the same level.

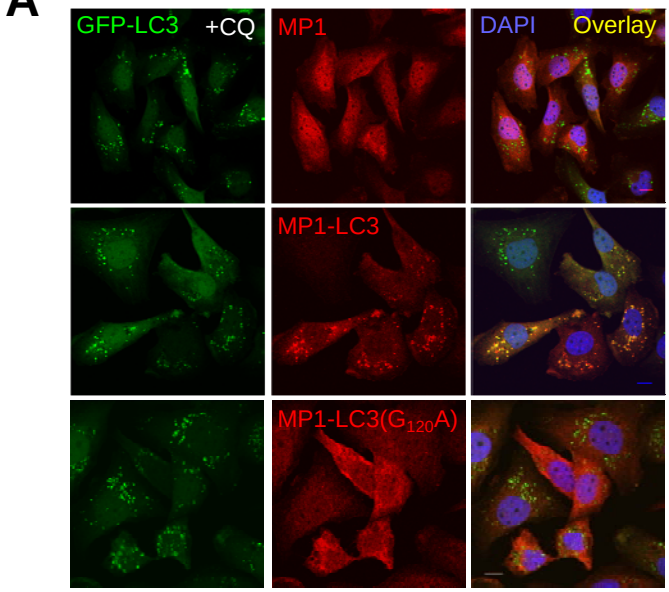
A
GFP-LC3
+CQ
MP1
DAPI
Overlay
MP1-LC3
MP1-LC3(G120A)

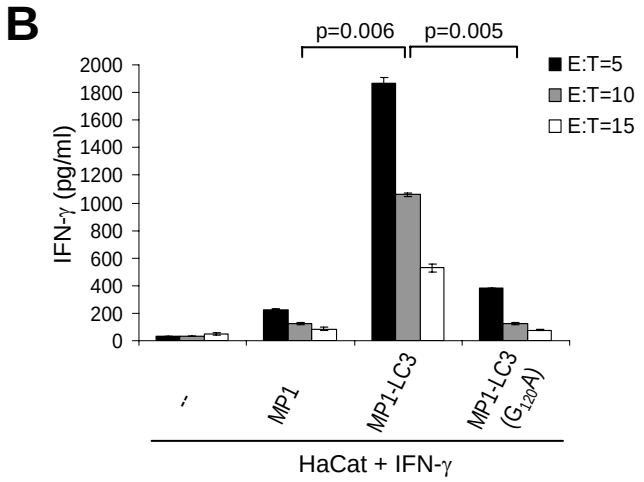
B
p=0.006
p=0.005
E:T=5
E:T=10
E:T=15
IFN-γ (pg/ml)
2000
1800
1600
1400
1200
1000
800
600
400
200
0
-
MP1
MP1-LC3
MP1-LC3 (G120A)
HaCat + IFN-γ

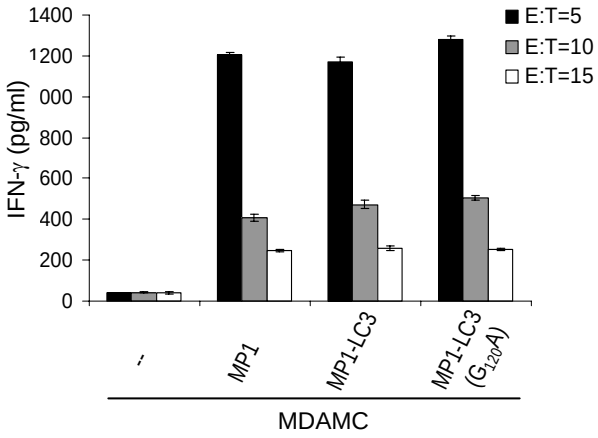
E:T=5
E:T=10
E:T=15
IFN-γ (pg/ml)
1400
1200
000
800
600
400
200
0
-
MP1
MP1-LC3
MP1-LC3 (G120A)
MDAMC

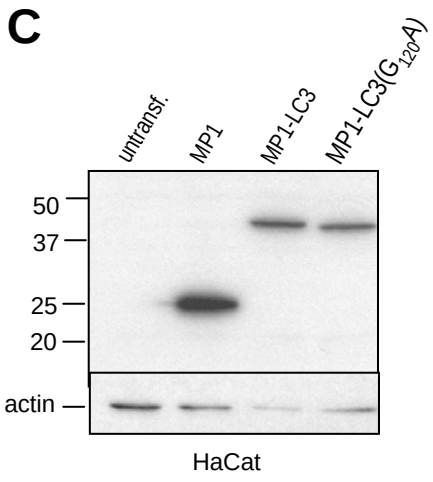
C
untransf.
MP1
MP1-LC3
MP1-LC3(G120A)
50
37
25
20
actin
HaCat

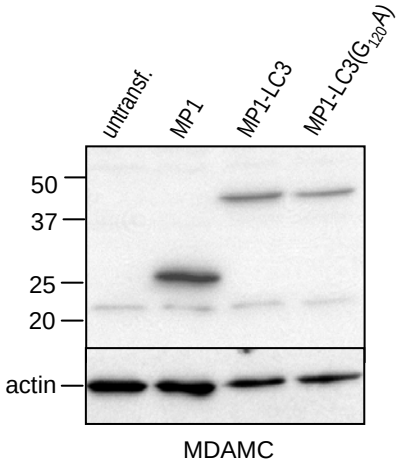
untransf.
MP1
MP1-LC3
MP1-LC3(G120A)
50
37
25
20
actin
MDAMC

Figure 27: Autophagy is required for delivery of MP1-LC3 to MHC class II loading compartments.

MDAMC cells stably expressing MP1-LC3 were transfected with control siRNA (specific for *firefly luciferase*) or siRNA specific for *atg12* (Atg12.2). After 36 h, cells were treated with 200 U/ml IFN-γ to upregulate MHC class II expression and were cultured for another 36 h. To prevent degradation of MP1-LC3 by lysosomal proteases, cells were treated with 50 μM chloroquine (CQ) during the last 6 hours of the culture, where indicated (+CQ). Cells were fixed, stained with MP1- and MHC class II-specific antibodies and DAPI and analyzed by confocal microscopy. Scale bar: 10 μm. Representative fields from one experiment out of two are shown. In control siRNA-treated cells, a substantial fraction of MP1-LC3-containing vesicles can be observed to colocalize with MHC class II compartments, whereas this colocalization is completely abrogated after *atg12* knockdown.

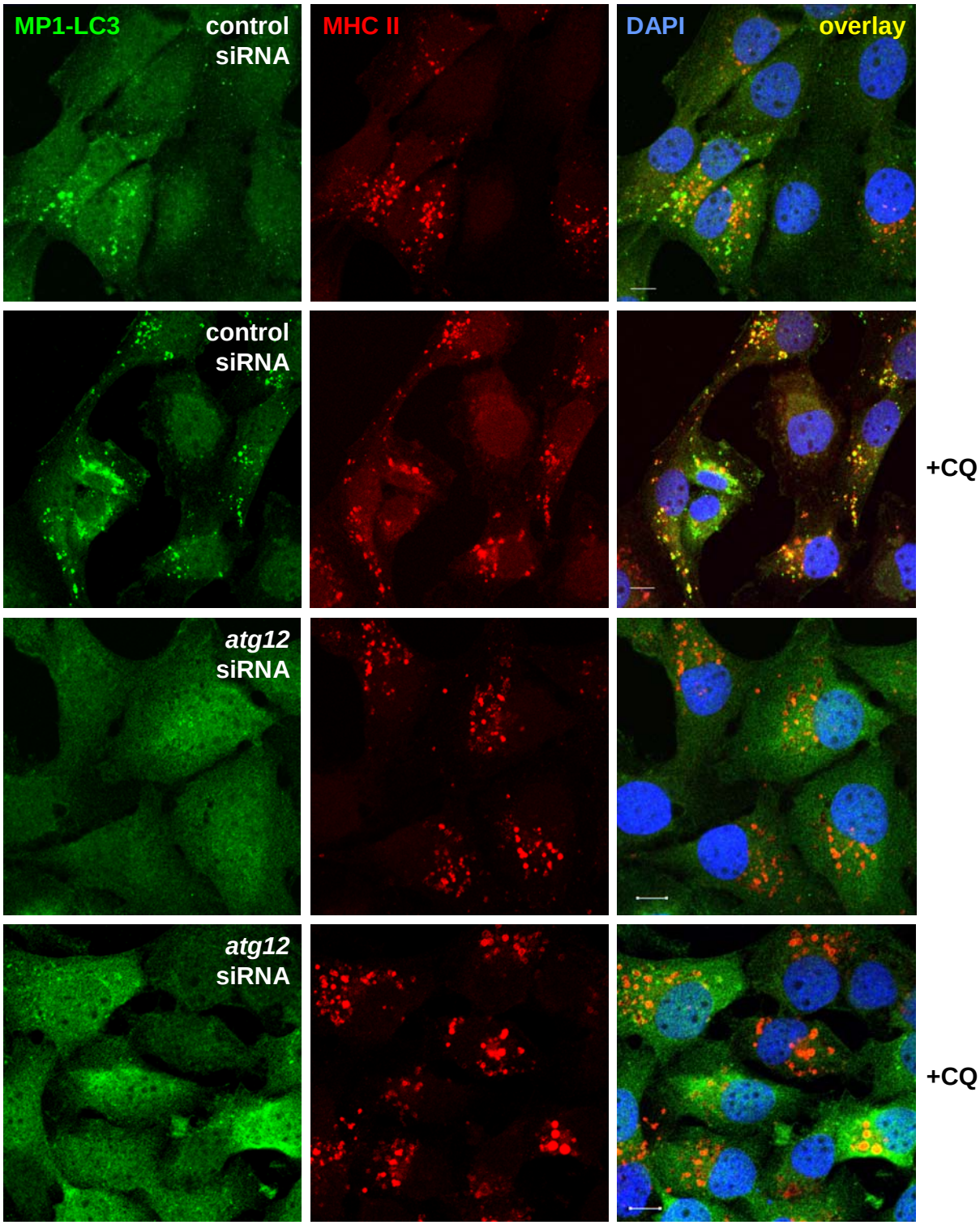
MP1-LC3
control siRNA
MHC II
DAPI
overlay
control siRNA
+CQ
atg12 siRNA
atg12 siRNA
+CQ

colocalize with punctate MHC class II compartments any more (Fig. 27). These experiments suggest that LC3 fusion antigens enter MHC class II loading compartments primarily via autophagy.

Taken together, the two ubiquitin-like conjugation systems, LC3-lipid and Atg12-Atg5, are required for targeting of LC3 fusion proteins for MHC class II loading and enhanced MHC class II presentation, because mutation of the residue involved in LC3 conjugation to the autophagic membrane as well as *atg12*-specific RNA interference inhibit this pathway.

3.2.13 Conclusions: Autophagy constitutively contributes to MHC class II presentation and can be targeted from improved T helper stimulation

By analyzing autophagosome formation in different MHC class II-positive human cell types, we have shown that constitutively MHC class II-positive APCs, such as B cell lines, monocytes and dendritic cells, as well as epithelial cell lines with IFN-γ inducible MHC class II expression display substantial amounts of steady-state autophagy. Furthermore, MHC class II loading compartments (MIICs) in epithelial and dendritic cells contain substantial amounts of GFP-LC3, suggesting that MIICs continuously receive input from the autophagy pathway. Finally, we demonstrated that by targeting this pathway via fusion to the autophagosome marker LC3, MHC class II presentation and $CD4^+$ T cell recognition of Influenza MP1 could be strongly enhanced, without compromising its $CD8^+$ T cell recognition. This novel MHC class II targeting strategy utilizes the unusual lipid coupling mechanism of the LC3 protein and is dependent on autophagosome formation. Together, our data demonstrate that autophagosomes

frequently and efficiently fuse with MHC class II loading compartments and that this pathway can be targeted for better $CD4^+$ T cell stimulation.

3.3 Autophagy regulation by influenza A virus

Our studies have demonstrated that autophagy is constitutively active in MHC class II-positive human cells and efficiently delivers cytosolic antigens for MHC class II loading in the steady state. We wondered if this process is further regulated by immune activation. We did not see an effect of IFNs on the autophagy level (Fig. 17B), although an enhancement of autophagy by IFN-γ has been reported for murine macrophages [102, 103]. Furthermore, autophagy did not seem to change during differentiation of monocytes into dendritic cells (DCs) or during DC maturation with proinflammatory cytokines, poly-IC or LPS (Fig. 16). Since activation of cells with cytokines did not lead to a detectable change in the autophagy level, we studied autophagy in the context of a more physiological immune system stimulus, namely viral infection. As a model virus, we used influenza virus, because it can productively infect different types of MHC class II-positive cells, such as lung epithelial cells and dendritic cells, allowing us to study autophagy and MHC class II presentation during the viral replication/infection cycle.

3.3.1 Autophagosomes are strongly increased after influenza A virus infection of human epithelial cell lines and dendritic cells

To investigate whether the cellular autophagy level is altered in response to influenza A virus infection, we infected stably GFP-LC3-transfected human epithelial cell lines with influenza virus strain A/Aichi/68 (H3N2). We infected cells at a low multiplicity of infection (MOI between 0.1 or 0.2), which typically resulted in an infection rate of 50-70% (Fig. 28A). At these MOIs, cell viability was still mostly unimpaired 24 hours post-infection, whereas 48 hours post-infection, a large number of apoptotic cells could be

Figure 28: Autophagosomes are strongly increased after influenza A virus infection of human epithelial cell lines and dendritic cells.

A: Titration of influenza virus A/Aichi/68 (H3N2) on human lung epithelial cells. A549 cells were infected with virus at different MOIs and 24 hours later cells were stained with an MP1-specific antibody. Percentage of MP1-positive cells was determined in 6 different fields for each MOI.

B: Cell viability of A549 cells 24 hours and 48 hours post-infection. Cells were infected with influenza virus A/Aichi/68 at low MOI (0.1-0.2). 24 hours and 48 hours later were stained for Annexin-V and the dead cell marker 7-AAD and analyzed by flow cytometry. One of two experiments is shown.

C: Left: Stably GFP-LC3-transfected epithelial cell lines A549, MLE12 and MDAMC were infected with influenza virus A/Aichi/68 and after 24 hours were analyzed in an epifluorescence microscope. **Right:** GFP-LC3+ A549 cells were infected with different strains of influenza virus (A/Aichi/68, A/WSN/33 and A/PR8/34) and 24 hours later were analyzed in an epifluorescence microscope. One of two experiments is shown.

D: The human epithelial cell lines HaCat and 293T and monocyte-derived immature DCs were infected with influenza virus A/Aichi/68 at low MOI. 24 hours post-infection, lysates of uninfected or infected cells were prepared and analyzed by Western blot for the LC3 protein. All cell types show an increase in LC3-II. The cross-reacting band marked with an asterisk (*) shows equal protein loading. One of two experiments is shown.

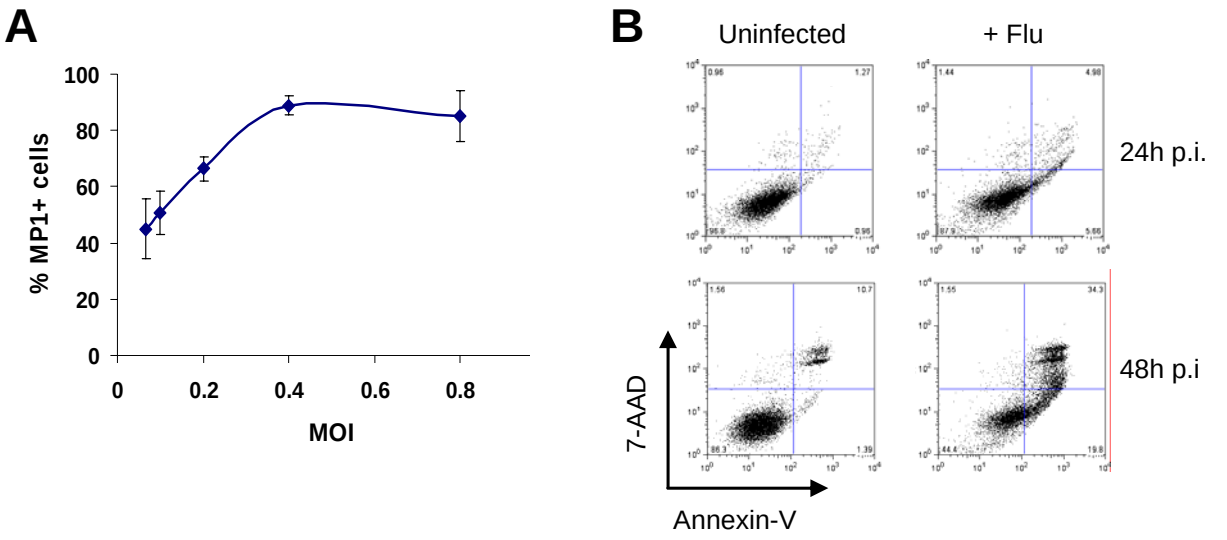
A
100
80
60
40
20
0
% MP1+ cells
0
0.2
0.4
0.6
0.8
MOI
B
Uninfected
+ Flu
24h p.i.
48h p.i
7-AAD
Annexin-V

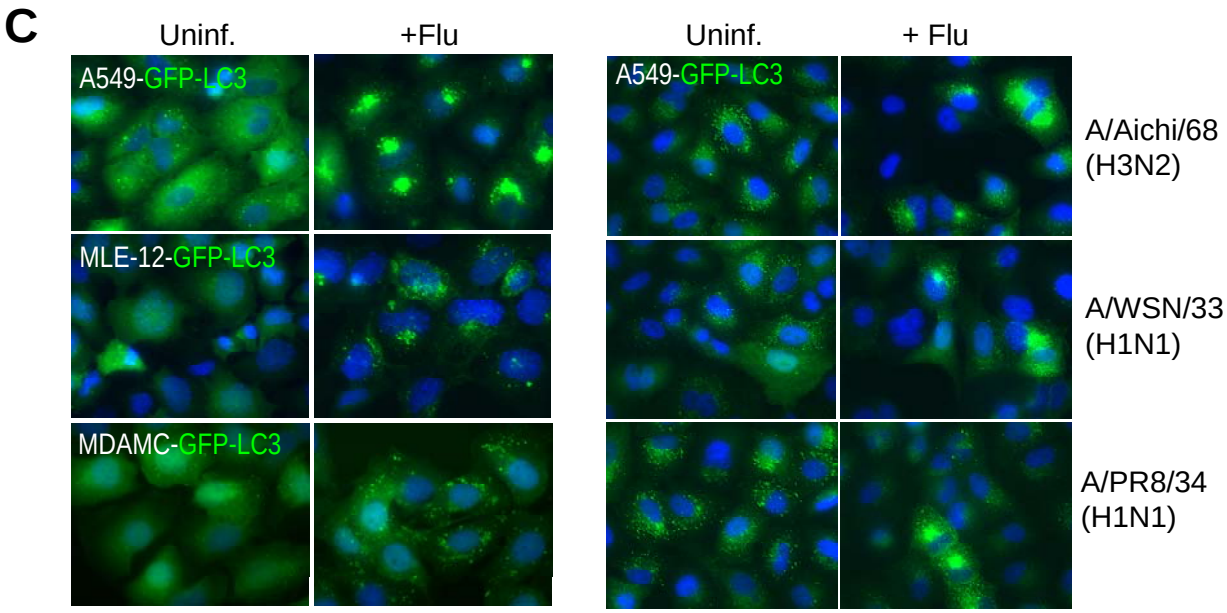
C
Uninf.
+Flu
Uninf.
+ Flu
A549-GFP-LC3
MLE-12-GFP-LC3
MDAMC-GFP-LC3
A549-GFP-LC3
A/Aichi/68
(H3N2)
A/WSN/33
(H1N1)
A/PR8/34
(H1N1)

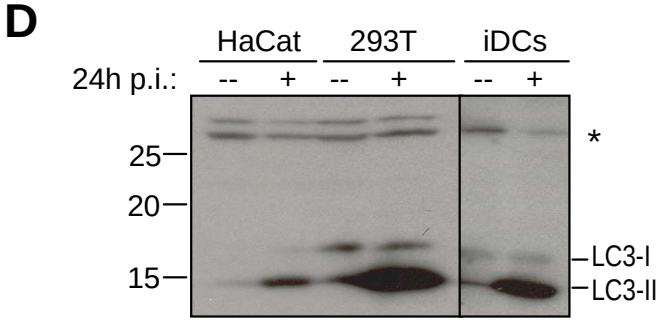
D
HaCat
293T
iDCs
24h p.i.:
-- + -- + -- +
25
20
15
*
LC3-I
LC3-II

detected (Fig. 28B). We therefore chose to analyze cells 24 hours post-infection. In comparison to uninfected cells, influenza-infected cells showed a strong increase in GFP-LC3-positive autophagosomes in all cell types examined (Fig. 28C, left). In infected human and murine lung epithelial cells, large GFP-LC3-positive structures could be observed in the perinulear area (Fig. 28C left, upper two rows). These structures probably are either very large autophagosomes or clusters of many small autophagosomes in close proximity to each other. The increase and swelling/clustering of autophagosomes in lung epithelial cells occurred after infection with different strains of influenza virus [A/Aichi/68 (H3N2), A/WSN/33 (H1N1) and A/PR8/34 (H1N1)] (Fig. 28C, right). The increased autophagosome number could also be observed by Western blot on the level of endogenous LC3: When lysates of uninfected and A/Aichi/68-infected cells were analyzed by anti-LC3 immunoblot, LC3-II was strongly increased in influenza-infected epithelial cell lines and dendritic cells (Fig. 28D). These data demonstrate that in different infectable cell types, autophagosomes are strongly increased after influenza A virus infection, suggesting that autophagy is a process that is regulated in response to influenza infection.

3.3.2 Ultrastructural analysis of influenza-infected cells reveals unusually large autophagosomes containing amorphous, electron-dense material

To see if the large GFP-LC3-positive structures that we observed in influenza-infected lung epithelial cells are autophagosomes of very large size or are clusters of small autophagosomes, we analyzed influenza-infected human lung epithelial cells (A549) by electron microscopy (in collaboration with Dr. Marc Pypaert, Yale University, New

Haven). This also allowed us to look at the autophagosome content/morphology at the ultrastructural level.

In uninfected cells, a few small (0.5 – 1 μm) autophagosomes or autolysosomes containing internal lipid vesicles and electron dense material could be observed (Fig. 29A black arrows). In contrast, 24 hours after influenza infection, cells contained many more multivesicular, membrane-rich autophagosomes of about 0.5 – 1.5 μm, which sometimes were in close proximity to each other (Fig. 29 B, left panels). In addition, some cells contained extremely large autophagosomes (up to 7 μm) that sometimes even reached the size of the nucleus (Fig. 29B, right panels). The giant autophagosomes contained electron-dense, amorphous material, which was not present in uninfected cells and therefore might consist of viral protein complexes or nucleic acids, such as viral RNPs. Autophagosomes did not seem to contain large amounts of other organelles, such as mitochondria or rough ER, as these organelles were mainly seen in the cytoplasm, but not inside autophagosomes (Fig. 29B).

Our ultrastructural analysis of influenza-infected cells confirms that autophagosome numbers are strongly increased after influenza infection. Furthermore, it suggests that at least some of the large GFP-LC3-positive structures observed in fluorescence microscopy represent unusually large autophagosomes that might contain viral components, such as protein or RNA complexes.

Figure 29: Influenza-infected cells contain unusually large autophagosomes with amorphous, electron-dense material *(Experiment performed in collaboration with Dr. Marc Pypaert, Yale University, New Haven.).*

Uninfected or influenza (A/Aichi/68)-infected A549 cells were fixed 24 hours post-infection with 2.5 % glutaraldehyde for 1 hour and were processed for electron microscopy. Representative pictures from one experiment are shown.

A: Uninfected A549 cells have few, small autophagosomes / autolysosomes containing lipid membranes and electron-dense material (black arrows). Scale bars: 2 μm (black line).

B: Influenza-infected A549 cells have numerous small and medium size (0.5-1.5 μm) autophagosomes containing internal lipid membranes or electron dense material (left panels). Some influenza-infected cells have in addition one or few extremely large autophagosomes (up to 7 μm) that often contained electron-dense, amorphous or fibrous material not present in uninfected cells (right panels). Scale bars: 2 μm (black line).

A

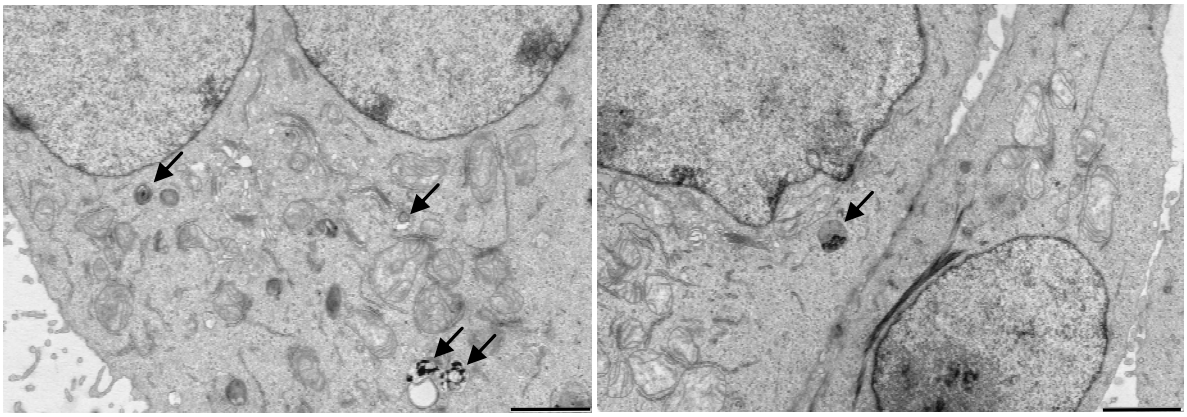

B

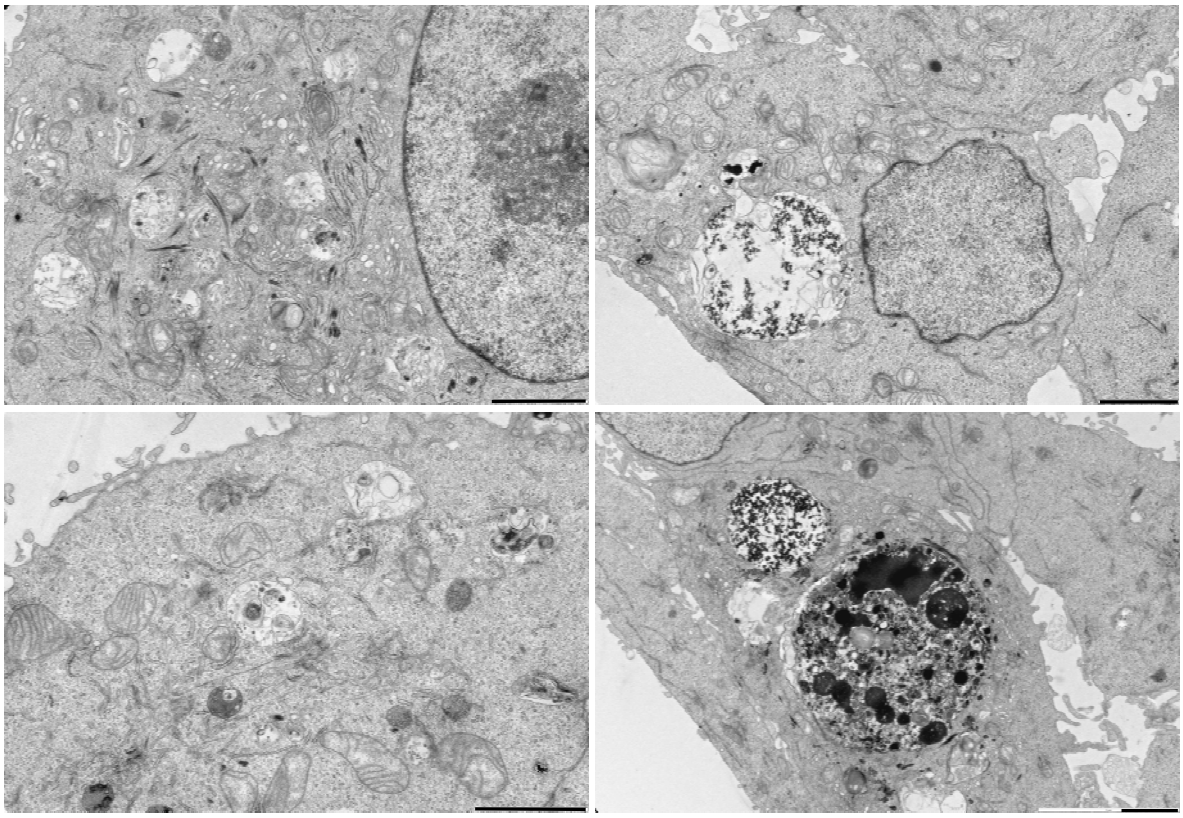

3.3.3 Small autophagosomes show highly increased mobility in influenza-infected cells

Since we observed both small and unusually large autophagosomes in influenza-infected cells, we wondered if these two different autophagosome pools have distinct mobility and how they interact with each other. To address this question, we observed live GFP-LC3-transfected A549 lung epithelial cells in spinning disc confocal microscopy. We confirmed that influenza-infected cells contained numerous small autophagosomes (Fig. 30A, middle) and sometimes one large GFP-LC3$^+$ vesicle of ≥ 5 μm diameter (Fig. 30A. right), whereas uninfected cells contained a smaller number of evenly distributed, small to medium size autophagosomes (Fig. 30A, left). The larger autophagosomes (≥ 1 μm) in both uninfected and infected cells moved only slowly; especially the very large vesicles appeared almost immobile when followed over a period of 10 min (Fig. 30B). In uninfected cells, smaller autophagosomes (< 1 μm) moved slightly more rapidly than large autophagosomes and therefore could be seen to move slowly when followed over a period of 30 seconds (average speed = 0.1 μm/s, Fig. 30C left). Strikingly, small autophagosomes in influenza-infected cells behaved very differently from the ones in uninfected cells and from large autophagosomes: Vesicle tracking showed that small autophagosomes in infected cells moved very rapidly throughout the whole cell body (Fig. 30C). The movement seemed to be random and non-directional, since vesicles moved towards and away from the central perinuclear region containing immobile large autophagosomes. The average speed of autophagosomes in infected cells was about 0.3 μm/s, however, this number is probably a severe underestimation, since it includes the

Figure 30: Mobility of autophagosomes in uninfected and influenza-infected cells analyzed by live cell spinning disc confocal microscopy.

Uninfected or influenza (A/Aichi/68)-infected GFP-LC3$^+$ A549 cells were transferred to CO_2-independent medium and analyzed at 37ºC on a spinning disc confocal microscope with a 63x oil immersion lens. One of two experiments is shown.

A: Still images showing that uninfected cells contain a smaller number of evenly distributed GFP-LC3$^+$ autophagosomes of normal size (0.5 – 1.5 μm), whereas infected cells contained much higher numbers of small autophagosomes (middle) and sometimes one or two extremely large (> 5 μm) autophagosomes (right). Scale bars: 10 μm.

B: Pictures were taken at 15 s intervals over a total period of 10 min. Snapshots from the indicated time points are shown. Large autophagosomes move very slowly or are immobile in both uninfected and influenza-infected cells. Smaller autophagosomes move more rapidly and therefore their movement is lost at this time resolution. Scale bars: 10 μm.

C: Pictures were taken at 200-600 ms intervals over a total period of 24-30 sec and vesicle movement was tracked using Imaris software. Vesicle tracks are represented as color-coded lines (t = 0 in blue, t = end in white). In uninfected cells, overall vesicle movement is slow. In influenza-infected cells, large autophagosomes are also slow to immobile, whereas small autophagosomes move rapidly throughout the whole cell body. Average speed of all vesicles from three representative fields was determined using Imaris software and is shown in the graph to the right. Error bars indicate standard deviations.

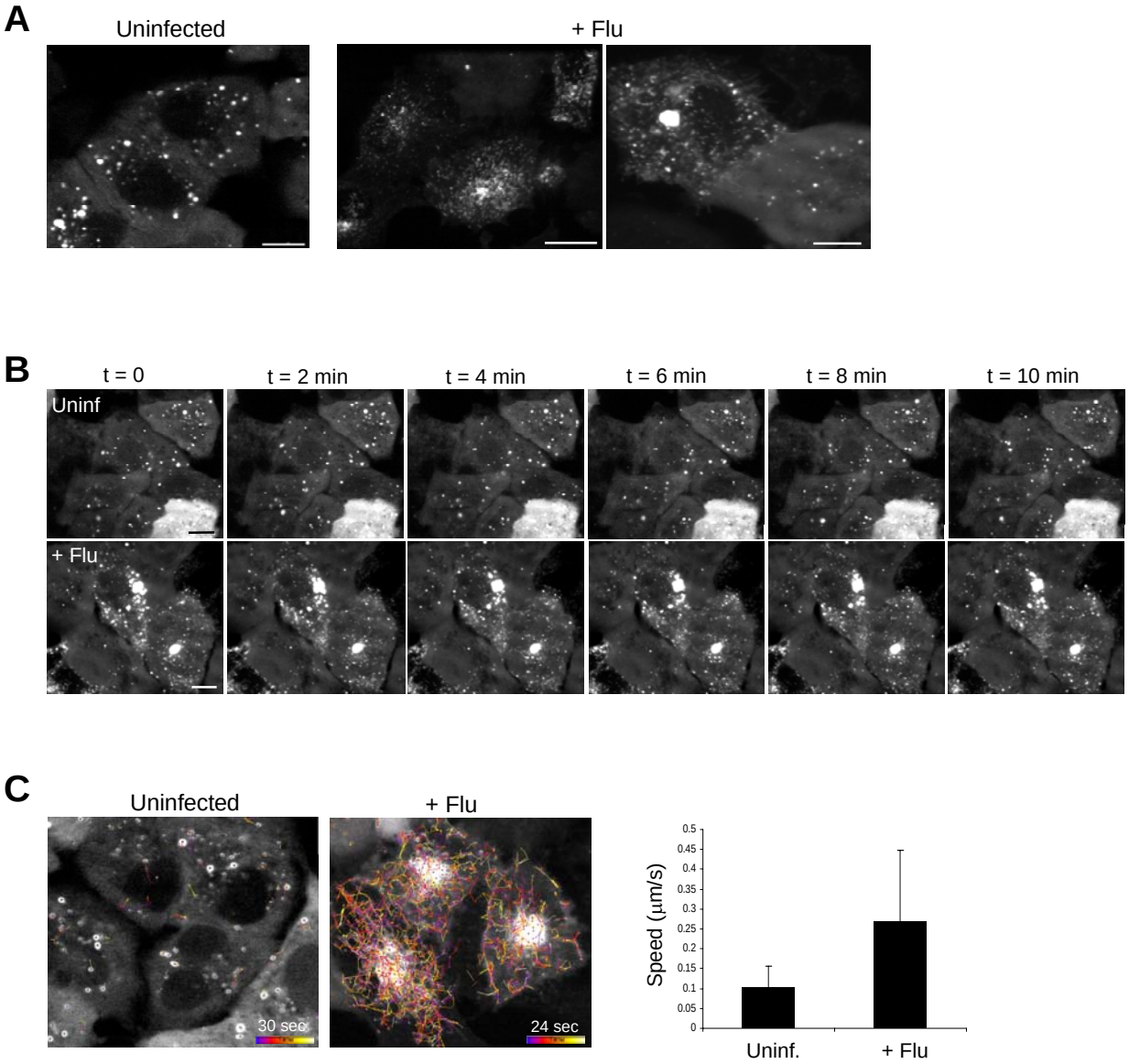
A
Uninfected
+ Flu
B
t = 0
t = 2 min
t = 4 min
t = 6 min
t = 8 min
t = 10 min
Uninf
+ Flu
C
Uninfected
+ Flu
30 sec
24 sec
Speed (µm/s)
0.5
0.45
0.4
0.35
0.3
0.25
0.2
0.15
0.1
0.05
0
Uninf.
+ Flu

values for the very large immobile autophagosomes, which are present in influenza-infected cells at large numbers.

Taken together, the two pools of autophagosomes in influenza-infected cells move with dramatically different speed: Large, strongly GFP-LC3-positive autophagosomes are very slow to immobile, as are autophagosomes in uninfected cells. In contrast, small and faintly GFP-LC3-labelled structures in influenza-infected cells move very rapidly throughout the whole cell body. The relationship between large, immobile and small, highly mobile autophagosomes and the physiological relevance of the accelerated autophagosome movement needs further investigation.

3.3.4 In influenza-infected cells, autophagosomes are not degraded in lysosomes

Since autophagosomes in influenza-infected cells show altered mobility and cellular distribution compared to uninfected cells, we wondered if altered autophagosomes still fused with lysosomes and were degraded by lysosomal proteases. To investigate fusion of autophagosome with lysosomes, we labelled acidic compartments with red fluorescent lysotracker 24 hours after influenza infection or mock infection and analyzed cells live under the spinning disc confocal microscope. In uninfected cells, about 25% of GFP-LC3$^+$ vesicles overlapped with lysotracker staining, indicating that a fraction of autophagosomes had fused with lysosomes and had become acidified (Fig. 31A). In contrast, in influenza-infected cells almost no overlap between autophagosomes and lysotracker staining was observed, especially large perinuclear autophagosomes were always devoid of lysotracker staining (Fig. 31A). This suggests that after influenza infection, autophagosomes do not fuse with acidic compartments.

Figure 31: Autophagosomes in influenza-infected cells are not degraded by lysosomal proteases.

A: Uninfected or influenza (A/Aichi/68)-infected GFP-LC3-expressing A549 cells were stained with lysotracker red for 30 min and then were imaged at 5 s intervals on a spinning disc confocal microscope. Green and red channels were imaged with a time lag of 2-3 s, therefore the degree of colocalization is probably underestimated for the smaller, more mobile vesicles. Still, a significant fraction (27%) of the larger, immobile autophagosomes in uninfected cells was stained with lysotracker, whereas almost no overlap with lysotracker was seen for the large, immobile autophagosomes in influenza-infected cells. Representative still images from two independent experiments are shown.

B: The GFP-LC3^{+} human epithelial cell lines (A549 and MDAMC) were infected with influenza virus (A/Aichi/68) at an MOI of 0.4, so that most cells in the culture would become infected. 24 h post-infection, cells were treated with chloroquine (CQ) for 6 h and lysates were analyzed by anti-LC3 Western blot. One of two experiments is shown.

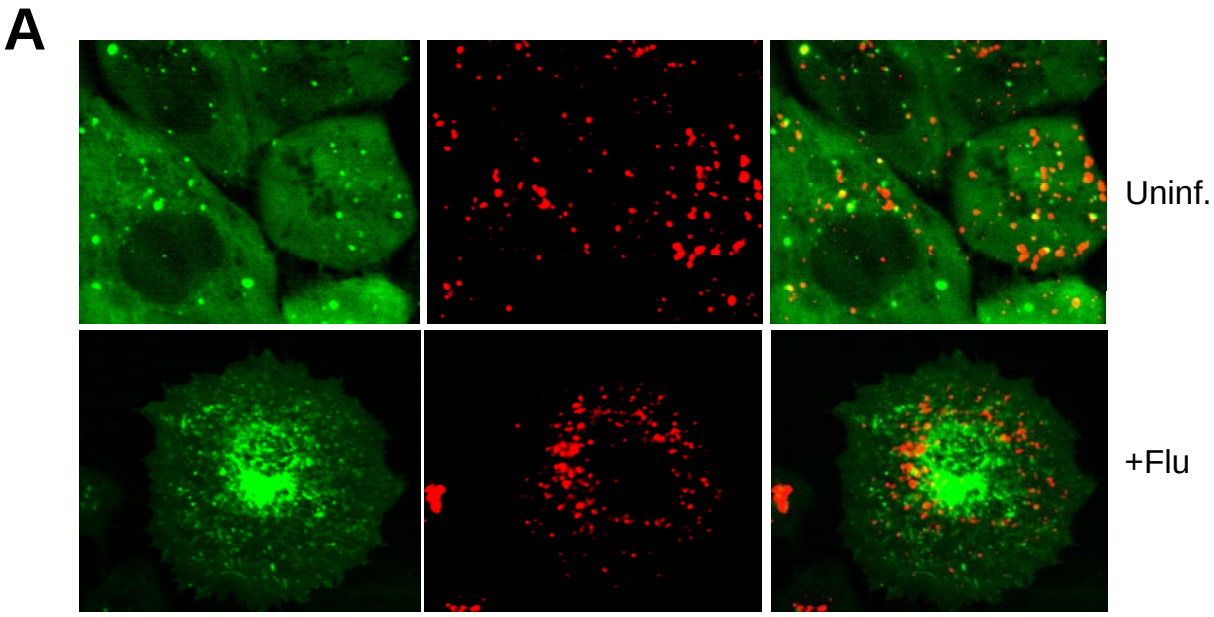
A
Uninf.
+Flu

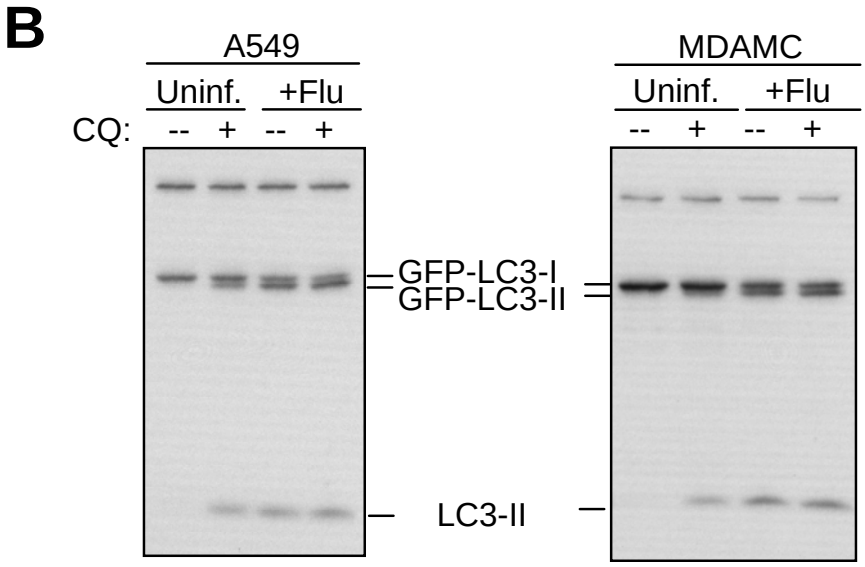
B
A549
MDAMC
Uninf.
+Flu
Uninf.
+Flu
CQ:
-- + -- +
-- + -- +
GFP-LC3-I
GFP-LC3-II
LC3-II

To confirm this result in a different assay, we infected cells with influenza virus or mock infected them and 24 hours post-infection treated them with the lysosomal proteolysis inhibitor chloroquine (CQ) for 6 hours. In uninfected cells, LC3-II and GFP-LC3-II accumulated upon CQ treatment, indicating that autophagosomes are turned over by lysosomal proteases (Fig. 31B). In contrast, in influenza-infected cells, no further accumulation of LC3-II and GFP-LC3-II could be observed in response to CQ treatment, demonstrating that autophagosomes were not turned over by lysosomal proteases in infected cells. This fits our observation that autophagosomes do not fuse with acidic compartments and suggests that autophagosome increase and swelling observed upon influenza infection is due to a block in autophagosome degradation. Although it cannot be excluded that an increased rate of autophagosome formation contributes to this effect, it seems very likely that the observed phenomenon is mainly due to a block in autophagosome-lysosome fusion.

3.3.5 Autophagosome increase occurs only in directly and productively infected cells

To investigate at what time point after infection the autophagosome increase first occurs, we prepared lysates at various time points post-infection and analyzed them by anti-LC3 Western blot. LC3-II was first increased 10 hours post-infection in infected dendritic cells and lung epithelial cells and gradually accumulated to higher levels at later time points (Fig. 32A). Thus, the increase in autophagosomes was not an extremely rapid response, indicating that viral or cellular factors might have to be produced first.

Figure 32: Autophagosome increase occurs only in directly and productively infected cells.

A: Immature DCs and the lung epithelial cell line A549 were infected with influenza virus (A/Aichi/68) and lysates were prepared at the indicated time points post-infection and then analyzed by anti-LC3 Western blot. LC3-II first increased 10 hours post-infection and accumulated to higher levels at later time points. One of two experiments is shown.

B: GFP-LC3-expressing epithelial cell lines (A549, MLE-12 and MDAMC) were either left untreated or were incubated with live or heat-inactivated (56ºC for 30 min) influenza virus A/Aichi/68. 24 hours later, cells were analyzed by anti-LC3 Western blot (top) or by fluorescence microscopy (bottom). LC3-II and GFP-LC3-II accumulated only in cells incubated with live virus, not in cells treated with heat-inactivated virus. One of two experiments is shown.

C: The GFP-LC3-expressing epithelial cell line MDAMC was left uninfected or was infected with influenza virus A/Aichi/68 and 24 hours later was stained for matrix protein 1 (MP1) and analyzed in an epifluorescence microscope. GFP-LC3-positive vesicles accumulated only in cells that were stained for MP1, not in MP1-negative, uninfected cells. One of two experiments is shown.

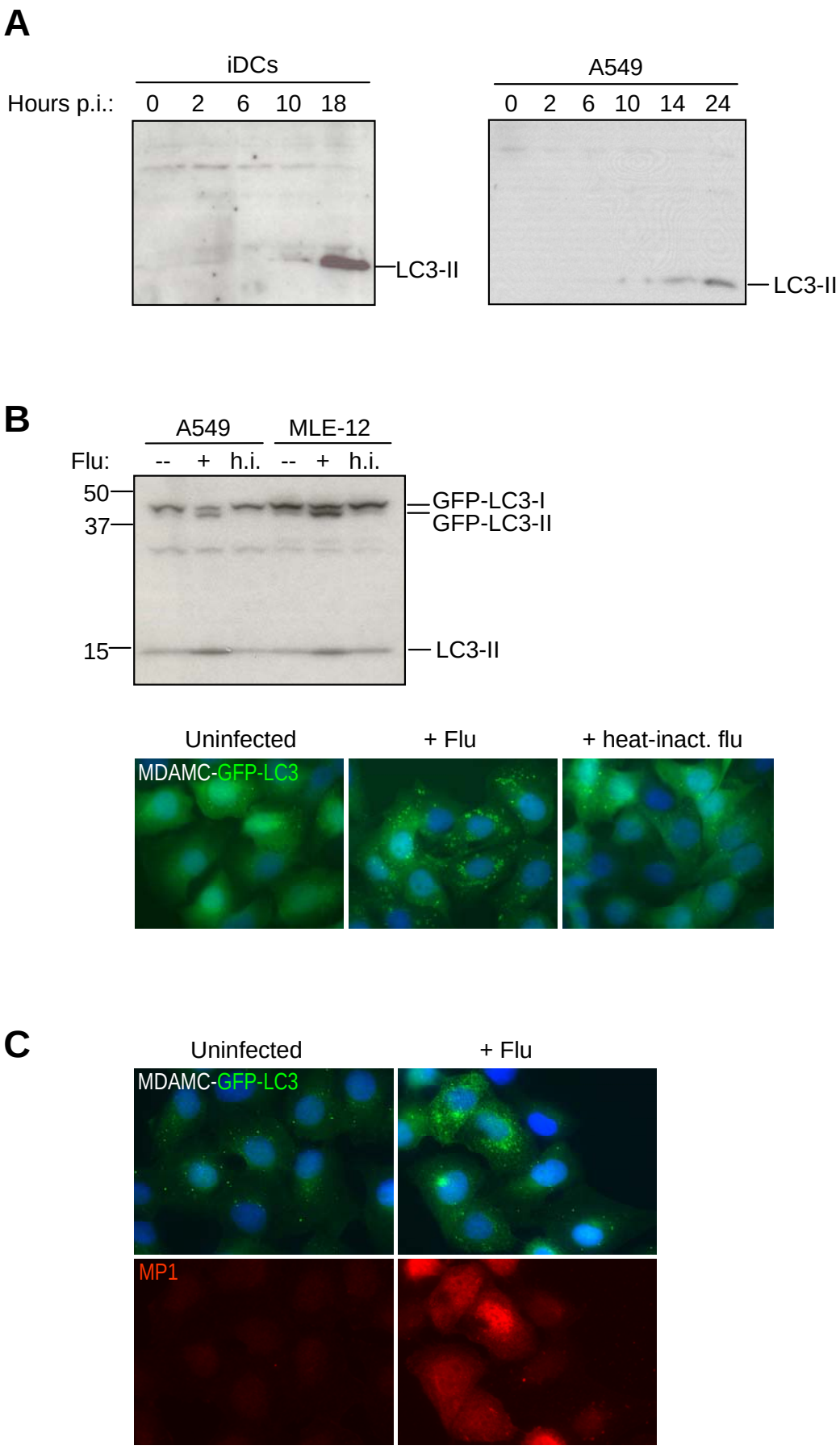
A
iDCs
Hours p.i.: 0 2 6 10 18
LC3-II
A549
0 2 6 10 14 24
LC3-II
B
A549
MLE-12
Flu: -- + h.i. -- + h.i.
50
37
15
GFP-LC3-I
GFP-LC3-II
LC3-II
Uninfected
+ Flu
+ heat-inact. flu
MDAMC-GFP-LC3
C
Uninfected
+ Flu
MDAMC-GFP-LC3
MP1

To see whether cells have to be directly and productively infected or whether uptake of inactivated viral particles is sufficient to mediate autophagosome accumulation, we exposed cells to live or heat-inactivated influenza virus and analyzed their autophagosome number by LC3 Western blot or fluorescence microscopy. Only live influenza virus was able to elicit an autophagosome accumulation, whereas heat-inactivated virus did not cause any change in LC3-II levels (Fig. 32B). Thus, contact with the viral envelope or endocytosis of inactivated virus particles is not sufficient to elicit an autophagosome increase.

To visualize more directly that productive infection is necessary for autophagosome regulation, we stained uninfected and infected cells with an MP1-specific antibody, to see if the autophagosome increase occurs only in cells that produce viral protein. Indeed, autophagosome accumulation and formation of large perinuclear autophagosomes only occurred in cells that expressed MP1, whereas MP1-negative cells did not change their autophagosome number (Fig. 32C). This indicates that autophagosome accumulation occurs only in directly and productively infected cells and is not mediated by a soluble factor present in the culture. In line with this, we could show that type I IFNs were not responsible for the observed effect, since blocking of the IFNα/β receptor did not abrogate the influenza-induced autophagosome accumulation (data not shown).

3.3.6 The viral proteins NS1 and PB1-F2 are not required and dsRNA is not sufficient for autophagosome accumulation

Since autophagosomes started to accumulate not before 10 hours post-infection and seemed to require direct and productive infection, we hypothesized that virally encoded products produced by infected cells might be responsible for the observed autophagosome accumulation. Two viral proteins that are not involved in virus replication, but rather have immunomodulatory functions, are the non-structural protein 1 (NS1) and PB1-F2. NS1 suppresses the host IFN response by preventing the activation of pro-IFN transcription factors and PKR [179, 193] and PB1-F2 accelerates apoptosis by inducing mitochondrial permeabilization [217]. Influenza virus deletion mutants that lack NS1 or PB1-F2 are able to infect cells normally and undergo productive replication and therefore can be studied in the context of a full replication cycle [179, 217]. We utilized isogenic NS1 and PB1-F2 deletion viruses to test if these proteins might be involved in modulating autophagy. However, cells infected with PR8ΔNS1 virus or WSNΔPB1-F2 still showed an increase in autophagosomes 24 hours post-infection, as did their wild-type counterparts (Fig. 33A and B). Therefore, NS1 and PB1-F2 are not required for autophagy regulation in influenza-infected cells.

To test if cytosolic double-stranded RNA (dsRNA) produced during the viral life cycle might mediate the autophagosome increase, we externally added or transfected the dsRNA mimic poly-IC. Western blot analysis showed that LC3-II levels were not increased by external addition of poly-IC (25 μg/ml) or cytosolic delivery of poly-IC (0.5 μg/ml) with different transfection reagents (Fig. 33C). Therefore, it seems unlikely that viral dsRNA is responsible for the observed phenomenon. Further experiments are

Figure 33: The viral proteins NS1 and PB1-F2 are not required and dsRNA is not sufficient for autophagosome accumulation.

A: The GFP-LC3$^+$ lung epithelial cell lines A549 was infected with influenza virus A/PR8/34 or the isogenic deletion mutant A/PR8/34ΔNS1 and 24 h post-infection cells were analyzed in an epifluorescence microscope. Cell death was slightly increased in ΔNS1-infected cells, but accumulation of GFP-LC3$^+$ vesicles occurred to a similar extend as in PR8 wt-infected cells, showing that NS1 is not responsible for autophagosome accumulation. Representative fields from one experiment are shown.

B: The GFP-LC3$^+$ lung epithelial cell lines A549 was infected influenza virus A/WSN/33 or the isogenic deletion mutant A/WSN/33-ΔPB1-F2 at different MOIs. 24 h post-infection, cell lysates were prepared and analyzed by anti-LC3 Western blot. Conversion of GFP-LC3-I into GFP-LC3-II occurred with both wt and ΔPB1-F2 virus, showing that PB1-F2 is not responsible for autophagosome accumulation. Experiment was repeated and confirmed by fluorescence microscopy.

C: A549 cells were left untreated (--), infected with influenza A/Aichi/68 or were treated extracellularly with a high dose of poly-IC (25 μg/ml, ++). In addition, small amounts of poly-IC (0.5 μg/ml, +) were introduced into the cytosol with two different transfection reagents. 24 h after treatment, lysates from all conditions were prepared and analyzed by anti-LC3 Western blot. The cross-reacting band indicated with an asterisk (*) shows equal protein loading. Poly-IC does not induce accumulation of LC3-II. One of two experiments is shown.

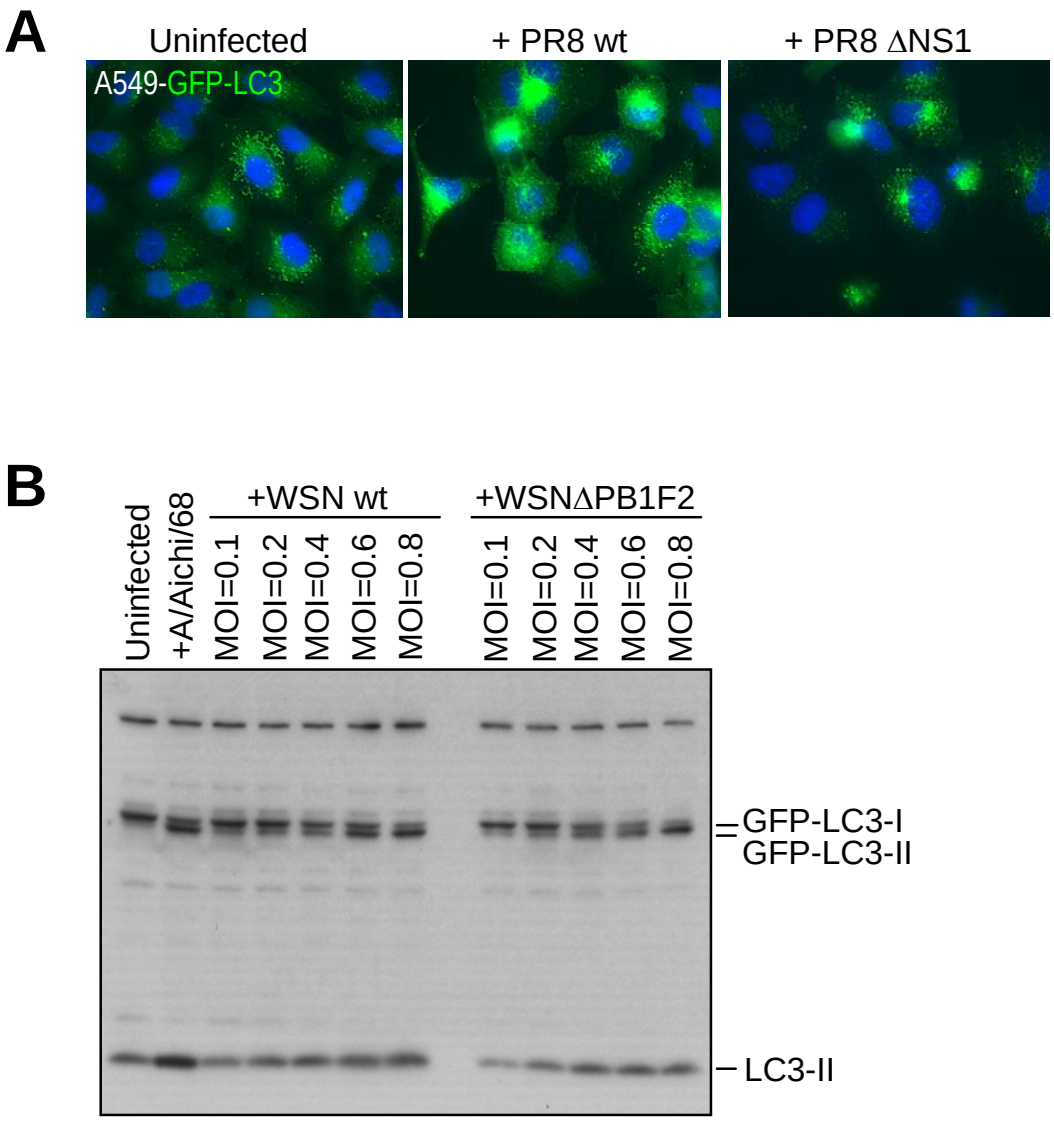
A
Uninfected
+ PR8 wt
+ PR8 ΔNS1
A549-GFP-LC3
B
+WSN wt
+WSNΔPB1F2
Uninfected
+A/Aichi/68
MOI=0.1
MOI=0.2
MOI=0.4
MOI=0.6
MOI=0.8
MOI=0.1
MOI=0.2
MOI=0.4
MOI=0.6
MOI=0.8
GFP-LC3-I
GFP-LC3-II
LC3-II
C
Fugene
Exgen
Poly-IC:
--
flu
++
+
--
+
--
*
25
20
15
LC3-I
LC3-II

required to investigate which viral components are responsible for modulating the autophagy pathway.

3.3.7 After inhibition of autophagy, influenza virus replicates more efficiently, suggesting that autophagy might restrict virus replication

Autophagosomes strongly accumulate in influenza-infected cells, however, it is not clear if and how autophagy influences viral replication. If viral components are indeed sequestered into autophagosomes, as our electron microscopy data suggest, autophagy might be a host cell response to restrict virus replication. However, it is also possible that influenza virus subverts autophagy for its own purposes and blocks autophagosome-lysosome fusion because autophagosomes are beneficial to virus replication.

To address if autophagy is beneficial for the host cell or the virus, we eliminated autophagy by siRNA-mediated silencing of *atg12* and then measured how many virus particles were produced by *atg12*-silenced or control cells upon influenza infection. *atg12*-silencing worked efficiently in at least 70% of the cells, as indicated by the lack of GFP-LC3^{+} vesicle formation (Fig. 34A). Larger amounts of virus particles were first detectable in supernatants of infected cells at 12 hours post-infection under conditions of single-round virus replication (Fig. 34B). Starting at 16 hours post-infection, virus titers were consistently increased in supernatants of *atg12*-silenced cells compared to control cells (increase between 1.4 - 2.7-fold) (Fig. 34B). This suggests that autophagy might impair virus replication and thus might restrict or delay virus replication in infected lung epithelial cells.

Figure 34: Influenza virus replicates more efficiently after inhibition of autophagy *(experiment performed in collaboration with Gina Conenello, Mt. Sinai School of Medicine, New York).*

The GFP-LC3-expressing lung epithelial cell lines A549 was transfected with *atg12*-specific siRNA (Atg12.2) or *firefly luciferase*-specific control siRNA. After 2 days, autophagosome accumulation in response to chloroquine (6 hours) was analyzed by fluorescence microscopy **(A).** Simultaneously, cells were infected with influenza virus (A/Aichi/68) and virus titers in culture supernatants collected at various time points post-infection were determined by plaque assay **(B).** The experiment was performed only once so far and needs to be repeated.

A: GFP-LC3^{+} autophagosomes accumulate after CQ treatment in control siRNA-treated cells, but not in the majority (70%) of *atg12*-siRNA-treated cells.

B: From 16 hours post-infection onwards, influenza virus titers were higher in supernatants of *atg12*-silenced cells compared to control siRNA-treated cells under conditions of single cycle replication. The experiment was performed in duplicate wells, error bars indicate standard deviations.

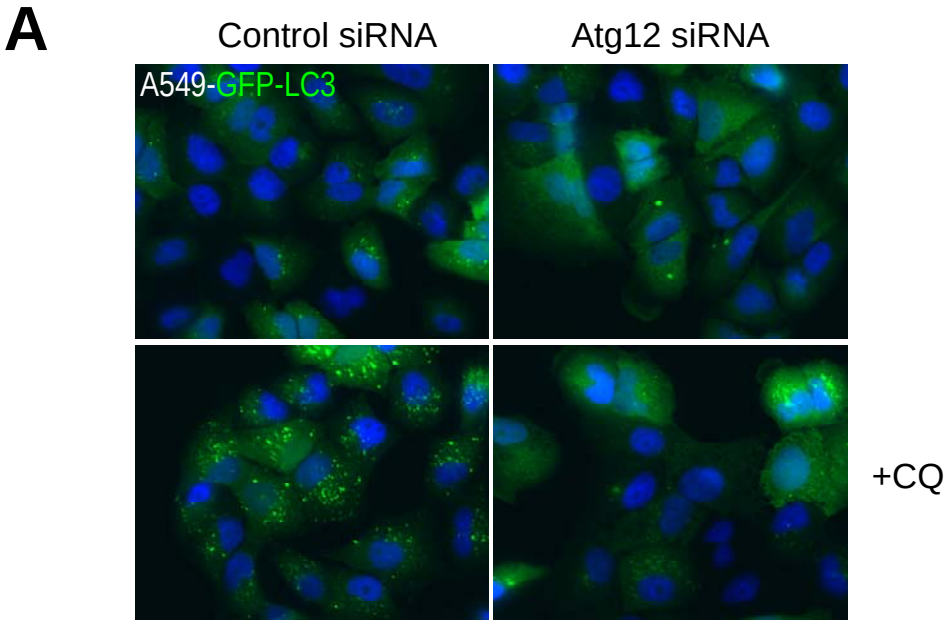
A
Control siRNA
Atg12 siRNA
A549-GFP-LC3
+CQ

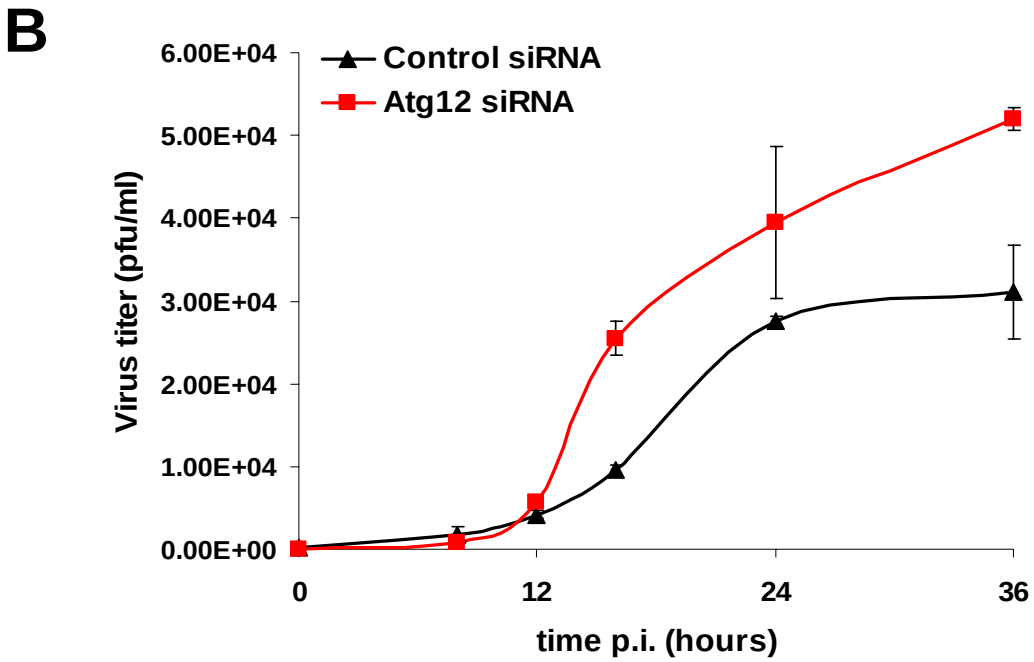
B
6.00E+04
5.00E+04
4.00E+04
3.00E+04
2.00E+04
1.00E+04
0.00E+00
Virus titer (pfu/ml)
Control siRNA
Atg12 siRNA
0
12
24
36
time p.i. (hours)

3.3.8 Conclusion: Autophagy is regulated by influenza A virus and restricts virus replication

Taken together, we observed a strongly increased number of autophagosomes in cells that are productively infected with influenza A virus. Two types of autophagosomes seem to be present in influenza-infected cells: A large number of small autophagosomes that move unusually rapidly and one or few giant autophagosomes (up to 7 μm) that are almost immobile and contain amorphous protein or nucleic acid, possibly of viral origin. The accumulation and swelling of autophagosomes are probably due to a block in autophagosome-lysosome fusion. The sequestration of viral components into autophagosomes might help to restrict virus replication, as our data indicate that influenza virus is able to replicate more efficiently when autophagy is inhibited. We propose that autophagy is an innate immune mechanism that helps to restrict or delay influenza A virus replication/dissemination until the adaptive immune response kicks in.

Chapter 4: Discussion

4.1 Endogenous MHC class II processing pathway of EBNA1

4.1.1 Evidence that lysosomal proteases and not cytosolic proteases are involved in the processing of EBNA1

It is well established that the glycine-alanine repeat domain of EBNA1 prevents proteasomal degradation of the full length protein in *cis* [175]. Nevertheless, EBNA1 is not completely resistant to proteolysis, as it can be endogenously processed for presentation on MHC class II molecules [43]. However, the proteases involved in this unusual antigen processing pathway have not been identified so far. We speculated that lysosomal enzymes might be responsible for processing of EBNA1. This indeed seemed to be the case, since treatment of an EBNA1-transfected B cell line with lysosomal acidification inhibitors led to an increase in the steady state levels of EBNA1 (Fig. 7A). After inhibitor treatment, EBNA1 accumulated in partially LAMP1-positive vesicles (Fig. 8A) and the microsomal fraction (Fig. 8B), indicating that EBNA1 degradation takes place in vesicular, partially lysosomal compartments and not the cytosol. Finally, an inhibitor of aspartyl proteases also led to an accumulation of EBNA1 (Fig. 7B and C), which is consistent with a role for the lysosomal aspartyl proteases cathepsin D and E. Both are expressed in B cells and have previously been implicated in antigen processing [204-208]: Cathepsin E was found to be upregulated in activated B cells [218] and cathepsin D was found to be involved in the processing of ovalbumin [204], glutamate decarboxylase (GAD) [44], and soluble leishmania antigen [205] *in vivo*. Cathepsin D was found to be optimally active at very acidic pH values (between pH 3.0 and 4.0) [16],

and its activity is probably strongly compromised after treatment with the lysosomal acidification inhibitors. Thus, the observation that EBNA1 is degraded less efficiently upon treatment with pH-raising drugs is consistent with a role of cathepsin D in the processing of EBNA1. Furthermore, the strongly acidic pH optimum of cathepsin D suggests that it would function best late in the endocytic pathway, i.e. in late endosomes or lysosomes [16]. Thus, it can be speculated that these compartments may be involved in the processing of EBNA1.

Cytosolic proteases, such as proteasomes and calpains, have been implicated in the processing and presentation of other endogenous proteins on MHC class II [44, 49], but do not seem to be involved in case of EBNA1: Treatment of an EBNA1-transfected B cell line with the proteasome inhibitor lactacystin did not change the steady state level of EBNA1 (Fig. 7D), which is consistent with the finding that EBNA1 is resistant to proteasomal degradation [178]. Similarly, inhibition of the cytosolic proteases calpain I and II, which were reported to play a role in the processing of endogenously expressed GAD [44], did not affect EBNA1 levels (Fig. 7D). The inhibitor concentrations we used seem to be sufficient to achieve effective inhibition of the proteasome and calpains, respectively: First, even the lowest inhibitor concentrations used in our experiments (0.25 μM lactacysteine and 5 μM calpeptin) have previously been reported to be effective in blocking antigen processing in B cells [44]. Second, FACS analysis revealed that the highest lactacystin concentration used (1 μM) was just below the lethality threshold and higher concentrations severely impaired the viability of the inhibitor treated B cells (data not shown). These observations suggest that the inhibitors were indeed effective in the presented experiment and that neither proteasomes nor calpains play a role in the

processing of EBNA1. Even though a role of other cytosolic proteases can not be excluded, the presented data suggest that EBNA1 is mainly degraded by endosomal/lysosomal proteases.

4.1.2 Evidence that macroautophagy is involved in MHC class II presentation of EBNA1

By immune-electron microscopy, EBNA1 was detected on isolation membranes or double membrane surrounded autophagosomes (Fig. 9) and inhibition of autophagy with the pharmacologic inhibitor 3-methyladenine (Fig. 10) or *atg12*-specific siRNAs (Fig. 11) significantly reduced MHC class II presentation of EBNA1 to $CD4^+$ T cell clones. These experiments suggested that EBNA1 is processed for MHC class II presentation by macroautophagic degradation.

Two model antigens (neomycin phosphotransferase II and cytosolic complement C5) and one tumor antigen (MUC-1) have also been suggested to be processed for MHC class II presentation by macroautophagy [45, 50, 53]. In all these studies, inhibitors of class III PI3 kinase, such as 3-methyladenine and wortmannin, were used to inhibit autophagosome formation and to down-regulate $CD4^+$ T cell recognition of the respective antigen. As discussed in chapter 1.3.4, these inhibitors can affect other vesicular transport and fusion processes and therefore the obtained results have to be interpreted with caution. We did not exclusively rely on the use of pharmacologic inhibitors and complemented our studies with a more specific approach to inhibit autophagy, involving siRNA-mediated silencing of *atg12*. Using this strategy, we observed that EBNA1-specific $CD4^+$ T cell recognition was reduced by about 40-60% (Fig. 11).

The fact that the EBNA1-specific $CD4^+$ T cell response was only partially (40-60%) reduced after *atg12* knockdown could be explained either by an incomplete knockdown (see residual *atg12* mRNA level in Fig. 11A), by the presence of long-lived MHC class II-peptide complexes on the cell surface [212]. Therefore, it is still possible that EBNA1 is processed for MHC class II presentation exclusively by macroautophagy. Alternatively, other endogenous processing routes, such as chaperone-medited autophagy or microautophagy might partially contribute to MHC class II presentation of EBNA1. Although we can not exclude that these alternative pathways are involved, our data provide good evidence that macroautophagy contributes significantly to MHC class II presentation and $CD4^+$ T cell recognition of EBNA1.

4.1.3 Chaperone-mediated autophagy in MHC class II presentation

In addition to macroautophagy, chaperone-mediated autophagy has been implicated in endogenous autoantigen processing for MHC class II presentation. For two autoantigens, glutamate decarboxylase 65 (GAD65) and the mutated immunoglobulin κ light chain SMA, overexpression of the LAMP-2a transporter was reported to enhance endogenous MHC class II presentation to GAD65- and Ig κ-specific T cell hybridomas [62]. In addition, the cognate GAD65-derived $CD4^+$ T cell epitope associated to a higher degree with MHC class II in LAMP-2a overexpressing cells as indicated by co-immunoprecipitation. Proteasomal degradation was required for endogenous MHC class II processing of both autoantigens [44, 219]. Therefore, proteasomal products or peptides of GAD65 and Ig κ seem to be transported into MHC class II loading compartments via chaperone-mediated autophagy.

Although chaperone-mediated autophagy can play a role in endogenous MHC class II processing, this does not seem to be the major processing route for EBNA1. First of all, EBNA1 was visualized in vesicles that are only partially LAMP1 positive (Fig. 8). Furthermore, in immuno-electron microscopy we detected EBNA1 on autophagic isolation membranes and double membrane autophagosomes rather than on classical lysosomes (Fig. 9). Finally, MHC class II presentation of EBNA1 required *atg12* (Fig. 11), which is specifically involved in macroautophagy, but not chaperone-mediated autophagy. Together, our data support a major role of macroautophagy and not chaperone-mediated autophagy in MHC class II presentation of EBNA1.

4.1.4 Relationship between half life and MHC class I vs. II presentation

Autophagic delivery seems to allow cytosolic and nuclear antigens to gain access to MHC class II presentation [45, 50, 53, 214]. Therefore, intracellular antigens can be monitored by $CD4^+$ T cells, although this pool of antigens was previously believed to be under the exclusive surveillance of $CD8^+$ T cells via MHC class I presentation [3]. Since antigen localization is not the decisive factor for MHC class I versus class II presentation anymore, the question arises what determines whether a nuclear/cytosolic antigen is preferentially presented on MHC class II or MHC class I.

We scrutinized the features of the most frequently identified natural MHC class I and II ligands (Table 9) and found that the half-life of proteins might determine in part on which class of MHC molecules an antigen is presented. The available evidence suggests that short-lived proteins are preferentially presented on MHC class I, while long-lived proteins preferentially access MHC class II loading (Table 9). Cyclin-derived peptides

Table 9: Natural MHC class I and class II ligands and their half lifes.

The three most frequent cytosolic/nuclear MHC class II ligands (HSC70, HSP70 and GAPDH) are compared to the most frequent natural MHC class I ligands (cyclins) in terms of half life and presentation on MHC class I or II, respectively. Data were compiled from the SYFPEITHI database of MHC ligands (www.syfpeithi.com) [30].

Protein	**Cellular compartm.**	**Half life**	**Restricting MHC II alleles**	**#**	**Restricting MHC I alleles**	**#**
HSC70	Cytosol	20 h [220]	H2-E^k HLA-DQB1*0603 HLA-DRB1*0401 HLA-DRB1*0402 HLA-DRB1*1101 HLA-DRB1*1104	6	HLA-A*6801 HLA-B*5101	2
HSP70	Cytosol	4 h [221] [222]	H2-A^k HLA-DQB1*0602 HLA-DRB1*0701 HLA-DRB1*1101 HLA-DRB1, unass.	5	HLA-A*0201 HLA-A*3004 HLA-A*6801 HLA-B*4601	4
GAPDH	Cytosol	130 h [223]	HLA-DQA1*0301 /DQB1*0301[224] HLA-DRB1*0402 HLA-DRB1*0404 HLA-DRB1*1101	4	-	0
Ornithine decarboxylase	Cytosol	12 min [223]	-	0	HLA-A*01 HLA-A*0201	2
Cyclins C, D, E	Nucleus	15 min [225-227]	-	0	H2-D^b (D1) HLA-A*01 (D2)[228] HLA-A*0201 (D1) HLA-A*6601 (D2) HLA-A*6801 (D1) HLA-B*1509 HLA-B*3801 HLA-B*39011 HLA-B*40 (B) HLA-B*4601 (B)	10

have frequently been eluted from a variety of human and mouse MHC class I molecules, and their half-lives are thought to be around 15 min [225]. In contrast, glyceraldehyde-3-phosphate dehydrogenase (GAPDH) is one of the most abundant natural MHC class II ligands [30, 32, 229] and its half-life was estimated to be 130 h [223]. Interestingly, cyclin peptides have so far not been eluted from MHC class II and vice versa GAPDH fragments were not found on MHC class I. Another example of a short-lived protein giving rise to MHC class I but not MHC class II ligands is ornithine decarboxylase (ODC) with a half-life of 12 min [223] (Table 9).

In line with these observations, half-life modification was shown to influence MHC class I versus MHC class II presentation: Only long-lived ($t_{1/2}$ = 5h) influenza matrix protein 1 (MP1) was presented endogenously on MHC class II to $CD4^+$ T cells [40]. When the protein half-life was shortened to 10 min via N-end rule modification, MHC class II presentation and $CD4^+$ T cell recognition were undetectable. Furthermore, EBNA1 is a very long-lived protein ($t_{1/2}$ > 20h in human B cells) [175] and EBV transformed B cells are only weakly detected by EBNA1-specific $CD8^+$ T cells [230]. However, when the glycine-alanine (GA) domain of EBNA1 is removed its half-life drops significantly [175] and $CD8^+$ T cell recognition is enhanced 4-fold [231]. In addition, defective ribosomal products, which are prematurely truncated or misfolded translation products, have a very short half-life and contribute significantly to MHC class I presentation [7, 232]. Together, these studies suggest that short-lived proteins are preferentially presented on MHC class I and long-lived proteins are preferentially loaded onto MHC class II.

Short-lived proteins, such as cyclins, DRiPs and GA domain-deleted EBNA1, have been found to be primarily degraded by proteasomes [5]. In contrast, long-lived proteins are classical substrates of autophagy [233]. In line with this, we found that the long-lived EBNA1 protein is degraded by autophagy (Fig. 9-11) and GAPDH was found to be both a substrate of chaperone-mediated autophagy [234] and to be contained in autophagosomes [235]. Therefore, we suggest that proteasomal degradation of short-lived nuclear/cytosolic antigens leads primarily to MHC class I presentation and autophagic catabolism of long-lived proteins leads primarily to MHC class II presentation. While substrate selection for proteasomal degradation via ubiquitinylation has been characterized in great detail [5], the mechanism by which long-lived proteins are selected for autophagic degradation is still unclear to date (see next paragraph).

4.1.5 Possible signals for autophagic degradation

Although no defined signal for substrate selection has been characterized so far, the selective degradation of damaged organelles and long-lived proteins argues that macroautophagy is not entirely non-selective. Several lines of evidence suggest that macromolecular assemblies and protein aggregates might be specifically selected for autophagy: First, in the related cytosol-to-vacuole (Cvt) pathway in yeast, the well-characterized Cvt substrate aminopeptidase I (ApeI) assembles into dodecamers in the cytosol, then binds to Atg9 and is delivered to the yeast vacuole via a double membrane-coated vesicle [236-238]. Second, *atg5* or *atg7* gene disruption in mouse liver or neurons leads to the accumulation of ubiquitin-positive protein aggregates in the cytosol [67, 69, 70]. Two candidates have been suggested to be involved in the recognition of ubiquitin-

positive protein aggregates: The autophagy-linked FYVE protein (Alfy) and p62/sequestosome. Both proteins localize partially to autophagosomes and to ubiquitin-positive protein aggregates and possibly target one to the other [239, 240]. Third, the proteasome, a large protein complex in the cytosol and nucleus, can be degraded by autophagy [241-243]. Overall, these observations suggest that protein aggregates or large protein complexes are preferentially degraded by autophagy, either because they are specifically recognized by the autophagosome machinery via a yet unknown mechanism, or simply because they cannot be unfolded and degraded by the proteasome.

For EBNA1, it has been speculated that newly synthesized EBNA1 might form aggregates due to the extended hydrophobic glycine-alanine repeat [244]. In neurodegenerative diseases, proteins with expanded polyglutamine and polyalanine repeats are known to form aggregates that in turn are degraded by autophagy *in vitro* and *in vivo* [245, 246]. Even though EBNA1 aggregates have not been described so far, it is possible that the GA repeat of EBNA1 favors microaggregate formation and thus degradation by the autophagy machinery. Alternatively, EBNA1 might associate with the proteasome and might be delivered for autophagic degradation along with this macromolecular protein complex. It has been shown that proteins that bind to the proteasome, but cannot be translocated into the catalytic core, stably associate with the proteasome and block its function [247]. The GA repeat of EBNA1 indeed can block the proteasome in *trans* [248]. Since the proteasome is one of the most abundant proteins, only a small fraction of the total proteasome pool would be inactivated by EBNA1 binding and subsequently discarded by autophagy. So far, no data exist to prove by which mechanism EBNA1 is shuttled into the autophagy pathway. Further studies are needed to

determine how EBNA1 and other long-lived proteins are preferentially selected for autophagic degradation and MHC class II presentation.

4.2 Autophagy as a constitutive and efficient mechanism for MHC class II presentation

4.2.1 Autophagy as a constitutive process in antigen presenting cells

Our analysis of MHC class II-positive cells has shown that a variety of human epithelial cell lines, B cell lines as well as primary monocytes and dendritic cells display substantial amounts of steady-state macroautophagy: A combination of fluorescence microscopy and biochemical analysis showed that autophagosomes form constitutively in all MHC class II-positive cell types under nutrient-rich conditions (Fig. 15 & 16). Autophagosome formation depended on *atg12* activity (Fig. 12D) and was not induced by starvation (Fig. 15E).

Our observations are in line with some other reports that have shown that autophagy is a constitutively active house-keeping mechanism in many mammalian tissues: First, analysis of GFP-LC3 transgenic mice has shown that in some murine tissues, e.g. thymus and kidney epithelium, autophagy occurs actively even under nutrient-rich conditions [68]. In response to starvation, autophagy seems to be differentially regulated in different tissues: In some organs (muscle and liver) autophagy is indeed strongly upregulated in response to starvation, presumably because these tissues are responsible for nutrient homeostasis of the body. However, other tissues, such as thymus and kidney epithelium, display high basal levels of autophagy even without

starvation. The authors concluded that the regulation of autophagy is organ dependent and the role of autophagy is not restricted to the starvation response [68]. Second, loss of *atg5* or *atg7* in neurons leads to accumulation of protein aggregates and neurodegeneration, suggesting that a basal level of autophagy is required in neurons for continuous clearance of microaggregates [69, 70]. Our study extends constitutive autophagy to cell types relevant to the immune system, including B cells, monocytes, dendritic cells and MHC class II-positive epithelial cells. MHC class II presentation of endogenous antigens after autophagy should enable the immune system to monitor these MHC class II-positive cell types for infections.

4.2.2 Fusion of autophagosomes with MHC class II loading compartments

Our analysis by immunofluorescence confocal and electron microscopy showed that MHC class II loading compartments (MIICs) contain substantial amounts of GFP-LC3 (Fig. 18-20), suggesting that autophagosomes continuously fuse with MIICs. Consistent with our findings, autophagosomes have been described to fuse with late endosomes [114, 115], but the significance of this fusion event for antigen targeting to MHC class II presentation had not been investigated. Our study closes this knowledge gap and implicates fusion of autophagosomes with late endosomal MHC class II loading compartments as a means to continually present cytosolic proteins to $CD4^+$ T cells.

Our analysis by electron micrsocopy suggests that autophagosome content meets MHC class II molecules in multivesicular bodies (Fig. 19). The ultrastructural features of these MHC class II- and LC3-containing compartments are consistent with previous descriptions of MHC class II loading compartments: MIICs were usually described to be

multivesicular or multilaminar and can be expanded and swollen after chloroquine treatment [3, 249, 250]. Interestingly, mature autophagosomes morphologically resemble multivesicular/multilaminar MHC class II loading compartments: Isolated autophagosomes often display multiple intravesicular membranes [251, 252] and autophagosomes have been shown to give rise to multilamellar bodies [253]. Therefore, the multivesicular/multilaminar nature of MHC class II loading compartments might in part be explained by the frequent fusion with autophagosomes containing a double membrane and multiple internal membrane sheets [114, 254].

4.2.3 Natural MHC class II ligands generated by autophagy

Our studies have provided evidence that autophagosomes frequently fuse with MHC class II loading compartments in different types of antigen presenting cells (Fig. 18-20) and that this pathway efficient delivers autophagy substrates, such as LC3 fusion proteins, for MHC class II loading and $CD4^+$ T cell stimulation (Fig. 24 and 27). To uncover this efficient MIIC delivery pathway, we relied on proteins that were excellent autophagy substrates (e.g. GFP-LC3 and MP1-LC3) and therefore were targeted into this pathway very efficiently. Our studies were nicely complemented by Dengjel et al., who analyzed the MHC class II ligandome of Epstein-Barr virus transformed B cell lines (B-LCL) and found that autophagy indeed can generate natural MHC class II ligands from cytosolic and nuclear proteins. In their studies, they characterized HLA-DR ligands with and without autophagy induction by starvation [37]. 24 hours after autophagy induction, MHC class II ligands derived from intracellular and lysosomal proteins were increased by 50%, while ligands derived from membrane and secreted proteins remained constant.

Three cytosolic/nuclear proteins (eukaryotic translation elongation factor 1 alpha, ubiquitin protein ligase NEDD4La and RAD23 homolog B nucleotide excision repair protein) and one lysosomal protein (cathepsin D) were most dramatically up-regulated in their presentation on HLA-DR. This suggested that upregulation of autophagy leads to enhanced MHC class II presentation of cytosolic/nuclear proteins.

In addition, in the same study two peptides derived from the autophagosome-associated protein Atg8/LC3 (MAP1LC3B) were found to be presented on HLA-DR under nutrient rich conditions. This suggested that Atg8/LC3, which is coupled to autophagosome membranes and partially degraded with autophagy substrates, is naturally processed onto MHC class II under steady-state conditions. This is consistent with our findings that autophagosomes frequently fuse with MHC class II loading compartments and that Atg8/LC3 is degraded in these compartments (Fig. 18). Therefore, not only under starvation conditions, but also in the steady state, natural MHC class II ligands are generated by autophagy.

4.2.4 Role of autophagy in professional and non-professional antigen presenting cells (APCs)

We detected constitutive autophagy and fusion with MHC class II loading compartments in both professional antigen presenting cells (B cells, dendritic cells, Fig. 16 & 20) and non-professional antigen presenting cells (epithelial cell lines, Fig. 15 & 18). Here I discuss what role autophagy might play in these different cell types during an immune response.

4.2.4.1 Role of autophagy in professional APCs

Pathogens that can infect professional APCs, such as B cells or dendritic cells, might be made detectable for the immune system by way of MHC class II presentation after autophagy. The case of EBNA1 exemplifies how autophagy can contribute to the immune surveillance of infected B cells. Cytolytic anti-viral $CD4^+$ T cells have been characterized in both mouse and man *ex vivo* [129, 130]. They have been demonstrated to control viral infections [255, 256]and can exert protective roles in the control of B cell tumors and viremia caused by murine and human γ-Herpesvirus infections [56, 257-260]. During persistent EBV infection, EBNA1-specific $CD4^+$ T cells might even be the only T cell response preventing the occurrence of EBV associated malignancies expressing EBNA1 as the sole antigen, e.g. Burkitt's lymphoma.

In dendritic cells, the most proficient antigen-presenting cells of the immune system, autophagy might contribute to two fundamental properties of DCs: Induction of $CD4^+$ T cell tolerance and stimulation of naïve $CD4^+$ T cells. Although DCs are very adept in picking up exogenous antigens, such as dying cells or environmental proteins, intracellular proteins might also be processed endogenously onto MHC class II molecules of DCs to comprehensively tolerize against DC specific antigens and efficiently prime naïve $CD4^+$ T cells after direct infection of DCs. The latter mechanism might be especially important for noncytolytic pathogens that leave infected host cells intact, so that dying cells are not readily available as a source of exogenous antigen. In these situations, autophagy might contribute to endogenous MHC class II antigen processing in DCs. This could be tested *in vivo* by DC-specific knockout of autophagy in mice.

4.2.4.2 Role of autophagy in non-professional APCs

MHC class II presentation by autophagy might be even more important for cell types that are not as phagocytic/endocytic as professional antigen presenting cells, such as DCs or macrophages. Cells that have only limited endocytic potential, e.g. epithelial and tumor cells, might depend on endogenous antigen processing routes, such as autophagy, to load antigens onto their MHC class II molecules. All epithelial EBV-associated malignancies, such as nasopharyngeal or gastric carcinoma, express MHC class II [149]. Furthermore, many epithelial and tumor cells upregulate MHC class II in response to inflammatory cytokines, such as IFN-γ [215]. Epithelial cells in inflamed tissues are often surrounded by cytolytic $CD4^+$ T cells, suggesting immune surveillance by $CD4^+$ T cells of these tissues *in vivo* [261-263].

Furthermore, thymic cortical epithelium was shown to have high levels of constitutive autophagy [68]. Cortical epithelial cells are capable of mediating positive selection of T cells in the thymus, including $CD4^+$ T cells that have to be educated on MHC class II [264]. Since thymic cortical epithelial cells are only weakly phagocytic, endogenous MHC class II antigen processing might play a major role in loading MHC class II molecules for positive selection of $CD4^+$ T cells and constitutive autophagy might contribute self-antigens for this positive T cell selection. This could be tested by specific Atg gene knockout in thymic epithelium in a mouse model.

4.2.5 Targeting antigens for autophagic degradation to enhance MHC class II presentation

In our studies, influenza matrix protein (MP1) could be targeted for enhanced MHC class II presentation by fusion to the autophagosome-associated LC3 protein (Fig. 24A). Although earlier work by Long and colleagues and our experiments with unmodified MP1 reveals access of MP1 to MHC class II presentation by an intracellular route [40], fusion to LC3 markedly increased MHC class II presentation of MP1 by up to 20 fold. This increase occurred in spite of the fact that the MP1-LC3 fusion protein was expressed at lower levels than wild-type MP1 after transfection (Fig. 22B) and did not influence surface expression of MHC class II (Fig. 24A).

Control experiments with an MP1-specific $CD8^+$ T cell clone showed that LC3 fusion did not impair MHC class I presentation of the targeted antigen (Fig. 25). This result might seem surprising, considering that the MP1-LC3 fusion protein is so efficiently shuttled into the autophagy pathway and thus away from proteasomal degradation. However, most likely both constructs give rise to similar amounts of defective ribosomal products (DRiPs), which are efficiently processed by the proteasome for MHC class I presentation [6].

In our experiments, unmodified matrix protein (MP1) was also endogenously presented on MHC class II molecules in all three types of target cells, although at a very low level (Fig. 24A). We excluded presentation from exogenous sources, because mixing of HLA-mismatched MP1-expressing epithelial cells with HLA-matched untransfected target cells was unable to stimulate $CD4^+$ T cells (Fig. 24A, top). Since autophagy is a constitutively active pathway in all three target cell types, it is tempting to speculate that

endogenous MHC class II presentation of MP1 might be due to autophagy. We tried to address this question by *atg12* silencing in target cells and subsequent T cell coculture (data not shown). However, we were unable to efficiently silence *atg12* in HaCat, B-LCL or dendritic cell targets, using the described *atg12*-specific siRNAs or shRNAs. Knockdown efficiency never reached more than 50% and therefore MHC class II presentation was not significantly reduced after treatment with *atg12* siRNAs. Therefore, we could not conclusively address whether endogenous MHC class II presentation of MP1 involves macroautophagy or other processing pathways.

4.2.6 Application of LC3 targeting strategy in recombinant viral vaccines and tumor immunotherapy

Strongly enhanced MHC class II presentation after LC3 targeting occurred in three different target cell types, among them dendritic cells, the most potent activators of naïve T cells (Fig. 24A, bottom). This suggests that the LC3 targeting strategy might be useful for vaccine antigens expressed in dendritic cells, for example after intracellular delivery via viral vectors. Notably, the MP1-LC3 fusion protein was also efficiently processed onto MHC class I molecules (Fig. 25). Therefore, DCs that express LC3 fusion antigens would be expected to efficiently prime both $CD4^+$ and $CD8^+$ T cell responses. $CD4^+$ T cells can have direct antiviral and cytolytic functions, but moreover they are crucial for the maintenance of protective $CD8^+$ T cell effector functions and memory [265]. Therefore, improved stimulation of helper T cells could be a valuable component of vaccine development.

In recombinant viral vaccines or DNA vaccines, vaccine antigens could easily be engineered to express the relatively small LC3 tag at their C-terminus. Therefore this strategy should be considered for recombinant viral vaccines or DNA vaccines. For tumor immunotherapy, dendritic cells electroporated with tumor-derived mRNA have been used to efficiently stimulate tumor-specific MHC class I-restricted responses, however presentation of the expressed antigens on MHC class II is often inefficient [266]. Modification of tumor antigens with the LC3 sequence might enhance MHC class II presentation in electroporated DCs and stimulate more efficient antitumor immunity.

4.2.7 Comparison of LC3 targeting with other MHC class II targeting strategies

Other targeting strategies have been explored to enhance MHC class II presentation of vaccine antigens. All strategies employ targeting sequences that delivers the antigen of interest for degradation in late endosomal/lysosomal compartments. The oldest MHC class II targeting method utilizes the cytosolic/transmembrane tail of the invariant chain fused to the N-terminus of the antigen [54, 267, 268]. Other targeting strategies use the cytosolic domains of LAMP1 or DC-LAMP plus a signal sequence for import into the ER [266, 269]. Antigens fused to these endosomal targeting sequences are indeed targeted to endosomal/lysosomal compartments and are more efficiently presented on MHC class II than the antigen itself [266].

Although we have not formally compared our targeting strategy with these existing targeting strategies, we think that MHC class II targeting via LC3 fusion could be advantageous over LAMP or invariant chain targeting for the following reason: Proteins carrying the invariant chain or LAMP targeting signal have to pass the quality

control for secreted and membrane proteins in the endoplasmic reticulum and therefore face the danger of retrograde transport and proteasomal degradation [270]. That this indeed seems to occur can be seen from the fact that MHC class I presentation is also somewhat enhanced by invariant chain or LAMP targeting [266]. ER quality control, retrograde transport and subsequent proteasomal degradation presumably reduces the efficiency with which the chimeric antigens are targeted to MHC class II loading compartments. In contrast, LC3 fusion proteins don't have to go through the ER quality control system because they gain direct access to MHC class II loading compartments. This probably leads to very efficient MHC class II presentation, as can be seen from our T cell assays, where LC3 fusion antigens were able to stimulate up to 95% of the maximal $CD4^+$ T cell recognition achieved with peptide pulsing of target cells (Fig. 24A).

However, a direct comparison of the different targeting strategies would be needed to determine which targeting method best enhances MHC class II presentation and $CD4^+$ T cell stimulation.

4.3 Autophagy regulation by influenza A virus

4.3.1 Autophagosome accumulation after influenza A virus infection: Reasons and consequences

When we studied influenza A virus infection of lung epithelial cell lines *in vitro*, we observed that autophagosomes strongly accumulated between 10-24 hours post-infection (Fig. 28 & 32). The phenomenon was not related to cell death and required live influenza

virus (Fig. 32). It occurred in different cell types, including epithelial and dendritic cells, and with different strains of influenza virus (Fig. 28).

The increase in autophagosomes/LC3-II could have two fundamentally different causes: First, autophagosome formation could be upregulated (e.g. by increased beclin-expression or increased PI3K activity), so that more LC3-I is converted to LC3-II and more autophagosomes and autolysosomes are formed. Alternatively, autophagosome degradation in lysosomes could be blocked, so that LC3-II-labeled autophagosomes accumulate over time. Several pieces of evidence argue for the second scenario: First, autophagosomes in influenza-infected cells do not seem to fuse with acidic compartments to the same extent as they do in uninfected cells (Fig. 31). Second, LC3-II is not degraded by lysosomal proteases in influenza-infected cells (Fig. 31). Finally, a block in autophagosome degradation would be expected to lead to a gradual accumulation of autophagosomes and LC3-II, which is exactly what we observed 10-24 hours post-infection (Fig. 32). Although we cannot exclude that an upregulation of autophagy contributes to the observed effect, it is very likely that a block in fusion with lysosomes is at least in part responsible for the increase in autophagosomes in influenza-infected cells.

The mechanism that causes a block in autophagosome-lysosome fusion remains to be determined. Acidic compartments do exist and move normally in influenza-infected cells (Fig. 31 and data not shown). Therefore, it is more likely that autophagosomes are the culprits and are modified in a way that renders them unable to fuse with lysosomes. The abnormally high mobility of small autophagosomes or the immobility of very large autophagosomes could be at the root of the autophagosomes' inability to fuse with acidic compartments. Alternatively, the protein machinery involved in autophagosome-

lysosome docking, tethering or fusion might be altered or impaired in influenza-infected cells.

One can speculate that influenza A virus evolved the autophagosome-lysosome fusion block as a mechanism to avoid autophagic degradation and MHC class II presentation of viral antigens. This would represent a novel immune escape mechanism of influenza A virus. Alternatively, the block in autophagosome-lysosome fusion might not have evolved as a viral immune escape mechanism, but might just be a byproduct of altered autophagosome physiology, e.g. altered mobility or protein composition. Nevertheless, it would be interesting to test whether endogenous MHC class II presentation of bystander (i.e. non-influenza) antigens is reduced after influenza infection.

4.3.2 Altered morphology and behavior of autophagosomes in influenza-infected cells

By both transmission electron microscopy and live cell fluorescence microscopy we observed unusually large autophagosomes in influenza-infected cells (Fig. 29 & 30). These "giant" autophagosomes were up to 7 μm in diameter and sometimes even reached the size of the nucleus. They contained electron-dense, amorphous material that did not resemble cellular organelles, such as ER or mitochondria, nor did it have the spherical shape of influenza virions [271]. Nevertheless, the material contained within the giant autophagosomes most likely consists of viral protein or nucleic acid, since these molecules would appear electron-dense and would be present in infected cells only.

The influenza A virus genome consist of ribonucleoprotein (RNP) complexes that have the shape of a twisted rod of 10-15 nm width and 30-120 nm length [271]. By transmission electron microscopy, RNPs can be seen as electron-dense rod-like structures within the viral envelope. Since RNPs are probably produced in high numbers in influenza-infected cells and their macromolecular nature would fit the criteria of preferred autophagy substrates (see chapter 3.1.5), it seems possible that the fibrous electron-dense material within influenza-induced autophagosomes are viral RNPs. This hypothesis should be addressed by immuno-staining for RNP components, such as the nucleoprotein (NP).

It is unclear how the giant autophagosomes arise in influenza-infected cells. The process of autophagosome formation could be altered such that isolation membranes elongate to unusually long structures, giving rise to very large autophagosomes. This might be caused by alterations in the Atg protein machinery or might be triggered by unusually large substrates. We did not observe unusually long isolation membranes by electron microscopy and the length of RNPs (30-120 nm) does not immediately explain an abnormal elongation of isolation membranes. Another possibility would be that the giant autophagosomes form by homotypic fusion between two or multiple autophagosomes, giving rise to one large autophagosome. Such fusion compartments would be expected to contain multiple internal membranes derived from the inner membranes of fusing autophagosomes. In our influenza-infected cells, autophagosomes were often seen in close proximity to each other and they almost always contained multiple internal membranes and vesicles (Fig. 29), suggesting homotypic fusion as a possible mechanism for giant autophagosome biogenesis. Although homotypic fusion

between autophagosome has not been described before, it might occur in influenza-infected cells as an alternative to fusion with lysosomes, e.g. due to a remodeled vesicle fusion machinery. Although the function of such an altered fusion behavior is unclear, it could explain how the autophagosomal membrane expands to such unusual size and why autophagosomes do not fuse with lysosomes in influenza-infected cells.

Apart from size, another property of autophagosomes that is altered in influenza-infected cells is mobility: Infected cells contained numerous small autophagosomes that moved very rapidly throughout the entire cytoplasm (Fig. 30). One can speculate that this change in autophagosome mobility might facilitate sequestration of viral components into autophagosomes. The rapidly moving GFP-LC3-positive structures observed in live cell fluorescence microscopy might be isolation membranes that formed in response to newly exported RNPs and that move with accelerated speed to ensure rapid sequestration of RNPs into newly forming autophagosomes. Alternatively, the accelerated speed of autophagosomes might not be related to the sequestration of viral components, but rather to the altered fusion behavior of autophagosomes discussed in the previous paragraph. More experiments are needed to determine the exact nature of the rapidly moving structures and to investigate the mechanism and functional of the accelerated autophagosome mobility.

4.3.3 Autophagy as an innate immune mechanism against viral infections

Our preliminary data suggest that influenza A virus replication might be restricted by autophagy: When we treated cells with *atg12*-siRNAs, the virus replicated more efficiently than in cells that had normal autophagy levels (Fig. 34). The enhancement in

virus replication achieved by *atg12* silencing was only 2-3 fold, however the experiment was done under conditions of single-round replication, i.e. the released virus particles were unable to reinfect cells and therefore amplify the infection. The experiment should be repeated under conditions of multicycle replication (different virus strain, such as influenza A/WSN/33, or addition of trypsin). Future experiments should also include later timepoints (e.g. 48 hours post-infection), since differences in virus replication might become more apparent at these very time points (see plateau in control cells in Fig. 34B).

Although the results presented in Fig. 34 are still preliminary, they suggest that autophagy might be a mechanism to impair or delay influenza A virus replication. A similar role of autophagy has been suggested for other viruses. In Sindbis virus infection, neuronal overexpression of the autophagy-inducing gene *beclin-1* protects mice against lethal Sindbis virus encephalitis [112]. In plants, *beclin-1*, *atg3* and *atg7* decrease TMV replication and prevent the spread of virus-induced cell death [272]. In contrast to these single-stranded RNA viruses, double-stranded DNA viruses with a more complex genome have developed escape mechanisms against autophagy: Karposi sarcoma-associated herpes virus (KSHV) encodes a viral Bcl-2 homologue that interacts with beclin-1 to inhibit autophagy [93]. Similarly, herpes simplex virus type 1 (HSV-1) encodes for an early antigen ICP34.5, which interacts with a different beclin-1 domain to inhibit PKR-induced autophagy [95, 273]. If these viral escape mechanisms are eliminated or if beclin-1 is overexpressed, autophagy is induced and virus replication and virulence are impaired, suggesting that autophagy may restrict virus replication and virulence [93, 95, 112].

Our preliminary finding that influenza A virus replication might be impaired by autophagy, would add an important human pathogen to the list of viruses that can be restricted by autophagy. Presumably, the small influenza virus RNA genome does not allow for an autophagy escape mechanism, although it remains to be seen if block in autophagosome-lysosome fusion represents a viral immune escape mechanism to prevent autophagy-mediated MHC class II presentation. Furthermore, *in vivo* experiments with mice are needed to determine if autophagosome accumulation also occurs during intranasal infection with influenza A virus. Recombinant influenza A virus carrying an autophagy inhibitor, such as ICP34.5, would be an ideal tool to further investigate the physiologic role of autophagy during *in vivo* infection.

Different models on how influenza A virus replication can be restricted by autophagy can be envisioned. One hypothesis could be that rough endoplasmic reticulum (ER) containing the viral glycoproteins HA and NA is sequestered into autophagosomes. It has recently been demonstrated in yeast that ER stress leads to ER expansion and sequestration of the expanded ER into autophagosomes, without degradation in lysosomes. However, our electron microscopy analysis failed to reveal the presence of rough ER inside influenza-induced autophagosomes and thus this model does not seem very likely. Alternatively, it can be proposed that the sequestration of RNPs by autophagosomes limits influenza virus replication. In influenza-infected cells, newly formed RNPs are exported into the cytoplasm at large quantities and might recognized by the autophagy machinery and taken up into autophagosomes due to their macromolecular nature. Our electron microscopy data would be consistent with the uptake of fibrous, protein- or nucleic acid-containing material, for example rod-like, electron dense RNPs

(Fig. 29). Although the sequestered RNPs may not be degraded in lysosomes (Fig. 31), uptake of RNPs into autophagosomes might limit the availability of RNPs for the assembly of new virus particles and thus reduce the number of new virions that bud from the infected cell (Fig. 34).

4.3.4 Inhibition of autophagy by viruses

Although influenza virus replication seems to be restricted by autophagy (see previous paragraph and Fig. 32), our data indicate that influenza virus interferes with the autophagy pathway at the level of autophagosome-lysosome fusion (Fig. 31). This represents a fundamental change in the autophagosomes' "life cycle", since they normally readily fuse with late endosomal/lysosomal compartments to deliver autophagy substrates for lysosomal degradation [76, 87].

Other viruses have been reported to inhibit autophagy, although at different stages and for different purposes than influenza A virus [108]. The first class of viruses, exemplified by KSHV and HSV-1, inhibit autophagosome generation by inhibiting beclin-1-dependent autophagy upregulation [93, 95]. In the case of HSV-1, this mechanism allows the virus to replicate efficiently in the central nervous system (CNS) and to cause fatal pathology [95]. The second class of viruses, exemplified by poliovirus and mouse hepatitis virus (MHV), block the degradation of autophagosomal membranes to use them as scaffolds for their RNA replication complexes [110, 111]. Accumulation of autophagosome-like structures is therefore a hallmark of poliovirus and MHV infections and interference with autophagosome formation compromises replication of these viruses [108, 110].

Influenza A virus also seems to inhibit degradation of autophagosomes (Fig. 31), although for different purposes than poliovirus and MHV. Influenza virus replicates its RNA in the nucleus [180], therefore it does not utilize autophagosomal membranes for its replication, like poliovirus and MHV do. Hence, inhibition of autophagy by influenza virus represents a new class of viral interference with the autophagy pathway, since the virus prevents autophagosome degradation, but does not utilize autophagosome membranes for its replication. It is possible that influenza virus utilizes autophagic membranes for a different step during the viral life cycle, such as virus assembly. Alternatively, the purpose of the autophagosome-lysosome fusion block might also be to evade MHC class II presentation of viral antigens. This would represent a novel immune escape mechanism. A third hypothesis could be that the accumulation of large numbers of autophagosomes depletes the cytosol from essential Atg proteins, (e.g. LC3), so that the formation of new autophagosomes is compromised and the sequestration of viral components, such as RNPs, is prevented. Since the bulk of LC3 and GFP-LC3 molecules seem to be engaged with autophagic membranes in influenza-infected cells (Fig. 28 and 30), it is conceivable that this is indeed the case. It remains to be tested if such a negative feedback loop exists to prevent the autophagic sequestration of viral components needed for virus replication.

References

1. O'Leary, J.G., et al., *T cell- and B cell-independent adaptive immunity mediated by natural killer cells.* Nat Immunol, 2006. **7**(5): p. 507-16.

2. Janeway, C.A., Jr., et al., *Immunobiology: The immune system in health and disease*. 6th edition ed. 2005, New York: Garland Publishing.

3. Trombetta, E.S. and I. Mellman, *Cell biology of antigen processing in vitro and in vivo.* Annu Rev Immunol, 2005. **23**: p. 975-1028.

4. Kloetzel, P.M., *Antigen processing by the proteasome.* Nat Rev Mol Cell Biol, 2001. **2**(3): p. 179-87.

5. Ciechanover, A., D. Finley, and A. Varshavsky, *Ubiquitin dependence of selective protein degradation demonstrated in the mammalian cell cycle mutant ts85.* Cell, 1984. **37**(1): p. 57-66.

6. Yewdell, J.W., E. Reits, and J. Neefjes, *Making sense of mass destruction: quantitating MHC class I antigen presentation.* Nat Rev Immunol, 2003. **3**(12): p. 952-61.

7. Schubert, U., et al., *Rapid degradation of a large fraction of newly synthesized proteins by proteasomes.* Nature, 2000. **404**(6779): p. 770-4.

8. Shastri, N., S. Schwab, and T. Serwold, *Producing nature's gene-chips: the generation of peptides for display by MHC class I molecules.* Annu Rev Immunol, 2002. **20**: p. 463-93.

9. Odorizzi, C.G., et al., *Sorting signals in the MHC class II invariant chain cytoplasmic tail and transmembrane region determine trafficking to an endocytic processing compartment.* J Cell Biol, 1994. **126**(2): p. 317-30.

10. Busch, R., et al., *Accessory molecules for MHC class II peptide loading.* Curr Opin Immunol, 2000. **12**(1): p. 99-106.

11. Neefjes, J., *CIIV, MIIC and other compartments for MHC class II loading.* Eur J Immunol, 1999. **29**(5): p. 1421-5.

12. Hiltbold, E.M. and P.A. Roche, *Trafficking of MHC class II molecules in the late secretory pathway.* Curr Opin Immunol, 2002. **14**(1): p. 30-5.

13. Villadangos, J.A. and H.L. Ploegh, *Proteolysis in MHC class II antigen presentation: who's in charge?* Immunity, 2000. **12**(3): p. 233-9.

14. Watts, C., *Antigen processing in the endocytic compartment.* Curr Opin Immunol, 2001. **13**(1): p. 26-31.

15. Chapman, H.A., *Endosomal proteases in antigen presentation.* Curr Opin Immunol, 2006. **18**(1): p. 78-84.

16. Riese, R.J. and H.A. Chapman, *Cathepsins and compartmentalization in antigen presentation.* Curr Opin Immunol, 2000. **12**(1): p. 107-13.

17. Chicz, R.M., et al., *Specificity and promiscuity among naturally processed peptides bound to HLA-DR alleles.* J Exp Med, 1993. **178**(1): p. 27-47.

18. Collins, D.S., E.R. Unanue, and C.V. Harding, *Reduction of disulfide bonds within lysosomes is a key step in antigen processing.* J Immunol, 1991. **147**(12): p. 4054-9.

19. Phan, U.T., B. Arunachalam, and P. Cresswell, *Gamma-interferon-inducible lysosomal thiol reductase (GILT). Maturation, activity, and mechanism of action.* J Biol Chem, 2000. **275**(34): p. 25907-14.

20. Castellino, F., et al., *Large protein fragments as substrates for endocytic antigen capture by MHC class II molecules.* J Immunol, 1998. **161**(8): p. 4048-57.

21. von Andrian, U.H. and T.R. Mempel, *Homing and cellular traffic in lymph nodes.* Nat Rev Immunol, 2003. **3**(11): p. 867-78.

22. Itano, A.A. and M.K. Jenkins, *Antigen presentation to naive CD4 T cells in the lymph node.* Nat Immunol, 2003. **4**(8): p. 733-9.

23. Mellman, I. and R.M. Steinman, *Dendritic cells: specialized and regulated antigen processing machines.* Cell, 2001. **106**(3): p. 255-8.

24. Steinman, R.M., D. Hawiger, and M.C. Nussenzweig, *Tolerogenic dendritic cells.* Annu Rev Immunol, 2003. **21**: p. 685-711.

25. Choi, J., et al., *T lymphocyte-endothelial cell interactions.* Annu Rev Immunol, 2004. **22**: p. 683-709.

26. Bottazzo, G.F., et al., *Role of aberrant HLA-DR expression and antigen presentation in induction of endocrine autoimmunity.* Lancet, 1983. **2**(8359): p. 1115-9.

27. Ostrand-Rosenberg, S., *Tumor immunotherapy: the tumor cell as an antigen-presenting cell.* Curr Opin Immunol, 1994. **6**(5): p. 722-7.

28. Bevan, M.J., *Cross-priming for a secondary cytotoxic response to minor H antigens with H-2 congenic cells which do not cross-react in the cytotoxic assay.* J Exp Med, 1976. **143**(5): p. 1283-8.

29. Heath, W.R. and F.R. Carbone, *Cross-presentation, dendritic cells, tolerance and immunity.* Annu Rev Immunol, 2001. **19**: p. 47-64.

30. Rammensee, H., et al., *SYFPEITHI: database for MHC ligands and peptide motifs.* Immunogenetics, 1999. **50**(3-4): p. 213-9.

31. Dongre, A.R., et al., *In vivo MHC class II presentation of cytosolic proteins revealed by rapid automated tandem mass spectrometry and functional analyses.* Eur J Immunol, 2001. **31**(5): p. 1485-94.

32. Friede, T., et al., *Natural ligand motifs of closely related HLA-DR4 molecules predict features of rheumatoid arthritis associated peptides.* Biochim Biophys Acta, 1996. **1316**(2): p. 85-101.

33. Jacobson, S., et al., *HLA class II-restricted presentation of cytoplasmic measles virus antigens to cytotoxic T cells.* J Virol, 1989. **63**(4): p. 1756-62.

34. Malnati, M.S., et al., *Processing pathways for presentation of cytosolic antigen to MHC class II-restricted T cells.* Nature, 1992. **357**(6380): p. 702-4.

35. Nuchtern, J.G., W.E. Biddison, and R.D. Klausner, *Class II MHC molecules can use the endogenous pathway of antigen presentation.* Nature, 1990. **343**(6253): p. 74-6.

36. Jaraquemada, D., M. Marti, and E.O. Long, *An endogenous processing pathway in vaccinia virus-infected cells for presentation of cytoplasmic antigens to class II-restricted T cells.* J Exp Med, 1990. **172**(3): p. 947-54.

37. Dengjel, J., et al., *Autophagy promotes MHC class II presentation of peptides from intracellular source proteins.* Proc Natl Acad Sci U S A, 2005. **102**: p. 7922-7927.

38. Muntasell, A., et al., *Dissection of the HLA-DR4 peptide repertoire in endocrine epithelial cells: strong influence of invariant chain and HLA-DM expression on the nature of ligands.* J Immunol, 2004. **173**(2): p. 1085-93.

39. Münz, C., et al., *Peptide analysis, stability studies, and structural modeling explain contradictory peptide motifs and unique properties of the NOD mouse MHC class II molecule H2-Ag7.* Eur J Immunol, 2002. **32**(8): p. 2105-2116.

40. Gueguen, M. and E.O. Long, *Presentation of a cytosolic antigen by major histocompatibility complex class II molecules requires a long-lived form of the antigen.* Proc Natl Acad Sci U S A, 1996. **93**(25): p. 14692-7.

41. Aichinger, G., et al., *Major histocompatibility complex class II-dependent unfolding, transport, and degradation of endogenous proteins.* J Biol Chem, 1997. **272**(46): p. 29127-36.

42. Chen, M., et al., *Efficient class II major histocompatibility complex presentation of endogenously synthesized hepatitis C virus core protein by Epstein-Barr virus-transformed B-lymphoblastoid cell lines to CD4(+) T cells.* J Virol, 1998. **72**(10): p. 8301-8.

43. Münz, C., et al., *Human CD4(+) T lymphocytes consistently respond to the latent Epstein-Barr virus nuclear antigen EBNA1.* J Exp Med, 2000. **191**(10): p. 1649-60.

44. Lich, J.D., J.F. Elliott, and J.S. Blum, *Cytoplasmic processing is a prerequisite for presentation of an endogenous antigen by major histocompatibility complex class II proteins.* J Exp Med, 2000. **191**(9): p. 1513-24.

45. Brazil, M.I., S. Weiss, and B. Stockinger, *Excessive degradation of intracellular protein in macrophages prevents presentation in the context of major histocompatibility complex class II molecules.* Eur J Immunol, 1997. **27**(6): p. 1506-14.

46. Weiss, S. and B. Bogen, *B-lymphoma cells process and present their endogenous immunoglobulin to major histocompatibility complex-restricted T cells.* Proc Natl Acad Sci U S A, 1989. **86**(1): p. 282-6.

47. Bonifaz, L.C., S. Arzate, and J. Moreno, *Endogenous and exogenous forms of the same antigen are processed from different pools to bind MHC class II molecules in endocytic compartments.* Eur J Immunol, 1999. **29**(1): p. 119-31.

48. Qi, L., J.M. Rojas, and S. Ostrand-Rosenberg, *Tumor cells present MHC class II-restricted nuclear and mitochondrial antigens and are the predominant antigen presenting cells in vivo.* J Immunol, 2000. **165**(10): p. 5451-61.

49. Mukherjee, P., et al., *Efficient presentation of both cytosolic and endogenous transmembrane protein antigens on MHC class II is dependent on cytoplasmic proteolysis.* J Immunol, 2001. **167**(5): p. 2632-41.

50. Nimmerjahn, F., et al., *Major histocompatibility complex class II-restricted presentation of a cytosolic antigen by autophagy.* Eur J Immunol, 2003. **33**(5): p. 1250-9.

51. Oukka, M., et al., *CD4 T cell tolerance to nuclear proteins induced by medullary thymic epithelium.* Immunity, 1996. **4**(6): p. 545-53.

52. Dani, A., et al., *The pathway for MHCII-mediated presentation of endogenous proteins involves peptide transport to the endo-lysosomal compartment.* J Cell Sci, 2004. **117**(Pt 18): p. 4219-30.

53. Dorfel, D., et al., *Processing and presentation of HLA class I and II epitopes by dendritic cells after transfection with in vitro transcribed MUC1 RNA.* Blood, 2005. **105**(8): p. 3199-3205.

54. Wang, R.F., et al., *Cloning genes encoding MHC class II-restricted antigens: mutated CDC27 as a tumor antigen.* Science, 1999. **284**(5418): p. 1351-4.

55. Bartido, S.M., S. Diment, and C.S. Reiss, *Processing of a viral glycoprotein in the endoplasmic reticulum for class II presentation.* Eur J Immunol, 1995. **25**(8): p. 2211-9.

56. Paludan, C., et al., *EBNA1 specific CD4+ Th1 cells kill Burkitt's lymphoma cells.* J Immunol, 2002. **169**: p. 1593-1603.

57. Weiss, S. and B. Bogen, *MHC class II-restricted presentation of intracellular antigen.* Cell, 1991. **64**(4): p. 767-76.

58. Lechler, R., G. Aichinger, and L. Lightstone, *The endogenous pathway of MHC class II antigen presentation.* Immunol Rev, 1996. **151**: p. 51-79.

59. Zhou, D. and J.S. Blum, *Presentation of cytosolic antigens via MHC class II molecules.* Immunol Res, 2004. **30**(3): p. 279-90.

60. Unanue, E.R., *Perspective on antigen processing and presentation.* Immunol Rev, 2002. **185**: p. 86-102.

61. Tewari, M.K., et al., *A cytosolic pathway for MHC class II-restricted antigen processing that is proteasome and TAP dependent.* Nat Immunol, 2005. **6**(3): p. 287-94.

62. Zhou, D., et al., *Lamp-2a facilitates MHC class II presentation of cytoplasmic antigens.* Immunity, 2005. **22**: p. 571-581.

63. Hershko, A., A. Ciechanover, and A. Varshavsky, *Basic Medical Research Award. The ubiquitin system.* Nat Med, 2000. **6**(10): p. 1073-81.

64. Klionsky, D.J. and S.D. Emr, *Autophagy as a regulated pathway of cellular degradation.* Science, 2000. **290**(5497): p. 1717-21.

65. De Duve, C. and R. Wattiaux, *Functions of lysosomes.* Annu Rev Physiol, 1966. **28**: p. 435-92.

66. Kuma, A., et al., *The role of autophagy during the early neonatal starvation period.* Nature, 2004. **432**(7020): p. 1032-6.

67. Komatsu, M., et al., *Impairment of starvation-induced and constitutive autophagy in Atg7-deficient mice.* J Cell Biol, 2005. **169**(3): p. 425-34.

68. Mizushima, N., et al., *In vivo analysis of autophagy in response to nutrient starvation using transgenic mice expressing a fluorescent autophagosome marker.* Mol Biol Cell, 2004. **15**(3): p. 1101-11.

69. Hara, T., et al., *Suppression of basal autophagy in neural cells causes neurodegenerative disease in mice.* Nature, 2006. **441**(7095): p. 885-9.

70. Komatsu, M., et al., *Loss of autophagy in the central nervous system causes neurodegeneration in mice.* Nature, 2006. **441**(7095): p. 880-4.

71. Cuervo, A.M. and J.F. Dice, *A receptor for the selective uptake and degradation of proteins by lysosomes.* Science, 1996. **273**(5274): p. 501-3.

72. Cuervo, A.M. and J.F. Dice, *Unique properties of lamp2a compared to other lamp2 isoforms.* J Cell Sci, 2000. **113 Pt 24**: p. 4441-50.

73. Chiang, H.L., et al., *A role for a 70-kilodalton heat shock protein in lysosomal degradation of intracellular proteins.* Science, 1989. **246**(4928): p. 382-5.

74. Agarraberes, F.A., S.R. Terlecky, and J.F. Dice, *An intralysosomal hsp70 is required for a selective pathway of lysosomal protein degradation.* J Cell Biol, 1997. **137**(4): p. 825-34.

75. Cuervo, A.M., *Autophagy: in sickness and in health.* Trends Cell Biol, 2004. **14**(2): p. 70-7.

76. Yoshimori, T., *Autophagy: a regulated bulk degradation process inside cells.* Biochem Biophys Res Commun, 2004. **313**(2): p. 453-8.

77. Juhasz, G. and T.P. Neufeld, *Autophagy: a forty-year search for a missing membrane source.* PLoS Biol, 2006. **4**(2): p. e36.

78. Reggiori, F., *1. Membrane origin for autophagy.* Curr Top Dev Biol, 2006. **74**: p. 1-30.

79. Yorimitsu, T. and D.J. Klionsky, *Autophagy: molecular machinery for self-eating.* Cell Death Differ, 2005. **12 Suppl 2**: p. 1542-52.

80. Klionsky, D.J., et al., *A unified nomenclature for yeast autophagy-related genes.* Dev Cell, 2003. **5**(4): p. 539-45.

81. Mizushima, N., et al., *A protein conjugation system essential for autophagy.* Nature, 1998. **395**(6700): p. 395-8.

82. Mizushima, N., et al., *Dissection of autophagosome formation using Apg5-deficient mouse embryonic stem cells.* J Cell Biol, 2001. **152**(4): p. 657-68.

83. Ichimura, Y., et al., *A ubiquitin-like system mediates protein lipidation.* Nature, 2000. **408**(6811): p. 488-92.

84. Kabeya, Y., et al., *LC3, a mammalian homologue of yeast Apg8p, is localized in autophagosome membranes after processing.* Embo J, 2000. **19**(21): p. 5720-8.

85. Kirisako, T., et al., *Formation process of autophagosome is traced with Apg8/Aut7p in yeast.* J Cell Biol, 1999. **147**(2): p. 435-46.

86. Lang, T., et al., *Aut2p and Aut7p, two novel microtubule-associated proteins are essential for delivery of autophagic vesicles to the vacuole.* Embo J, 1998. **17**(13): p. 3597-607.

87. Tanida, I., et al., *Lysosomal turnover, but not a cellular level, of endogenous LC3 is a marker for autophagy.* Autophagy, 2005. **1**(2): p. 84-91.

88. Mizushima, N., *Methods for monitoring autophagy.* Int J Biochem Cell Biol, 2004. **36**(12): p. 2491-502.

89. Petiot, A., et al., *Distinct classes of phosphatidylinositol 3'-kinases are involved in signaling pathways that control macroautophagy in HT-29 cells.* J Biol Chem, 2000. **275**(2): p. 992-8.

90. Ogier-Denis, E. and P. Codogno, *Autophagy: a barrier or an adaptive response to cancer.* Biochim Biophys Acta, 2003. **1603**(2): p. 113-28.

91. Kihara, A., et al., *Beclin-phosphatidylinositol 3-kinase complex functions at the trans-Golgi network.* EMBO Rep, 2001. **2**(4): p. 330-5.

92. Kametaka, S., et al., *Apg14p and Apg6/Vps30p form a protein complex essential for autophagy in the yeast, Saccharomyces cerevisiae.* J Biol Chem, 1998. **273**(35): p. 22284-91.

93. Pattingre, S., et al., *Bcl-2 antiapoptotic proteins inhibit Beclin 1-dependent autophagy.* Cell, 2005. **122**(6): p. 927-39.

94. Espert, L., P. Codogno, and M. Biard-Piechaczyk, *Involvement of autophagy in viral infections: antiviral function and subversion by viruses.* J Mol Med, 2007.

95. Orvedahl, A., et al., *HSV-1 ICP34.5 confers neurovirulence by targeting the Beclin 1 autophagy protein.* Cell Host & Microbe, 2007. **in press**.

96. Levine, B., *Eating oneself and uninvited guests: autophagy-related pathways in cellular defense.* Cell, 2005. **120**: p. 159-162.

97. Kirkegaard, K., M.P. Taylor, and W.T. Jackson, *Cellular autophagy: surrender, avoidance and subversion by microorganisms.* Nat Rev Microbiol, 2004. **2**(4): p. 301-14.

98. Shintani, T. and D.J. Klionsky, *Autophagy in health and disease: a double-edged sword.* Science, 2004. **306**(5698): p. 990-5.

99. Rich, K.A., C. Burkett, and P. Webster, *Cytoplasmic bacteria can be targets for autophagy.* Cell Microbiol, 2003. **5**(7): p. 455-68.

100. Nakagawa, I., et al., *Autophagy defends cells against invading group A Streptococcus.* Science, 2004. **306**(5698): p. 1037-40.

101. Ogawa, M., et al., *Escape of Intracellular Shigella from Autophagy.* Science, 2005. **307**(5710): p. 727-31.

102. Gutierrez, M.G., et al., *Autophagy Is a Defense Mechanism Inhibiting BCG and Mycobacterium tuberculosis Survival in Infected Macrophages.* Cell, 2004. **119**(6): p. 753-66.

103. Singh, S.B., et al., *Human IRGM induces autophagy to eliminate intracellular mycobacteria.* Science, 2006. **313**(5792): p. 1438-41.

104. Amer, A.O. and M.S. Swanson, *Autophagy is an immediate macrophage response to Legionella pneumophila.* Cell Microbiol, 2005. **7**(6): p. 765-78.

105. Gutierrez, M.G., et al., *Autophagy induction favours the generation and maturation of the Coxiella-replicative vacuoles.* Cell Microbiol, 2005. **7**(7): p. 981-93.

106. Dorn, B.R., W.A. Dunn, Jr., and A. Progulske-Fox, *Porphyromonas gingivalis traffics to autophagosomes in human coronary artery endothelial cells.* Infect Immun, 2001. **69**(9): p. 5698-708.

107. Pizarro-Cerda, J., et al., *Virulent Brucella abortus prevents lysosome fusion and is distributed within autophagosome-like compartments.* Infect Immun, 1998. **66**(5): p. 2387-92.

108. Munz, C., *Viral evasion from innate immune control via autophagy.* Cell Host & Microbe, 2007. **in press**.

109. Suhy, D.A., T.H. Giddings, Jr., and K. Kirkegaard, *Remodeling the endoplasmic reticulum by poliovirus infection and by individual viral proteins: an autophagy-like origin for virus-induced vesicles.* J Virol, 2000. **74**(19): p. 8953-65.

110. Jackson, W.T., et al., *Subversion of cellular autophagosomal machinery by RNA viruses.* PLoS Biol, 2005. **3**(5): p. e156.

111. Prentice, E., et al., *Coronavirus replication complex formation utilizes components of cellular autophagy.* J Biol Chem, 2004. **279**(11): p. 10136-41.

112. Liang, X.H., et al., *Protection against fatal Sindbis virus encephalitis by beclin, a novel Bcl-2-interacting protein.* J Virol, 1998. **72**(11): p. 8586-96.

113. Ashford, T.P. and K.R. Porter, *Cytoplasmic components in hepatic cell lysosomes.* J Cell Biol, 1962. **12**: p. 198-202.

114. Liou, W., et al., *The autophagic and endocytic pathways converge at the nascent autophagic vacuoles.* J Cell Biol, 1997. **136**(1): p. 61-70.

115. Berg, T.O., et al., *Isolation and characterization of rat liver amphisomes. Evidence for fusion of autophagosomes with both early and late endosomes.* J Biol Chem, 1998. **273**(34): p. 21883-92.

116. Fass, E., et al., *Microtubules support production of starvation-induced autophagosomes but not their targeting and fusion with lysosomes.* J Biol Chem, 2006. **281**(47): p. 36303-16.

117. Kochl, R., et al., *Microtubules facilitate autophagosome formation and fusion of autophagosomes with endosomes.* Traffic, 2006. **7**(2): p. 129-45.

118. Seglen, P.O. and P.B. Gordon, *3-Methyladenine: specific inhibitor of autophagic/lysosomal protein degradation in isolated rat hepatocytes.* Proc Natl Acad Sci U S A, 1982. **79**(6): p. 1889-92.

119. Barry, M. and R.C. Bleackley, *Cytotoxic T lymphocytes: all roads lead to death.* Nat Rev Immunol, 2002. **2**(6): p. 401-9.

120. Russell, J.H. and T.J. Ley, *Lymphocyte-mediated cytotoxicity.* Annu Rev Immunol, 2002. **20**: p. 323-70.

121. Murphy, K.M. and S.L. Reiner, *The lineage decisions of helper T cells.* Nat Rev Immunol, 2002. **2**(12): p. 933-44.

122. Pardoll, D.M. and S.L. Topalian, *The role of CD4+ T cell responses in antitumor immunity.* Curr Opin Immunol, 1998. **10**(5): p. 588-94.

123. Toes, R.E., et al., *CD4 T cells and their role in antitumor immune responses [comment].* J Exp Med, 1999. **189**(5): p. 753-6.

124. Zajac, A.J., et al., *Therapeutic vaccination against chronic viral infection: the importance of cooperation between CD4+ and CD8+ T cells.* Curr Opin Immunol, 1998. **10**(4): p. 444-9.

125. Maloy, K.J., et al., *CD4(+) T cell subsets during virus infection. Protective capacity depends on effector cytokine secretion and on migratory capability.* J Exp Med, 2000. **191**(12): p. 2159-70.

126. Rentenaar, R.J., et al., *Development of virus-specific CD4(+) T cells during primary cytomegalovirus infection.* J Clin Invest, 2000. **105**(4): p. 541-8.

127. Stalder, T., S. Hahn, and P. Erb, *Fas antigen is the major target molecule for CD4+ T cell-mediated cytotoxicity.* J Immunol, 1994. **152**(3): p. 1127-33.

128. Hahn, S., R. Gehri, and P. Erb, *Mechanism and biological significance of CD4-mediated cytotoxicity.* Immunol Rev, 1995. **146**: p. 57-79.

129. Jellison, E.R., S.K. Kim, and R.M. Welsh, *Cutting edge: MHC class II-restricted killing in vivo during viral infection.* J Immunol, 2005. **174**(2): p. 614-8.

130. Appay, V., et al., *Characterization of CD4(+) CTLs ex vivo.* J Immunol, 2002. **168**(11): p. 5954-8.

131. Franco, A., et al., *Pathogenetic effector function of CD4-positive T helper 1 cells in hepatitis B virus transgenic mice.* J Immunol, 1997. **159**(4): p. 2001-8.

132. Christensen, J.P., et al., *CD4(+) T cell-mediated control of a gamma-herpesvirus in B cell- deficient mice is mediated by IFN-gamma.* Proc Natl Acad Sci U S A, 1999. **96**(9): p. 5135-5140.

133. Mumberg, D., et al., *CD4(+) T cells eliminate MHC class II-negative cancer cells in vivo by indirect effects of IFN-gamma.* Proc Natl Acad Sci U S A, 1999. **96**(15): p. 8633-8.

134. Schoenberger, S.P., et al., *T-cell help for cytotoxic T lymphocytes is mediated by CD40-CD40L interactions [see comments].* Nature, 1998. **393**(6684): p. 480-3.

135. Bennett, S.R., et al., *Help for cytotoxic-T-cell responses is mediated by CD40 signalling [see comments].* Nature, 1998. **393**(6684): p. 478-80.

136. Cardin, R.D., et al., *Progressive loss of CD8+ T cell-mediated control of a gamma-herpesvirus in the absence of CD4+ T cells.* J Exp Med, 1996. **184**(3): p. 863-71.

137. Grakoui, A., et al., *HCV persistence and immune evasion in the absence of memory T cell help.* Science, 2003. **302**(5645): p. 659-62.

138. Shedlock, D.J. and H. Shen, *Requirement for CD4 T cell help in generating functional CD8 T cell memory.* Science, 2003. **300**(5617): p. 337-9.

139. Sun, J.C. and M.J. Bevan, *Defective CD8 T cell memory following acute infection without CD4 T cell help.* Science, 2003. **300**(5617): p. 339-42.

140. Sun, J.C., M.A. Williams, and M.J. Bevan, *CD4+ T cells are required for the maintenance, not programming, of memory CD8+ T cells after acute infection.* Nat Immunol, 2004. **5**(9): p. 927-33.

141. Addo, M.M. and E.S. Rosenberg, *Cellular immune responses in transplantation-associated chronic viral infections.* Transpl Infect Dis, 2002. **4**(1): p. 31-40.

142. Brown, D.M., E. Roman, and S.L. Swain, *CD4 T cell responses to influenza infection.* Semin Immunol, 2004. **16**(3): p. 171-7.

143. Leen, A., et al., *Differential immunogenicity of Epstein-Barr virus latent-cycle proteins for human CD4$^+$ T-helper 1 responses.* J Virol, 2001. **75**(18): p. 8649-59.

144. Welters, M.J., et al., *Frequent display of human papillomavirus type 16 E6-specific memory t-Helper cells in the healthy population as witness of previous viral encounter.* Cancer Res, 2003. **63**(3): p. 636-41.

145. van der Burg, S.H., et al., *The status of HPV16-specific T-cell reactivity in health and disease as a guide to HPV vaccine development.* Virus Res, 2002. **89**(2): p. 275-84.

146. Bui, M., et al., *Role of the influenza virus M1 protein in nuclear export of viral ribonucleoproteins.* J Virol, 2000. **74**(4): p. 1781-6.

147. Rosenberg, S.A., *A new era for cancer immunotherapy based on the genes that encode cancer antigens.* Immunity, 1999. **10**(3): p. 281-7.

148. Wang, R.F., *The role of MHC class II-restricted tumor antigens and CD4+ T cells in antitumor immunity.* Trends Immunol, 2001. **22**(5): p. 269-76.

149. Rickinson, A.B. and E. Kieff, *Epstein-Barr Virus*, in *Fields Virology*, D.M. Knipe and P.M. Howley, Editors. 2001, Lippincott-Raven: Philadelphia. p. 2575-2627.

150. Epstein, M.A., B.G. Achong, and Y.M. Barr, *Virus particles in cultured lymphoblasts from Burkitt's lymphoma.* Lancet, 1964. **1**: p. 702-703.

151. Epstein, M.A., et al., *Morphological and biological studies on a virus in cultured lymphoblasts from Burkitt's lymphoma.* J Exp Med, 1964. **121**: p. 761-770.

152. Klein, G., *Epstein-Barr virus strategy in normal and neoplastic B cells.* Cell, 1994. **77**(6): p. 791-3.

153. Pope, J.H., M.K. Horne, and W. Scott, *Transformation of foetal human keukocytes in vitro by filtrates of a human leukaemic cell line containing herpes-like virus.* Int J Cancer, 1968. **3**(6): p. 857-66.

154. Cohen, J.I., *Epstein-Barr virus infection.* N Engl J Med, 2000. **343**(7): p. 481-92.

155. Khanna, R. and S.R. Burrows, *Role of Cytotoxic T Lymphocytes in Epstein-Barr Virus-Associated Diseases.* Annu Rev Microbiol, 2000. **54**: p. 19-48.

156. Thorley-Lawson, D.A., *Epstein-Barr virus: exploiting the immune system.* Nature Reviews Immunology, 2001. **1**: p. 75-82.

157. Yates, J.L., N. Warren, and B. Sugden, *Stable replication of plasmids derived from Epstein-Barr virus in various mammalian cells.* Nature, 1985. **313**(6005): p. 812-5.

158. Bochkarev, A., et al., *Crystal structure of the DNA-binding domain of the Epstein-Barr virus origin-binding protein, EBNA1, bound to DNA.* Cell, 1996. **84**(5): p. 791-800.

159. Kaiser, C., et al., *The proto-oncogene c-myc is a direct target gene of Epstein-Barr virus nuclear antigen 2.* J Virol, 1999. **73**(5): p. 4481-4.

160. Ling, P.D., et al., *EBNA-2 upregulation of Epstein-Barr virus latency promoters and the cellular CD23 promoter utilizes a common targeting intermediate, CBF1.* J Virol, 1994. **68**(9): p. 5375-83.

161. Tomkinson, B., et al., *Epstein-Barr virus recombinants from overlapping cosmid fragments.* J Virol, 1993. **67**(12): p. 7298-306.

162. Parker, G.A., et al., *Epstein-Barr virus nuclear antigen (EBNA)3C is an immortalizing oncoprotein with similar properties to adenovirus E1A and papillomavirus E7.* Oncogene, 1996. **13**(12): p. 2541-9.

163. Harada, S. and E. Kieff, *Epstein-Barr virus nuclear protein LP stimulates EBNA-2 acidic domain-mediated transcriptional activation.* J Virol, 1997. **71**(9): p. 6611-8.

164. Komano, J., et al., *Oncogenic role of Epstein-Barr virus-encoded RNAs in Burkitt's lymphoma cell line Akata.* J Virol, 1999. **73**(12): p. 9827-31.

165. Vuyisich, M., R.J. Spanggord, and P.A. Beal, *The binding site of the RNA-dependent protein kinase (PKR) on EBER1 RNA from Epstein-Barr virus.* EMBO Rep, 2002. **3**(7): p. 622-7.

166. Babcock, G.J., et al., *EBV persistence in memory B cells in vivo.* Immunity, 1998. **9**(3): p. 395-404.

167. Babcock, G.J. and D.A. Thorley-Lawson, *Tonsillar memory B cells, latently infected with Epstein-Barr virus, express the restricted pattern of latent genes previously found only in Epstein-Barr virus-associated tumors.* Proc Natl Acad Sci U S A, 2000. **97**(22): p. 12250-5.

168. Laichalk, L.L. and D.A. Thorley-Lawson, *Terminal differentiation into plasma cells initiates the replicative cycle of Epstein-Barr virus in vivo.* J Virol, 2005. **79**(2): p. 1296-307.

169. Murray, R.J., et al., *Identification of target antigens for the human cytotoxic T cell response to Epstein-Barr virus (EBV): implications for the immune control of EBV-positive malignancies.* J Exp Med, 1992. **176**(1): p. 157-68.

170. Khanna, R., et al., *Identification of cytotoxic T cell epitopes within Epstein-Barr virus (EBV) oncogene latent membrane protein 1 (LMP1): evidence for HLA A2 supertype-restricted immune recognition of EBV-infected cells by LMP1- specific cytotoxic T lymphocytes.* Eur J Immunol, 1998. **28**(2): p. 451-8.

171. Lee, S.P., et al., *Conserved CTL epitopes within EBV latent membrane protein 2: a potential target for CTL-based tumor therapy.* J Immunol, 1997. **158**(7): p. 3325-34.

172. Reedman, B.M. and G. Klein, *Cellular localization of an Epstein-Barr virus (EBV)-associated complement-fixing antigen in producer and non-producer lymphoblastoid cell lines.* Int J Cancer, 1973. **11**(3): p. 499-520.

173. Kieff, E. and A. Rickinson, *Epstein-Barr Virus and its replication*, in *Fields Virology*, D.M. Knipe and P.M. Howley, Editors. 2001, Lippincott-Raven: Philadelphia. p. 2511-2573.

174. Yin, Y., B. Manoury, and R. Fahraeus, *Self-inhibition of synthesis and antigen presentation by Epstein-Barr virus-encoded EBNA1.* Science, 2003. **301**(5638): p. 1371-4.

175. Levitskaya, J., et al., *Inhibition of ubiquitin/proteasome-dependent protein degradation by the Gly-Ala repeat domain of the Epstein-Barr virus nuclear antigen 1.* Proc Natl Acad Sci U S A, 1997. **94**(23): p. 12616-21.

176. Voo, K.S., et al., *Evidence for the Presentation of Major Histocompatibility Complex Class I-restricted Epstein-Barr Virus Nuclear Antigen 1 Peptides to CD8+ T Lymphocytes.* J Exp Med, 2004. **199**(4): p. 459-70.

177. Tellam, J., et al., *Endogenous presentation of CD8+ T cell epitopes from Epstein-Barr virus nuclear antigen 1.* J Exp Med, 2004. **199**: p. 1421-1431.

178. Levitskaya, J., et al., *Inhibition of antigen processing by the internal repeat region of the Epstein-Barr virus nuclear antigen-1.* Nature, 1995. **375**(6533): p. 685-8.

179. Yewdell, J. and A. Garcia-Sastre, *Influenza virus still surprises.* Curr Opin Microbiol, 2002. **5**(4): p. 414-8.

180. Lamb, R.A. and R.M. Krug, *Orthomyxoviridae: The Viruses and Their Replication*. 4th edition ed. Fundamental Virology, ed. D.M. Knipe and P.M. Howley. 2001, Philadelphia: Lippincott Williams & Wilkins.

181. Martin-Benito, J., et al., *Three-dimensional reconstruction of a recombinant influenza virus ribonucleoprotein particle.* EMBO Rep, 2001. **2**(4): p. 313-7.

182. Skehel, J.J. and D.C. Wiley, *Receptor binding and membrane fusion in virus entry: the influenza hemagglutinin.* Annu Rev Biochem, 2000. **69**: p. 531-69.

183. Bui, M., G. Whittaker, and A. Helenius, *Effect of M1 protein and low pH on nuclear transport of influenza virus ribonucleoproteins.* J Virol, 1996. **70**(12): p. 8391-401.

184. Martin, K. and A. Helenius, *Transport of incoming influenza virus nucleocapsids into the nucleus.* J Virol, 1991. **65**(1): p. 232-44.

185. Martin, K. and A. Helenius, *Nuclear transport of influenza virus ribonucleoproteins: the viral matrix protein (M1) promotes export and inhibits import.* Cell, 1991. **67**(1): p. 117-30.

186. Thomas, P.G., et al., *Cell-mediated protection in influenza infection.* Emerg Infect Dis, 2006. **12**(1): p. 48-54.

187. Lawrence, C.W. and T.J. Braciale, *Activation, differentiation, and migration of naive virus-specific CD8+ T cells during pulmonary influenza virus infection.* J Immunol, 2004. **173**(2): p. 1209-18.

188. Lawrence, C.W., R.M. Ream, and T.J. Braciale, *Frequency, specificity, and sites of expansion of CD8+ T cells during primary pulmonary influenza virus infection.* J Immunol, 2005. **174**(9): p. 5332-40.

189. Belz, G.T., et al., *Compromised influenza virus-specific CD8(+)-T-cell memory in CD4(+)-T-cell-deficient mice.* J Virol, 2002. **76**(23): p. 12388-93.

190. Belz, G.T., et al., *Absence of a functional defect in CD8+ T cells during primary murine gammaherpesvirus-68 infection of I-A(b-/-) mice.* J Gen Virol, 2003. **84**(Pt 2): p. 337-41.

191. Garcia-Sastre, A. and C.A. Biron, *Type 1 interferons and the virus-host relationship: a lesson in detente.* Science, 2006. **312**(5775): p. 879-82.

192. Stetson, D.B. and R. Medzhitov, *Antiviral defense: interferons and beyond.* J Exp Med, 2006. **203**(8): p. 1837-41.

193. Donelan, N.R., C.F. Basler, and A. Garcia-Sastre, *A recombinant influenza A virus expressing an RNA-binding-defective NS1 protein induces high levels of beta interferon and is attenuated in mice.* J Virol, 2003. **77**(24): p. 13257-66.

194. Katze, M.G., Y. He, and M. Gale, Jr., *Viruses and interferon: a fight for supremacy.* Nat Rev Immunol, 2002. **2**(9): p. 675-87.

195. Grasser, F.A., et al., *Monoclonal antibodies directed against the Epstein-Barr virus-encoded nuclear antigen 1 (EBNA1): immunohistologic detection of EBNA1 in the malignant cells of Hodgkin's disease.* Blood, 1994. **84**(11): p. 3792-8.

196. Chen, M.R., et al., *The major immunogenic epitopes of Epstein-Barr virus (EBV) nuclear antigen 1 are encoded by sequence domains which vary among nasopharyngeal carcinoma biopsies and EBV-associated cell lines.* J Gen Virol, 1999. **80**(Pt 2): p. 447-55.

197. Gorga, J.C., et al., *Purification and characterization of class II histocompatibility antigens from a homozygous human B cell line.* J Biol Chem, 1987. **262**(33): p. 16087-94.

198. Kube, D., et al., *Expression of epstein-barr virus nuclear antigen 1 is associated with enhanced expression of CD25 in the Hodgkin cell line L428.* J Virol, 1999. **73**(2): p. 1630-6.

199. Fonteneau, J.F., et al., *Generation of high quantities of viral and tumor-specific human CD4+ and CD8+ T-cell clones using peptide pulsed mature dendritic cells.* J Immunol Methods, 2001. **258**(1-2): p. 111-26.

200. Subklewe, M., et al., *Dendritic Cells Expand Epstein Barr Virus Specific CD8(+) T Cell Responses More Efficiently Than EBV Transformed B Cells.* Hum Immunol, 2005. **66**(9): p. 938-49.

201. Chen, Y., M. Schindler, and S.M. Simon, *A mechanism for tamoxifen-mediated inhibition of acidification.* J Biol Chem, 1999. **274**(26): p. 18364-73.

202. McLean, I.W. and P.K. Nakane, *Periodate-lysine-paraformaldehyde fixative. A new fixation for immunoelectron microscopy.* J Histochem Cytochem, 1974. **22**(12): p. 1077-83.

203. Subklewe, M., et al., *Presentation of Epstein-Barr virus latency antigens to CD8+, interferon-gamma-secreting, T lymphocytes.* Eur J Immunol, 1999. **29**(12): p. 3995-4001.

204. Diment, S., *Different roles for thiol and aspartyl proteases in antigen presentation of ovalbumin.* J Immunol, 1990. **145**(2): p. 417-22.

205. Zhang, T., et al., *Pepstatin A-sensitive aspartic proteases in lysosome are involved in degradation of the invariant chain and antigen-processing in antigen presenting cells of mice infected with Leishmania major.* Biochem Biophys Res Commun, 2000. **276**(2): p. 693-701.

206. Bennett, K., et al., *Antigen processing for presentation by class II major histocompatibility complex requires cleavage by cathepsin E.* Eur J Immunol, 1992. **22**(6): p. 1519-24.

207. Hewitt, E.W., et al., *Natural processing sites for human cathepsin E and cathepsin D in tetanus toxin: implications for T cell epitope generation.* J Immunol, 1997. **159**(10): p. 4693-9.

208. Nishioku, T., et al., *Involvement of cathepsin E in exogenous antigen processing in primary cultured murine microglia.* J Biol Chem, 2002. **277**(7): p. 4816-22.

209. Rickinson, A.B. and D.J. Moss, *Human cytotoxic T lymphocyte responses to Epstein-Barr virus infection.* Annu Rev Immunol, 1997. **15**: p. 405-31.

210. Voo, K.S., et al., *Identification of HLA-DP3-restricted peptides from EBNA1 recognized by CD4(+) T cells.* Cancer Res, 2002. **62**(24): p. 7195-9.

211. Fenteany, G., et al., *Inhibition of proteasome activities and subunit-specific amino-terminal threonine modification by lactacystin.* Science, 1995. **268**(5211): p. 726-31.

212. Nelson, C.A., S.J. Petzold, and E.R. Unanue, *Peptides determine the lifespan of MHC class II molecules in the antigen-presenting cell.* Nature, 1994. **371**(6494): p. 250-2.

213. Kuma, A., et al., *Formation of the approximately 350-kDa Apg12-Apg5.Apg16 multimeric complex, mediated by Apg16 oligomerization, is essential for autophagy in yeast.* J Biol Chem, 2002. **277**(21): p. 18619-25.

214. Paludan, C., et al., *Endogenous MHC class II processing of a viral nuclear antigen after autophagy.* Science, 2005. **307**(5709): p. 593-6.

215. Reith, W. and B. Mach, *The bare lymphocyte syndrome and the regulation of MHC expression.* Annu Rev Immunol, 2001. **19**: p. 331-73.

216. Codogno, P. and A.J. Meijer, *Autophagy and signaling: their role in cell survival and cell death.* Cell Death Differ, 2005. **12**: p. 1509-1518.

217. Zamarin, D., et al., *Influenza virus PB1-F2 protein induces cell death through mitochondrial ANT3 and VDAC1.* PLoS Pathog, 2005. **1**(1): p. e4.

218. Sealy, L., et al., *Regulation of cathepsin E expression during human B cell differentiation in vitro.* Eur J Immunol, 1996. **26**(8): p. 1838-43.

219. Dul, J.L., et al., *Hsp70 and antifibrillogenic peptides promote degradation and inhibit intracellular aggregation of amyloidogenic light chains.* J Cell Biol, 2001. **152**(4): p. 705-16.

220. Jiang, J., et al., *CHIP is a U-box-dependent E3 ubiquitin ligase: identification of Hsc70 as a target for ubiquitylation.* J Biol Chem, 2001. **276**(46): p. 42938-44.

221. Li, D. and R.F. Duncan, *Transient acquired thermotolerance in Drosophila, correlated with rapid degradation of Hsp70 during recovery.* Eur J Biochem, 1995. **231**(2): p. 454-65.

222. Landry, J., et al., *Phosphorylation of HSP27 during development and decay of thermotolerance in Chinese hamster cells.* J Cell Physiol, 1991. **147**(1): p. 93-101.

223. Dice, J.F. and A.L. Goldberg, *A statistical analysis of the relationship between degradative rates and molecular weights of proteins.* Arch Biochem Biophys, 1975. **170**(1): p. 213-9.

224. Rammensee, H.-G., J. Bachman, and S. Stevanovic, *MHC ligands and peptide motifs*. 1997, Austin: Springer, Landes Bioscience.

225. Barette, C., et al., *Human cyclin C protein is stabilized by its associated kinase cdk8, independently of its catalytic activity.* Oncogene, 2001. **20**(5): p. 551-62.

226. Germain, D., et al., *Ubiquitination of free cyclin D1 is independent of phosphorylation on threonine 286.* J Biol Chem, 2000. **275**(16): p. 12074-9.

227. Singer, J.D., et al., *Cullin-3 targets cyclin E for ubiquitination and controls S phase in mammalian cells.* Genes Dev, 1999. **13**(18): p. 2375-87.

228. Falk, K., et al., *Peptide motifs of HLA-A1, -A11, -A31, and -A33 molecules.* Immunogenetics, 1994. **40**(3): p. 238-41.

229. Harris, P.E., et al., *Predominant HLA-class II bound self-peptides of a hematopoietic progenitor cell line are derived from intracellular proteins.* Blood, 1996. **87**(12): p. 5104-12.

230. Blake, N., et al., *Human CD8+ T cell responses to EBV EBNA1: HLA class I presentation of the (Gly-Ala)-containing protein requires exogenous processing.* Immunity, 1997. **7**(6): p. 791-802.

231. Lee, S.P., et al., *CD8 T cell recognition of endogenously expressed Epstein-Barr virus nuclear antigen 1.* J Exp Med, 2004. **199**: p. 1409-1420.

232. Reits, E.A., et al., *The major substrates for TAP in vivo are derived from newly synthesized proteins.* Nature, 2000. **404**(6779): p. 774-8.

233. Henell, F., et al., *Degradation of short- and long-lived proteins in perfused liver and in isolated autophagic vacuoles--lysosomes.* Exp Mol Pathol, 1987. **46**(1): p. 1-14.

234. Aniento, F., et al., *Uptake and degradation of glyceraldehyde-3-phosphate dehydrogenase by rat liver lysosomes.* J Biol Chem, 1993. **268**(14): p. 10463-70.

235. Fengsrud, M., et al., *Autophagosome-associated variant isoforms of cytosolic enzymes.* Biochem J, 2000. **352 Pt 3**: p. 773-81.

236. Kim, J. and D.J. Klionsky, *Autophagy, cytoplasm-to-vacuole targeting pathway, and pexophagy in yeast and mammalian cells.* Annu Rev Biochem, 2000. **69**: p. 303-42.

237. Shintani, T., et al., *Mechanism of cargo selection in the cytoplasm to vacuole targeting pathway.* Dev Cell, 2002. **3**(6): p. 825-37.

238. Suzuki, K., Y. Kamada, and Y. Ohsumi, *Studies of cargo delivery to the vacuole mediated by autophagosomes in Saccharomyces cerevisiae.* Dev Cell, 2002. **3**(6): p. 815-24.

239. Simonsen, A., et al., *Alfy, a novel FYVE-domain-containing protein associated with protein granules and autophagic membranes.* J Cell Sci, 2004. **117**(Pt 18): p. 4239-51.

240. Bjorkoy, G., et al., *p62/SQSTM1 forms protein aggregates degraded by autophagy and has a protective effect on huntingtin-induced cell death.* J Cell Biol, 2005. **171**(4): p. 603-14.

241. Cuervo, A.M., et al., *Degradation of proteasomes by lysosomes in rat liver.* Eur J Biochem, 1995. **227**(3): p. 792-800.

242. Hendil, K.B., *The 19 S multicatalytic "prosome" proteinase is a constitutive enzyme in HeLa cells.* Biochem Int, 1988. **17**(3): p. 471-7.

243. Tanaka, K. and A. Ichihara, *Half-life of proteasomes (multiprotease complexes) in rat liver.* Biochem Biophys Res Commun, 1989. **159**(3): p. 1309-15.

244. Dantuma, N.P., et al., *Inhibition of proteasomal degradation by the gly-Ala repeat of Epstein- Barr virus is influenced by the length of the repeat and the strength of the degradation signal.* Proc Natl Acad Sci U S A, 2000. **97**(15): p. 8381-5.

245. Ravikumar, B., R. Duden, and D.C. Rubinsztein, *Aggregate-prone proteins with polyglutamine and polyalanine expansions are degraded by autophagy.* Hum Mol Genet, 2002. **11**(9): p. 1107-17.

246. Ravikumar, B., et al., *Inhibition of mTOR induces autophagy and reduces toxicity of polyglutamine expansions in fly and mouse models of Huntington disease.* Nat Genet, 2004. **36**(6): p. 585-95.

247. Navon, A. and A.L. Goldberg, *Proteins are unfolded on the surface of the ATPase ring before transport into the proteasome.* Mol Cell, 2001. **8**(6): p. 1339-49.

248. Leonchiks, A., et al., *Inhibition of ubiquitin-dependent proteolysis by a synthetic glycine- alanine repeat peptide that mimics an inhibitory viral sequence.* FEBS Lett, 2002. **522**(1-3): p. 93-8.

249. Li, P., et al., *Compartmentalization of class II antigen presentation: contribution of cytoplasmic and endosomal processing.* Immunol Rev, 2005. **207**: p. 206-17.

250. Zwart, W., et al., *Spatial separation of HLA-DM/HLA-DR interactions within MIIC and phagosome-induced immune escape.* Immunity, 2005. **22**(2): p. 221-33.

251. Fengsrud, M., et al., *Ultrastructural characterization of the delimiting membranes of isolated autophagosomes and amphisomes by freeze-fracture electron microscopy.* Eur J Cell Biol, 2000. **79**(12): p. 871-82.

252. Stromhaug, P.E., et al., *Purification and characterization of autophagosomes from rat hepatocytes.* Biochem J, 1998. **335 (Pt 2)**: p. 217-24.

253. Hariri, M., et al., *Biogenesis of multilamellar bodies via autophagy.* Mol Biol Cell, 2000. **11**(1): p. 255-68.

254. Niemann, A., A. Takatsuki, and H.P. Elsasser, *The lysosomotropic agent monodansylcadaverine also acts as a solvent polarity probe.* J Histochem Cytochem, 2000. **48**(2): p. 251-8.

255. Fu, T., K.S. Voo, and R.F. Wang, *Critical role of EBNA1-specific CD4+ T cells in the control of mouse Burkitt lymphoma in vivo.* J Clin Invest, 2004. **114**(4): p. 542-50.

256. Sparks-Thissen, R.L., et al., *An optimized CD4 T-cell response can control productive and latent gammaherpesvirus infection.* J Virol, 2004. **78**(13): p. 6827-35.

257. Stevenson, P.G., et al., *Immunological control of a murine gammaherpesvirus independent of CD8+ T cells.* J Gen Virol, 1999. **80**(Pt 2): p. 477-83.

258. Robertson, K.A., E.J. Usherwood, and A.A. Nash, *Regression of a murine gammaherpesvirus 68-positive b-cell lymphoma mediated by CD4 T lymphocytes.* J Virol, 2001. **75**(7): p. 3480-2.

259. Nikiforow, S., K. Bottomly, and G. Miller, *CD4+ T-cell effectors inhibit Epstein-Barr virus-induced B-cell proliferation.* J Virol, 2001. **75**(8): p. 3740-52.

260. Nikiforow, S., et al., *Cytolytic CD4(+)-T-Cell Clones Reactive to EBNA1 Inhibit Epstein-Barr Virus-Induced B-Cell Proliferation.* J Virol, 2003. **77**(22): p. 12088-12104.

261. Wu, Z., et al., *Perforin expression by thyroid-infiltrating T cells in autoimmune thyroid disease.* Clin Exp Immunol, 1994. **98**(3): p. 470-7.

262. Muller, S., et al., *Activated CD4+ and CD8+ cytotoxic cells are present in increased numbers in the intestinal mucosa from patients with active inflammatory bowel disease.* Am J Pathol, 1998. **152**(1): p. 261-8.

263. Yawalkar, N., et al., *A comparative study of the expression of cytotoxic proteins in allergic contact dermatitis and psoriasis: spongiotic skin lesions in allergic*

contact dermatitis are highly infiltrated by T cells expressing perforin and granzyme B. Am J Pathol, 2001. **158**(3): p. 803-8.

264. Starr, T.K., S.C. Jameson, and K.A. Hogquist, *Positive and negative selection of T cells.* Annu Rev Immunol, 2003. **21**: p. 139-76.

265. Bevan, M.J., *Helping the CD8(+) T-cell response.* Nat Rev Immunol, 2004. **4**(8): p. 595-602.

266. Bonehill, A., et al., *Messenger RNA-electroporated dendritic cells presenting MAGE-A3 simultaneously in HLA class I and class II molecules.* J Immunol, 2004. **172**(11): p. 6649-57.

267. Sanderson, F., et al., *Accumulation of HLA-DM, a regulator of antigen presentation, in MHC class II compartments.* Science, 1994. **266**(5190): p. 1566-9.

268. Dengjel, J., et al., *Identification of a naturally processed cyclin D1 T-helper epitope by a novel combination of HLA class II targeting and differential mass spectrometry.* Eur J Immunol, 2004. **34**(12): p. 3644-51.

269. Fernandes, D.M., L. Vidard, and K.L. Rock, *Characterization of MHC class II-presented peptides generated from an antigen targeted to different endocytic compartments.* Eur J Immunol, 2000. **30**(8): p. 2333-43.

270. Kostova, Z. and D.H. Wolf, *For whom the bell tolls: protein quality control of the endoplasmic reticulum and the ubiquitin-proteasome connection.* Embo J, 2003. **22**(10): p. 2309-17.

271. Noda, T., et al., *Architecture of ribonucleoprotein complexes in influenza A virus particles.* Nature, 2006. **439**(7075): p. 490-2.

272. Liu, Y., et al., *Autophagy regulates programmed cell death during the plant innate immune response.* Cell, 2005. **121**(4): p. 567-77.

273. Talloczy, Z., et al., *Regulation of starvation- and virus-induced autophagy by the eIF2alpha kinase signaling pathway.* Proc Natl Acad Sci U S A, 2002. **99**(1): p. 190-5.